Method Development for Catalyst Discovery using

Electrospray Ionization Mass Spectrometry

by

Matthew Alex Henderson
B.Sc., University of Calgary, 2004

A Dissertation Submitted in Partial Fulfillment of the
Requirements for the Degree of

DOCTOR OF PHILOSOPHY

In the Department of Chemistry

Supervisory Committee

Method Development for Catalyst Discovery using

Electrospray Ionization Mass Spectrometry

by

Matthew Alex Henderson
B.Sc., University of Calgary, 2004

Supervisory Committee

Dr. J. Scott McIndoe, Supervisor
(Department of Chemistry)

Dr. Robin G. Hicks, Departmental Member
(Department of Chemistry)

Dr. Peter C. Wan, Departmental Member
(Department of Chemistry)

Dr. Jay T. Cullen, Outside Member
(Department of Earth and Ocean Sciences)

Abstract

Supervisory Committee

Dr. J. Scott McIndoe, Supervisor
(Department of Chemistry)

Dr. Robin G. Hicks, Departmental Member
(Department of Chemistry)

Dr. Peter C. Wan, Departmental Member
(Department of Chemistry)

Dr. Jay T. Cullen, Outside Member
(Department of Earth and Ocean Sciences)

Electrospray ionization mass spectrometry (ESI-MS) is a powerful tool for characterizing organometallic catalytic reactions. It does however, have some problems, and this thesis presents three of them along with solutions that have been developed for overcoming these challenges.

Gas phase reactivity has typically been done with highly specialized and sophisticated equipment. However, concurrent with instrument sophistication is cost, leading to decreased access to gas phase reactivity for practicing synthetic chemists seeking only to scan the fundamental reactivity of a given molecule or complex across a range of substrates. This thesis presents a cost effective solution to accessing gas phase chemistry by ESI-MS employing common equipment found in any synthetic laboratory and a case study with the anionic ruthenium cluster $[H_3Ru_4(CO)_{12}]^-$.

The second development of this thesis involved the synthesis and design of a range of charged alkynes which were used to study the Pauson-Khand reaction. Applying the techniques of gas-phase reactivity, some elusive intermediates were observed in the catalytic cycle.

Polar solvents such as water, acetonitrile, methanol, ethanol, and acetone are most common for ESI-MS, with non-polar solvents such as toluene and hexane being totally inert in the ESI process. Highly sensitive organometallic compounds generally

decompose rapidly in polar solvents, hindering the study of these systems by ESI-MS. A discovery presented in this thesis was that addition of lipophilic ionic liquids to hexane or toluene facilitated the required electrochemistry in the ionization process. This allows characterization of highly sensitive organometallic catalysts in solvents such as hexane and toluene that were previously unsuited to study by ESI-MS.

Methylaluminoxane (MAO) is an important cocatalyst in homogeneous Ziegler-Natta polymerization. Despite its importance however, very little structural information is known. This thesis presents the first known ESI-MS study of both MAO and hydrolyzed triisobutylaluminum (TiBA). The presence of several known structural features are apparent in detailed MS/MS experiments, confirming the validity of these results, and for the first time molecular masses of this oligomeric mixture are obtained. Furthermore, results from the hydrolysis of TiBA give insight into a structure that may potentially be an active cocatalyst in the activation process.

Table of Contents

List of Tables

List of Figures

List of Schemes

Abbreviations

a.m.u.	Atomic mass unit
APCI	Atmospheric pressure chemical ionization
BMIM	Butylmethylimidazolium
CE	Collision energy
CI	Chemical ionization
CID	Collision induced dissociation
CV	Cone voltage
EAN	Effective atomic number rule
EDESI-MS	Energy dependent electrospray ionization mass spectrometry
EI	Electron ionization (electron impact)
ESI-MS	Electrospray ionization mass spectrometry
FAB	Fast atom bombardment
FT-ICR	Fourier transform ion cyclotron resonance
GPI	Gas phase ion
GPR	Gas phase reactivity
HPLC	High performance liquid chromatography
IL	Ionic Liquid
LSIMS	Liquid secondary ionization mass spectrometry
m/z	Mass to charge ratio
MALDI	Matrix assisted laser desorption
MAO	Methylaluminoxane
MCP	Multi channel plate
MS	Mass spectrometry
NMR	Nuclear magnetic resonance
PhF	Fluorobenzene
Q-Tof	Quadrupole time of flight
Quad	Quadrupole
Tof	Time of flight

Acknowledgments

First and foremost I want to thank Scott McIndoe for everything he has taught me over the past five years. His patience and encouragement are welcome reprieves when the downs of graduate school are overwhelming. Scott also seems to have an unending stockpile of answers to questions about the totally not-obvious (at least to me), *most* of which he answers without even cracking a smile. I have sometimes wondered if he regrets his open-door policy.

I am lucky to have worked very closely with an incredible group of coworkers, who pleasantly though reluctantly, have put up with a variety of childish antics over the years. Nicky, Krista, Keri, and Jenny always seemed able to tolerate with a smile; no doubt wishing they had better friends to work with. Danielle though…Grape throwing contests across the office require two players, arguments have two sides, and coffee always tastes better when it's some else's money. I think "partner-in-crime" might better describe our working relationship.

Ori Granot is a new addition to the chemistry support staff at UVIC, but over the last year has helped enormously in dealing with the various issues of maintaining a sensitive instrument. Chris Greenwood is another valuable member of the department whose patience in teaching the complexities of NMR are much appreciated. I don't know how many times both Ori and Chris have re-answered the same question that I've had.

My family has been an incredible support group for me. Mom and Dad: always patient, encouraging, and helpful in every way parents love to be. Anouk, (Princess): the thought of you puts a smile on my face (that's usually all I need). And Kim: for the endless little things that you do to keep me on my toes; thank you and I love you.

Dedication

I would like to dedicate this thesis to three people.

To my daughter Anouk, because I love you. Your thousands of questions are an inspiration to me, and I often remind myself of them while working quietly alone in the evenings – they make me smile and my tasks easier. I look forward to your exciting future, and I am eager to be there and to help in any way that I can.

To my Mom and Dad: Merle and Bruce Henderson. I cannot thank you enough for the support that you've given me over my whole life. Be it in swimming, school, parenting, or other; you have helped me through everything in the biggest and smallest of ways. Of you both, I know that you place your children's educations and goals at the top of your priorities, and this is a lesson that I will never forget. I hope to pass this on to my family (present and future). You are both incredible role models to me. Thank you for everything.

Chapter 1 Electrospray Ionization Mass Spectrometry

1.1 Introduction

Mass spectrometry is a technique that has become a ubiquitous tool in chemical analysis. Its origins date back to 1886 when Eugene Goldstein discovered that rays passing through a cathode tube (later determined to be electrons) moving toward an anode were paired with opposing rays moving towards the cathode and composed of positive ions whose identity depended on the gas inside the tube.[1] This phenomenon was further studied by Wilhelm Wien who learned that these rays could be controlled with electric and magnetic fields.[2] Wien took this discovery a step further by actually separating the positively charged rays and measuring their mass to charge ratios, earning him credit for the discovery of the proton and creating the basis for characterizing particles based on such ratios. J. J. Thomson further improved on this design,[3] and demonstrated that electrons were particles with measurable mass, a discovery that later earned him a Nobel prize. Another of Thomson's important contributions came in 1913 when he discovered that neon gas was actually composed of a mixture of two isotopes (^{20}Ne and ^{22}Ne: Figure 1-1).[1] This result was hotly contested, but it was later confirmed by his understudy F.W. Aston who also reported that chlorine was a 3:1 mixture of the isotopes ^{35}Cl and ^{37}Cl (Figure 1-1).[4]

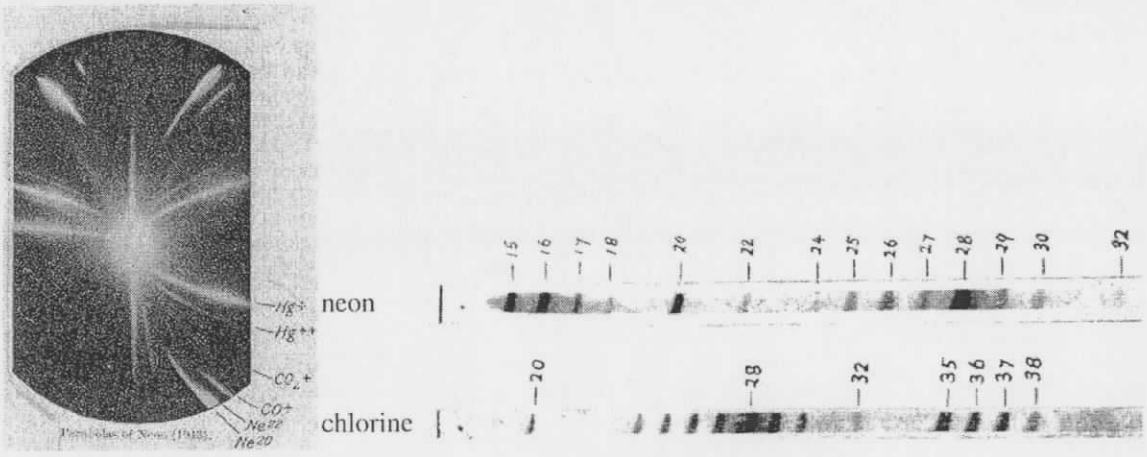

Figure 1-1: J. J. Thomson's first report of ^{20}Ne and ^{22}Ne (at left),[3] which was later confirmed by F.W. Aston in a report (at right) that also discovered chlorine was composed of the isotopes ^{35}Cl and ^{37}Cl.[5]

In 1918 Arthur Dempster designed the first instrument that resembles the modern mass spectrometer of today.[6] In what appears to be the only publication employing this instrument, Dempster reported the spectrum of Na^+ and K^+ (shown in Figure 1-2) by varying the potential difference through which a ray of ions was accelerated before being bent by a strong magnetic field and detecting them at an electrometer. With reference to Equation 1-1, ions of the same mass-to-charge ratio (*m/z*), bent by the same magnetic field (H_0), follow the same radius of curvature (r) depending on the applied potential difference (V).

$$\frac{m}{z} = \frac{H_0^2 r^2}{2V}$$

Equation 1-1

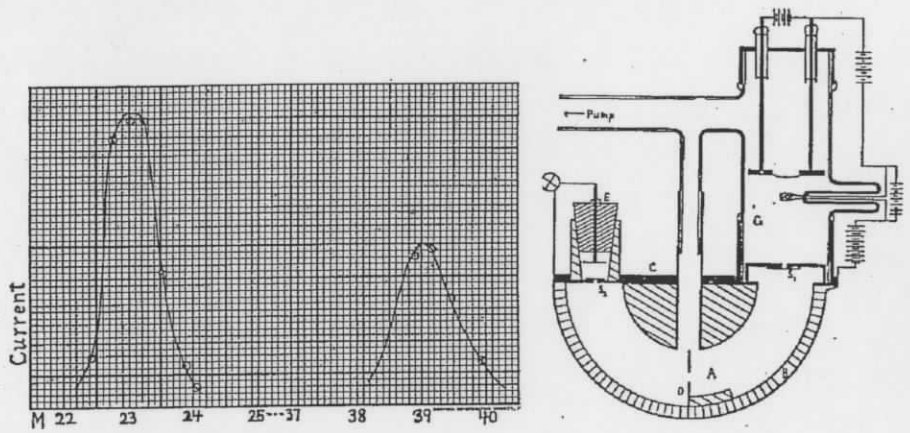

Figure 1-2: Dempster's spectrum of both Na^+ and K^+ (at left) obtained from his own instrument (at right), which is a close relative of modern mass spectrometers.[6]

Such is the essence of all mass spectrometers; a charged particle is characterized based on its mass (in amu) and its integer charge in a ratio (*m/z*), which is a dimensionless unit. In terms of interpreting the mass of an ion, this ratio refers to the atomic mass scale, which is defined with reference to the most abundant isotope of carbon: ^{12}C. Under this definition one mass unit is 1/12 the mass of ^{12}C and is given the term Dalton (Da).[7] Multiply charged species will therefore have a smaller *m/z* ratio than their singly charged analogues, even if their molecular weights are higher.

1.2 Ionization in mass spectrometry

The process of obtaining a gas phase ion is central to all types of mass spectrometry experiments, and in the decades since Dempster's experiments a number of methods have evolved. Transporting ions into the gas phase is not an easy task, and most methods towards this end require considerable amounts of energy. The manner in which a molecule or ion finds its way from the source (where it is ionized) to the detector (where its *m/z* ratio is determined) in a mass spectrometer has been an important feature distinguishing all types of mass spectrometry. The following is a short review of selected ionization methods that have been deemed relevant to the evolution of electrospray ionization.

1.2.1 Electron ionization (EI)

Electron ionization is the oldest and most widely used ionization method, and was first developed by Dempster in his initial experiments,[8] but has been repeatedly improved upon over the decades.[9,10] Essentially, a metal filament is heated to incandescence, a temperature that emits continuous free electrons. This emitted electron beam is accelerated with a voltage between 10 V and 100 V (70 V being standard). The vaporized sample is introduced into the path of this high energy electron beam in the source where an energetic electron interacts with an electron in the molecule forcing it out of its orbital. The process is very energy intensive in order to ensure efficient ionization accompanied by extensive fragmentation of the molecule. Resultant spectra generally consist of fragments of the parent ion, with only traces of the molecular ion.

1.2.2 Chemical Ionization (CI)

Chemical ionization (CI) was the first in a series of "soft" ionization techniques, with spectra consisting mainly of a single intact molecular ion, instead of being dominated by fragment ions as seen in EI mass spectrometry.[7] The technique was originally developed by Munson and Field in 1966 and is well reviewed.[11] The ionization source is essentially the same as the EI source[12] with the difference is that the energetic electron beam first ionizes a neutral gas molecule, commonly methane or other small alkane, but here is

demonstrated with NO. The neutral sheath gas is first ionized by loss of an electron ($NO + e^- \rightarrow NO^{\bullet+} + 2e^-$) which can react with further neutral gas molecules ($NO^{\bullet+} + R \rightarrow R^{\bullet+} + NO$). This is followed by a gas phase hydride abstraction with the analyte of interest ($NO^{\bullet+} + R'\text{-}H \rightarrow HNO + R'^{+}$).[13] Initially, this reaction occurred under a high vacuum (10^{-4} Pa), but a further development by Horning allowed for ionization at atmospheric pressure (APCI).[14] Munson and Field's CI technique was considerably less sensitive than EI at the time which significantly reduced its application to relatively polar molecules that provided low intensity molecular ions. Conversely, APCI has proven very sensitive with detection limits down to femtogram concentrations.[15]

1.2.3 Liquid secondary ionization and fast atom bombardment (LSIMS)

Fast atom bombardment[16] and liquid secondary ionization mass spectrometry (FAB-MS and LSIMS respectively) are quite similar. FAB functions by focusing a beam of fast moving high energy atoms (argon or xenon atoms) on a sample that is dissolved in a liquid matrix;[17] the only difference with LSIMS is that the beam consists of ions (Cs^+ usually) rather than atoms. The analyte is dissolved in the liquid matrix, and the matrix itself functions to absorb much of the energy of the beam whilst donating a proton to the analyte, so this is also considered a "soft" ionization technique. The liquid nature of the matrix also provides a constantly refreshed surface of matrix/analyte, which adds quality to the spectrum and gives a consistent ion current. The focused beam forces both matrix and dissolved analyte into the gas phase. The matrix is then pumped away, leaving the ions behind to be controlled by the various electric and magnetic fields to guide them to the detector. Overall, the process has been compared to analyzing the analyte dissolved in the splashed up water droplets after firing a cannonball into a lake.[18]

1.2.4 Matrix assisted laser desorption ionization (MALDI)

The technique of matrix assisted laser desorption ionization (MALDI) is another "soft" ionization method in mass spectrometry which has been well reviewed.[19] Laser desorption ionization (LDI) evolved in the early eighties from developments of FAB and LSIMS, but the introduction of a matrix (Co powder) was conceived by Tanaka[20] earning him part of the 2002 Nobel prize in chemistry.[21] In modern MALDI (as refined by Karas

and Hillenkamp), the analyte is dissolved and crystallized in a suitable *organic* matrix (ratio of ~ 1:5000[1]), chosen for its propensity to crystallize, the presence of a chromophore, and often for its protic nature. A high intensity laser beam (either UV or IR) is focused on the dried matrix, and most of the energy is imparted to the matrix which quickly vaporises. Both the matrix and analyte arrive in the gas phase, and ionization occurs by a proton transfer from the matrix to the analyte, much like in CI. The role of the matrix is to absorb most of the incoming radiation, but also to dilute the analyte and thereby reduce the extent of ion clusters that form. MALDI has found applications in characterizing very large molecules with masses up to >300 000 *m/z*[22,23] and down to attomolar detection limits,[1] making it the most sensitive technique for detecting biomolecules of its time.

1.2.5 Electrospray ionization (ESI)

Electrospray ionization (ESI) was the next improvement to soft ionization methods for mass spectrometry. The process was originally develloped in the late sixties[24] but was not applied to mass spectrometry until the eighties by Yamashita and Fenn.[25,26] Their experiments eventually led to a share of the 2002 Nobel Prize in chemistry along with Tanaka.[27] Compared to other ionization processes, electrospray is considered to be the softest,[28] an important feature considering many molecules have bonds that easily break under the highly energetic conditions common to electron impact mass spectrometry (EI-MS). Notably, it has been determined that weak molecular interactions such as hydrogen bonding are retained throughout ionization.[29] In effect the method of ionization imparts very little increase in internal energy (vibrational or rotational)[28] to the ion itself; the energy is instead focused on evaporating the solvent (a highly endothermic process). This feature has been used to characterize the non-denatured three-dimensional structure of proteins,[30] as much weaker non-covalent bonding interactions are preserved in the ionization process.[31]

1.3 ESI: The Ionization Process

During the ionization process pre-existing ions in solution are passed through a charged stainless steel capillary (Figure 1-3) with an applied potential of around 3 kV which acts to either oxidize or reduce the counterion of the analyte of interest, the solvent, or the capillary.[32] This electrochemistry functions to impart an excess of charge to the solution, and upon exiting the capillary, the sample is subjected to a stream of heated desolvation gas (usually N_2) to rapidly evaporate all solvent, leaving behind the ions, now in the gas phase. The charged capillary, the flow rate, and the desolvation gas all function to generate a fine mist of charged droplets. The actual mechanism by which the ion finds its way from these charged droplets (containing similarly charged ions and many solvent molecules), to being a lone ion in the gaseous state is presently the subject of considerable debate with the ion evaporation[33] mechanism and the charge residue model (whereby successive Coulombic explosions lead to gas phase ions) likely acting together.[34,35] Electrospray ionization can be used in a number of different types of instruments, but when coupled with mass spectrometry, ESI becomes a powerful tool for characterizing compounds quickly and efficiently.

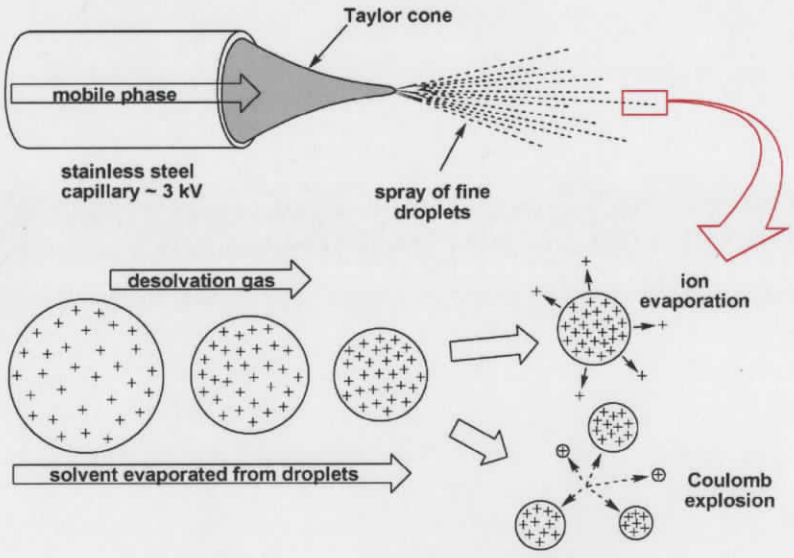

Figure 1-3: The process of electrospray ionization.

It was observed early on that ESI-MS was well suited to the characterization of proteins.[36] Being extremely large biomolecules with molar masses on the order of thousands of g/mol and containing multiple charges on amino acid residues (making them highly water soluble), proteins are perfectly suited to the method. The instrument itself is designed to desolvate all water from the peptide in just a fraction of a second with high temperatures and desolvation flow rates generating the gas phase ion for detection in the MS.[37] Such conditions are somewhat harsh, as water has an unusually high boiling point and surface tension to overcome; other solvents such as methanol, acetonitrile, acetone, ethanol, isopropanol, and dichloromethane have both lower surface tensions and boiling points making them more conducive to ESI-MS.[38] As such, generating ions from these solutions allows for milder conditions. Given that many charged organometallic and inorganic compounds are soluble in these solvents, it follows that their characterization by ESI-MS is facile.[39] The quality of data obtained is impressive, usually with just a single peak for the analyte of interest.

1.4 Q-Tof Micro

The specific instrument used in this laboratory was a Micromass Quadrupole Time of Flight (Q-Tof) Micro tandem mass spectrometer (Figure 1-4). Ionization occurs at the source under atmospheric conditions with a stream of nitrogen gas. Gas phase ions pass through the skimmer cones in a region of differential pumping (from atmospheric pressure down to approximately 10^{-2} torr)[28] and are initially focused with a hexapole ion guide. The high vacuum conditions in this region are provided by the first of two turbo pumps. Ions then enter a quadrupole, the first mass analyzer. The quadrupole can function either to simply focus the ions further (its most common function), or for MS/MS experiments it can allow ions of a specific *m/z* value to pass into the collision cell for *tandem-in-space* MS/MS analysis.[40] In a routine experiment, the focused ion beam passes into the collision cell, which contains argon gas at a pressure of about 10^{-3} torr. In an MS/MS experiment the collision voltage is increased and ion fragmentation occurs. From the collision cell, ions pass into the time of flight (Tof) tube[41] where the pusher

sends them on a trajectory orthogonal to their original path. The reflectron (a type of ion mirror) helps to focus the ion beam by redirecting the ions towards the detector,[18] which is a microchannel plate (MCP). The reflectron ensures that all ions of the same *m/z* ratio, regardless of initial kinetic energies, arrive at the detector at the same time,[42] i.e. resolution is maximized. The ion path in the Tof is about one meter, and since all ions are pulsed with the same voltage they are given the same kinetic energy. From the Newtonian formula for kinetic energy ($E_k = \frac{1}{2}mv^2$), ions of different mass will have different velocities. With path length and energy held constant, the masses of the ions are determined based on how long it takes them to travel the length of the flight tube and reach the MCP detector, hence the name "Time of Flight." The MCP is an array detector with thousands of electron multiplier tubes, and an ion arriving at any one of them will set off a cascade of electrons that is eventually converted to an electronic signal.

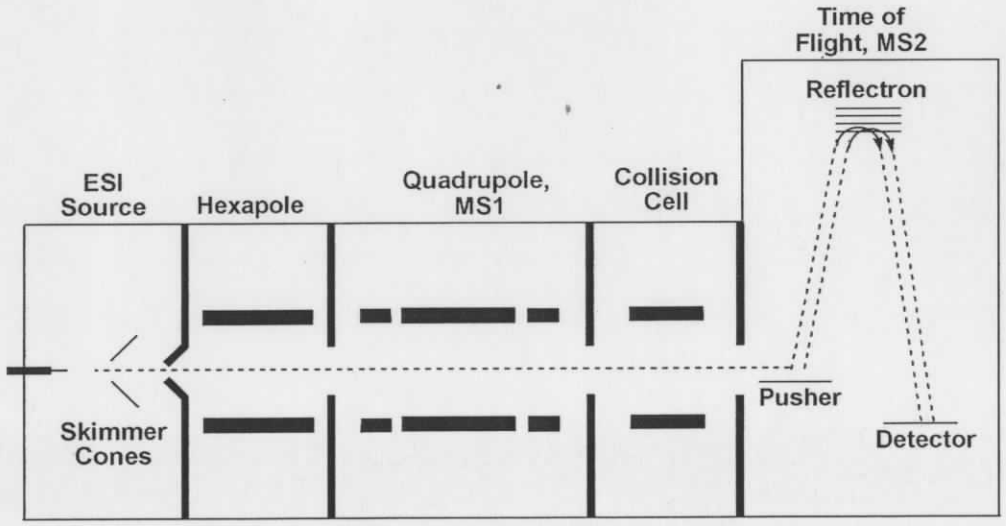

Figure 1-4: Block diagram of the Q-Tof mass spectrometer.

1.5 Energy Dependent ESI-MS

Collision induced dissociation (CID) occurs at either the electrospray ionization source or in the collision cell. The internal energy of an ion governs the fragmentation process,[43] and it is a very large increase of internal energy that explains the extensive fragmentation

associated with electron impact ionization. Because most of the energy involved in forming gas-phase ions in ESI-MS is aimed at the desolvation process, very little energy is imparted to the analyte of interest and very little fragmentation is then observed. A further benefit to ESI-MS however, is that the internal energy of the ion can be controlled by means of accelerating voltages, allowing the experimenter to control the extent of fragmentation.[44]

Energy dependent electrospray ionization mass spectrometry (EDESI-MS) is a fairly new tool in mass spectrometry.[45,46] It is a method of representing information gathered in CID experiments, which typically generate an enormous amount of data that is cumbersome to handle and interpret. Usually, data that appear uninformative are discarded and only those spectra that contribute to the story at hand are retained.

The process involves sequentially fragmenting the ions (as in CID) and the EDESI mass spectrum reports the *entire* fragmentation process in one spectrum. If fragmentation occurs at the source, all ions will be subjected to CID and the resulting spectrum will include fragments from each ion. If CID is performed on a mass selected ion (by MS1, Figure 1-4) in the collision cell, the fragmentation pattern will represent only those product ions from a single precursor ion. Although such fragmentation patterns are commonly reported in mass spectrometry, EDESI-MS aims to control the energies producing the fragments and to unselectively report *all* processes along a continuum of voltages.

At the source, cone voltages begin at 0 V and only very weak spectra are obtained with minimal fragmentation ($[PtBr_6]^{2-}$ in Figure 1-5). Increasing the voltage stepwise in a region of differential pumping increases the ions' mean free path along with its translational energy. When the ion collides with a relatively stationary neutral gas molecule (typically nitrogen) or atom (argon), this energy is distributed internally to the bonds of the ion. Those bonds that are weakest, and cannot tolerate this increase in energy break first, and a fragment is lost[47] (either $Br^{\bullet}$ or Br^{-} in Figure 1-5). The resulting spectrum consists mostly of product ions. EDESI-MS spectra are a summation of each spectrum taken at each cone voltage across the entire range of accessible voltages.[48] The resulting three dimensional surface (with ion intensity as the z-axis) can be represented

by a two dimensional contour plot with *m/z* and cone voltage forming the two axes of interest, and ion intensity represented by the contour lines (Figure 1-5).

The only difference when the same experiment is done with a mass selected ion in the collision cell is that the collision gas is argon instead of nitrogen, and the resulting spectrum is generally simpler (because only one precursor ion is involved). For larger molecules with multiple fragments this approach accurately depicts the complex processes that are occurring. Weaker molecular interactions can also be probed, and towards this end protonated water droplets, $[H(H_2O)_n]^+$ (n = up to 76) have been studied and EDESI-MS studies have shown gas phase water droplets to sequentially fragment.[49] Special stabilities for droplets containing multiples of n = 12 or 13, with importance given to n = 21 were also observed. A free and downloadable computer program (EDit)[50] to assist in the depiction of EDESI-MS spectra has also been developed.[a]

---

[a] EDit may be downloaded freely from the following website along with a step-by-step instruction guide: http://web.uvic.ca/~mcindoe/edit.html

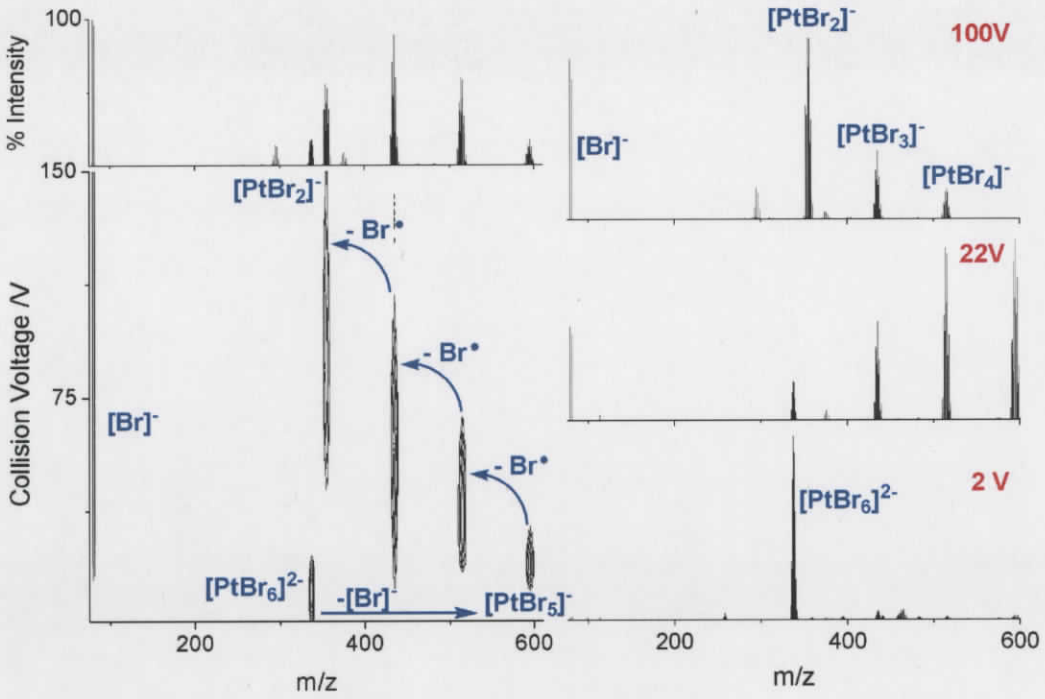

Figure 1-5: At left is the EDESI-MS spectrum of $[PtBr_6]^{2-}$ consisting of the entire voltage range for the whole CID experiment. At right are the spectra for three selected cone voltages, ignoring data from 147 other voltages.

1.6 ESI-MS and catalytic studies

The research in this thesis is aimed at elucidating metal-catalyzed transformations of organic molecules. In general, catalysts function to lower the energy barrier between the starting material and the desired product. This barrier is usually lowered by creating an alternate path with lower activation energies that may be overcome more readily at lower temperatures. The new path usually brings substrates together such that they are positioned close to one another in a manner that certain reactant bonds have been disrupted and also that product bonds may easily form.

In discussing catalytic reactions, most inorganic chemistry textbooks place the catalytic cycle at the center of the picture (as in Scheme 1-1), with non-purposeful side reactions such as solvations and dimerizations occurring tangentially to the cycle. This depiction often misrepresents the activity of the metal complex in solution because it suggests the cycle constitutes the bulk of reactivity, which may not be the case. Many reactions occur

at high temperatures or pressures just to enable sufficient catalytic turnovers (occurring as side reactions to the main reactivity of the complex). For such systems it is entirely reasonable to suggest the bulk of the catalyst's reactivity is not within the catalytic cycle but is instead dominated by several non-productive (but reversible) side reactions;[51] the productive catalytic reaction occurring tangentially to these reactions. This concept was expertly discussed in studies of asymmetric hydrogenation by chiral rhodium catalysts.[52] It was determined in these systems that the preferred binding mode of prochiral substrates led to a dead end, where the major diastereomer was too stable to react further. Rather, it was the much more active rates of a minor catalytic diastereomer, which did not build up in sufficient concentrations to be detected, that dominated the enantioselective reactivity for this asymmetric hydrogenation.[53] The minor diastereomers were found to be up to one thousand times more reactive than the stable, crystallographically characterized major diastereomer, which more than compensated for their undetectable concentrations by NMR and other spectroscopic techniques.

In other systems, it can happen that a catalyst is so effective that the reaction happens extremely rapidly under ambient conditions, thus confounding mechanistic studies by conventional means.[54] Non-productive side reactions are a minimal occurrence, but minute loadings are the norm, making typical spectroscopic studies poorly tailored to their study. Furthermore, short-lived intermediates throughout the cycle are so fleeting that they barely effect any observable changes should a spectrum actually be attainable.

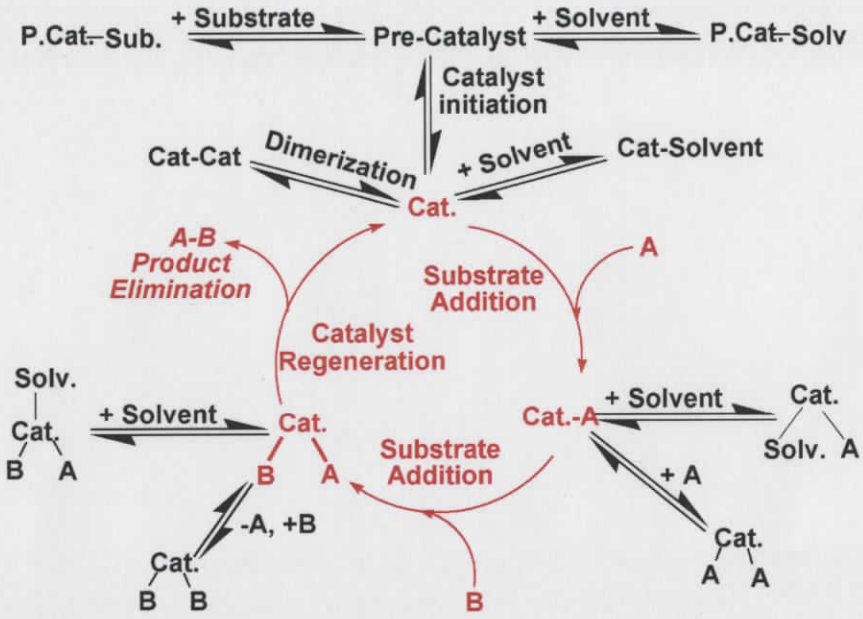

Scheme 1-1: This is a generic representation of several types of reactions that may occur in the solution of a metal catalyzed reaction. The productive cycle (in red) need not constitute the main reactivity of the metal complex. Dimerizations and solvations may be the more abundant reaction even though they are not useful.[52]

For these reasons, elucidating catalytic mechanisms is not an easy task, but a number of methods are employed to shed light on each system. Kinetic studies of reaction mixtures are common and important because catalysis is primarily a kinetic phenomenon.[51, 55] By varying concentrations of reagents, catalysts, reaction conditions, and by manipulating substituent electronics, a large body of information can be obtained about how all components come together to form the desired product. With the introduction of Reaction Progress Kinetic Analysis the complications generally associated with detailed kinetic studies are lessened,[56] although several careful experiments must still be performed to gain a full understanding of the kinetics of a reaction. Metal catalysts themselves often require elaborate syntheses just to obtain small quantities of potentially expensive precatalyst. At loadings greater than 1 or 2%, one batch of metal complex may not last long enough for complete mechanistic studies and cost becomes a limiting factor.

Nuclear magnetic resonance (NMR) experiments are prominent in such research.[57] Almost every atom in the periodic table has an NMR active isotope in sufficient abundance to give a reasonable signal; albeit quadrupolar nuclei give spectra that are

considerably more complex than dipolar nuclei. A given metal precatalyst will undoubtedly have at least one such atom that may be probed for studies, with ^{1}H, ^{31}P, and ^{13}C being the favorites. Such experiments can be done directly on a reaction mixture without interfering with the sample at all (no solution is lost). The quantitative nature of NMR allows signals to be compared to each other, and in conjunction with variable temperatures, kinetic studies can also be performed directly on the sample. NMR functions to characterize magnetic environments and anything that may disrupt this environment will reveal itself in some form or another: chemical shift, splitting patterns, coupling constants, or peak intensities.

There are however, a couple of problems with NMR studies. First of all, the instrumentation is not particularly sensitive.[58] In order to get a detectable peak, high concentrations of the desired analyte (catalyst in this case) are required. The best metal catalysts often operate effectively at loadings less than 1%, but in order to perform an NMR experiment much higher loadings are usually required. This puts the catalyst in a different chemical environment than it is in during ideal catalysis, and observed peaks may not be associated with the catalytic cycle. In-situ studies with pressurizable NMR tubes generally only facilitate 10-20 catalytic turnovers, which is not enough for an acceptable signal to noise ratio of suspected intermediates.[59] Furthermore, at pressures of about 10 bar, the solubility of most gases is so low that one catalytic turnover will consume all dissolved reactant and hours will be needed for more to dissolve.[59]

Detailed NMR studies of phosphine-containing metal complexes have been done previously.[60,61] Interestingly, one paper avoided firm peak assignments because chemical shifts for the tris-phosphinated metals were unknown, however subsequent investigations of this issue are difficult to find.[62] Other groups have also commented on the ambiguity of such studies.[63]

Another method of studying a catalytic cycle is to isolate and purify potential intermediates along the cycle. As such, isolable intermediates can be conclusively characterized by standard spectroscopic methods. Once this is done, stoichiometrically introducing them to a reaction mixture and observing their reactivity (in the form of peak shifts or splitting pattern changes) provides a way of monitoring the reaction from a well

known starting point. One must question though, whether a species which is thermodynamically stable enough to be isolated, purified, and stored can also be kinetically labile enough to participate in a catalytic cycle.[51]

Given the facility of ESI-MS characterization, and the rapidly expanding literature base concerning its application to inorganic chemistry, it seems a logical next step to begin exploring catalytic chemistry as well. There are a few notable points to make:

1. Catalytic reaction mixtures are generally quite complex with a large number of side reactions occurring at the same time as the main catalytic cycle (Scheme 1-1). These side reactions may confound various spectroscopic studies, but ESI-MS, on the other hand, transfers the entire solution to the gas phase. Any intermediates of all reactions will find themselves in a deeper local minimum, making them longer lived in the gas phase.[64] As such, a more complete snapshot of the reaction mixture may be obtained. From this point, each peak of a different molecular formula can be distinguished and subjected to MS/MS. The reactivity of those ions with coordinated substrate can be probed individually without signal interference from other complexes, and the true catalyst can be identified, even if in minute concentrations.

2. Structurally similar molecules may have similar magnetic environments, numerous bonds of similar type or strength, and HOMO-LUMO energy gaps that are very close. If these similar molecules are present at the same time in solution, their spectra will be a result of overlapping signals in NMR, IR, and UV-Vis experiments. Mass spectrometry characterizes compounds based on mass to charge ratios alone. As such, any chemical similarities will not affect an observed spectrum. The one condition however, is that these similar compounds cannot be isomeric.

3. As long as the desired analyte is charged, it appears as a single peak in the spectrum. Absent are any signals associated with solvent (in enormous excess over the analyte) or other neutral compounds.

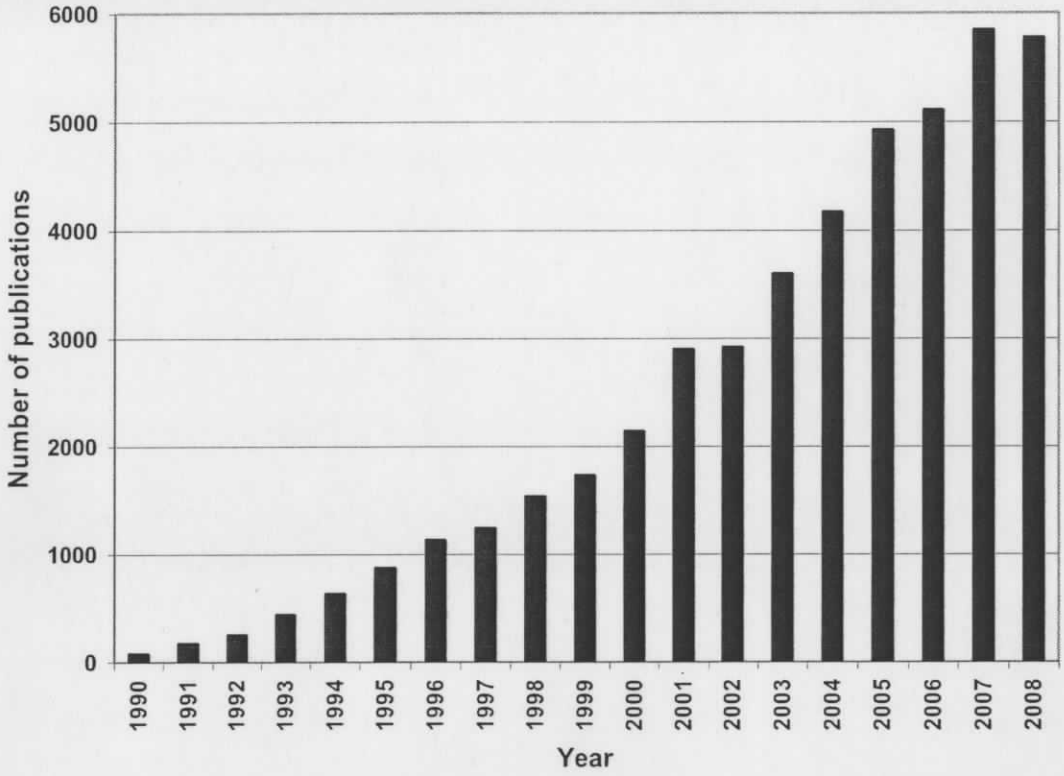

Figure 1-6: Histogram of publications involving electrospray mass spectrometry. Generated with a SciFinder scholar search of "electrospray mass spectrometry" on September 26, 2008.

Despite this reputation, it would be irresponsible to suggest perfection. In fact, with the aim of studying catalytic reactions there are a number of issues that need to be addressed in order to obtain meaningful results that stand up to reasonable scientific criticism.

1. Only ionic species are detected. This point is considered an advantage when the catalyst of interest is charged, but what about when the catalyst is neutral? There is a vast library of neutral catalysts,[65] or catalytic cycles that pass through neutral intermediates, all of which would be important to consider in order to properly understand the chemistry of the experiment. Imparting a charge to a neutral complex without disrupting the catalytic center would significantly expand the available chemistry to be studied by ESI-MS.

2. Once the ion is in the gas phase, it is detected almost immediately. Any reactivity for a given complex usually occurs before this, while still in solution. At times

though, it is difficult to know the order of reactivity for certain observed species. For example, in generating an ion which was transferred to the gas phase, was there an intermediate solvent complex that has since disappeared, or other subtle reactions that led to its formation? To understand the fundamental reactivity of a complex there must be a way to probe it once in the gas phase. This is accomplished by gas phase reactivity, but when coupled with ESI-MS such instruments are highly specialized and issues of complexity and cost make them unavailable to virtually every practicing wet chemist and most mass spectrometrists around the world. Overcoming the obstacles to gas phase reactivity would represent a considerable improvement and significantly expand the utility of ESI-MS to any chemist with access to such an instrument.

3. Non-polar solvents do not facilitate the required electrochemistry needed to generate gas phase ions by ESI-MS. Polar solvents must be used because they are able to solvate and stabilize electrolytes which allow them to be conductive in the presence of an electric field. The problem with polar solvents is that they are commonly coordinating as well, which deactivates certain highly reactive catalysts. To prevent this deactivation, the reaction is performed in non-polar solvents (such as toluene), making them unsuitable for study by ESI-MS. Often times, the most active catalysts function in these non-polar solvents, so ESI-MS has had little contribution to understanding their chemistry.

This thesis is aimed at expanding the knowledge base of organometallic catalysis by studying known reactions. More pointedly, it aims to expand the utility of electrospray ionization mass spectrometry by addressing the above points in hopes that new tools and methods may be developed to enhance studies of catalysis. Each chapter presents a problem associated with studying catalytic systems by ESI-MS as well as the solutions developed over the course of this project to overcome the given obstacle. As often as possible a case study on a particular catalyst, cycle, or metal complex has been provided to lend support to the new technique. The chapters have been arranged in increasing order according to the perceived impact of the technique in the community of those studying similar systems.

1.8 References

[1] Becker, J.S., Inorganic Mass Spectrometry: Principles and Applications, John Wiley & Sons Ltd.: Hoboken, **2007**.

[2] Robertson, A.J.B., Mass Spectrometry, John Wiley & Sons Inc., New York, **1954**.

[3] Thomson, J.J., Proceedings of the Royal Society. **1913**, *A89*, 1-20.

[4] Aston, F.W., *Phil. Mag.,* **1920**, *39*, 449.

[5] Squires, G., *Dalton Trans.* **1998**, 3893-3899.

[6] Dempster, A.J., *Physical Reviews,* **1918**, *11*, 316-325.

[7] Watson, J.T.; Sparkman, O.D., *Introduction to Mass Spectrometry: Instrumentation, Applications, and Strategies for Data Interpretation,* John Wiley & Sons, Ltd.: Hoboken, **2007**.

[8] Dempster, A.J., *Phil. Mag.,* **1916**, *31*, 438.

[9] Bleakney, W., *Phys. Rev.,* **1929**, *34*, 157-160.

[10] Tate, J.T.; Smith, D.H., *Phys. Rev.,* **1934**, *46*, 773-776.

[11] Harrison, A.G., *Chemical ionization mass spectrometry.* CRC Press, Boca Raton, 2nd Ed.1992.

[12] Munson, M.S.B.; Field, F.H., *J. Am. Chem. Soc.,* **1966**, *88*, 2621.

[13] Subba Rao, S.C.; Fenselau, C., *Anal. Chem.,* **1978**, *50 (3)*, 511-515.

[14] Horning, E.C.; Horning, M.G.; Carroll, D.I.; Dzidic, I.; Stillwell, R.N., *Anal. Chem.,* **1973**, *45 (6)*, 936-943.

[15] Carroll, D.I.; Stillwell, R.N.; Horning, M.G.; Horning, E.C., *Anal. Chem.,* **1974**, *46 (6)*, 706-710.

[16] Barber, M.; Bordoli, R.S.; Sedgwick, R.D.; Tyler, A.N., *J. Chem. Soc., Chem. Commun.,* **1981**, 325-327.

[17] Barber, M.; Bordoli, R.S.; Elliot, G.J.; Sedgwick, R.D.; Tyler, A.N., *Anal. Chem.,* **1982**, *54*, 645-657.

[18] Henderson, W.; McIndoe, J.S., *Mass spectrometry of inorganic and organometallic compounds.* John Wiley and Sons, Ltd.: Hoboken, **2005**.

[19] A) Dreiseward, K., *Chem. Rev.,* **2003**, *103,* 395-426. B) Karas, M.; Krüger, R., *Chem. Rev.,* **2003**, *103*, 427-440. C) Knochenmuss, R.; Zenobi, R., *Chem. Rev.,* **2003**, *103,* 441-452.

[20] Tanaka, K.; Waki, H.; Ido, H.; Akita, S.; Yoshida, T., *Rapid Commun. Mass Spectrom.,* **1988**, *2*, 151-153.

[21] Tanaka, K., *Angew. Chem. Int. Ed. Engl.,* **2003**, *42*, 3861-3870.

[22] Karas, M.; Bahr, U.; Ingendoh, A.; Hillenkamp, F., *Angew. Chem. Int Ed. Engl.,* **1989**, *28*, 760-761.

[23] Bahr, U.; Karas, M.; Hillenkamp, F., *Fresenius J. Anal. Chem.,* **1994**, *348*, 783-791.

[24] Dole, M.; Mack, L.L.; Hines, R.L.; Mobley, R.C.; Ferguson, L.D.; Alice, M.B., *J. Chem. Phys.,* **1968**, *49*, 2240-2249.

[25] Yamashita, M.; Fenn, J.B., *J. Phys. Chem.,* **1984**, *88*, 4451-4459.

[26] Fenn. J.B.; Mann, M.; Meng, C.K., *Science,* **1989**, *246*, 64-71.

[27] Fenn, J.B., *Angew. Chem. Int. Ed. Engl.,* **2003**, *42*, 3871-3894.

[28] Cole, R.B., *J. Mass Spectrom.,* **2000**, *35*, 763-772.

[29] McQuinn, K.; Hof, F.; McIndoe, J.S., *Chem. Eur. J.,* **2008**, *14*, 6483-6489.

[30] Suckau, D.; Shi, Y.; Beu, S.C.; Senko, M.W.; Quinn, J.P.; Wampler, F.W.; McLafferty, F.W., *Proc. Natl. Acad. Sci. USA.,* **1993**, *90*, 790-793.

[31] Loo, J.A., *J. Mass Spectrom.,* **1997**, *16*, 1-23

[32] Blades, A.T.; Ikonomou, M.G.; Kebarle, P., *Anal. Chem.,* **1991**, *63*, 2109-2114.

[33] McQuinn, K.; Hof, F.; Mcindoe, J.S., *Chem. Commun.,* **2007**, 4099-4101.

[34] Kebarle, P., *J. Mass Spectrom.,* **2000**, *35*, 804-817.

[35] Gamero-Castano, M.; de la Mora, J.F., *Anal. Chim. Acta,* **2000**, *406*, 67-91.

[36] Winger, B.E.; Hofstadler, S.A.; Bruce, J.E.; Udseth, H.R.; Smith, R.D., *J. Am. Soc. Mass Spectrom.,* **1993**, *4,* 566-577.

[37] Zaia, J.; Annan, R.S.; Biemann, K., *Rapid Commun. Mass Spectrom.,* **1992**, *6*, 32-36.

[38] Tang, L.; Kebarle, P., *Anal. Chem.,* **1991**, *63*, 2709-2715.

[39] Chen, P., *Angew. Chem. Int. Ed. Engl.,* **2003**, *42*, 2832-2847.

[40] Miller, P.E.; Denton, M.B., *J. Chem. Educ.,* **1986**, *63*, 617-622.

[41] Price, D.; Williams, J.D., *Time-of-Flight Mass Spectrometry*, Pergamon Press: Toronto, **1969**.

[42] Mamyrin, B.A., *Int. J. Mass Spectrom.*, **1994**, *131*, 1-19.

[43] Collette, C.; De Pauw, E., *Rapid Commun. Mass Spectrom.*, **1998**, *12*, 165-170.

[44] Collette, C.; Drahos, L.; De Pauw, E.; Vekey, K., *Rapid Commun. Mass Spectrom.*, **1998**, *12*, 1673-1678.

[45] Dyson, P.J.; Johnson, B.F.G.; McIndoe, J.S.; Langridge-Smith, P.R.R., *Rapid Commun. Mass Spectrom.*, **2000**, *14*, 311-313.

[46] Butcher, C.P.G.; Dinca, A.; Dyson, P.J.; Johnson, B.F.G.; Langridge-Smith, P.R.R.; McIndoe, J.S., *Angew. Chem. Int. Ed. Engl.*, **2003**, *42*, 5752-5755.

[47] Levsen, K.; Schwarz, H., *Mass Spectrom. Rev.*, **1983**, *2*, 77-148.

[48] McIndoe, J.S., The Encyclopedia of Mass Spectrometry, Elsevier, **2007**, *Vol. 6*, 467-474.

[49] McQuinn, K.; Hof, F.; McIndoe, J.S., *Int. J. Mass Spectrom.*, **2009**, *279*, 32-36.

[50] Husheer, S.L.G.; Forest, O.; Henderson, M.A.; McIndoe, J.S., *Rapid Commun. Mass Spectrom.*, **2005**, *19*, 1352-1354.

[51] Halpern, J., *Inorg. Chim. Acta,* **1981**, *50*, 11-19.

[52] Halpern, J.; *SCIENCE*, **1982**, *217 (4558)*, 401-407.

[53] Chan, A.S.C.; Pluth, J.J.; Halpern, J., *J. Am. Chem. Soc.*, **1980**, *102*, 5952-5954.

[54] Halpern, J.; Wong, C.S., *J. Chem. Soc. Chem. Commun.*, **1973**, 629-630.

[55] Tolman, C.A.; Meaking, P.Z.; Lindner, D.L.; Jesson, J.P., *J. Am. Chem. Soc.*, **1974**, *96 (9)*, 2762-2774.

[56] Blackmond, D.G., *Angew. Chem. Int. Ed. Engl.*, **2005**, *44*, 4302-4320.

[57] Friebolin, H., *Basic One- and Two-Dimensional NMR Spectroscopy,* 3rd Ed., Toronto, Wiley-VCH, **1998**.

[58] Roe, D.C.; Kating, P.M.; Krusic, P.J.; Smart, B.E., *Top. Catal.*, **1998**, *5*, 133-147.

[59] Van Leeuwen, P.W.N.M., *Homogeneous Catalysis: Understanding the Art,* Kluwer Academic Publishers: Boston , **2004**.

[60] Mann, B.E.; Musco, A., *J. Chem. Soc., Dalton Trans.*, **1975**, 1673-1677.

[61] Tolman, C.A.; Seidel, W.C.; Gerlach, D.H., *J. Am. Chem. Soc.*, **1972**, *94(8)*, 2669-2676.

[62] Kuran, W.; Musco, A., *Inorg. Chim. Acta.*, **1975**, *12*, 187-193.

[63] Ahlquist, M.; Fristrup, P.; Tanner, D.; Norrby, P.O., *Organometallics,* **2006**, *25*, 2066-2073.

[64] Richardson, D.E.; Plattner, D.A., *Comprehensive Organometallic Chemistry*, Elsevier, **2007**, *1*, 801-822.

[65] *Applied homogeneous catalysis with organometallic compounds: A comprehensive handbook in three volumes;* Cornils, B.; Herrmann, W.A., Eds.; Wiley-VCH: Weinheim, 2002.

Chapter 2 Accessible gas phase chemistry by ESI-MS

2.1 Introduction

The past few decades have seen an impressive evolution of gas phase chemistry. Although the method has yet to become a firsthand tool to practicing chemists, the argument for its relevance has been made in a number of detailed reviews.[1] Most scientists prefer to think of the gas phase in terms of a simplified environment which may be used to determine factors not easily found in solution phase experiments. Information relating to potential energy surfaces,[2] reaction rate constants,[3] and solvation dynamics[4] are only a few of the many chemical questions that may be addressed by theory. Theoretical studies do not have to be the extent of the utility of the gas phase though. Experiments performed on gas phase systems, and in conjunction with mass spectrometry, can be useful in elucidating complex molecular dynamics that would be difficult to interpret by more conventional spectroscopic methods.[5,6]

There are some obvious points of difference between the gas phase and condensed phase systems, but with a proper understanding of how molecules behave in the gas phase it is possible to extract useful chemical information easily and concisely.

1. In the absence of solvent and their respective "cages," electrostatic forces maintain the complex. Interactions such as charge-dipole, but also charge-induced dipole, and dipole-dipole, keep an ion-molecule complex together in the gas phase.[7,8] These interactions allow sufficient time for the ion-molecule complex to redistribute itself and find a potential minimum.[9]
2. Ion-molecule reactions in the gas phase occur via long-lived complexes, which may undergo up to 10^8 molecular vibrations[10] in 10-100μs,[11] which is far faster than the rate of molecular collisions under conditions of high vacuum. This means the orientation of the ion-molecule complex immediately after collision is not especially important because it has more than enough time to find an orientation favourable to reaction before the next collision breaks the complex apart.

3. Organometallic reactions are essentially non-polar. There is very little change in the energy of solvation because there is very little change in the polarity of a complex along a given mechanistic profile. Chen has suggested that this explains why there are many similarities between gas phase and solution phase transformations for organometallic reactions.[1e]

Notwithstanding such claims, speculation as to the connection between gas phase and solution phase chemistry is still prominent. A recent exchange between the groups of Chen[12] and Bercaw[13] on the nature of CH activation by a new platinum catalyst effectively illustrates the hesitation to accepting these gas phase conclusions.[14]

The comparison of gas phase results to the condensed phase is normally made on a case-by-case basis.[15] In solution, solvent effects have the potential to completely change a reaction. The same reaction in different solvents may change ligand binding preferences or alter the geometry of the final product. Furthermore, the number of collisions per second a molecule undergoes in solution (around 10^9 /s) is orders of magnitude higher than in the gas phase.[16] The result in the gas phase is that some product ions of exothermic reactions will not be able to dissipate their excess energy, allowing them to participate in reactions not accessible in solution.[16] With these points in mind gas phase chemistry may perhaps better be used as a screening tool for discovering new reactions *before* they have been tried in the condensed phase. Once a substrate has shown to be reactive, it can be tested in solution with solvents that would be expected to favour such a reaction. This screening process would considerably reduce the amount of benchtop chemistry and dramatically improve synthetic efficiency.

The question as to why gas phase studies are useful is a good one considering that most tangible chemistry almost always occurs on condensed phase systems. Intuitively, any synthetic chemist has an intimate understanding that the same reaction may have an entirely different outcome in different solvents, so it would likely also have a different outcome in the absence of solvent altogether. Gas phase chemistry does however, have a place in mechanistic elucidation studies, and it comes with notable advantages.

1. The gas phase benefits from far fewer variables. The absence of acidic or basic sites, counterion effects, aggregation, and surface inhomogeneities that would clutter the solution phase experiment and otherwise occlude the relevant chemistry at hand is absent in the gas phase.[1b]
2. Reactive intermediates find themselves in deeper local minima,[1d] making them longer lived. This allows detection of short lived intermediates that would otherwise disappear almost as soon as they appear in solution phase experiments. The reactivity of these intermediates is not dependent on any solvent effects.[17]
3. When studied via mass spectrometry, experiments can be very fast and require only a few milligrams of material, a particular advantage for studying hard to synthesize and/or expensive compounds.[1e]
4. With carefully designed experiments and the appropriate instrument, quantitative thermodynamic data on metal-substrate binding can be established.[17]

2.2 Differences in reactivity between solution and the gas phase

A simple example of differences between solution and gas phase reactivity is the reaction of silver nitrate with benzenethiol (Figure 2-1). In solution $AgSC_6H_{5(s)}$ precipitates from acetonitrile, but the reaction of Ag^+ with benzenethiol in the gas phase produces the ion $[Ag(HSC_6H_5)]^+$ without deprotonation.[18] In this reaction, acetonitrile functions to deprotonate an intermediate; since it is absent in the gas phase no deprotonation occurs and the outcome is different (essentially, the intermediate is trapped)

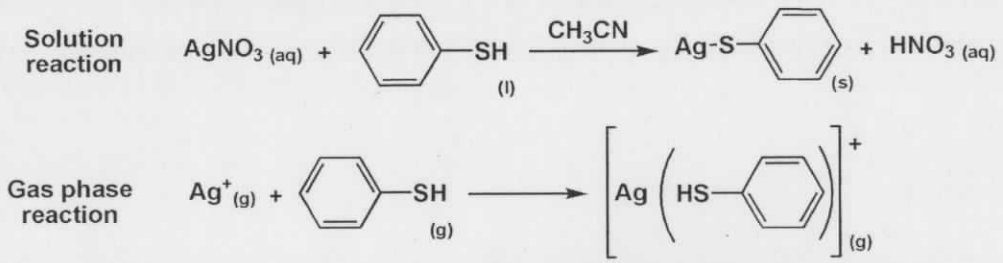

Figure 2-1: The reaction of the silver ion with benzene thiol is different in solution as compared to the gas phase.

As mentioned above, far fewer collisions occur in the gas phase making it less likely for species to dissipate energy gained in their exothermic formation reactions. An Ir(I) ethene complex has been observed to quantitatively convert to a Ir(III) peroxo-ethene complex in the gas phase reaction with molecular oxygen (Figure 2-2).[16] This reaction only goes to ~25% completion in solution, and the proposed explanation is that an unknown electron transfer process, which would occur during a charge separation step and degrade the peroxo-ethene complex, is inhibited in the gas phase but contributes significantly to the low yield in solution.

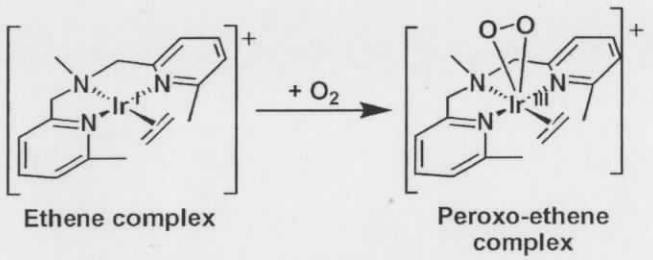

Figure 2-2: Plattner's coordination of O_2 to an iridium complex.

These two cases exemplify how the gas phase is less cluttered than in solution. That the first case does not deprotonate the thiol is simply because there is no base present to do the job, and that Plattner's peroxo-ethene complex does not decompose, but appears to react quantitatively was attributed to the absence of an unknown reductant in the gas phase. Fundamentally though, the chemistry of the two states is very similar without confounding details present in the gas phase.

2.3 Gas phase cluster chemistry

The comparison to the condensed phase has also been made for heterogeneous systems.[19] The chemistry of highly reactive metallic nanoparticles is difficult to study directly, so any method revealing mechanistic information would be useful in understanding these systems. The literature pertaining to oxo-metallate studies by ESI-MS is quickly expanding,[20] revealing structural information about the formation of these very large

solution species[21] and in modelling solid state metallic reactivity.[22] Studies of metal clusters have also revealed that it is possible to generate naked metal clusters in the gas phase by collision induced dissociation (CID).[23] In this way, a metal core of only a few atoms can be probed for reactivity after loss of all ligands and used as a well defined model with a known geometry for representing what occurs at the surface of a heterogeneous metallic surface.[24] Such comparisons have been done with very close correlation of niobium oxide and molybdenum oxide clusters to their native reactions.[25,26] Gold nanoparticles with up to 25 gold atoms and 18 ligands, with an $m/z > 7400$ have been studied in both ion modes, exemplifying the scope of ESI-MS for these cluster studies.[27]

Ridge has previously reported on the gas phase reactivity of partially ligated, odd-electron cobalt-carbonyl clusters.[28] $[Co_2]^+$ (generated by electron ionization) was shown to break the alkyl bromide bond of $(CH_3)_2CHBr$, whereas $[Co_2(CO)]^+$ led to C-H activation with loss of HBr. A further study with an FTICR mass spectrometer demonstrated that certain cationic carbonyl clusters reacted with cyclohexane and 1-hexene, but that anionic clusters failed to react at all.[29]

This chapter presents a case study of the gas phase reactivity of a tetrahedral ruthenium carbonyl cluster. In order to access the gas phase chemistry, some simple modifications to an electrospray ionization Micromass Q-Tof *micro* mass spectrometer were implemented.

2.4 Data Interpretation

Electrospray ionization mass spectrometry (ESI-MS) as a tool is well suited to studying ions in the gas phase. Current interest has focused on those systems where catalytic reactions are modelled in an attempt to identify the active catalyst within a cycle. The soft ionization of ESI and high sensitivity of MS can function on a complex reaction mixture where the catalyst is at its normal concentration, instead of requiring the catalyst to be in enormous concentration to facilitate an acceptable signal to noise ratio. Furthermore, the problem of peak overlap is avoided; each species can unambiguously be distinguished based simply on differences in m/z ratios.

An important aspect of gas phase chemistry, one that is often not clearly quoted or understood, is the ion energy at which a reaction takes place. In solution the energy of reactants can be quite closely estimated by the temperature of the reaction. If a mixture is heated to the boiling point of the solvent, the kinetic energy of all molecules is very close.

Ions in the gas phase however, have energies that depend not only on the boiling point of the solvent from whence they came, but also on various voltage parameters throughout the instrument that direct and guide the ions. Many of these voltages are insignificant and do not affect the average kinetic energy of an ion significantly, but for an electrospray ionization mass spectrometer both cone voltage (at the source) and collision voltage (in the collision cell) have the potential to affect the chemistry of an ion quite drastically through CID.

CID involves two possible processes. The first is simply unimolecular fragmentation of the molecular ion to generate a product ion; this occurs when the translational energy of the ion is converted to internal vibrational energy following collisions with a (usually inert) gas molecule or atom. The second is a reaction, where a neutral, reactive molecule has added to the ion either by simple coordination or by oxidative addition.[9] Mechanistic studies of the Pauson-Khand reaction have been done in this way, with norbornene as a reactive gas.[30] The general principle can be seen in Scheme 2-1 where ion A is mass selected for CID with a non-reactive gas (argon), or with a reactive gas in the collision cell.

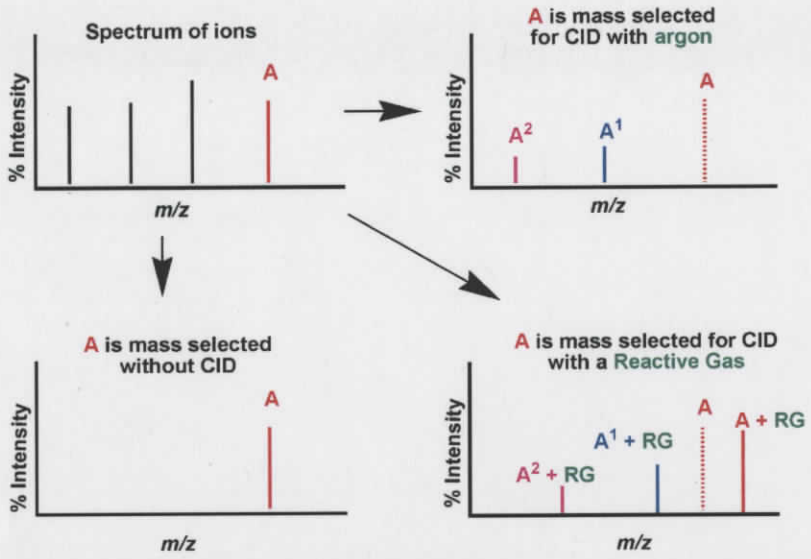

Scheme 2-1: A representation of gas phase reactivity of ion A, for reaction via CID in the collision cell with a reactive gas. A^1 and A^2 are product ions from the fragmentation of A.

It is possible to induce reactivity between an ion and a neutral molecule by incrementing the internal energy of the ion, but to simply view a 2-dimensional spectrum of this process does not accurately represent the conditions of the experiment. EDESI-MS spectra however, show the reactivity across the entire energy range of a given experiment.[31] From this, it is possible to observe how the coordination sphere of an ion changes at higher energies, as well as to understand the reactivity of the ion at those energies. Metal clusters are examples that show just such changes, and the left-hand spectrum of Figure 2-3 shows the sequential loss of twelve CO molecules across the entire energy range. In such a way, the reactivity or fragmentation of these clusters can be observed at low energies where reactions are more akin to solution reactivity, and also at high energies where reactivity may be better compared to a heterogeneous system.

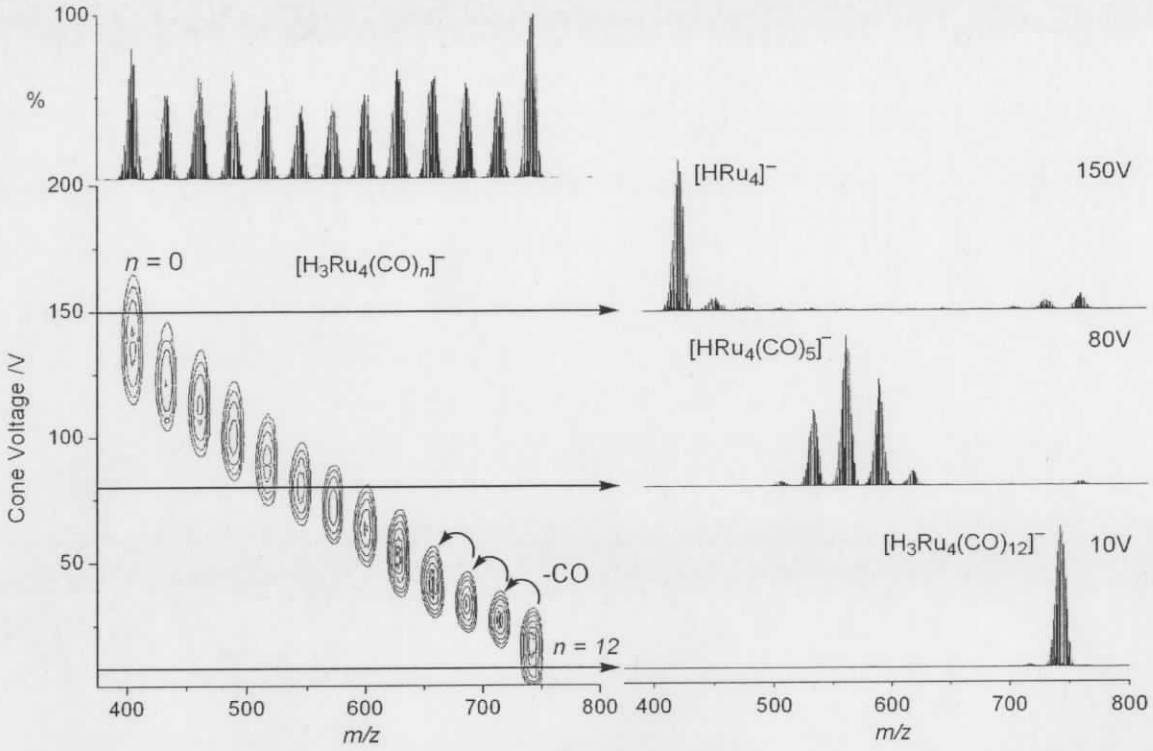

Figure 2-3 The left spectrum is an EDESI-MS of $[H_3Ru_4(CO)_{12}]^-$ clearly showing the loss of 12 CO groups at progressively higher cone voltages. The stacked plot at right shows that at three different voltages, a regular 2-dimensional mass spectrum can be drastically different.

2.5 Instrumental Design

Ion-molecule reactions have been extensively probed by mass spectrometry, but experimental designs are not trivial. Chen has modified his instrument by adding a 24-pole reaction chamber to facilitate such experiments. Gerlich has added a 22-pole reaction chamber to his instrument,[32] O'Hair has used a modified ion-trap,[33] and Schwarz has used a triple quadrupole mass spectrometer,[34] all with the aim of probing organometallic and catalytic chemistry. These modifications can be quite extensive and present a considerable challenge for any synthetic chemist seeking to study their system (or catalyst) in a similar way. Also, their complexity creates a mental barrier to acceptance; scientists are less likely to accept a result (especially if it opposes their own) when they have difficulty understanding the fundamentals of an experiment or instrument. The modifications introduced here sought to overcome the accessibility and

complexity issues as well as to provide some support for correlating gas phase to solution phase chemistry.

The electrospray ionization source was initially designed to desolvate large biomolecules from water in fractions of a second; this is no simple task and a combination of high source temperature, high flow rate of desolvation gas, and differential pumping are required. Desolvating organometallic species from more volatile solvents such as methanol, acetonitrile, or dichloromethane is considerably easier, and as such, most commercial instruments are greatly over-specified for these purposes.

Most chambers of a typical electrospray ionization mass spectrometer (those not under high vacuum) are bathed in varying pressures of an inert gas, and the source in particular has two N_2 inlets for desolvating the ions. One of them, the "cone gas," can be easily hijacked without any detriment to desolvation or detection sensitivity (Figure 2-4). This gas line can be switched from N_2 to any reactive gas (O_2, C_2H_4, H_2, CO_2, CH_4, etc...), or it can be spliced and N_2 can be passed through a vial containing a volatile liquid, thus introducing some of the liquid as a vapour to the electrospray source.

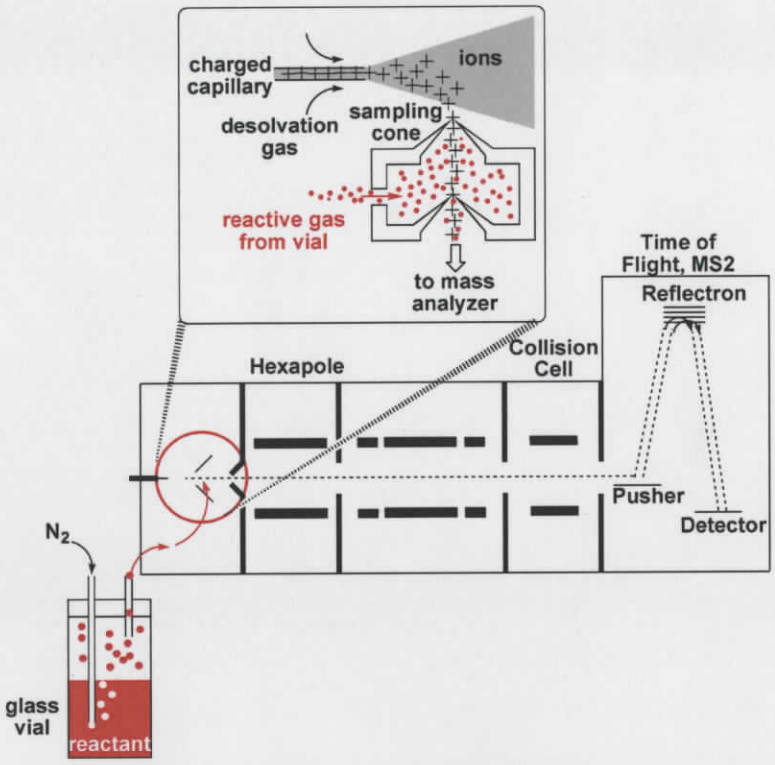

Figure 2-4: Instrumental setup showing specifically where the gas phase reactivity occurs in the instrument.

After a series of modifications and improvements to the first design, the final materials were: a new source housing with an access arm, three flow meters, a vial, a septum, two stainless steel needles, about two meters of both plastic and copper tubing, a tubing union, and an additional tank of dry nitrogen (Figure 2-5). A hole was cut in the source housing to facilitate the new gas line, but this had no effect on the electrospray ionization process, and other users have not reported any interference. At the skimmer cones in the source, the tube can easily be removed from the cone gas inlet and replaced with the new tube (and just as easily reversed) which will carry the reactive gas. With the volatile liquid in the vial, the N_2 flow rate can be controlled with the gas tank regulator and the flow meters, with vapours introduced at the electrospray ionization source housing. It is at this point and beyond that the gas phase reaction occurs; precursor and product ions are accelerated through the skimmer cones and on through the instrument for detection.

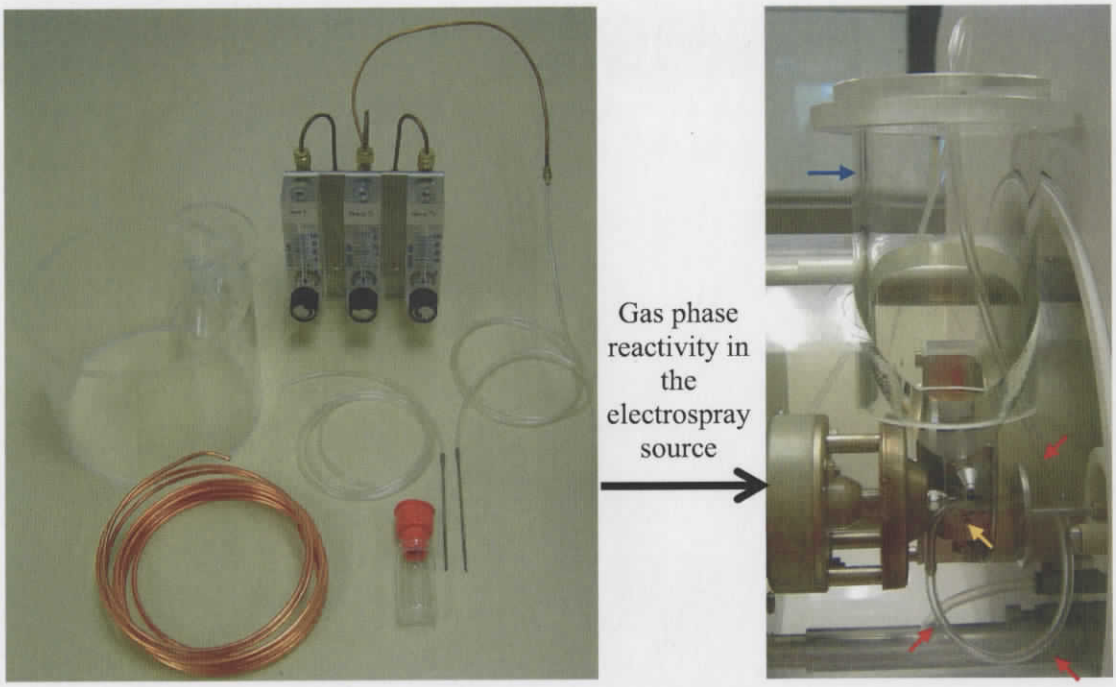

Figure 2-5: Photograph of materials used (left) to facilitate gas phase reactivity at the cone in an ESI-MS. Red arrow shows the line carrying the reactive gas. Blue arrow shows the access arm on the new source housing. Yellow arrow shows both the capillary and the skimmer cones where the gas phase reaction occurs.

This design can be set up with minimal cost, and is transformative in converting a commercial mass spectrometer from an analytical tool to a small scale laboratory, able to detect product ions immediately after they form. Typical experiments generally take between a few seconds to a few minutes.

From the literature, it seems that both Posey[35] and Vekey[36] have separately reported similar designs. Both Kebarle[37] and Fenn[38] reported reactivity of low valent metal ions with gases water under similar, but more controlled systems. Posey's system introduced solvents such as DMF and DMSO (typically unsuitable for ESI-MS)[39] for reaction with naked transition metal ions in a stream of solvent laden dry nitrogen gas, whereas Vekey used a saturated curtain gas to detect ions accompanied by up to 100 solvent molecules. Exact experimental details were not revealed, but the systems seem closely related to the design described herein, albeit used for different purposes.

2.6 Results and Discussion

The rapidity of these experiments is such that many volatile substrates can be probed for reactivity in minutes. Structural elucidation by ESI-MS is made simple by analysis of the EDESI-MS spectra for both MS and MS/MS experiments. With three different flow meters, gases can be either switched from one to another at the turn of a dial, or mixed together to observe more complex gas phase transformations. Such studies may also facilitate competition reactions, but these are not the focus of the present study. This project is an introduction to both the easy access to gas phase reactivity and to the advantages of representing the information in the EDESI-MS format.

The anionic cluster $[H_3Ru_4(CO)_{12}]^-$, synthesized as the $[Ph_3PNPPh_3]^+$ salt,[40] was chosen as a model system for a number of reasons. First of all, the precursor cluster $H_4Ru_4(CO)_{12}$ is easily synthesized in high yield,[41,42] and deprotonation to form the anionic trihydride is facile.[43] The cluster contains both hydride and carbonyl ligands and may undergo reactivity involving either of them, but importantly the tetraruthenium core itself has previously shown catalytic activity in a large number of reactions including: the water-gas shift reaction,[44] hydrogenation of both olefins[45] and arenes,[46] reduction of molecular oxygen to water,[46] and hydroformylation reactions.[47]

2.6.1 Alkenes

This study focused on the reactivity of $[H_3Ru_4(CO)_{12}]^-$ with a range of functional groups. The simplicity of interpreting the EDESI-MS spectrum was immediately apparent on reaction with 1-hexene (Figure 2-6). Clearly evident from the EDESI-MS spectrum is the coordination of up to three equivalents of hexene. The first addition occurs after loss of 3 CO's, with trace amounts showing up after loss of only 2 CO's, generating the ion $[H_3Ru_4(CO)_9(C_6H_{12})]^-$. Coordination of the second and third hexene moieties occurs for CO = 8 and 3 respectively. This example is a powerful demonstration of the ability of EDESI-MS to clearly and concisely represent data gathered over a large range of voltages; taken separately, as in the three 2-dimensional spectra, peak assignment is significantly more difficult (eg: the 2D spectrum at 80 V; Figure 2-6).

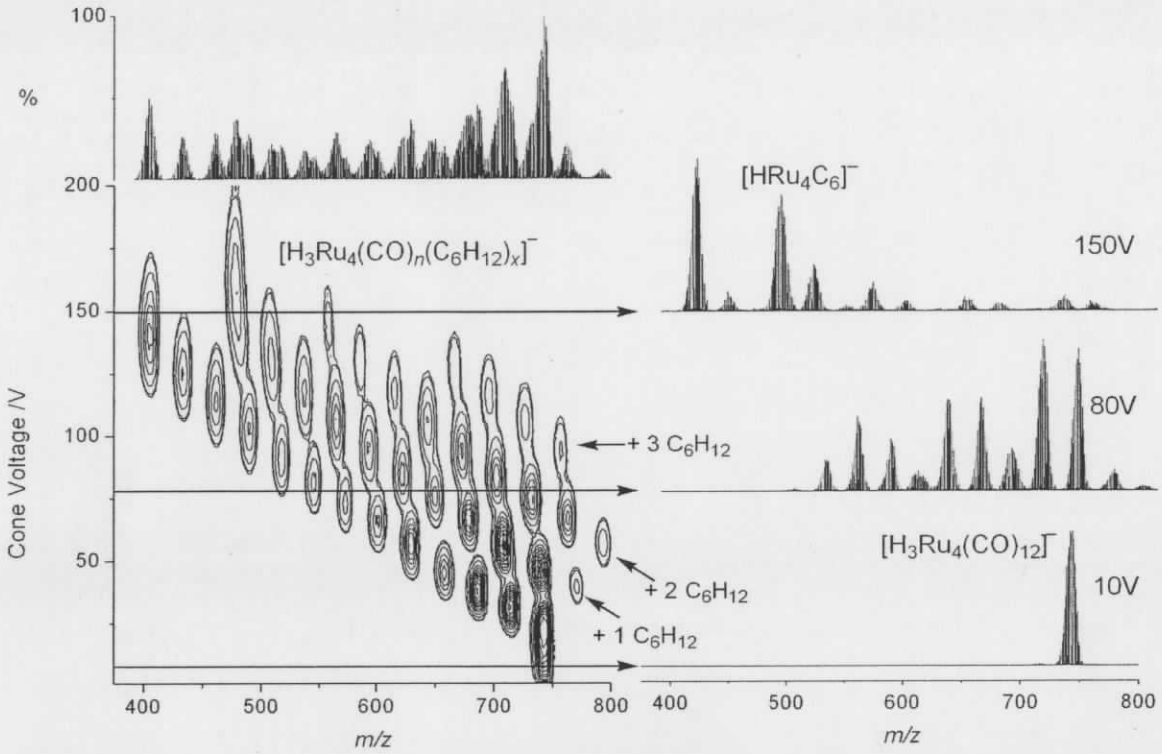

Figure 2-6: EDESI-MS of $[H_3Ru_4(CO)_{12}]^-$ in the presence of hexene vapors. Interpretation is made easy with the contour plot. Assigning 2-dimensional mass spectra of these high energy reactions (80V and 150V) is tedious and difficult due to the presence of overlapping signals.

A feature of these spectra that is not apparent in these plots, but which was easily detected in subsequent MS/MS experiments, is the occurrence of intramolecular C-H activation. This reactivity is perhaps not too surprising given that more than one vacant coordination site is available on the cluster when the first hexene molecule binds. There is precedent for this occurrence in the literature as well, albeit mainly for mononuclear metal complexes.[48] The MS/MS spectrum of the peak at 742 *m/z*, representing the first addition of hexene after loss of three CO moieties, shows the consecutive loss of three H_2 molecules before loss of another CO group (Figure 2-7). Close inspection of the peak shows that the cluster has in fact *already* lost at least two equivalents of H_2 before CID in the collision cell caused the loss of three more. The fact that loss of H_2 occurs at low collision voltages suggests that intramolecular C-H activation, followed by loss of H_2, occurs very quickly when other coordination sites are also available. At high enough

cone voltage (>180 V), it is obvious that this reactivity has occurred to the extent that nearly all H's have been removed, leaving only an $[HRu_4C_6]^-$ carbide cluster.

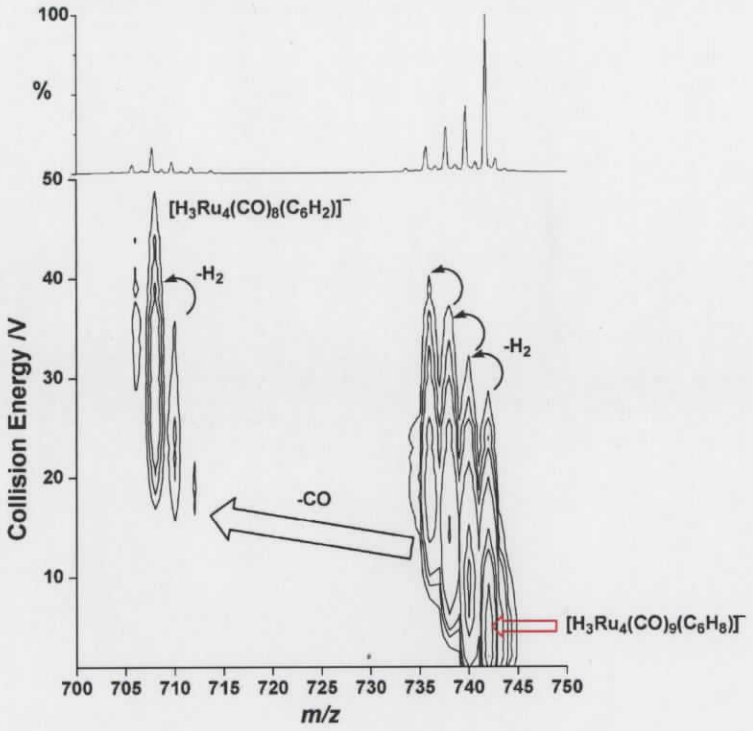

Figure 2-7: MS/MS of 742 *m/z* showing loss of H_2.

Such reactivity would probably occur by activation of a C-H bond by an adjacent metal atom that has already lost a CO ligand (Scheme 2-2). After coordination to the cluster by means of the vinyl group, adjacent sp^3 carbon atoms would be well positioned with respect to either an adjacent metal atom or the same metal center to undergo intramolecular activation of a C-H bond. With hydrides already present on the cluster, it seems reasonable that two hydrides could then be reductively eliminated as H_2. In this way the cluster maintains its three anionic ligands (two hydrides and now an alkyl group). Repeating this process successively replaces all hydride bonds with alkyl bonds from hexene to lose three equivalents of H_2. After this, the hexene group can activate further C-H bonds after the additional loss of CO that occurs under highly energetic conditions.

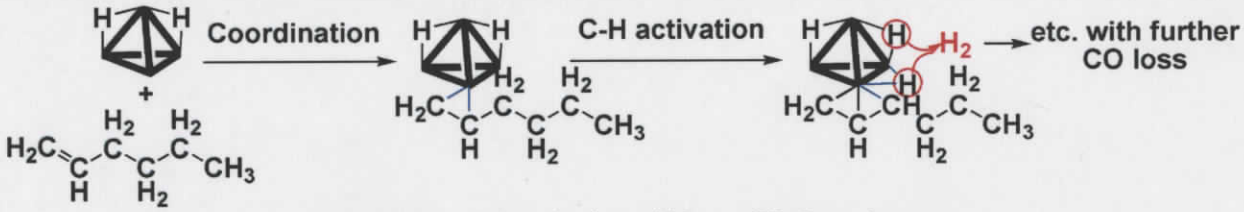

Scheme 2-2: C-H activation with loss of H_2 from cluster.

Given the nature of this system, with both hydride and carbonyl ligands surrounding the metal core, it seemed possible that some reactions central to catalytic processes of hydrogenation and hydroformylation might be observed (Scheme 2-3). Their occurrence would appear in the MS/MS experiment with reductive elimination of either hexane at 86 *m/z* (hydrogenation) or 1-heptanal at 114 *m/z* (hydroformylation; an alkyl group would first have to migrate to a CO ligand). As mentioned above though, C-H activation with very fast loss of H_2 seemed to prevent any sort of potential catalysis. Indeed for hydroformylation a high pressure of CO is required[49] to favour the insertion of CO into the Ru-C bond, and it seems likely that a pressure of H_2 would also be required to slow the rapid dehydrogenation. The high vacuum conditions of the mass spectrometer would reasonably limit such occurrences.

Hydrogenation: $[H_3Ru_4(CO)_9]^- + C_6H_{12} \longrightarrow [HRu_4(CO)_9]^- + C_6H_{14}$

Hydroformylation: $[H_3Ru_4(CO)_9]^- + C_6H_{12} \longrightarrow [HRu_4(CO)_8]^- + C_6H_{13}COH$

Scheme 2-3: Two potential catalytic reactions that may occur with an alkene in the gas phase.

Given the surprising simplicity of the addition of hexene, and the facility of C-H activation, the possibility of generating a cyclopentadienyl ligand from reaction with cyclopentene seemed a reasonable proposition. Although cyclopentene proved highly

reactive with rapid loss of H_2 as with hexene, there was no unusual stability for ions with greater than five hydride ligands.[a]

2.6.2 Arenes

Arenes may coordinate a metal center through the aromatic ring in an η^6-fashion, which presents different but still interesting chemistry with the cluster at hand.[50] Classic examples of arene coordination after removal of CO are with group 6 hexacarbonyl ligands to form piano stool complexes, but the cluster coordination of arenes has also been studied.[51] Three carbonyl groups can be replaced by the aryl group, coordinating in an η^6-fashion to maintain the electron count of the metal at 18 (Equation 2-1). Aryl cluster chemistry has also been reported with the ligand binding to a triangular cluster face in η^6-μ_3- fashion.[52] This binding mode activated the benzene to catalytic hydrogenation generating cyclohexane.[51] It seemed reasonable to expect that after suitable activation by CID and loss of CO, an aryl group might coordinate and potentially hydrogenate with the hydride ligands under MS/MS conditions.

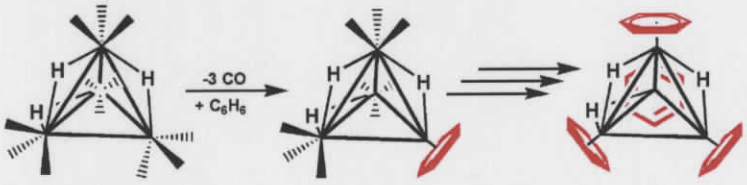

Equation 2-1: Expected arene coordination after loss of sufficient CO.

Both toluene and chlorobenzene were tried as potentially reactive gases, but both proved surprisingly unreactive in the gas phase (Figure 2-8). A toluene molecule was added after loss of five CO ligands from the cluster and was quite stable under MS/MS conditions. Chlorobenzene was even less reactive, adding only after all but one of the CO groups were removed from the cluster.

---

[a] See the appendix for the assigned spectrum (Appendix fig. 3) of the gas phase reaction of $[H_3Ru_4(CO)_{12}]^-$ with cyclopentene.

The decreased reactivity for these aryl reactions may be justified by considering the electron counts of each metal center in the cluster. The loss of five CO ligands needed for toluene coordination would be from the cluster as a whole,[53] with the remaining ligands distributing themselves equally. For the unreactive ion ($[H_3Ru_4(CO)_8]^-$) immediately preceding the reactive ion (at ~60 V; Figure 2-8), each metal center has between 16 and 17 electrons assuming all carbonyls and hydrides are fluxional. This level of unsaturation amounts to less than one coordination site per metal. Loss of one more CO to make $[H_3Ru_4(CO)_7]^-$ drops the electron count of one metal below 16, making it more likely to coordinate a substrate. No immediate loss of H_2 is observed at this energy, but at higher energies, multiple losses of H_2 occurs to give the $[HRu_4C_7]^-$ carbide cluster.

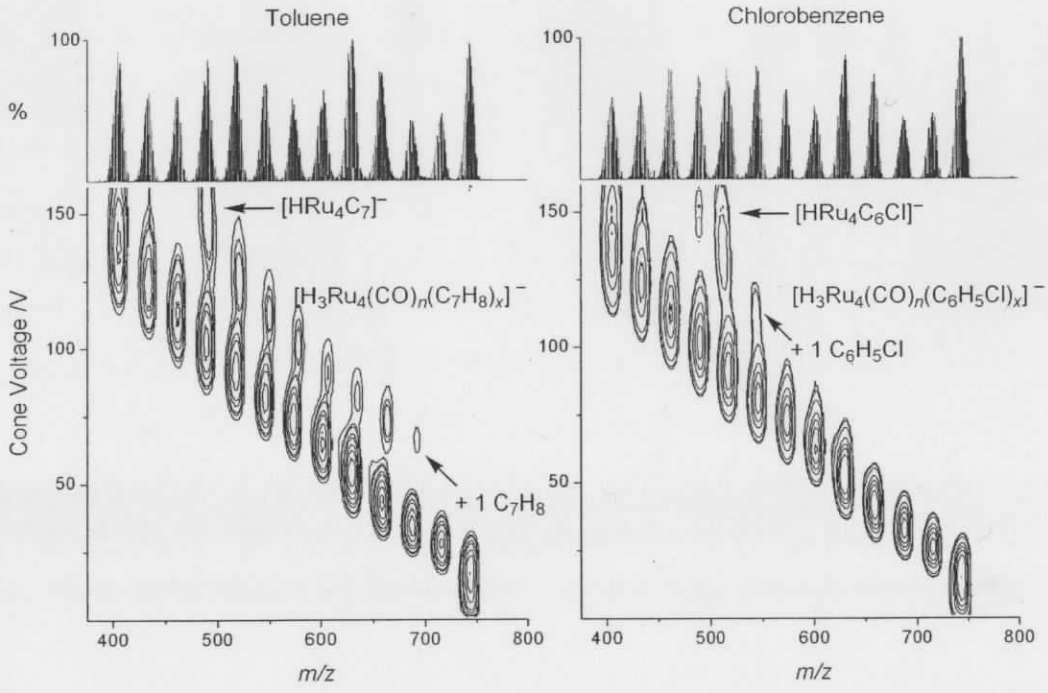

Figure 2-8: EDESI-MS of $[H_3Ru_4(CO)_{12}]^-$ in the presence of toluene (left) and chlorobenzene (right) vapors.

The decreased reactivity of chlorobenzene suggests that an electronic component to gas phase reactivity may be presenting itself, or possibly that the methyl group of toluene is

involved in the initial reaction. Minimal amounts of reactivity were observed and only with the highly reactive ion containing only one CO group.

2.6.3 Silanes

Silanes proved more reactive than both alkenes and arenes. This result was not surprising, as many cluster complexes with various silyl ligands have been crystallized and fully characterized.[54,55] The Si-H bond is slightly weaker than the C-H bond[56] and seemed to undergo more facile oxidative addition in the gas phase than alkanes, adding an equivalent of silane to the cluster ion that had lost just a single CO ligand.

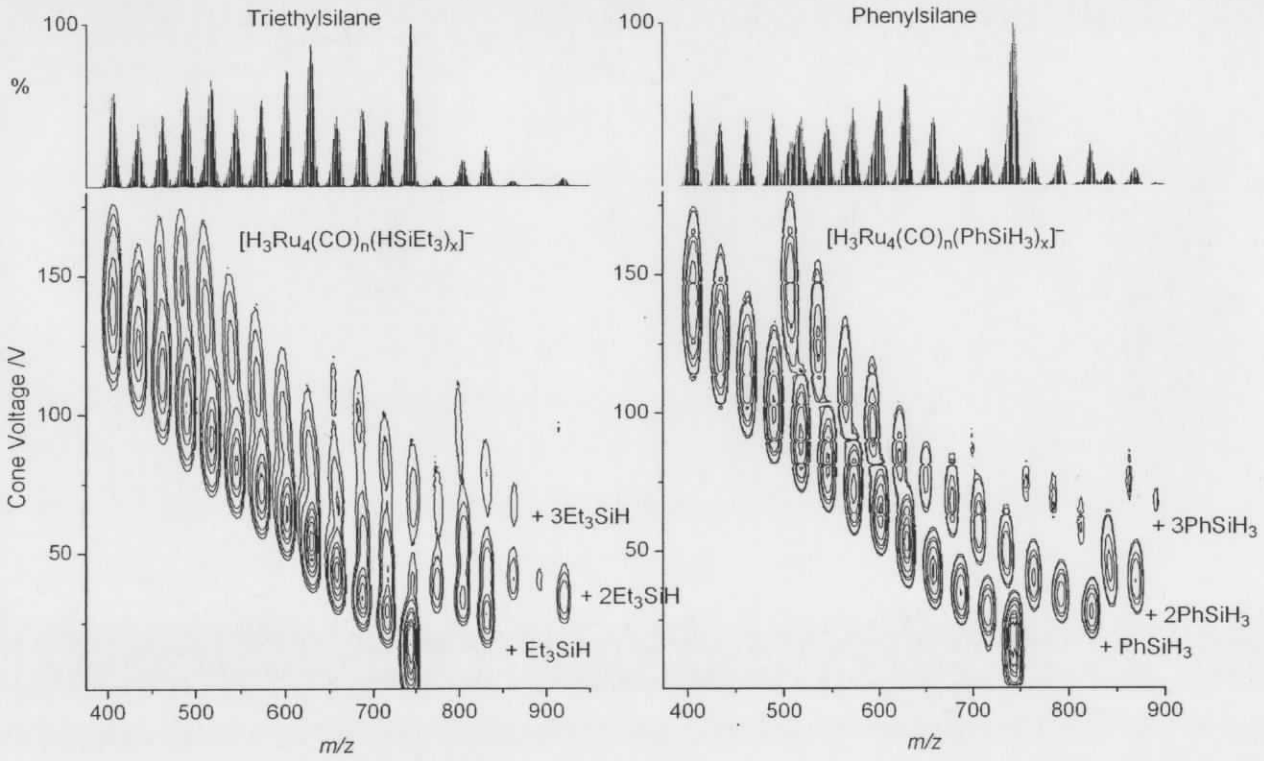

Figure 2-9: EDESI-MS of $[H_3Ru_4(CO)_{12}]^-$ in the presence of triethylsilane (left) and phenylsilane (right) vapors.

Both triethylsilane and phenylsilane were tested for reactivity, and although both were quite reactive on addition of the first silane moiety, their respective stabilities in MS/MS studies were quite different. Reductive elimination of the silane was favoured for triethylsilane, but loss of CO was preferred for phenylsilane. This suggested that all three

Si-H bonds were activated for phenylsilane, but the Si-C bonds remain inactive for triethylsilane. This was more evident in the MS/MS experiment (Figure 2-10) of the double addition products where the peak that should correspond to $[H_3Ru_4(CO)_{10}(PhSiH_3)_2]^-$ has already lost the equivalent of three H_2 equivalents, and peak assignment corresponds to the ion $[H_3Ru_4(CO)_{10}(PhSi)_2]^-$. Both phenylsilanes must therefore be bound as silylynes. On the other hand, triethylsilane does not activate its Si-C bonds to become a silylene ligand, but instead reductively eliminates the tertiary silane.

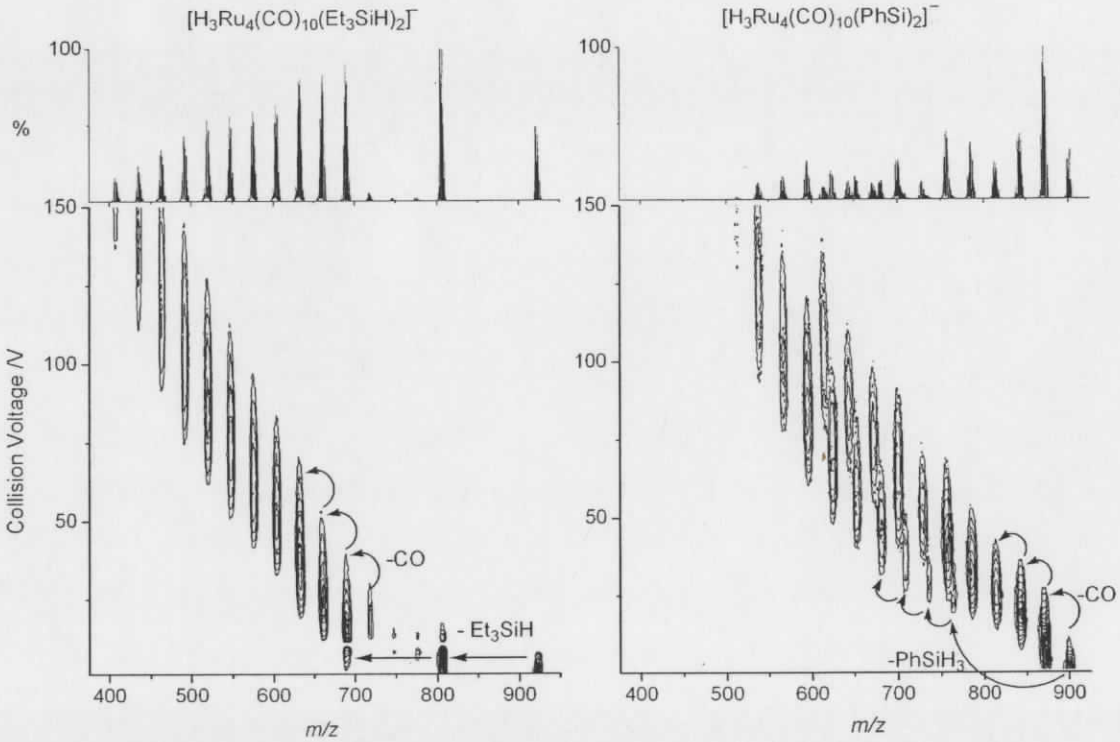

Figure 2-10: MS/MS of the ions following addition of two silane groups. Reactivity for MS/MS is considerably different for both species because they have different numbers of Si-H groups that may oxidatively add.

The potential for catalysis was again presented in the instance of reactivity with phenylsilane (Equation 2-2).[57,58,59] For the second time however, the very fast activation of E-H (E = Si in this instance but C in the case of hexene) followed by loss of H_2 prevented the opportunity to observe a dehydrocoupling reaction. A likely solution would be to conduct this experiment under a pressure of H_2 to favour the reverse

reaction; but increasing the pressure too much above atmospheric levels around the electrospray source would interfere with the ionization process and most likely lead to considerable arcing. In the case of the bis-triethylsilane complex, the MS/MS spectra show that loss of one silane occurs before loss of the second silane indicating that dehydrosilyl coupling has not occurred; this would appear as the simultaneous loss of both silanes.

Equation 2-2: Catalytic dehydrocoupling of phenylsilane.

2.6.4 Pentane

Given the facility of intramolecular C-H activation in reactions with alkenes, it seemed reasonable to inquire to the nature of *inter*molecular C-H activation. Ligand-free metallic ions[60,61,62] have shown to react extensively with saturated alkanes in the gas phase[63] with coordination after loss of H_2, as well as specifically designed C-H activation catalysts.[64] It seemed reasonable to expect that under sufficiently energetic conditions, C-H bonds would oxidatively add to the cluster, with subsequent loss of H_2 by reductive elimination. This was indeed observed although, not surprisingly, pentane was less reactive than the alkene systems (Figure 2-11). Pentane reacted in reasonable amounts with the ion $[H_3Ru_4(CO)_5]^-$. The first product ion of this reaction had already undergone extensive C-H activation and H_2 loss before detection, as expected given the extent of unsaturation about the metal core. These observations are in keeping with the rapid nature of C-H activation in the gas phase,[65] but contrast with a report by Ridge that anionic clusters were unreactive towards cyclohexane.[29]

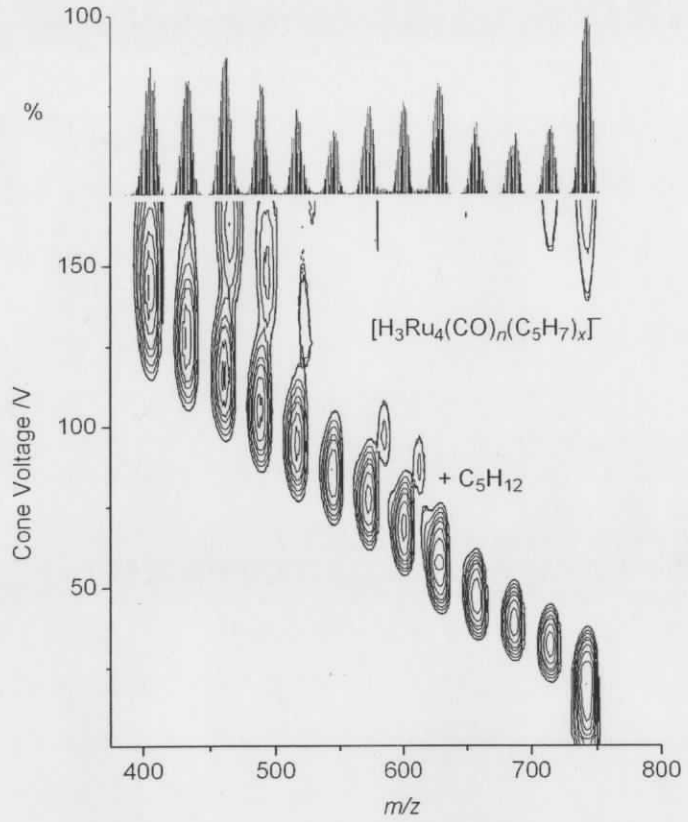

Figure 2-11: EDESI-MS of $[H_3Ru_4(CO)_{12}]^-$ in the presence of pentane gas.

2.6.5 Oxygen

Perhaps the most interesting result came upon reaction with molecular oxygen (Figure 2-12). This type of reactivity has been observed and reported on before for other anionic transition metal complexes.[66] There is no apparent reaction until four CO ligands have been removed at which point some rather dramatic changes occur. The cluster rapidly loses all of the remaining CO ligands and metal-metal bonds are broken to give heavily oxidized product ions with smaller cluster cores. The occurrence of CO oxidation to CO_2 was carefully investigated by MS/MS of product peaks, but no sign of this reaction was observed though it has been observed in other systems.[67]

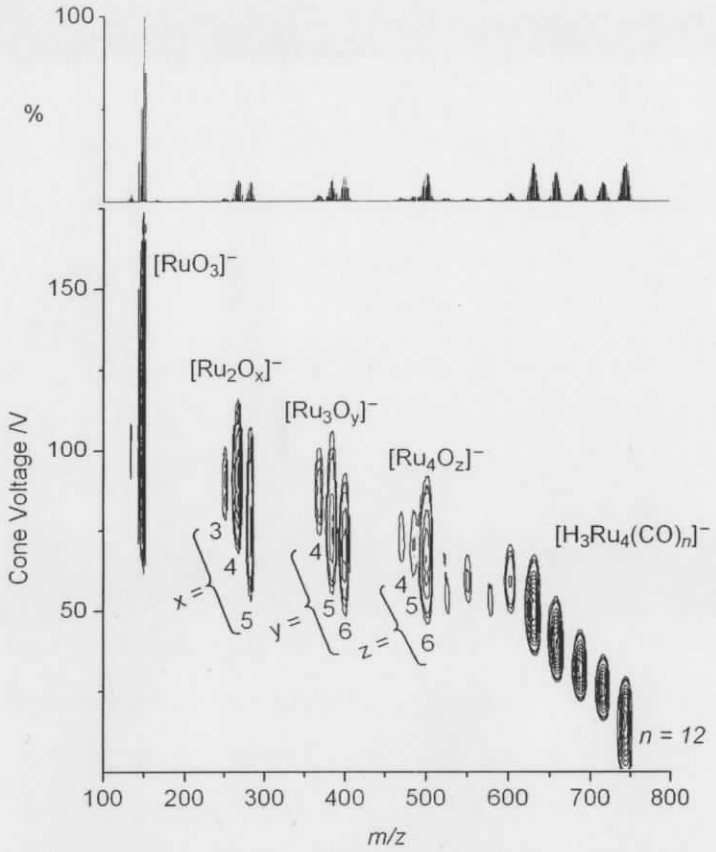

Figure 2-12: EDESI-MS of $[H_3Ru_4(CO)_{12}]^-$ in the presence of molecular oxygen.

The most stable product ion from this oxidation is $[RuO_3]^-$ with trace amounts of both $[RuO_4]^-$ and $[RuO_2]^-$ on either side. From MS/MS studies, fragmentation occurs via loss of Ru_nO_m (n = 1-3; m = 1-6). The major product ion ($[RuO_3]^-$) however, is never observed in MS/MS spectra of higher cluster species suggesting its formation requires fast fragmentation followed by addition of another O_2 molecule to the precursor ion, or that it is actually a product ion of $[RuO]^-$ on addition of O_2.

The rapidity of cluster breakdown after 4 CO ligands have been lost is unsurprising given that CO is a good ligand for *low* oxidation state metals. Oxygen does not appear to coordinate the cluster before this point, but upon loss of a fifth CO ligand, oxygen seems to react more vigorously. There is no sign of the complex $[H_3Ru_4(CO)_7]^-$, presumably because once O_2 coordinates, the ability of each ruthenium atom to back donate electron density to the π^* orbitals of their CO ligands is decreased. This would then make it even

easier for the remaining CO's to be shaken off the core by CID, and from Figure 2-12 we see that this occurs above a cone voltage of 50 V. As the CO ligands are rapidly lost, it is also possible for more O_2 to coordinate thereby oxidizing the Ru-Ru bonds and effectively breaking the cluster apart.

Reactions of ruthenium complexes with molecular oxygen have been observed in the past,[68] but always in the positive ion mode and generally with tris(2,2-bipyridine) ruthenium dichloride complexes. Furthermore, only MS/MS studies have been done whereby a mass selected ion that was expected to react (namely $[Ru(bipy)_2]^{2+}$) was mass selected and allowed to react in the collision cell with oxygen. The expected $+O_2$ adduct was observed, but it seems that little attempt was made to probe reactivity against other potential ions. The setup presented here allows the entire solution of ions to react in the gas phase, and all product ions to be observed at the same time (Figure 2-13). As such, the reaction of the monocation $[Ru(bipy)_2Cl]^+$ with both water and molecular oxygen can be observed in the same spectrum, which was not observed previously.

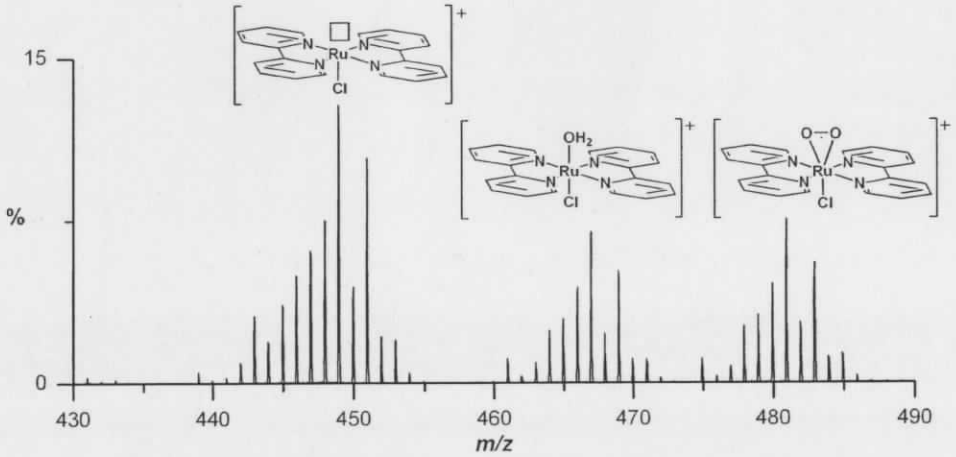

Figure 2-13: Gas phase reaction of $Ru(bipy)_3Cl_2$ with molecular oxygen in the electrospray source reveals a competition between water and molecular oxygen. Water is present as the complex was dissolved as the hexahydrate salt.

2.6.6 Volatile organometallic liquids

Volatile organometallic liquids are not excluded from past investigations into gas phase reactivity,[69] and they present an interesting and different type of reaction to investigate.

Beauchamp[70,71] and Ridge[72] have separately studied the gas phase chemistry of $Fe(CO)_5$, but never before has the correspondence to solution phase reactivity been so close. Electron impact or photon impact ion cyclotron resonance studies[73] of $Fe(CO)_5$ are extremely energetic and they generate ions such as $[Fe(CO)_x]^+$, where x = 1 or 2. Such ions are sufficiently unsaturated and already have excessive energy from the ionization process, that it is unsurprising they should coordinate the unreacted monomer, or any other moderately electron rich molecule in the vicinity.

The motivation for these experiments is not to observe *catalytic* reactions, but instead to examine cluster build-up reactions.[74] This would give insight to the order of reactivity in cluster formation in a manner that might more closely parallel the condensed phase reaction than past studies. From Figure 2-14 it is quite clear that the anionic ruthenium cluster reacts readily with iron pentacarbonyl, adding up to three iron atoms and varying numbers of carbonyl ligands. The difference between this reaction and those of organic substrates described above is that $Fe(CO)_5$ does not behave as a ligand, but rather it forms bonds with the metal core and shares its carbonyls about the $[Ru_4Fe]^-$ framework.

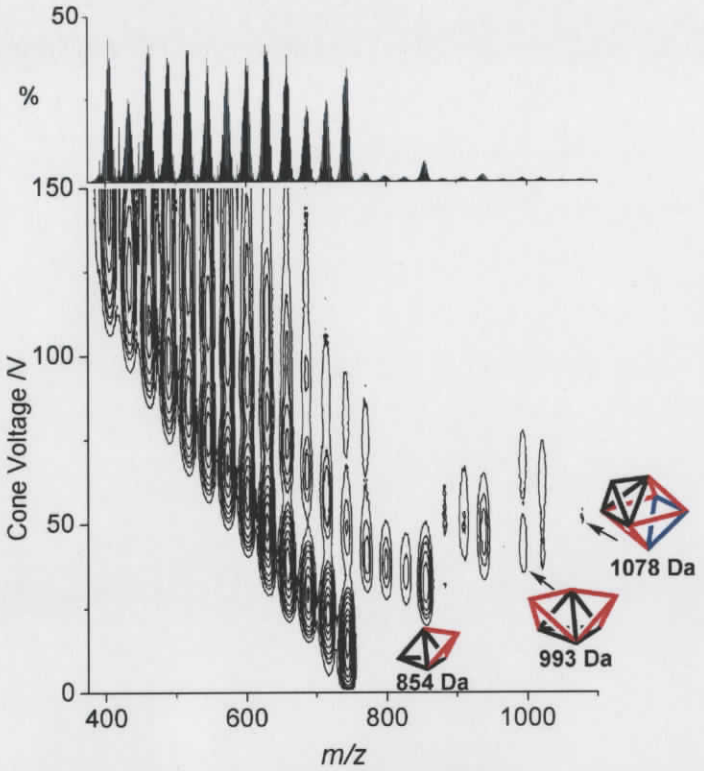

Figure 2-14: EDESI-MS of $[H_3Ru_4(CO)_{12}]^-$ in the presence of $Fe(CO)_{5\,(g)}$. Bonds in red are from ruthenium to iron, and bonds in blue are between iron atoms.

Evidence for the newly bound iron atom becoming part of the embedded cluster core can be seen from the MS/MS fragmentation patterns (Figure 2-15). For each of the identified base peaks in Figure 2-14, loss of CO is the only fragment that is observed. At very high collision voltages, where no further COs are observed to fall off, peak assignment of the bare cluster corresponds to the tetraruthenium core plus the requisite number of iron atoms that were added as $Fe(CO)_5$. Had the iron been bound weakly, or reversibly to the cluster, and had the carbonyl ligands not redistributed themselves onto the cluster framework, then elimination of the neutral $Fe(CO)_5$ molecule would have been expected. This is never observed, and therefore it must be presumed that the metal has bonded to the cluster.

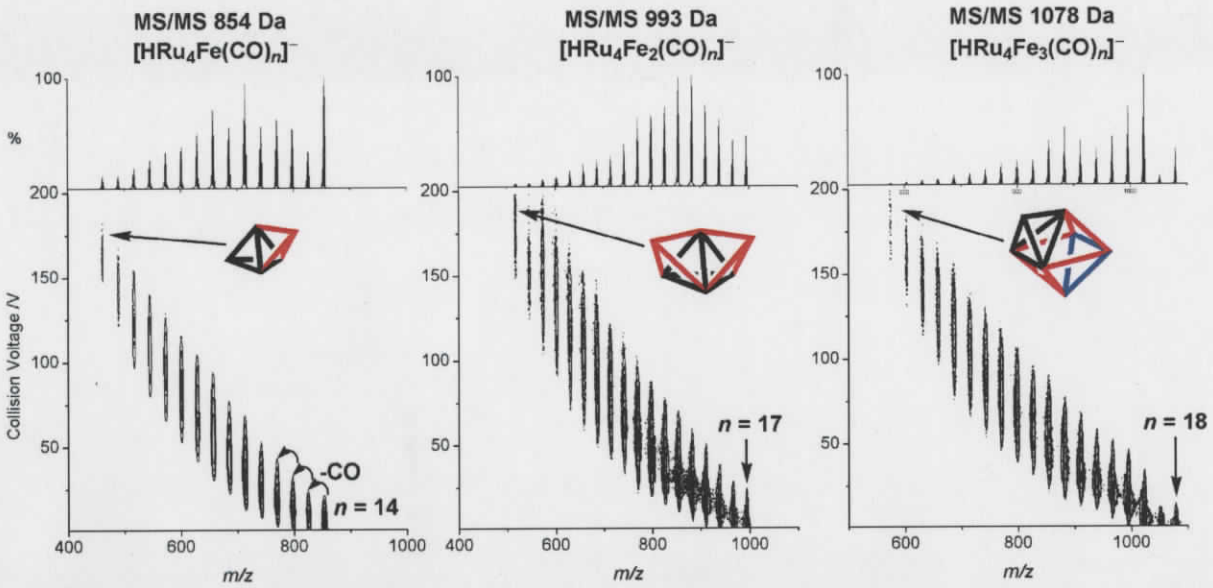

Figure 2-15: MS/MS spectra of the three base product clusters that form in the reaction with the sufficiently activated $[H_3Ru_4(CO)_{12}]^-$ cluster.

An observation in Ridge's $Fe(CO)_5$ system, is that the more unsaturated the metal was the more reactive it was.[75] This is simply a cluster based extension of the 18-electron rule for monometallic complexes. The more electron deficient a cluster is, the greater its propensity to add another metal or ligand (*ie:* greater reactivity). This theory, as well as the effective atomic number rule for electron counting in clusters[76] (EAN) can be used to explain the observed reactivity in this system. After loss of three CO's and one molecule of H_2 from $[H_3Ru_4(CO)_{12}]^-$, the cluster $[HRu_4(CO)_9]^-$ is deficient in 8 electrons, which corresponds to a vacant coordination site per metal atom (structure **1** in Scheme 2-4). This deficiency is sufficient to activate the cluster for addition of one equivalent of $Fe(CO)_5$, and with CO distribution about all of the metals, the trigonal bipyramidal cluster is observed at 854 *m/z* (structure **2** in Scheme 2-4). This product ion only has a $2e^-$ deficiency, but it is important to note that its presence in such intensity is attributed to the electron deficiency of the reacting cluster and not to the stability of the product ion. The $2e^-$ deficiency can be shared by having two metal atoms with electron counts of only 17 electrons, with the remaining metals having 18 electrons.

Loss of 2 COs from structure **2**, with addition of another $Fe(CO)_5$ generates a bicapped tetrahedron (structure **3**; Scheme 2-4) at 993 *m/z*. As such, this $84e^-$ cluster is not

deficient in electrons at all. Structure **4** is a 94 e^- cluster, and based on the EAN rule the nearest cluster this would correspond to is a capped octahedron. It may occur after loss of four COs from **3** followed by addition of $Fe(CO)_5$, which would occur by rearrangement of Ru-Fe bonds-a possible process in the gas phase.[77] It may also happen that structure **2** reacts with two equivalents of $Fe(CO)_5$, and after loss of six COs, generate structure **4**; such a reaction would bypass the bicapped tetrahedron to form the capped octahedron without breaking any metal-metal bonds.

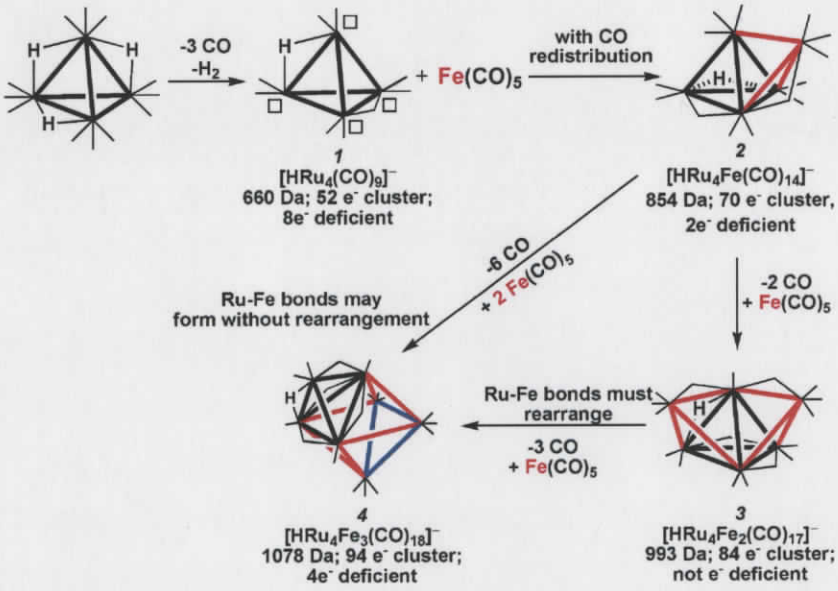

Scheme 2-4: Reactivity of $[H_3Ru_4(CO)_{12}]^-$ with $Fe(CO)_5$ in the gas phase to generate larger nuclearity clusters.

Studies of building up iron clusters ($[Fe_x(CO)_n]^-$) can be seen in this system (Figure 2-16), but only at very high cone voltages, where translational energies might be expected to parallel conditions of EI-MS. Notably, the relative abundance of $[Fe(CO)_3]^-$ and $[Fe(CO)_2]^-$ are quite low at all voltages where $[Fe(CO)_4]^-$ is observed. This low abundance is attributed to their unsaturation and increased reactivity with neutral $Fe(CO)_5$ to make the higher mass clusters. All of these ions have uneven electron counts attributed to an initial $1e^-$ reduction, with CO loss, that occurs at the capillary on the $Fe(CO)_5$ vapor.

A control experiment, whereby the $Fe(CO)_5$ vapor was introduced to the cone without any injected analyte was also attempted to try to simplify the spectrum and view only iron clusters. This experiment however, gave a very weak spectrum lacking the sensitivity that was observed at the end of the $[H_3Ru_4(CO)_{12}]^-$ experiments.

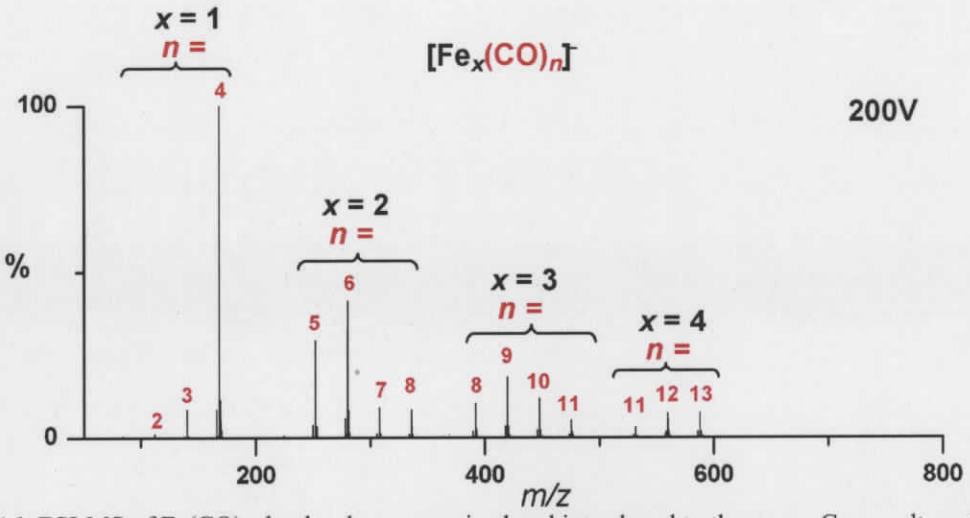

Figure 2-16: ESI-MS of $Fe(CO)_5$ that has been vaporized and introduced to the cone. Cone voltage is set to 200 V. Ionization is expected to occur by reduction of a small amount of the monomer to generate $[Fe(CO)_4]^-$, which goes on to react with further $Fe(CO)_5$ vapor.

This type of cluster buildup is similar to O'Hair's method of generating silver clusters from electrosprayed solutions of silver nitrate.[78] Other reports of building clusters in the gas phase have been noted for platinum,[79] and ruthenium[80]. These results also mimic the more energetic experiments of Ridge by EI-MS with $Fe(CO)_5$.[81] Given the energetics at which Ridge's clusters form, the correspondence to solution reactivity is minimal. Wallace has employed MALDI mass spectrometry to study the manner in which $CpCo(CO)_2$ coordinates large alkanes by mass spectrometry.[82] It was observed that $[Co_xCp_n]^+$ (up to x = 4 and n = 7), were formed in the gas phase, even though they were not present in the sample to begin with. Their presence however, was attributed to the chemistry that occurred in the laser ablation process which generated the reactive $[CoCp]^+$ monomer in the ablation plume. Further gas phase reactivity allowed the

clusters to build up, and with the variable hapticity of cyclopentadienyl ligands, the clusters were able to accommodate more than four ligands.

2.7 Experimental

The cluster salt $[PPN][H_3Ru_4(CO)_{12}]$ was made by a published method.[43] Cyclopentene, 1-hexene, toluene, pentane, chlorobenzene, triethylsilane, and iron pentacarbonyl were purchased from Aldrich and used as supplied (the toluene and pentane were HPLC grade). Phenylsilane was prepared in a $LiAlH_4$ reduction from trichlorophenylsilane (purchased from Aldrich). Oxygen and nitrogen (99.99%) were purchased from Airgas. Electrospray ionization mass spectra were collected using a Micromass QTof *micro* instrument. Capillary voltage was set at 2900 V, source and desolvation gas temperatures were at 50 and 100°C, respectively. A minimum of the $[PPN][H_3Ru_4(CO)_{12}]$ salt was dissolved in dichloromethane and infused via syringe pump at 5-10 $\mu L\ min^{-1}$ in order to acquire a spectra consisting of about 500 ion counts per second. EDESI-MS(/MS) spectra were collected using published procedures and processed using the program EDit.[83] The reactive gas was introduced by passing a stream of nitrogen through the appropriate liquid and directing the saturated gas through the cone gas port. The flow rate was approximately 15 $L\ h^{-1}$, compared to a desolvation gas flow rate of 100 $L\ h^{-1}$. Incrementing the cone voltage or collision voltage (for MS/MS experiments) was achieved using the program Autohotkey (freely available from http://www.autohotkey.com/).

2.7.1 Pictures of the gas phase setup

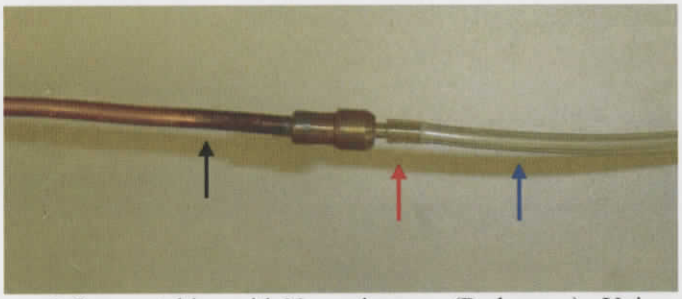

Figure 2-17: (Black arrow) Copper tubing with N_2 carrier gas. (Red arrow): Union piece between copper tubing and plastic tubing. (Blue arrow): Plastic tubing that is directed to the vial with the volatile liquid.

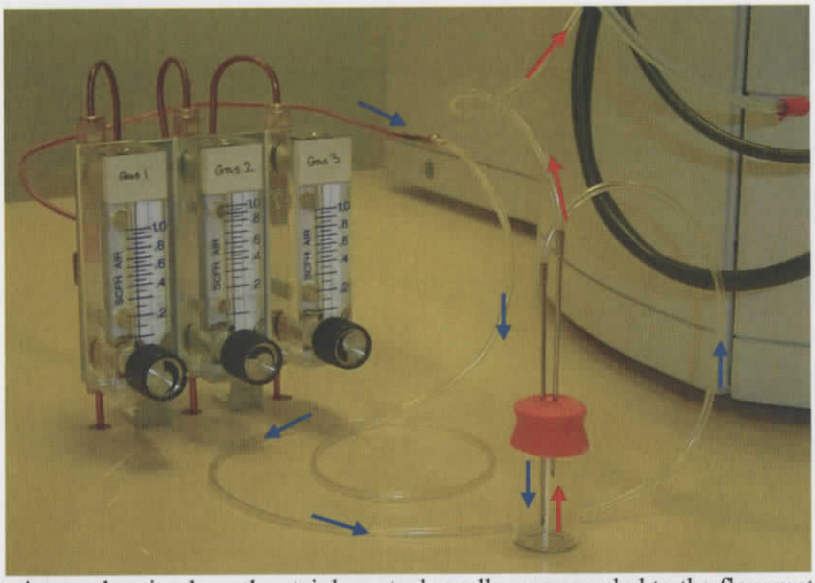

Figure 2-18: A picture showing how the stainless steel needles are coupled to the flow meters, then to the vial with the volatile liquid (blue arrows) and then from the vial to the mass spectrometer (red arrows).

2.8 References

[1] a) Morton, T.H., *Tetrahedron,* **1982**, *38*, 3195-3243. b) Bohme, D.K.; Schwarz, H., *Angew. Chem. Int. Ed. Eng.,* **2005**, *44*, 2336-2354. c) Eller, K; Schwarz, H., *Chem. Rev.,* **1991**, *91*, 1121-1177. d) Plattner, D.A., *Int. J. Mass. Spectrom.,* **2001**, *207*, 125-144. e) Chen, P., *Angew. Chem. Int. Ed. Engl.,* **2003**, *42*, 2832-2847. f) Richardson, D.E.; Plattner, D.A., *Comprehensive organometallic chemistry: Organometallic chemistry in the gas phase.* **2007**, *Vol. 1*, 801-822. g) Water, T.; O'Hair, R.A.J., *Annu. Rep. Prog. Chem., Sect. B,* **2002**, *98*, 433-501.

[2] Dedieu, A.; Veillard, A., *J. Am. Chem. Soc.,* **1972**, *94*, 6730-6738.

[3] Olmstead, W.N.; Brauman, J.I., *J. Am. Chem. Soc.,* **1977**, *99*, 4219-4228.

[4] Truong, T.N.; Stefanovich, E.V., *Chem. Phys. Lett.,* **1995**, *240,* 253-260.

[5] Waters, T.; O'Hair, R.A.J.; Wedd, A.G., *J. Am. Chem. Soc.,* **2003**, *125,* 3384-3396.

[6] Jarrold, M.F. In *Gas phase inorganic chemistry;* Ed. Russell D.H.; Metal and semiconductor cluster ions; Plenum Press: New York, **1989**; 137-192.

[7] Gioumousis, G.; Stevenson, D.P., *J. Chem. Phys.,* **1958**, *29*, 294-299.

[8] Marcalo, J.; Pires de Matos, A., *J. Organomet. Chem.,* **2002**, *647*, 216-224.

[9] Hinderling, C.; Adlhart, C.; Chen, P., *Angew. Chem. Int. Ed. Eng.*, **1998**, *37*, 2685-2689.

[10] Bowen, R.D.; Williams, D.H., *J. Am. Chem. Soc.*, **1980**, *102*, 2752-2756.

[11] Bowen, R.D., *Acc. Chem. Res.*, **1991**, *24*, 364-371.

[12] Gerdes, G.; Chen, P., *Organometallics*, **2006**, *25*, 809-811.

[13] Labinger, J.A.; Bercaw, J.E.; Tilset, M., *Organometallics*, **2006**, *25*, 805-808.

[14] Gerdes, G.; Chen, P., *Organometallics*, **2003**, *22*, 2217-2225.

[15] Cornehl, H.H.; Wesendrup, R.; Harvey, J.N.; Schwarz, H., *J. Chem. Soc., Perkin Trans.*, **1997**, *2*, 2283-2291.

[16] Thewissen, S.; Plattner, D.A.; de Bruin, B., *Int. J. Mass spectrom.* **2006**, *249/250*, 446-450.

[17] Armentrout, P.B., *Topics in Organometallic Chemistry*, **1999**, *4*, 1-45.

[18] Fisher, K.J.; Dance, I.G., Willett, G.D., *Rapid Commun. Mass Spectrom.*, **1996**, *10*, 106-109.

[19] Liu, F.Y.; Zhang, X.G.; Liyanage, R.; Armentrout, P.B., *J. Chem. Phys.*, **2004**, *121*, 10976-10990.

[20] Waters, T.; O'Hair, R.A.J.; Wedd, A.G., *Chem. Commun.*, **2000**, 225-226.

[21] Miras, H.N.; Wilson, E.F.; Cronin, L., *Chem. Commun.*, **2009**, 1297-1311.

[22] Butcher, C.P.G.; Dyson, P.J.; Johnson, B.F.G.; McIndoe, J.S., *Chem. Eur. J.*, **2003**, *9*, 944-950.

[23] Khairallah, G.N.; O'Hair, R.A.J., *Dalton Trans.*, **2005**, 2702-2712.

[24] O'Hair, R.A.J.; Khairallah, G.N., *J. Cluster Sci.*, **2004**, *15*, 331-363.

[25] Deng, H.T.; Kerns, K.P.; Castleman, A.W.Jr., *J. Phys. Chem.* **1996**, *100*, 13386-13392.

[26] Fialko, E.F.; Kikhtenko, A.V.; Goncharov, V.B.; Zamaraev, K.I., *J. Phys. Chem. B.*, **1997**, *101*, 5772-5773.

[27] Tracy, J.B.; Crowe, M.C.; Parker, J.F.; Hampe, O.; Fields-Zinna, C.A.; Dass, A.; Murray, R.W., *J. Am. Chem. Soc.*, **2007**, *129*, 16209-16215.

[28] Freas, R.B; Ridge, D.P., *J. Am. Chem. Soc.*, **1984**, *106*, 825-826.

[29] Pan, Y.H.; Ridge, D.P., *J. Phys. Chem.*, **1989**, *93*, 3375-3378.

[30] Gimbert, Y.; Lesage, D.; Milet, A.; Fournier, F.; Greene, A.E.; Tabet, J.C., *Org. Lett.*, **2003**, *5*, 4073-4075.

[31] Butcher, C.P.G.; Dinca, A.; Dyson, P.J.; Langridge-Smith, P.R.R.; McIndoe, J.S., *Angew. Chem. Int. Ed. Engl.* **2003**, *42*, 5752-5755.

[32] Gerlich, D., *J. Chem. Soc., Faraday Trans.*, **1993**, *89*, 2199-2208.

[33] O'Hair, R.A.J., *Chem. Commun.*, **2006**, 1469-1481.

[34] Trage, C.; Diefenbach, M.; Schroder, D.; Schwarz, H., *Chem. Eur. J.*, **2006**, *12*, 2454-2464.

[35] Spence, T.G; Burns, T.D.; Posey, L.A., *J. Phys. Chem. A,* **1997**, *101*, 139-144.

[36] Schlosser, G.; Takats, Z.; Vekey, K., *J. Mass Spectrom.*, **2003**, *38*, 1245-1251.

[37] Jayaweera, P.; Blades, A.T.; Ikonomou, M.G.; Kebarle, P., *J. Am. Chem. Soc.*, **1990,** *112,* 2452-2454.

[38] Zhan, D.; Rosell, J.; Fenn, J.B., *J. Am. Soc. Mass Spectrom.*, **1998**, *9*, 1241-1247.

[39] Ikonomou, M.G.; Blades, A.T.; Kebarle, P., *Anal. Chem.*, **1991**, *63*, 1989-1998.

[40] Jackson, P.F.; Johnson, B.F.G.; Lewis, J.; McPartlin, M.; Nelson, W.J.H., *J. Chem. Soc. Chem. Commun.*, **1978**, 920-921.

[41] Knox, S.A.R.; Koepke, J.W.; Andrews, M.A.; Kaesz, H.D., *J. Am. Chem. Soc.*, **1975**, *97*, 3942-3947.

[42] Bruce, M.I.; Williams, M.L., *Inorg. Synth.*, **1989,** *26*, 262.

[43] Koepke, J.W.; Johnson, J.R.; Knox, S.A.R.; Haesz, H.D., *J. Am. Chem. Soc.*, **1975**, *97*, 3947-3952.

[44] Ungermann, C.; Landis, V.; Moya, S.A.; Cohen, H.; Walker, H.; Pearson, R.G.; Rinker, R.G.; Ford, P.C., *J. Am. Chem. Soc.*, **1979**, *101*, 5922-5929.

[45] Meister, G.; Rheinwald, G.; Stoeckli-Evans; H.; Suss-Fink, G., *J. Chem. Soc. Dalton Trans.*, **1994**, 3215-3223.

[46] Plasseraud, L.; Suss-Fink, G., *J. Organomet. Chem.*, **1997**, *539*, 163-170.

[47] Tominaga, K.; Sasaki, Y., *J. Mol. Catal. A: Chem.*, **2004**, *220*, 159-165.

[48] Byrd, H.C.M.; Guttman, C.M.; Ridge, D.P., *J. Am. Soc. Mass Spectrom.*, **2003**, *14*, 51-57.

[49] Kamer, P.C.J.; Reek, J.N.H.; van Leeuwen, P.W.N.M., *Mechanisms in Homogeneous Catalysis: A Spectroscopic Approach,* Weinheim, **2005**, 231-269.

[50] Crabtree, R.H.: *The Organometallic Chemistry of the Transition Metals*, Ed. 3rd. John Wiley & Sons: New York, **2001**.

[51] Dyson, P.J.; Ellis, D.J. Parker, D.G.; Welton, T., *Chem. Commun.*, **1999**, 25-26.

[52] Campagnola, D.; Castiglioni, M.; Dastru, W.; Deabate, S.; Giordano, R.; King, P.J.; Sappa, E., *Inorg. Chim. Acta,* **1997**, *262*, 157-165.

[53] Roberts, Y.V.; Johnson, B.F.G.; Benfield, R.E., *Inorg. Chim. Acta,* **1995**, *229*, 221-227.

[54] Suss-Fink, G., *Inorg. Synth.* **1989,** *26*, 269.

[55] Nagashima, H.; Suzuki, A.; Iura, T.; Ryu, K.; Matsubara, K., *Organomet.,* **2000**, *19*, 3579-3590.

[56] Walsh, R., *Acc. Chem. Res.,* **1981**, *14*, 246-252.

[57] Rosenberg, L.; Davis, C.W.; Junzhi, Y., *J. Am. Chem. Soc.,* **2001**, *123*, 5120-5121.

[58] Aitken, C. T.; Harrod, J.F.; Samuel, E., *J. Am. Chem. Soc.,* **1986**, *108*, 4059-4066.

[59] Dioumaev, V.K.; Harrod, J.F., *J. Organomet. Chem.,* **1996**, *521*, 133-143.

[60] Chowdhury, A.K.; Wilkins, C.L., *J. Am. Chem. Soc.,* **1987**, *109,* 5336-5343.

[61] Byrd, G.D.; Freiser, B.S., *J. Am. Chem. Soc.,* **1982**, *104,* 5944-5950.

[62] Aristov, N.; Armentrout, P.B., *J. Am. Chem. Soc.,* **1986**, *108,* 1806-1819.

[63] Chen, R.; Liang Li, *J. Am. Soc. Mass Spectrom.,* **2001**, *12*, 367-375.

[64] Hinderling, C.; Plattner, D.A.; Chen, P., *Angew. Chem. Int. Ed. Engl.,* **1997**, *36,* 243-244.

[65] Schwarz, H., *Mass Spectrom. Rev.,* **1983**, *2*, 77-148.

[66] Siu, C. K.; Reitmeier, S. J.; Balteanu, I.; Bondybey, V. E.; Beyer, M. K., *Eur. Phys. J. D,* **2007**, *43*, 189-192.

[67] Squires, R. R., *Chem. Rev.,* **1987**, *87*, 623-646.

[68] Molina-Svendsen, H.; Bojesen, G.; McKenzie, C.J., *Inorg. Chem.,* **1998**, *37*, 1981-1983.

[69] Russell, D.H., *Gas Phase Inorganic Chemistry*, Plenum Press: New York, **1989**.

[70] Foster, M.S.; Beauchamp, J.L., *J. Am. Chem. Soc.,* **1971**, *93*, 4924-4926.

[71] Foster, M.S.; Beauchamp, J.L., *J. Am. Chem. Soc.,* **1975**, *97*, 4808-4814.

[72] Pan, Y.H.; Ridge, D.P., *J. Am. Chem. Soc.,* **1992**, *114*, 2773-2780.

[73] Dunbar, R.L.; Ennever, J.F.; Fackler, J.P.Jr., *Inorg. Chem.,* **1973**, *12*, 2734-2736.

[74] Kéki, S.; Szilágyi, L.Sz.; Török, J.; Deák, G.; Zsuga, M., *J. Phys. Chem.,* **2003**, *107*, 4818-4825.

[75] Wronka, J.; Ridge, D.P., *J. Am. Chem. Soc.,* **1984**, *106*, 67-71.

[76] Dyson, P.J.; McIndoe, J.S., *Transition Metal Carbonyl Cluster Chemistry*, Gordon and Breach Science Publishers: Canada, **2000**.

[77] Butcher, C.P.G.; Dyson, P.J.; Johnson, B.F.G.; Khimyak, T.; McIndoe, J.S., *Chem. Eur. J.,* **2003**, *9*, 944-950.

[78] Khairallah, G.N.; O'Hair, R.A.J., *Angew. Chem. Int. Ed. Engl.,* **2005**, *44,* 728-731.

[79] McNeal, C.J.; Hughes, J.M.; Lewis, G.J.; Dahl, L.F., *J. Am. Chem. Soc.,* **1991**, *113*, 372-373.

[80] Dale, M.J.; Dyson, P.J.; Johnson, B.F.G.; Langridge-Smith, P.R.R.; Yates, H.T., *J. Chem. Soc., Dalton Trans.,* **1996**, 771-774.

[81] Ridge, D.P.; Meckstroth, W.K., Reactions in ionized metal carbonyls: clustering and oxidative addition. In *Gas phase inorganic chemistry,* Russell D.H. Ed.; Plenum Press: New York, **1989**; 93-113.

[82] Wallace, W.E., *Chem. Commun.,* **2007**, 4525-4527.

[83] Husheer, S.L.G.; Forest, O.; Henderson, M.; McIndoe, J.S., *Rapid Commun. Mass Spectrom.* **2005**; *19*: 1352-1354.

Chapter 3 Neutral complexes and the Pauson-Khand reaction

3.1 Charging neutral complexes

Although ESI-MS has considerable merits as an analytical technique in the study of catalytic systems, it comes with the caveat that neutral, non-polar compounds are invisible to the technique. With many catalysts being[1] neutral metal complexes this disadvantage presents a considerable challenge to the broad application of ESI-MS in organometallic catalysis. Five commonly employed solutions to this problem are illustrated in Scheme 3-1 along with a fifth that has good potential but has been little-used.

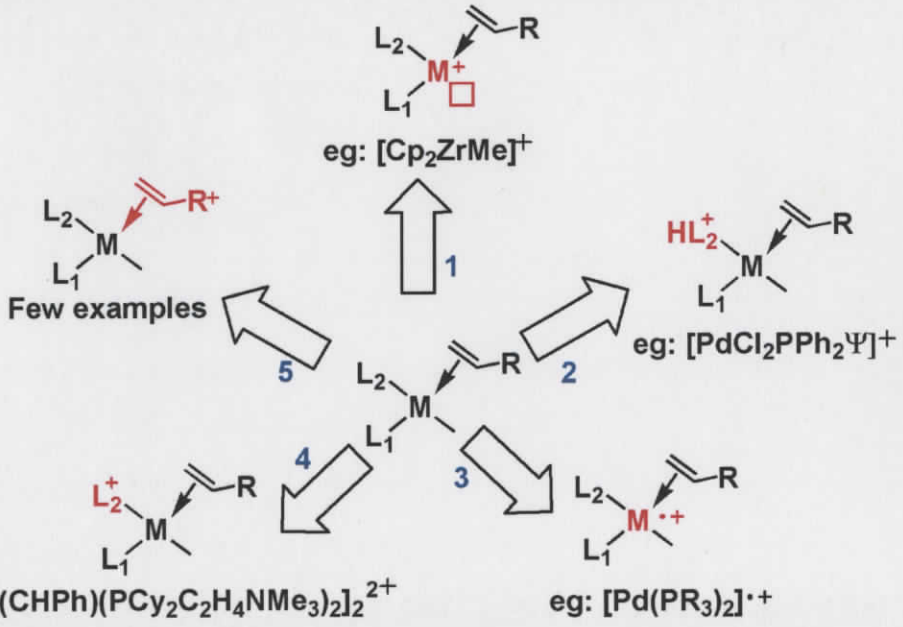

Scheme 3-1: Five methods of ionizing neutral metal complexes. 1) Loss of an ionic ligand. 2) Association with a charged species (such as a proton). 3) Loss of an electron from the metal center. 4) Addition of a charge to an ancillary ligand. 5) Adding a charge to the substrate.

1. The simplest method of charging a neutral complex is loss of an anionic ligand such as CH_3^- or Cl^-.

2. A second method is by association with a charged species, typically addition of H^+,[2] Na^+,[3] or Ag^+[4] somewhere on the complex remote from the metal. This has

been used in the development of proton sponge phosphine ligands, as well as Henderson's "electrospray friendly ligands."[5] Chemically sensible corollaries, such as addition of a halide (H^-, Cl^-, Br^-, I^-) are able to generate negatively charged complexes as well.[6]

3. Another method is to inject the neutral catalytic mixture directly. If the metal center itself has an accessible oxidation potential, the capillary voltage may be sufficient to expel an electron.[7] This type of oxidation generates a cationic complex that may be detected. Intermediates would also lose an electron, but the analogy of subsequent gas phase reactivity to solution phase chemistry is poor because the metal is in a different oxidation state.

4. A fourth solution is to incorporate a charged ancillary ligand. This method has been used by Chen to study olefin metathesis,[8] and also by McIndoe for studying homogeneous hydrogenation by Wilkinson's catalyst.[9] This method leaves the metal center in a relatively undisturbed environment when properly designed,[10] but often requires considerable time investment in the design and synthesis of viable ligands.

5. A fifth option, and one that will be further explored in this chapter, is to expand on a relatively unexplored method of ionizing neutral metal compounds for catalytic studies. This method demonstrates that charged substrates may also be used, for when an ionic substrate (such as a charged alkene or alcohol) is coordinated to a metal, the substrate's charge is imparted to the entire complex. Provided that the soft ionization of ESI-MS does not disrupt the potentially weak bonds between a substrate and catalytic intermediate, ESI-MS would be ideally suited to studying such systems. The literature reports few examples of this method of ionization, mainly by Chen involving studies of ruthenium catalyzed olefin metathesis.[11] The technique however, has yet to gain widespread utility. One goal of this thesis is to show the method to be a viable alternative with advantages of simple ligand design and facile syntheses.

3.2 The Pauson-Khand reaction

The Pauson-Khand reaction was discovered in 1971 during investigations of cobalt carbonyl clusters[12] derived from the reaction of $Co_2(CO)_8$ with various organic moieties.[13] Under a high pressure of CO, an alkene, an alkyne and CO were observed to combine in a [2+2+1] cycloaddition reaction to generate a cyclopentenone ring (Equation 3-1).[14] The reaction has since found applications in natural product synthesis[15] because of the high stereoselective control and good yields.[16]

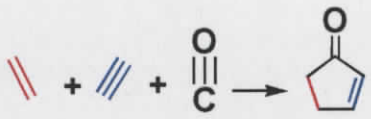

Equation 3-1

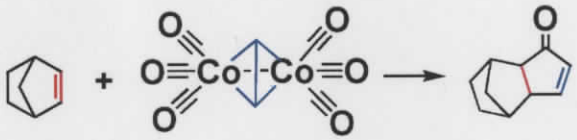

Equation 3-2

The reaction was initially developed in a stoichiometric protocol, whereby a dicobalt hexacarbonyl alkyne species is prepared in high yield, and in the presence of an alkene, the metal is oxidized away to give the cyclic product (Equation 3-2). Yields were quite poor and reaction conditions required pressures of CO and extended reaction times.[17,18] The reaction has however, evolved with a number of notable improvements:

1. Both intermolecular and intramolecular reactions are now available.
2. Activating agents such as 4-methyl morpholine N-oxide (NMO) and trimethyl amine N-oxide (TMNAO) react with a CO ligand expelling CO_2 and generating a vacant coordination site. This approach has reduced the need for high CO pressures. Other activators, mainly Lewis bases such as cyclohexylamine,[19] sulfides,[20] phosphine oxides,[21] and even water[22] have also been reported.

3. Catalytic variants have been introduced that operate under milder reaction conditions.[23] Several different metal carbonyl complexes have shown reactivity including $Ru_3(CO)_{12}$,[24] several Rh containing complexes,[25,26] $MoCp_2(CO)_4$,[27] $W(CO)_5$-THF,[28] $Fe(CO)_5$.[29,30]

4. Complexes without carbonyls have also been shown to enable the reaction, e.g. $ZrCp_2Cl_2$.[31]

5. The reaction has been performed in ionic liquids, enabling the recycling of the catalyst, making the system greener, cheaper, and more efficient.[32]

As widely used as this reaction is, there is little known about the mechanism. Magnus and co-workers have proposed the stoichiometric mechanism based solely on their observations of the unique stereospecificity of the cyclization.[33] This pathway is still widely accepted despite little to no evidence for any intermediate structures beyond the well-characterized dicobalt hexacarbonyl-alkyne structure (**2** in Scheme 3-2).[34] The catalytic mechanism (Scheme 3-2) was proposed in 1990, again with little evidence beyond analogues of **2**.[35] Another catalytic protocol used high intensity visible light and one atmosphere of CO, but these authors stressed the importance of ultra-high purity $Co_2(CO)_8$ with repeated sublimations and a very specific light source limiting its widespread utility.[36]

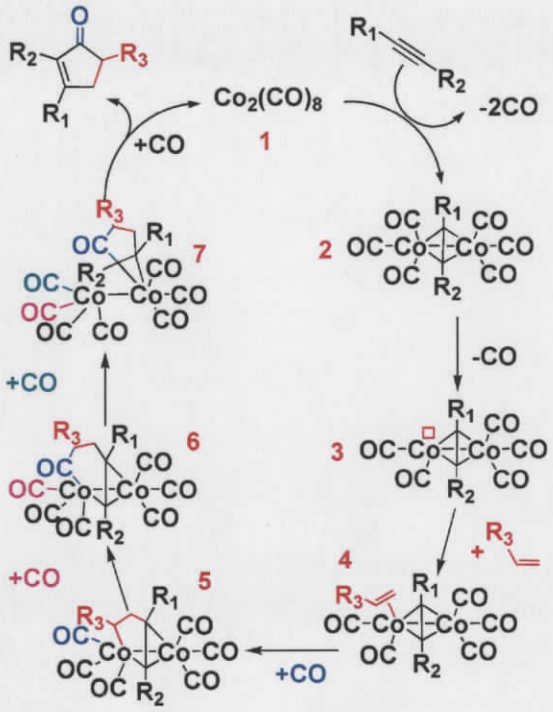

Scheme 3-2: Rautenstrauch catalytic mechanism.[35]

3.2.1 Selected studies

There are a couple of published reports that give evidence of the importance of a pentacarbonyl complex in this reaction. The first is a photochemical study with *in situ* characterization by IR spectroscopy.[37] Upon irradiation with UV light, IR bands corresponding to the pentacarbonyl species grew in. The authors note that in a nitrogen matrix, N_2 fills the vacant coordination site.

The alkene insertion reaction seems to be the step that has confounded most studies. It is the rate determining step,[38] with subsequent reactions occurring very quickly. As a result, no intermediates beyond the insertion product have been characterized, and most known studies seem to focus on controlling this particular step in an attempt to isolate the inserted product for crystallographic characterization. Towards this end, Evans employed a bisfunctionalized substrate with alkene and alkyne moieties.[39] Substrate design was strained however, and did not facilitate the subsequent insertion reaction. Even though they were able to crystallize a pentacarbonyl dicobalt-enyne complex with the alkene

filling the sixth coordination site, correspondence to an unhindered intramolecular enyne system was tenuous.

Another study employed a chiral cyclopropene complex in an intermolecular reaction with a $Co_2(CO)_6$(alkyne) complex.[40] A small amount of a dicobaltpentacarbonyl-enyne complex was collected and crystallized. Notably, the alkene had undergone the insertion reaction, but strangely the cyclopropene ring had opened. The authors propose this reactivity to be a dead end because the coordination of the chiral alkene did not occur with the required regiospecificity to generate the product (which was also collected in good yield, with the cyclopropene ring still intact). In effect, they managed to trap the inserted product down a reaction pathway that would never yield any product. This study is however a milestone towards understanding what is actually occurring in this system. When the alkene binds with a favorable orientation, then alkene insertion follows along with CO insertion and subsequent reductive elimination of the product. When the alkene binds in an unfavorable geometry, alkene insertion follows because this reaction is not dependent on the stereochemistry of the alkene, but subsequent CO insertion was prevented indicating that stereospecificity is dictated by this reaction. In order to satisfy the valencies of both cobalt atoms, the cyclopropene ring opens for anionic coordination of the third carbon atom. The complex reacts no further and can be isolated and crystallized.

Another study with evidence of pentacarbonyl complexes employed alkynes with donor atoms such as sulfur.[41,42] These donors displace one CO ligand and trap the coordination site. Complexes were characterized crystallographically and subsequently used in the stoichiometric reaction, but this system has yet to be developed into a catalytic version.

Although the Pauson-Khand reaction has been around for several decades, it appears there is just one detailed kinetic study.[43] This is a recent report employing (trimethylsilyl)-ethyne and norbornadiene (NBD). The authors used reaction progress kinetic analysis[44] to determine the rate equation shown in Equation 3-3, and two important points are immediately apparent. First of all, the alkyne does not appear in the rate equation at all. This means that the alkyne is not involved in the rate determining step, and higher concentrations of alkyne have no effect on the rate of the reaction.

Secondly, carbon monoxide appears to be a poison in the reaction. Increasing the concentration of CO decreases the reaction rate.

$$v = \frac{k[Co_2(CO)_8]^{1.3}[NBD]^{0.3-1.2}}{[CO]^{1.9}}$$

Equation 3-3

If carbon monoxide does in fact limit this system then it seems plausible that past accounts of high CO pressures are needed in conjunction with excesses of CO activators because the two effects act against each other. While a high pressure of CO would favor coordination to a metal at a vacant site, the activator would act to remove it. One known study has shown good catalytic results using an excess pressure of argon and minimal amounts of CO.[45] This study employed a rhodium based catalyst, so corollaries may not be direct, but it does suggest a possible error in past applications of high CO pressures.

3.2.2 Precedent for Pauson-Khand studies by ESI-MS

The Pauson-Khand reaction represents an ideal system for study by ESI-MS for a number of reasons:

1. It is easy to functionalize the alkyne substrate with a charge, and given the ease with which the alkyne group reacts with Co_2CO_8, it would seem reasonable to predict that a charged hexacarbonyl dicobalt-acetylene species would form easily and in good yield.[46] This represents an effective example of applying charged substrates to the task of ESI-MS of neutral metal complexes. From a synthetic perspective, charged substrates of different variations would be very simple to prepare. This gives the opportunity to study the intermolecular version by gas phase reaction with an alkene, and the intramolecular version by synthesizing a charged enyne substrate. Also, a charge may be appended to either the alkene or the alkyne separately.

2. One known study by Gimbert has been described whereby the bis(diphenylphosphino)methane (DPPM) ligand was coordinated to the phenylacetylene cluster to make $Co_2(CO)_4(DPPM)(\mu^2\text{-}C_2HC_6H_5)$. Subsequent deprotonation of the methylene carbon gave an anionic complex that could be characterized by ESI-MS.[47] This anionic compound was subjected to collisional activation with norbornene gas in the collision cell, and coordination of one alkene moiety was observed after loss of one CO ligand. This system demonstrated: a) that the Pauson-Khand reaction could be studied by ESI-MS if the system is carefully designed and b) that alkene coordination in the gas phase was possible.

3. Very little evidence has been put forth in establishing a solid mechanism beyond retrospective interpretation of product stereochemistry, creating the potential for new chemical discovery in a well documented and very useful system. The only well-characterized intermediate is the hexacarbonyl dicobalt-acetylene (**2** in Scheme 3-2) complex.[48]

4. The reaction combines three substrates, all three of which may be either gases or volatile liquids. This presents an opportunity to study the reaction by employing the previously discussed gas phase reactivity design.[47]

5. More than one catalyst has been shown to perform this reaction, thereby expanding the scope of the reaction should one metal complex prove unreactive or too difficult to study.

6. Carbonyl clusters can easily and unambiguously be characterized by ESI-MS.[49,50]

3.3 Results and Discussion

3.3.1 Design of charged substrate

Initial efforts focused on designing a library of charged ligands, which are the substrates in this system and will impart a charge to the catalyst upon coordination. Dyson has reported that alkyne functionalized imidazolium based ionic liquids are effective ligands for $Co_2(CO)_8$,[46] and this provided an early strategy for ionizing this complex. Indeed,

simply mixing a small amount of the ionic liquid methyl propargylimidazolium bis(trifluoromethyl)sulfonylamide with $Co_2(CO)_8$ in dichloromethane gave a reasonable, albeit cluttered spectrum.[a] Although this protocol has proven to be successful in obtaining high quality ESI-MS spectra of the catalyst, further study of the Pauson-Khand reaction does not seem likely. This is because a bis-functionalized derivative with both an alkene and an alkyne moiety on both imidazolium nitrogens would likely not react intramolecularly to form the cyclopentenone product simply because the reacting partners would be too far apart. Two different nitrogen based ionic liquid scaffolds were chosen based on pyrrolidine[51] and piperidine[52] because they would allow dual functionalization at the same nitrogen center (Figure 3-1).

The logic for having two different amines was to observe and compare reactivity between bisfunctionalized complexes, thereby adding credence to any similar phenomena. Also, allylpyrrolidine decolorized rapidly upon exposure to the atmosphere whereas allylpiperidine was far more stable and did not decolorize, even after several months. Both amines allowed functionalization of up to two substrates for intramolecular enyne reactivity, but were also cheap to buy, easy to handle, and sufficiently reactive, thereby easing synthetic challenges.

---

[a] See appendix 2 for spectrum of the ionic liquid methyl propargylimidazolium bis(trifluoromethyl)sulfonylamide mixed with Co_2CO_8: Appendix fig. 10 .

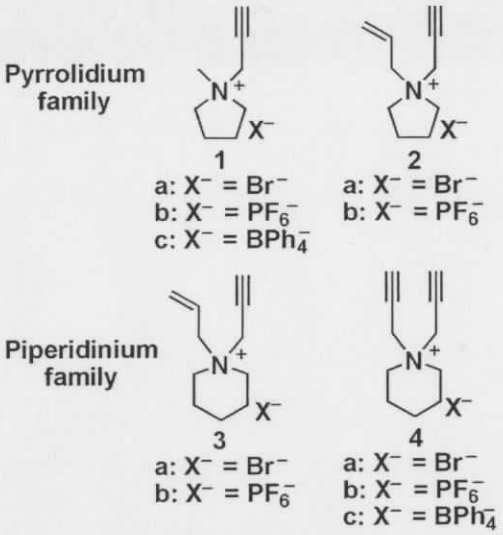

Figure 3-1: Substrate salts synthesized for studying the Pauson-Khand reaction

The synthesis of these salts was a two step process (Scheme 3-3) beginning from the tertiary amine. The amine was first reacted with one equivalent of propargyl bromide in a nucleophilic substitution reaction to generate the bromide salt. This reaction proceeded fairly smoothly in ether at room temperature. The bis-functionalized salts also underwent a preliminary reaction whereby the first functional group (either the alkene or alkyne) was added following a literature procedure.[53] The second reaction was a salt metathesis with either sodium hexafluorophosphate or sodium tetraphenylborate. All of the metatheses were performed open to the atmosphere in water, and most proceeded with respectable yields (27 % up to 87 %). The melting points of certain hexafluorophosphate salts were under 100°C, so by definition they may be classified as "room temperature ionic liquids".[b]

---

[b] A detailed description of ionic liquids may be found in the section 4.2 .

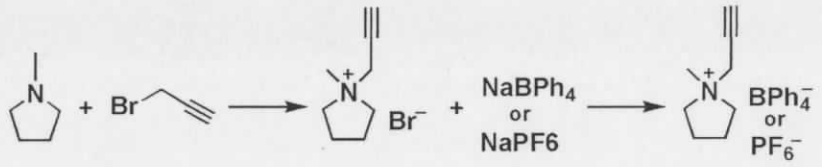

Scheme 3-3: Synthetic strategy applied to the charged acetylene substrates.

3.3.2 Synthesis of cobalt complexes

The reaction of each salt (**1b,c-4b,c**) with dicobalt octacarbonyl proceeded smoothly according to Equation 3-4 at room temperature in dichloromethane. The salts **1c** and **4c** were not particularly soluble in CH_2Cl_2, but dissolved in the presence of an excess of the metal cluster. For the synthesis of $Co_2(CO)_5$(**4b**), the reaction mixture required heat to expel the third CO ligand in a reasonable amount of time.

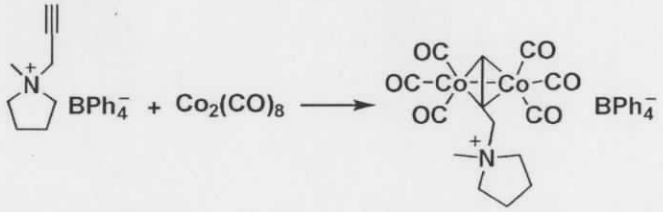

Equation 3-4: Synthetic strategy for ionizing neutral metal complexes.

High quality ESI-MS spectra were obtained for all metal complexes where the observed peak corresponded to the expected ion as exemplified in Figure 3-2.

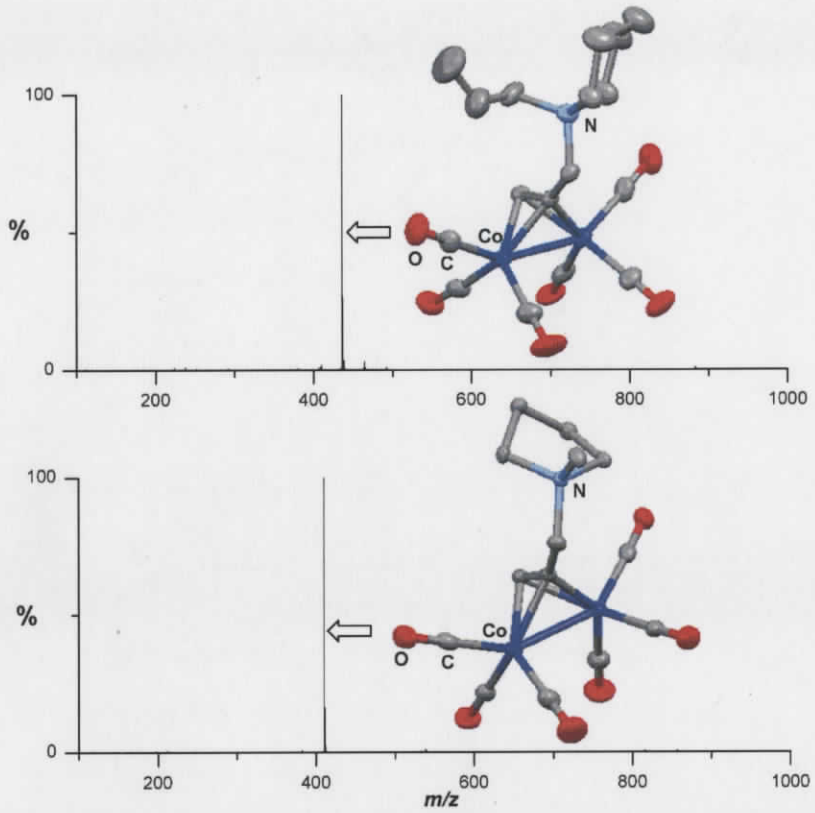

Figure 3-2: ESI-MS and crystal structure of$[Co_2(CO)_6(\mathbf{1c})]^+$ (bottom) and $[Co_2(CO)_6(\mathbf{3b})]^+$ (top).

3.3.3 Bis-functionalized complexes

The enyne complexes ($Co_2(CO)_6$(**2b** and **3b**)) designed here had the potential to form cyclic products (Figure 3-3). If the cyclic product were to appear for one enyne complex, it should also be expected for the second salt as well, because the difference between the two structures is not one that would affect substrate binding to the metal nor a catalytic cycle.

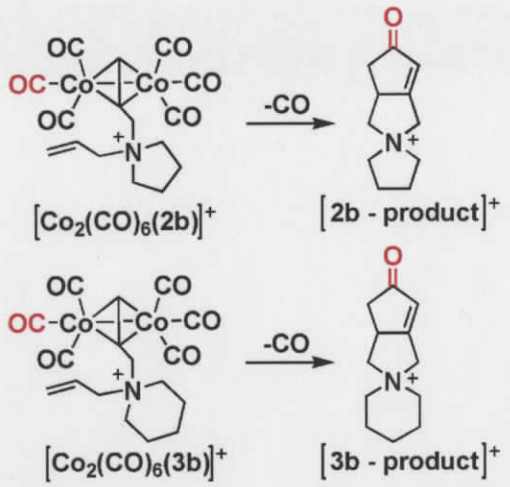

Figure 3-3: Cyclic products for both **2b** and **3b** precursors.

The reactivity of bis-alkyne compounds is less explored;[54,55] some reports of bis-alkyne complexes employing $Co_2(CO)_8$ are in the bis-cyclopentenone reaction within the same organic moiety (ie: both alkynes undergo separate *inter*molecular Pauson-Khand reactions without any *intra*molecular interference from the other alkyne).[56,57] In this system however, the alkyne groups are positioned such that they may react with each other as an alkene and alkyne, as two alkenes, or as two alkynes.

Surprisingly, it was not possible to isolate the hexacarbonyl complex $Co_2(CO)_6$(**4b**) in pure form, because even at room temperature the second alkyne moiety was sufficiently reactive to displace a third CO ligand to form the pentacarbonyl complex (Figure 3-4). The proximity of the second alkyne *did* lead to new reactivity.

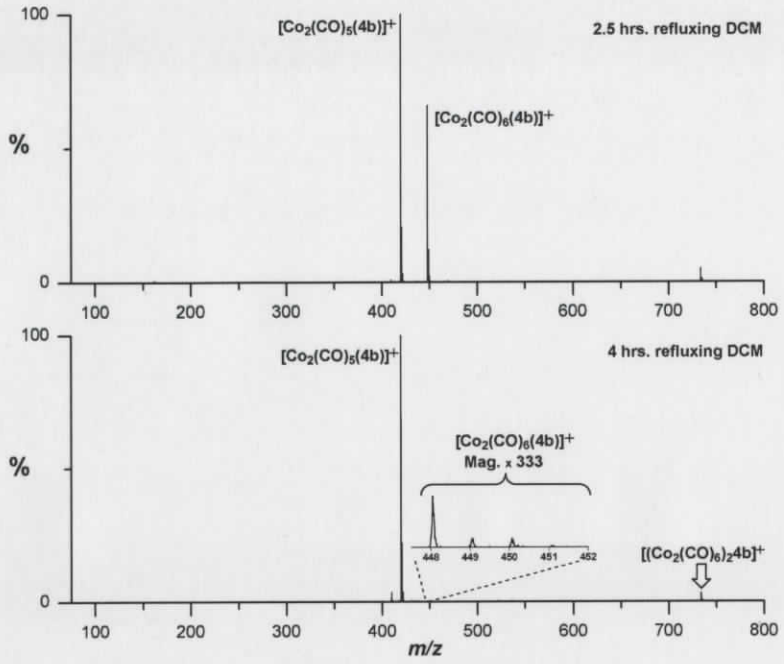

Figure 3-4: $Co_2(CO)_5$(**4b**) forms after about four hours in refluxing dichloromethane (DCM).

The occurrence of the pentacarbonyl complex $Co_2(CO)_5$(**4b**) in good yield was encouraging as it represented the possible isolation of an intermediate complex whereby a cyclic product could be reductively eliminated with the same regiochemistry of an intramolecular enyne system (Equation 3-5).[58]

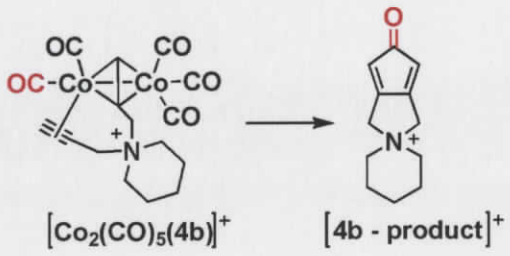

Equation 3-5: Cyclic product for the **4b** precursor.

3.3.4 IR and UV-Vis characterization

The IR spectra of all metal complexes correlated well with literature data (Table 3-1).[37] For complexes $Co_2(CO)_6$**L** (**L** = **1b**, **2b,** and **3b**) four bands were visible in the terminal bonding region. As reported for neutral enyne complexes,[59] the alkene group does not displace a CO ligand and occupy a coordination site on the metal complex. The spectrum of $Co_2(CO)_5$(**4b**) however, was slightly different as it had an additional broad absorption at 1983 cm^{-1} indicative of a bridging carbonyl ligand.[37]

Table 3-1: IR frequencies measured in cm^{-1}. All spectra run from dichloromethane. (st = strong, vs = very strong, m = medium, sh = shoulder)

Complex	Terminal CO	Bridging CO
$Co_2(CO)_6$(**1b**)	2105 (st), 2067 (vs), 2045 (vs), 2027 (sh)	–
$Co_2(CO)_6$(**2b**)	2105(st), 2067 (vs), 2045 (vs), 2034 (sh)	–
$Co_2(CO)_6$(**3b**)	2105 (st), 2066 (vs), 2045 (vs), 2033 (sh)	–
$Co_2(CO)_5$(**4b**)	2099 (st), 2066 (m), 2044 (vs), 2027 (sh)	1983 (st, broad)

The UV-Vis spectra of the four metal complexes were also collected as it was noted that in the solid phase, the powders were different shades of red. The spectra of complexes $Co_2(CO)_6$(**1b, 2b,** and **3b**) were quite similar (Figure 3-5) to each other; peaks have been tabulated for comparison (Table 3-2). Complex $Co_2(CO)_5$(**4b**) however, had a blue shift of the peak in the visible region and the notable lack of a peak in the region of 360 nm. This evidence does not confirm or refute the coordination of the second alkyne moiety to the metal complex in place of a CO ligand, but supports the notion that the second alkyne group is not simply an innocent spectator ligand, it is somehow altering the solution phase chemistry of this complex.

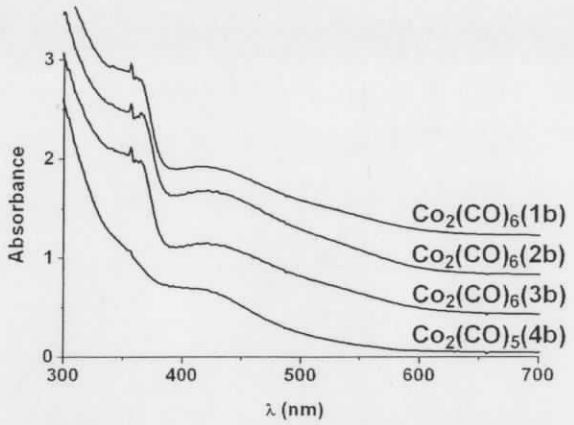

Figure 3-5: UV-Vis spectra for cobalt complexes

Table 3-2: UV-Vis peaks for cobalt complexes.

Complex	UV-Vis Absorbancies (nm)
$Co_2(CO)_6$(**1b**)	356, 364, 421
$Co_2(CO)_6$(**2b**)	356, 365, 421
$Co_2(CO)_6$(**3b**)	356, 364, 421
$Co_2(CO)_5$(**4b**)	405

3.3.5 Probing the intermolecular system by ESI-MS

A first experiment was to examine the EDESI-MS spectrum of $Co_2(CO)_6$(**1b**) in the absence of any reactive gas (Figure 3-6). The spectrum is more complicated than those of the tetraruthenium trihydrido dodecacarbonyl system, but this is unsurprising because the alkyne ligand ($[\mathbf{1b}]^+$) is much more likely to participate in side reactions than carbon monoxide or hydride ligands. Some obvious features are present. Loss of six carbon monoxide ligands occurs at a relatively low cone voltage and is complete at approximately 35 V. The ligand also begins to appear at relatively low voltages, below 25 V. The complexity observed at higher cone voltages is the result of a multitude of different fragmentation processes. The Co-Co bond can break to make a $[Co(CO)_x(\mathbf{1b})]^+$ complex; the $N\text{-}CH_{2\ (propargyl)}$ also breaks to give the methyl pyrrolidinium ion or $[Co_x(CO)_nC_3H_3]^+$ ions; C-H activation of the pyrrolidinium ring is also apparent at higher energies as discussed in section 2.6.1. This spectrum is essentially a baseline to which future gas phase experiments may be compared.

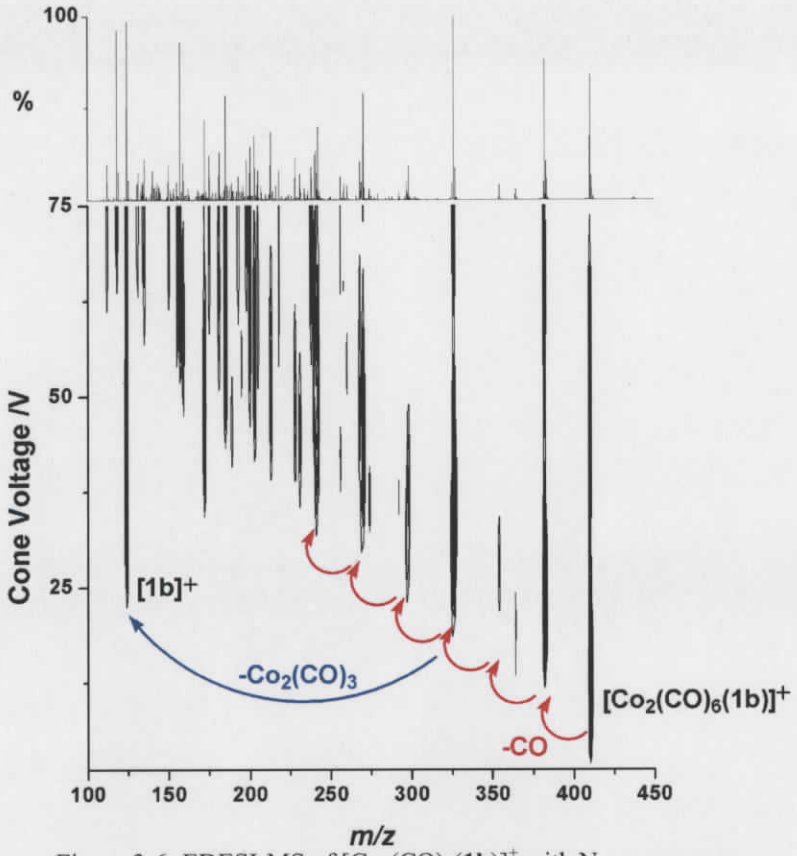

Figure 3-6: EDESI-MS of $[Co_2(CO)_6(\mathbf{1b})]^+$ with N_2 as cone gas.

3.3.5.1 Probing alkene coordination

CO removal by CID allows for the facile generation of intermediate **3** (Scheme 3-2), namely the $[Co_2(CO)_5(\mathbf{1b})]^+$ complex. This structure is proposed to add an alkene in the next step of the catalytic reaction. Performing gas phase reactivity on the hexacarbonyl complex as described in section 2.3 employing alkenes as the reactive partner revealed coordination of an alkene after loss of one carbon monoxide group. Shown in Figure 3-7 is the reaction of $[Co_2(CO)_6(\mathbf{1b})]^+$ with cyclopentene. It is apparent that at cone voltages below 25 V, the alkene adds to the metal complex. This is an important observation and is in keeping with the literature proposal for alkene coordination.[14] From the MS/MS spectrum, it can be seen that the alkene is the first fragment lost, suggesting that the subsequent insertion into the Co-$C_{(alkyne)}$ bond has not occurred, or at least that it is an easily reversible reaction.

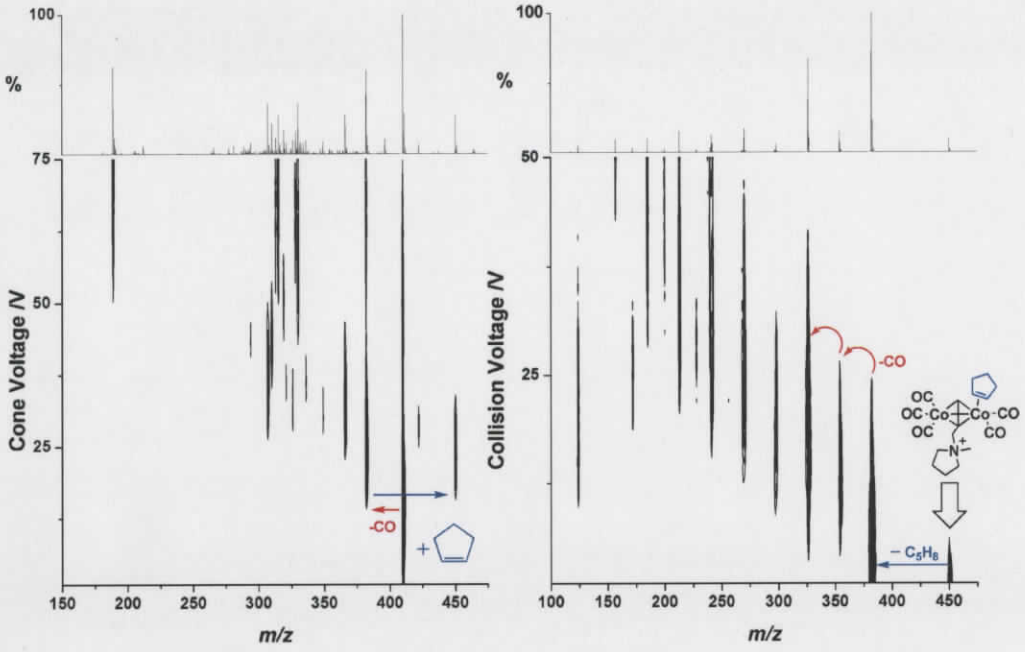

Figure 3-7: (Left) EDESI-MS contour plot of the reaction of $[Co_2(CO)_6(\mathbf{1b})]^+$ with cyclopentene gas. (Right) MS/MS spectrum of the only product ion showing that the alkene is the first fragment to fall off the complex. This suggests it has not undergone the insertion reaction yet.

It is not possible from this analysis to determine where on the metal complex the alkene has coordinated, so it is possible that it is not positioned very close to C2 (Figure 3-8), thereby inhibiting subsequent insertion. In Figure 3-8, alkene coordination to positions 1 or 2 could lead to an insertion into the Co-C1 bond. The regiochemical control of this reaction dictates that this is the bond that undergoes insertion and not the Co-C2 bond. Based on the positioning of the pyrrolidinium group, position 1 should also be sterically favored over 2. Alkene insertion after coordination to position 3 would require first a redistribution of ligands in order to facilitate insertion into Co-C1. Position 3 would perhaps favor coordination over 1 and 2 on steric grounds, because of proximity of the pyrrollidinium moiety. One report suggests that a trans effect favors loss of CO from position 3, implicating an electronic component to this dissociation in solution[60] and supporting the notion that this is potentially the location of the vacant site.

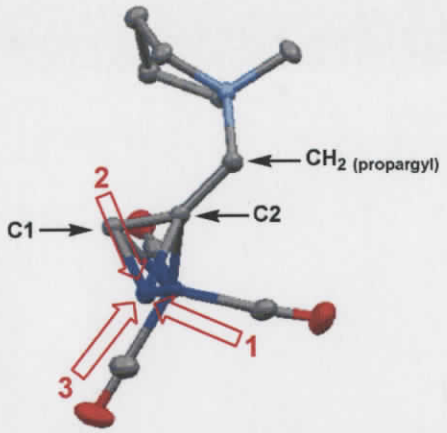

Figure 3-8: Illustration of the three possible coordination sites after loss of one CO from the hexacarbonyl precursor. The three CO groups on this Co atom have been removed for clarity.

The reactivity of other alkenes was also probed. Strained alkenes (such as cyclopentene) are known to react preferentially in the Pauson-Khand reaction, and this has been attributed to a lower energy LUMO.[38] Back donation from the metal *d*-orbitals into the alkene LUMO was a critical aspect of metallacycle formation (which is also the alkene insertion reaction). Those alkenes with more accessible LUMOs were more reactive. Estimates of reactivity can be made by considering the C=C–C bond angles. Cyclohexene, with an angle of 128° is sluggish to react, but both norbornene (107°) and cyclopentene (112°) are more reactive.[16c]

Alkenes activated by electron withdrawing groups also show good reactivity,[61] so a comparison of the reactivity of the cyclopentene system with both 1-hexene (an unstrained alkene) and 2,3-dihydrofuran (a strained and electronically activated alkene) was performed.[c] Their spectra are comparable to the cyclopentene system, and Figure 3-9 shows that at a cone voltage of only 20 V, coordination of an alkene occurs to *approximately* the same extent in the gas phase. Although it was expected that different reactivity would be observed, the similarities between these alkenes may simply be

---

[c] The respective EDESI-MS spectra of the gas phase reactions are included in appendix 2: Appendix fig. 11.

explained by the fact that alkene coordination is independent of the subsequent insertion reaction. As soon as a CO ligand dissociates, alkene coordination would occur regardless of strain or electronic effects. It is the insertion reaction that is rate determining and therefore it is this step that dictates the necessity for strain or electronic activation.

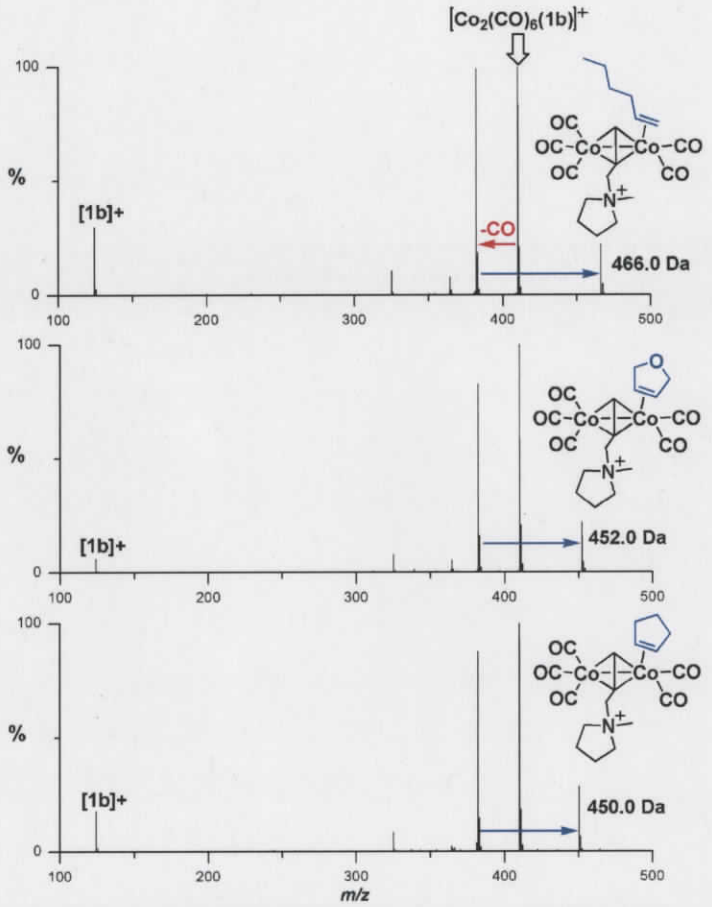

Figure 3-9: Gas phase reaction of $[Co_2(CO)_6(\mathbf{1b})]^+$ with three different alkenes at a cone voltage of 20 V.

The alkene coordination can be further investigated by analyzing the breakdown plots of the first products of each of these reactions. These graphs are generated by plotting the percent of each ion's ion-current with respect to the TIC (total ion current) of the spectrum at each cone voltage value. In such a way, the occurrence of an ion can be distinguished as either a fragment that occurs in the gas phase, or as a solution species whose appearance does not depend on any gas phase phenomena. If a species is a result

of a gas phase reaction, then it would be expected to be entirely absent at very low voltages, then to grow in as the appropriate collision voltage for that reaction is optimized and subsequently disappear when energies have surpassed the optimal range of reaction. If a species is present in solution at the start of the experiment, then its % TIC would be consistent throughout the EDESI-MS experiment (ie: it would look like a straight line instead of a curve).

From the breakdown plots (Figure 3-10), all three alkene adducts grow in at the same time as the pentacarbonyl complex, which is a strong suggestion that the alkene adduct reacts specifically with the pentacarbonyl complex, and not with the hexacarbonyl complex followed by CO loss. These breakdown plots cannot be compared quantitatively to each other however, because the reactivity depends on the concentration of the alkene in the gas phase, and the alkene concentration depends upon their volatilities. Cyclopentene is the most volatile (b.p. 45°C) followed by 2,3-dihydrofuran (54°C) then 1-hexene (63°C). While all gases are vaporized at room temperature with a stream of nitrogen gas, it is expected that a different amount of each gas will be available for reaction at the source, and this may explain why the intensities are different at room temperature.

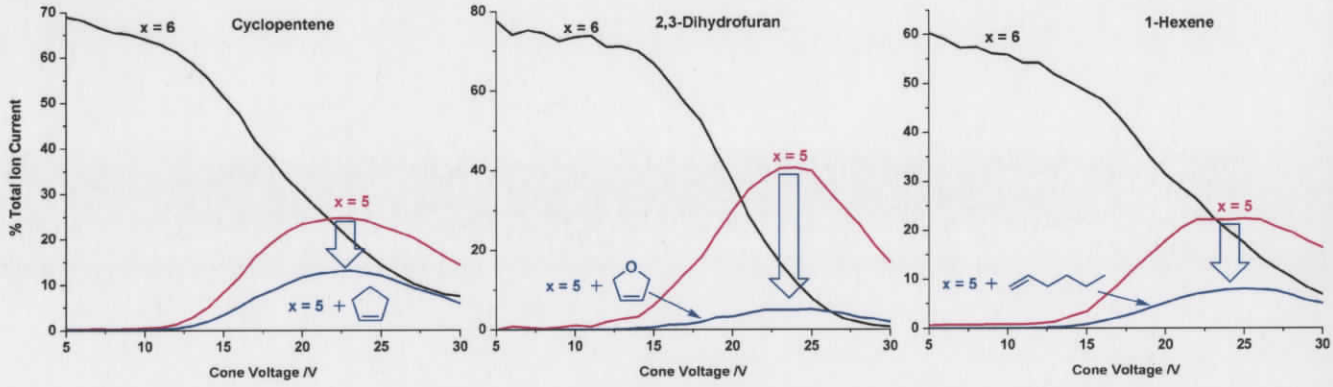

Figure 3-10: Breakdown plots of the gas phase reaction of $[Co_2(CO)_x(\mathbf{1b})]^+$ with three alkenes. The alkene adduct grows in at the same time that the pentacarbonyl complex is formed.

Under the very high CO pressures that this solution phase reaction is normally conducted under, the alkene insertion into the Co-alkyne bond is likely in competition with alkene dissociation and re-coordination of CO to regenerate the hexacarbonyl complex. It stands to reason that at these pressures, and considering that CO is a much better ligand for zero-valent metal clusters than alkenes,[62] the equilibrium for this occurrence would likely favor the hexacarbonyl complex. This may also explain why alkene dissociation is the first occurrence in the MS/MS spectra, without any trace of CO loss from this complex for all three alkenes (Figure 3-11).[d]

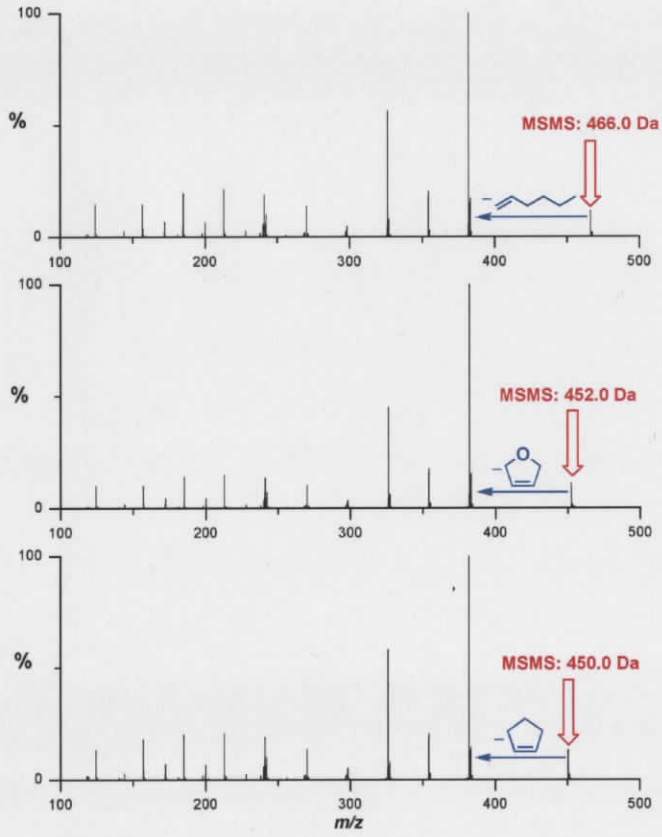

Figure 3-11: Combined spectra from the MS/MS experiments from the gas phase reactions of $[Co_2(CO)_6(\mathbf{1b})]^+$ with three alkene gases.

[d] EDESI-MS and MS/MS spectra of reactions with 2,3-dihydrofuran (Appendix fig. 13) and 1-hexene (Appendix fig. 14) are in appendix 2.

In Gimbert's ESI-MS gas phase experiment,[47] they reported that the most energetically demanding step was loss of CO from the hexacarbonyl complex, and that subsequent alkene coordination, alkene insertion, and CO insertion should occur rapidly. Upon this argument they tested for gas phase reactivity between $[Co_2(CO)_4DPPM]^-$ and norbornene, but no other alkenes. The results presented in this chapter suggest that alkene coordination is not as discriminating as may have been previously presumed.

3.3.5.2 The role of cyclohexylamine

The effects of activating agents in the catalytic Pauson-Khand reaction have been investigated.[63] Several hard bases have been tried including amine oxides,[64] phosphine oxides,[65] and sulfoxides.[66] Cyclohexylamine is another activator which has an accessible boiling point allowing the study of this reaction in the gas phase.[19] Although the boiling point of this amine is rather high (134°C), results from the gas phase reaction showed that a sufficient amount could be vaporized and coordinated to the metal complex at a cone voltage of 25 V (Figure 3-12).

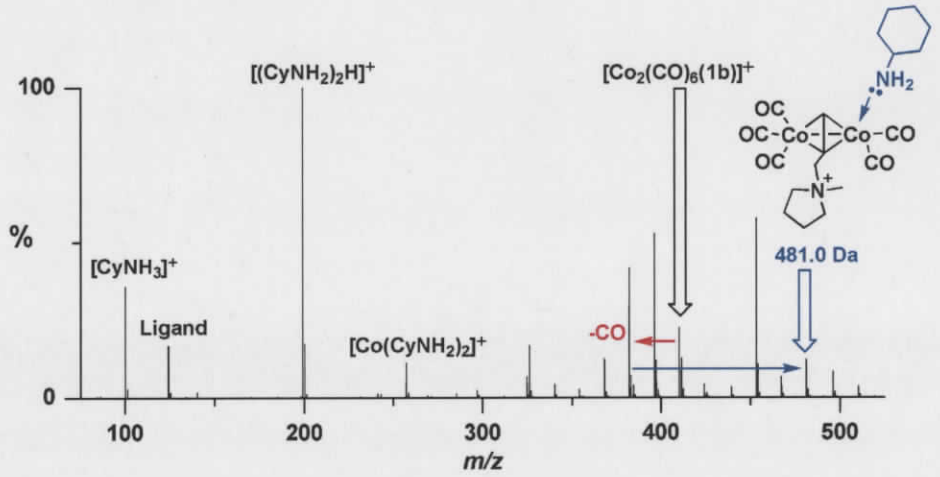

Figure 3-12: Spectrum of the gas phase reaction of $[Co_2(CO)_6(\mathbf{1b})]^+$ with cyclohexylamine (cone voltage = 25 V). See Figure 3-13 for further interpretation of this system.

This spectrum is complicated, but it is a result of several overlapping series. It is known that amines are very effective at decomposing cobalt carbonyl complexes through

disproportionation;[67] for example, treatment of $Co_2(CO)_8$ with excess NRH_2 rapidly produces $[Co(NRH_2)_6][Co(CO)_4]_2$.

An important point is that the complexity of Figure 3-12 appears at a relatively low cone voltage of 25 V, which is not so high as to remove several CO ligands and generate multiple coordination sites. A protonation reaction has occurred to protonate the amine, which then aggregates with a neutral amine to generate the base peak $[(CyNH_2)_2H]^+$. Also present are the free ligand and a single cobalt(I) ion with two coordinated amines $[Co(CyNH_2)_2H]^+$, which may be a precursor to the cation of the disproportionation reaction.[67] Elucidation of this spectrum can only be done by MS/MS, but the effect of this bulky amine appears rather quickly (Figure 3-13). Once the amine coordinates, it effectively promotes CO loss from the complex. It may further activate C-H bonds on its cyclohexyl group, with loss of H_2, to fill any of those coordination sites should they not otherwise be filled with another amine (as in the case of peaks at 496 *m/z* and 510 *m/z*). In essence, it appears that the role of the amine is to function as a bulky ligand and to free up some coordination sites. MS/MS spectra (Figure 3-13) of various ions seen in Figure 3-12 show that each peak can be accounted for by juggling the number of cyclohexylamine units that have coordinated and the number of CO ligands that it has subsequently displaced.

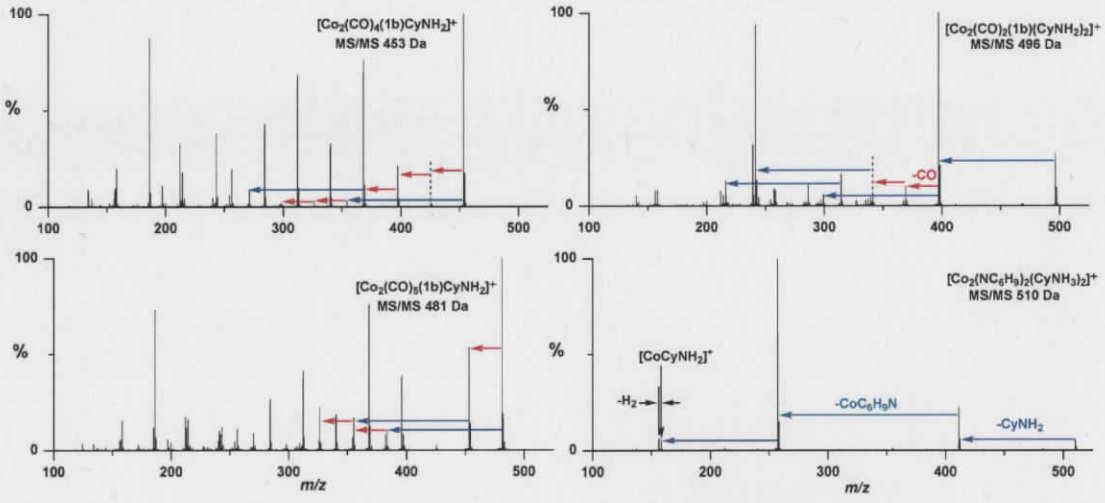

Figure 3-13: MS/MS of selected peaks in the gas phase reaction with cyclohexylamine.

3.3.6 Probing the intramolecular system by ESI-MS

Following the same methodology as for the intermolecular system, a first experiment was to simply look at the EDESI-MS spectra (Figure 3-14). These are very complicated spectra, so the MS/MS spectrum of the precursor ions are also shown.[e] Fragmentation is dominated by loss of CO with the ligand appearing at a cone voltage of about 20 V. At slightly higher energies, the $N\text{-}CH_{2\ (propargyl)}$ activation is present, consistent with the $Co_2(CO)_6$(**1b**) system.

Complexes $Co_2(CO)_6$(**2b** and **3b**) have the ability to form intramolecular product ions (recall Figure 3-3), so their appearance would be an important observation. From the insets of the EDESI-MS plots we see that they are both present (Figure 3-14).[f, g] This is a point of interest because both complexes have all the elements of intermediate **5** (Scheme 3-2): they are both hexacarbonyls, and they both possess the alkene and alkyne functional groups. As reported in the literature: "once the acetylene complex forms in the reaction mixture, it goes immediately to the product without any trace of observable intermediates."[68] It seems however that it is not possible for a CO ligand to insert into the Co-C1 bond of the alkyne (Figure 3-8) *before* alkene coordination. This is further confirmed by the MS/MS of $Co_2(CO)_6$(**2b** and **3b**), and the absence of product in both spectra (inset of EDESI-MS/MS: Figure 3-14). The alkene coordination must occur before any CO insertion, by way of a less carbonylated intermediate ($Co_2(CO)_n$(**2b** and **3b**) where $n \leq 5$). This is not an unusual result; these intramolecular systems commonly employ one of a variety of activating agents, suggesting that product formation from enyne complexes is more complicated than simply reductively eliminating a product by whatever means allows it to occur.

---

[e] The EDESI-MS and MS/MS spectra of $[Co_2(CO)_6(\mathbf{2b})]^+$ can be found in appendix 2: Appendix fig. 16.

[f] Only the first 30 spectra are summed in these insets because there is only a trace amount forming, and the baseline noise resulting from higher energies collisions (CV > 50) overwhelms the quality of products **2b** and **3b** from the lower energies.

[g] $Co_2(CO)_6$(**2b**) is in appendix 2: Appendix fig. 17.

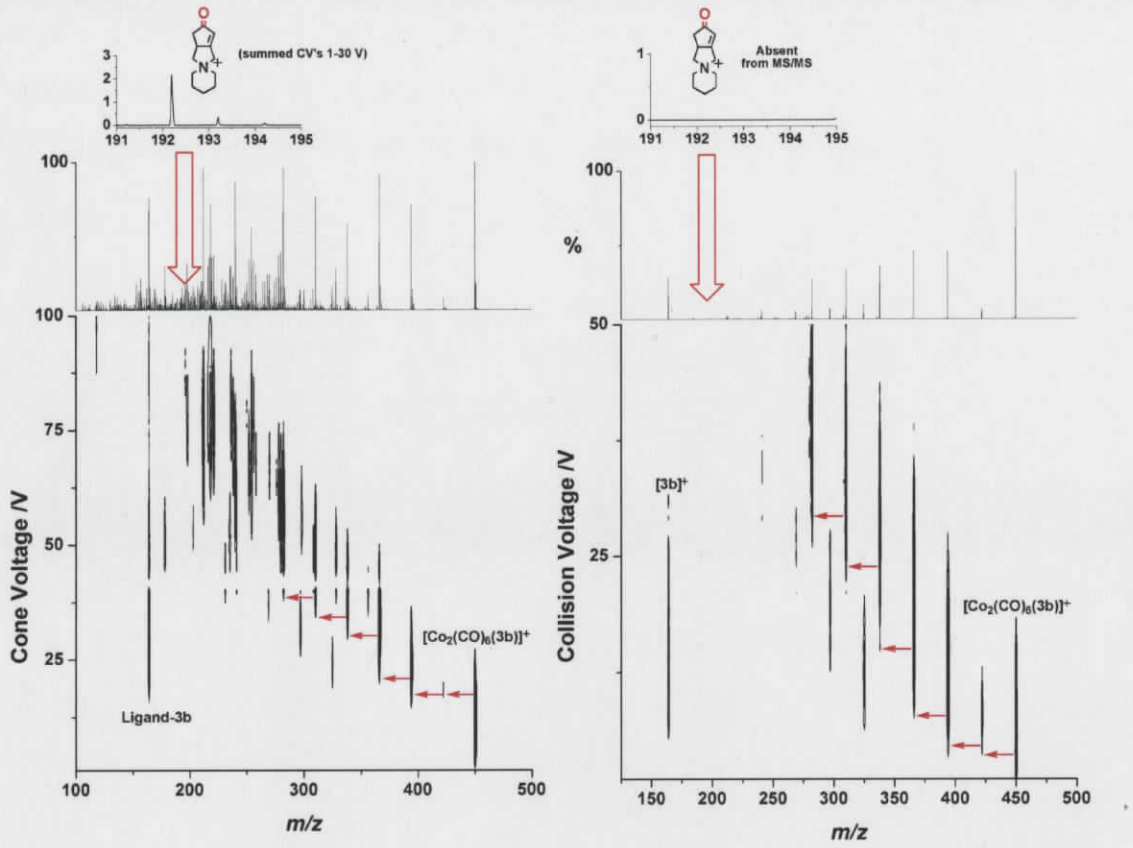

Figure 3-14: (Left) EDESI-MS of $Co_2(CO)_6$(**3b**). Inset shows product formation at low cone voltages. (Right) MS/MS spectrum of $Co_2(CO)_6$(**3b**). Inset shows no cyclic product is observed from the parent ion.

If lower coordinate complexes are indeed product-eliminating species in this reaction, then it is possible that the observed product may be forming as a result of reductive elimination from the pentacarbonyl complex (or even lower coordinate derivatives). This can only be confirmed upon analysis of their respective MS/MS spectra. Shown in Figure 3-15 are the summed MS/MS spectra of the x = 5,4,3 derivatives of the cobalt complexes. Again there is no apparent sign of product elimination from any of these intermediates.

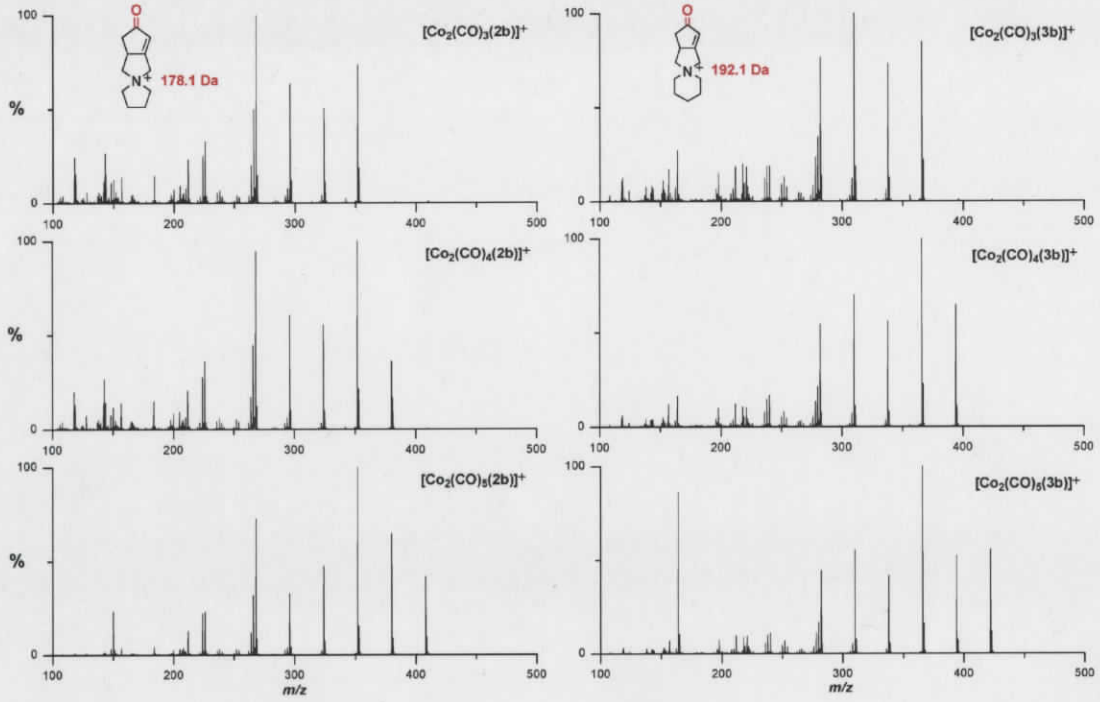

Figure 3-15: MS/MS spectra of tri,tetra, and pentacarbonyl derivatives of both $Co_2(CO)_x$(**2b** and **3b**). No product is observed to form from either complex.

To consider the Rautenstrauch mechanism again (Scheme 3-2), each insertion reaction occurs with coordination of CO. In these MS/MS spectra, there is no re-coordination of any ligand concurrent with fragmentation. Hence a lack of product elimination in these spectra, although not proof that Rautenstrauch is correct, is at least consistent with their proposal. If ligand re-coordination to the metal center is an essential factor in driving this reaction forward to product elimination, then it seems reasonable that alkenes and amines might function to stabilize the complex as substitutes for CO. This suggestion has precedent from the fact that higher alkene concentrations increase the reaction rate (Equation 3-3),[43] and that cyclohexylamine is an effective activator.[19]

3.3.7 Probing reactivities with coordinating substrates

The motivation for gas phase reactivity this time was slightly different than for the intermolecular system. Instead of looking for a reaction with a substrate, the interest was in addressing the stability of the metal complex. The reactive gas in this case would

function to fill vacant coordination sites, maintaining an 18 electron count on each metal, and presumably enhancing the insertion reactions. Upon reaction with an alkene in the gas phase however, neither $Co_2(CO)_6$(**2b** or **3b**) adds an alkene nor cyclohexylamine to the pentacarbonyl intermediate as did $Co_2(CO)_6$(**1b**). Shown in Figure 3-16 is the summed *m/z* spectra of the gas phase reactions of $Co_2(CO)_6$(**3b**) with the cyclopentene and the cyclohexylamine. The insets of Figure 3-16 show that no peaks have grown in where they were expected in the reaction with the pentacarbonyl complex.[h] The lack of coordination suggests there is no site for the ligand to coordinate, which implies then that the alkene is filling the vacant coordination site and has not yet inserted. Perhaps this is unsurprising since the same trend was observed for the intermolecular system; the MS/MS of $Co_2(CO)_6$(**1b**)(alkene) lost the alkene first before losing any CO's.

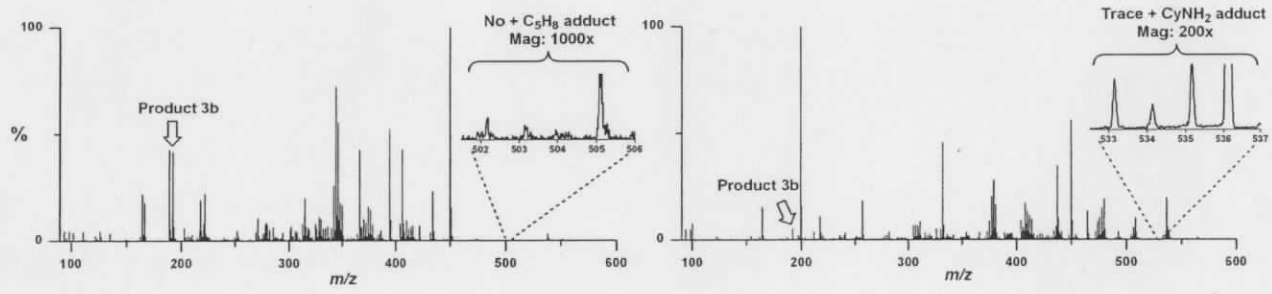

Figure 3-16: The summed EDESI spectrum of the gas phase reactions of $Co_2(CO)_6$(**3b**) with cyclopentene (left) and cyclohexylamine (right). No coordination of either species occurs upon loss of a CO ligand from the parent compound.

Here again though, the cyclic product ions were observed in both systems. In an attempt to approach the occurrence of this product from another perspective, the breakdown plots of the EDESI-MS spectra were analyzed upon collision with nitrogen, cyclopentene, and cyclohexylamine (Figure 3-17). For all three gas phase reactions, the product ion appears at very low cone voltages, and lasts throughout the entire experiment; it maintains a relatively straight line over all cone voltages, which implies that it is *not* a product of fragmentation from the metal complex. Two conclusions can be drawn from these

---

[h] This is consistent with $Co_2(CO)_6$(**2b**), shown in the appendix 2: Appendix fig. 18.

graphs: 1) nitrogen (N_2) coordinates the metal in place of CO and in preferance to cyclopentene and cyclohexylamine. This occurrence has been observed by IR in the UV[37] light activated system,[i] but would be undetectable by ESI-MS because both CO and N_2 have a nominal mass of 28 Da. 2) The product is a genuine ion in solution, not the result of a gas phase reaction.

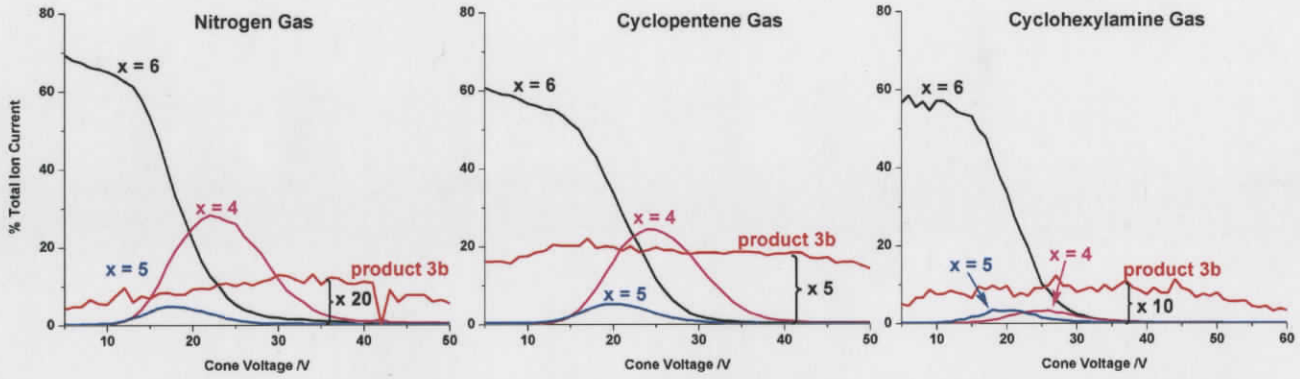

Figure 3-17: Breakdown plots of $[Co_2(CO)_x(\mathbf{3b})]^+$ from EDESI experiments with nitrogen, cyclopentene, and cyclohexylamine.

It is the latter of these conclusions that is most reasonable as it is unlikely that nitrogen would be sufficiently reactive to fill the vacant site. Although the solution phase occurrence of the product ions is somewhat unfortunate in the search for the active catalytic species, it presents the opportunity to study this system employing standard solution phase techniques. It is also confirmation that cyclization is not affected by the proximity of the positively charged ammonium center. Because all components necessary for product formation are present in the molecule, it is possible to track the occurrence of product over time with periodic sampling, and this will constitute an important part of future work for this system. Even if the product only forms in tiny amounts, as shown here, it will still be possible to track its evolution.

---

[i] This UV activated study required temperatures of 12 K, and the solvent was either liquid nitrogen or liquid argon. Upon irradiation, nitrogen coordinated the vacant position of the pentacarbonyl complexes, but argon did not.

3.3.8 The bis-alkyne system

The reactivity and behavior of the bis-alkyne complex $Co_2(CO)_5$(**4b**) was also worth addressing in a similar manner to the above systems. To confirm first that the pentacarbonyl complex is a genuine solution phase species and not the product of gas phase fragmentation, the breakdown plot must be considered. This is similar to previous structures of neutral bis-alkynyl amines in which a third CO ligand was displaced by a second alkyne group.[69] From Figure 3-18 the pentacarbonyl complex clearly disappears with the appearance of lower carbonylated intermediates. This is a good indication that $Co_2(CO)_5$(**4b**) exists in solution, complementing the IR data for this complex.

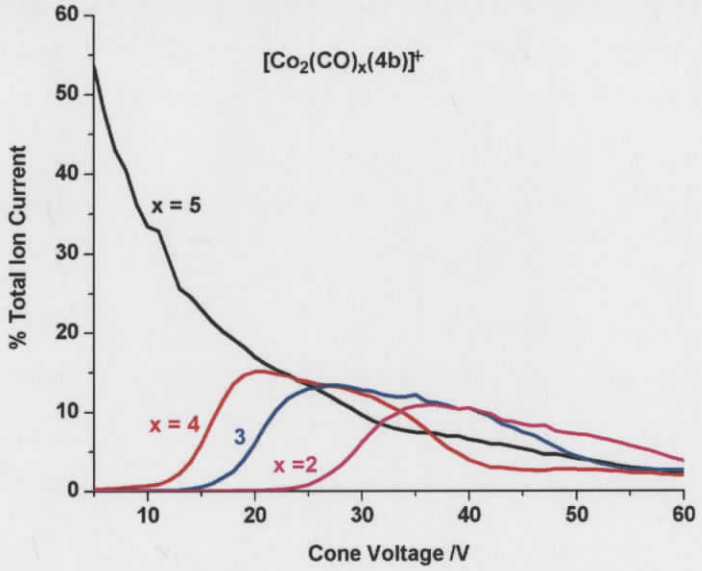

Figure 3-18: Breakdown plot of $[Co_2(CO)_5$(**4b**)$]^+$ showing that the occurrence of the pentacarbonyl complex is not a phenomenon of collision in the gas phase, but is rather a genuine and isolable complex in solution.

The EDESI-MS spectrum for $[Co_2(CO)_5$(**4b**)$]^+$ is a little different than for the previous complexes (Figure 3-19). There is an absence of ligand **4b** at low cone voltage which suggests the double coordination of the two alkyne ligands strengthens its attachment to the metal complex. The MS/MS spectrum of the parent complex is much simpler than for the hexacarbonyl complexes of **1b**, **2b**, and **3b**. Fragmentation is dominated entirely by loss of CO; notably absent is the N-CH_2 activation further suggesting the alkyne groups somehow reinforce their binding.

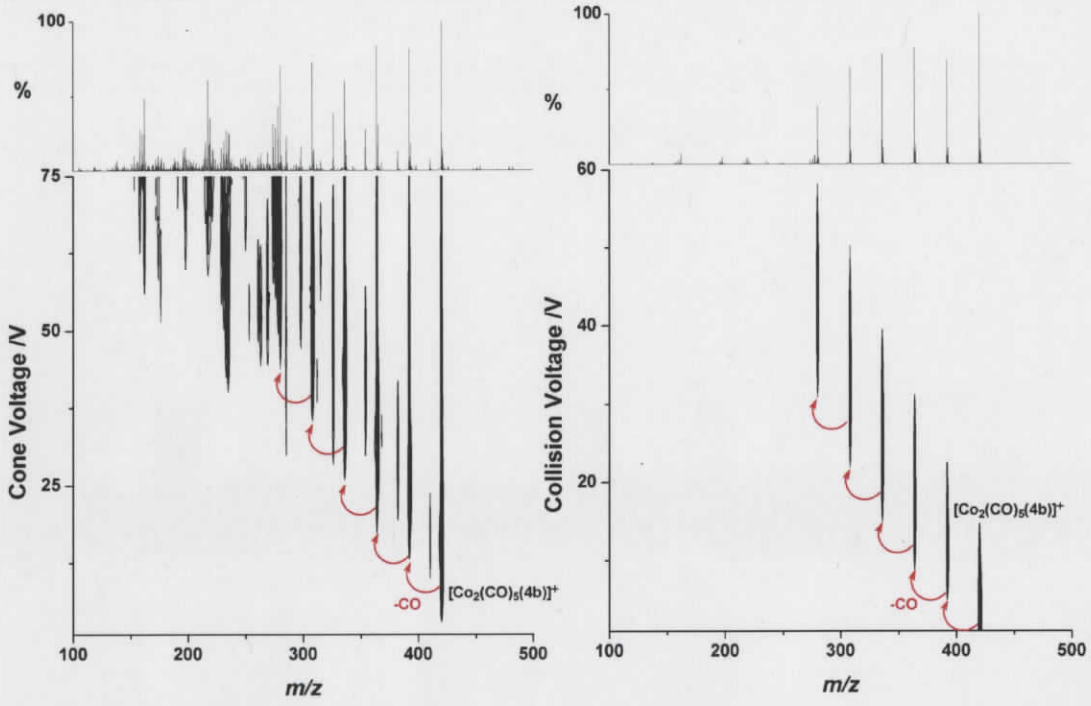

Figure 3-19: (Left) EDESI-MS spectrum of $[Co_2(CO)_5(\mathbf{4b})]^+$. (Right) MS/MS spectrum of $[Co_2(CO)_5(\mathbf{4b})]^+$.

Crystallization of this pentacarbonyl complex was attempted, but the only product that crystallized was the bis(hexacarbonyldicobalt) bispropargylpiperidinium hexafluorophosphate complex shown in Figure 3-20. Analogous compounds of bis-alkynyl amines have been reported in the literature with little subsequent work.[70] Along with these crystals, a brown powder formed at the bottom of each tube, hinting at some form of decomposition product. This complex is in relatively low concentration in solution (Figure 3-4), so its preferential crystallization may be a result of CO liberated from the decomposition products, that re-coordinates another pentacarbonyl complex (generating the hexacarbonyl complex), and with some ligand redistribution, forms the more crystalline product that was isolated.

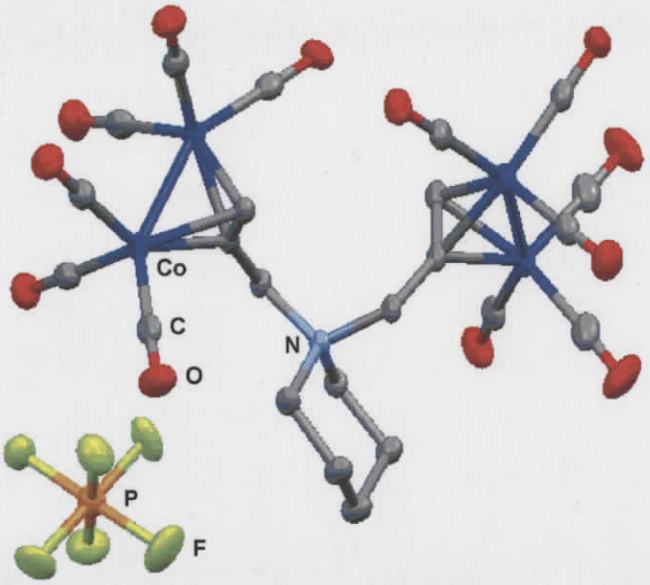

Figure 3-20: Crystal structure of $\{Co_2(CO)_6\}_2$**4b**, obtained from the attempted crystallization of $Co_2(CO)_5$(**4b**).

The gas phase reactions of $Co_2(CO)_5$(**4b**) with cyclopentene and cyclohexylamine were uneventful (appendix 2). There was no trace of cyclic product **4b** (Equation 3-5) at 190 *m/z*. Higher energy collisions gave a very strong signal at 189 *m/z*, but this was not reasonably assigned and was presumed to be the result of some higher energy gas phase reactions. One equivalent of cyclopentene adds to the metal complex after loss of two CO ligands generating $[Co_2(CO)_3$(**4b**)$C_5H_8]^+$, maintaining an 18 electron count on each cobalt center. Probing the solution phase chemistry in the presence of activators will also be important.

3.4 Future Work

The Pauson-Khand reaction is a very difficult system to study and has to date received limited attention by ESI-MS analysis. This study supplements one other report where ESI-MS was used or proved critical to the understanding of the chemistry at hand.[47] This work goes further though, in showing that by carefully designing the system to carry a charge on the substrate, meaningful data may be obtained that correlates closely with the more ubiquitous neutral system.

One experiment that would reveal a great deal of information is to perform a gas phase reaction between $Co_2(CO)_6$(**1b**) and an alkene at the source, but this time with CO as the collision gas in the collision cell, instead of argon. This experiment was tried once on this mass spectrometer, but it led to the unexpected venting of the instrument. If this experiment is instead performed on a triple quad or ion trap mass spectrometer, CO may be better tolerated.[71] Furthermore, ion trap instruments provide a time domain, allowing the potential for kinetic studies in the gas phase.

There is a great deal of potential for studying both inter- and intramolecular Pauson-Khand reactions. One of the most important things to be explored is the reactivity of the alkene. As mentioned previously, alkene reactivity can be related to C=C-C bond angles, and highly strained cyclopropene (64°)[72] has proven to be a very reactive partner for this reaction.[73] The alkene is so reactive that it is generally made *in situ*, and proceeds to completion. It may therefore be possible to investigate the gas phase reactivity of $Co_2(CO)_6$(**1b**) with cyclopropene by attaching the cone gas line to a flask where the alkene forms from solution. Given the higher degree of strain in cyclopropene as compared to cyclopentene, it may be more reactive in the gas phase, and in such a manner, it may be possible to identify the inserted product by MS/MS of $[Co_2(CO)_x(\mathbf{1b})C_3H_4]^+$ species (x = 1-6).

The enyne systems with both $Co_2(CO)_6$(**2b** and **3b**), demonstrated that the cyclization reaction can occur in solution. This raises the potential of studying the formation of product over time, concurrent with the disappearance of starting material; hence rate information may be obtained to supplement the only published kinetics study.[43] Also, the reactivity of the alkene in this system may be increased by introducing strain. Instead of employing a linear alkene, a cyclopentene, cyclobutene, or cyclopropene ring may destabilize the LUMO sufficiently in order to again observe the gas phase elimination of a product ion in an MS/MS experiment. This process will require some synthetic initiative, but so long as the system is carefully designed it is reasonable to expect that useful insights may be gained.

The new chemistry of the $Co_2(CO)_5$(**4b**) complex will also need to be explored. An important goal will be to crystallographically characterize the complex as this will give

insight into how the second alkyne moiety is coordinating the metal centre. Furthermore, the solution phase chemistry will require investigation to determine what manner of cyclization the complex undergoes, and if it is indeed as described in Equation 3-5.

Charged alkyne substrates seem to be rather effective in the goal of appending a charge to otherwise neutral metal complexes. Salts **1b** and **4b** may also be worthy of study in other catalytic reactions employing alkenes or alkynes.

3.5 Experimental

All solvents were dispensed from an MBRAUN solvent purification system and used within minutes. Inert atmosphere techniques were used for all syntheses involving $Co_2(CO)_8$. Methyl pyrrolidine, pyrrolidine, piperidine, allyl bromide, propargyl bromide, sodium hexafluorophosphate, sodium tetraphenylborate, sodium hydride, sodium chloride, sodium hydroxide, and dicobalt octacarbonyl were purchased from Aldrich and used without subsequent purification. UV-Vis spectra were collected on an Agilent 8453 UV-Vis spectrometer, and IR spectra were collected on a Perkin-Elmer FT-IR spectrum 1000 instrument. Gas phase reactions were performed using the experimental design described in section 2.5 .

3.5.1 Synthesis of 1a

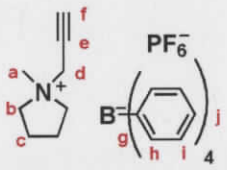

Methyl pyrrolidine (3.84 g, 45.1 mmol) and diethyl ether (30 mL) were cooled to 0°C in a 100 mL round bottom flask. Propargyl bromide (5 mL of an 80% solution in toluene, 6.90 g, 57.5 mmol) in ether (25 mL) was added dropwise. The mixture was subsequently allowed to warm to room temperature and stirred overnight. The solvent was then evaporated and the white product dried under vacuum for 24 hours. (8.97 g, 44.0 mmol, 97.6 %) M.P.: 62-68°C. ^{1}H NMR (CD_3OD): δ (ppm) 4.50 (d, 2H, CH_2-d); 3.75 (m, 4H, CH_2-b); 3.52 (t, 1H, CH-f); 3.29 (s, 3H, CH_3-a); 2.31 (m, 4H, CH_2-c). ^{13}C NMR (CD_3OD): δ (ppm) 81.96 (e); 73.33 (f); 65.25 (b); 54.50 (d); 50.44 (a); 23.20 (c).

3.5.2 Synthesis of 1b

An aqueous solution (20 mL H_2O) of **1a** (1.413 g, 6.96 mmol) and sodium hexafluorophosphate (1.19 g, 7.08 mmol) was prepared. The mixture was heated to facilitate dissolution, and then cooled to room temperature. The white crystals were filtered with a cold water wash and dried overnight under vacuum. (0.62 g, 2.30 mmol, 33.0 %) M.P.: 146-147°C. ^{1}H NMR (CD_3OD): δ (ppm) 4.33 (d, 2H, CH_2-d); 3.67 (m, 4H, CH_2-b); 3.45 (t, 1H, CH-f); 3.22 (s, 3H, CH_3-a); 2.28 (m, 4H, CH_2-c). ^{13}C NMR (CD_3OD): δ (ppm) 81.78 (e); 73.05 (f); 65.15 (b); 54.27 (d); 50.24 (a); 23.08 (c). ^{31}P NMR (CD_3OD): δ (ppm) -143.22 (septet for PF_6^-).

3.5.3 Synthesis of 1c

A 5 mL aqueous solution of **1a** (0.102 g, 0.502 mmol) was added to a 5 mL aqueous solution of sodium tetraphenylborate (0.161g, 0.470 mmol) and stirred for 15 minutes. A white product formed immediately. An extra 5 mL of water was added to enhance stirring. The product (0.183 g, 0.413 mmol, 87.8 %) was collected by vacuum filtration with a wash of water. Decomposes > 200°C. ^{1}H NMR (CD_3CN): δ (ppm) 7.31 (m, 8H, CH-i); 7.05 (t, 8H, CH-h); 6.87 (t, 4H, CH-j); 4.11 (d, 2H, CH_2-d); 3.53 (m, 4H, CH_2-b); 3.14 (t, 1H, CH-f); 3.14 (s, 3H, CH_3-a); 2.14 (m, 4H, CH_2-c). ^{13}C NMR (CD_3CN): δ (ppm) 165.79 (g), 136.74 (i), 126.60 (h), 122.77 (j), 81.47 (f), 72.63 (e), 65.09 (b), 54.29 (d), 50.58 (a), 22.77 (c).

3.5.4 Synthesis of allyl pyrrolidine[74]

Allyl bromide (6 mL, 8.4 g, 69.4 mmol) in diethyl ether (20 mL) was added dropwise to pyrrolidine (5.1 g, 71.7 mmol) in ether (20 mL) at 0°C over 30 minutes. The solution was then allowed to warm to room temperature and stirred overnight, followed by a potassium hydroxide extraction (3 x 25 mL of a 3M solution). The subsequent aqueous phase was then extracted with dichloromethane and all organic portions were combined, dried with anhydrous magnesium sulfate, and filtered. The solvent was removed on the rotary evaporator and the orange liquid was distilled (fraction that boiled at 120°C was retained) to give a colorless product. (3.5 g, 31.5mmol, 45.4 %) ^{1}H NMR ($CDCl_3$): δ

(ppm) 5.88 (m, 1H); 5.21 (m, 2H); 3.02 (d, 2H); 2.43 (m, 4H); 1.71 (m, 4H) ^{13}C NMR ($CDCl_3$): δ (ppm) 136.23, 116.53, 59.22, 53.96, 23.40.

3.5.5 Synthesis of 2a

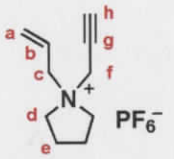

Allyl pyrrolidine (0.667 g, 6.00 mmol) and propargyl bromide (0.80mL, 1.07 g, 7.19 mmol) were stirred in ether (30 mL) overnight. The white product was filtered and collected (0.453 g, 1.86 mmol, 31.0 %). M.P.: 140-146°C. ^{1}H NMR (CD_3OD): δ (ppm) 6.11 (m, 1H, CH-b); 5.76 (m, 2H, CH_2-a); 4.30 (s, 2H, CH_2-f); 4.16 (d, 2H, CH_2-c); 3.68 (m, 4H, CH_2-d); 3.49 (t, 1H, CH-h); 2.28 (m, 4H, CH_2-e). ^{13}C NMR (CD_3OD): δ (ppm) 129.40 (a); 126.55 (b); 82.03 (h); 73.04 (g); 64.55 (c); 63.10 (d); 51.25 (f); 23.22 (e).

3.5.6 Synthesis of 2b

An aqueous solution of **2a** (0.265 g, 1.16 mmol, 20 mL H_2O) was added to an aqueous solution of sodium hexafluorophosphate (0.208 g, 1.24 mmol, 10 mL H_2O). The mixture was reduced to a volume of 10 mL and left overnight in the fridge at 5°C. The white crystals were filtered with a water wash and the filtrate was then reduced again to a smaller volume and transferred back into the fridge for further crystallization. The combined yield of both aliquots was 0.092g, 0.312mmol, 27.0 %. M.P.: 78-80°C. ^{1}H NMR (CD_3OD): δ (ppm) 5.96 (m, 1H, CH-b); 5.70 (m, 2H, CH_2-a); 4.15 (d, 2H, CH_2-f); 4.01 (d, 2H, CH_2-c); 3.55 (m, 4H, CH_2-d); 3.36 (t, 1H, CH-h); 2.16 (m, 4H, CH_2-e). ^{13}C NMR (CD_3OD): δ (ppm) 129.37 (a); 126.43 (b); 81.96 (h); 72.95 (g); 64.53 (c); 63.03 (d); 51.10 (f); 23.13 (e). ^{31}P NMR (CD_3OD): δ (ppm) -143.23 (septet for PF_6^-).

3.5.7 Synthesis of allyl piperidine[53]

Allyl bromide (15.6 g, 128.9 mmol), piperidine (10.5 g, 123.3 mmol), and sodium hydride (3.3g, 145.9 mmol) were combined as described in the literature to yield allyl piperidine (11.9 g, 95.0mmol, 77 %) after a partial dynamic vacuum distillation. ^{1}H NMR ($CDCl_3$): δ (ppm) 5.82 (m, 1H); 5.05 (m, 2H); 2.89 (d, 2H); 2.30 (s, 4H); 1.52 (m, 4H); 1.37 (m, 2H). ^{13}C NMR ($CDCl_3$): δ (ppm) 135.5, 117.33, 62.56, 54.37, 25.86, 24.26.

3.5.8 Synthesis of 3a

Propargyl bromide (2.42 g of 80% solution in toluene, 16.2 mmol) in toluene (20 mL) was added to allyl piperidine (1.94 g, 15.5 mmol) in toluene (20 mL). The mixture was stirred at room temperature for 48 hours, and the resulting white product was vacuum filtered, followed by vacuum drying overnight. (2.47 g, 10.1 mmol, 67 %) M.P.: 154-156°C ^{1}H NMR (CD_3CN): δ (ppm) 5.99-5.70 (m, 3H, CH-a,b); 4.43 (d, 2H, CH_2-g); 4.15 (d, 2H, CH_2-c); 3.53 (m, 4H, CH_2-d); 3.27 (t, 1H, CH-i); 1.91 (m, 4H, CH_2-e); 1.69 (m, 2H, CH_2-f). ^{13}C NMR (CD_3CN): δ (ppm) 129.88 (a); 125.01 (b); 82.68 (c); 71.77 (g); 62.33 (h); 59.23 (d); 50.38 (i); 21.39 (f); 20.31 (e).

3.5.9 Synthesis of 3b

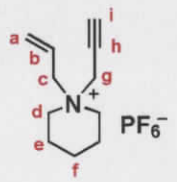

To 30 mL of water was added **3a** (0.45 g, 1.85 mmol) and sodium hexafluorophosphate (0.37 g, 2.20 mmol). The mixture was stirred for fifteen minutes and the white product was filtered (0.216 g). The filtrate was boiled to reduce the volume down to 15 mL, and transferred to the freezer (-10 °C) for four hours. These crystals were then filtered (0.171 g) to give a combined yield of 0.387 g, 1.25 mmol, 67.6 %. M.P.: 85-86°C. ^{1}H NMR (CD_2Cl_2): δ (ppm) 5.76 (m, 3H, CH-a,b); 3.99 (d, 2H, CH_2-g); 3.95 (d, 2H, CH_2-c); 3.36 (m, 4H, CH_2-d); 2.85 (t, 1H, CH-i); 1.86 (m, 4H, CH_2-e); 1.70 (q, CH_2-f). ^{13}C NMR (CD_2Cl_2): δ (ppm) 131.46 (a); 122.74 (b); 82.22 (c); 70.17 (g); 62.73 (h); 59.22 (d); 49.45 (i); 20.90 (f); 20.15 (e). ^{31}P NMR (CD_2Cl_2): δ (ppm) -143.82-septet for $[PF_6]^-$.

3.5.10 Synthesis of propargyl piperidine[53]

Piperidine (7.5 mL, 6.5 g, 75.9 mmol) in tetrahydrofuran (50 mL) was added to a slurry of sodium hydride (2.05 g, 85.5 mmol) in tetrahydrofuran (75 mL) over 1 hour. The mixture was allowed to stir at room temperature for another hour. A mixture of propargyl bromide (9.93 g of an 80% toluene solution, 66.2 mmol) in tetrahydrofuran was then added dropwise over an hour and the mixture was left to stir overnight. The mixture was quenched with a sodium chloride solution (1 mol L^{-1}) and the organic phase separated. The aqueous phase was then extracted with ethyl acetate (3 x 50mL) followed by

tetrahydrofuran (2 x 50mL) and combined with the original organic fraction. After drying with anhydrous magnesium sulfate, and filtering with a THF wash, the solvent was removed on a rotary evaporator and the orange product distilled to give a light yellow liquid (5.41 g, 43.9 mmol, 66 %). ^{1}H NMR ($CDCl_3$) δ (ppm): 4.24 (t, 1H); 3.16 (d, 2H); 2.39 (m, 4H); 1.51 (m, 4H); 1.34 (m, 2H). ^{13}C ($CDCl_3$) δ (ppm): 72.80, 68.36, 52.98, 47.43, 25.73, 23.74.

3.5.11 Synthesis of 4a

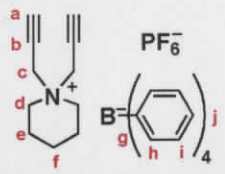

Propargyl piperidine (1.00 g, 8.1 mmol) was added to propargyl bromide (1.38 g of an 80% toluene solution, 9.2 mmol) along with toluene (30 mL) and allowed to stir at room temperature for 24 hours. The solution was then refluxed for 1 hour, and the brown product was vacuum filtered with a toluene wash and dried under vacuum overnight. (0.839 g, 3.5 mmol, 43.2 %) Decomposes above 200°C. ^{1}H NMR (CD_3OD): δ (ppm) 2.73 (d, 4H, CH_2-c); 1.91 (t, 4H, CH_2-d); 1.57 (t, 2H, CH-a); 0.23 (m, 4H, CH_2-e); 0.02 (m, 2H, CH_2-f). ^{13}C (CD_3CN): δ (ppm) 83.00 (c); 71.09 (a); 59.45 (d); 51.01 (b); 21.19 (f); 20.29 (e).

3.5.12 Synthesis of 4b

The synthesis of **4b** was performed as described for **1b** with the following amounts of reagents and solvents: **4a** (0.166 g, 0.689 mmol), sodium hexafluorophosphate (0.18 g, 1.07 mmol), water (30 mL), isolated product (0.0799 g, 0.26 mmol, 37.8 %). M.P.: 160-161. ^{1}H NMR (CD_3OD): δ (ppm) 4.46 (s, 4H, CH_2-c); 3.62 (t, 4H, CH_2-d); 3.53 (t, 2H, CH-a); 1.97 (m, 4H, CH_2-e); 1.74 (m, 2H, CH_2-f). ^{13}C NMR (CD_3OD): δ (ppm) 83.39 (c); 71.33 (a); 59.90 (d); 51.05 (b); 21.81 (f); 20.68 (e). ^{31}P (CD_3OD): δ (ppm) -143.24 (septet for PF_6^-).

3.5.13 Synthesis of 4c

A 20 mL aqueous solution of **4a** (0.37 g, 1.53 mmol), was added to a 20 mL aqueous of sodium tetraphenyl borate (0.60 g, 1.75 mmol) and stirred for 20 minutes. The white product (0.578 g, 1.20 mmol, 78.4 %) was vacuum filtered with a water wash. X-ray quality crystals were grown by the slow evaporation of an acetone solution. M.P.: 134-

136°C. ^{1}H NMR (CD_3CN): δ (ppm) 7.19 (m, 8H, CH-i); 6.91 (t, 8H, CH-h); 6.76 (t, 4h, CH-j); 4.15 (d, 4H, CH_2-c); 3.36 (t, 4H, CH_2-d); 3.11 (t, 2H, CH-a); 1.86 (m, 4H, CH_2-e); 1.76 (m, 2H, CH_2-f). ^{13}C NMR (CD_3CN): δ (ppm) 163.8 (g), 135.42 (i), 125.26 (h), 121.46 (j), 81.83 (a), 69.57 (b), 58.47 (d), 49.81 (c), 19.89 (f), 18.96 (e).

3.5.14 Synthesis of $Co_2(CO)_6$(1b)

Dicobalt octacarbonyl (0.207 g, 0.604 mmol) and **1b** (0.122 g, 0.45 mmol) were mixed as solids in a Schlenk flask. Dry dichloromethane was then added (10 mL) and the mixture was stirred at room temperature for 4 hours under N_2. The solvent was evacuated and the mixture was washed with ether (4 x 8 mL). The red solid was then dried under vacuum for two hours and collected (0.068 g, 0.122 mmol, 27.1 %). Decomposes above 120°C. ^{1}H NMR (CD_2Cl_2): δ (ppm) 6.32 (s, 1H,); 4.77, (s, 2H); 3.59 (m, 4H); 3.13 (s, 3H); 2.25 (s, 4H). ^{13}C NMR (CD_2Cl_2): δ (ppm) 75.09, 67.67, 65.03, 49.50, 22.16. ^{31}P NMR (CD_2Cl_2): δ (ppm) -143.79 (septet for PF_6^-). IR (cm^{-1}, CH_2Cl_2); 2105 (st), 2067 (vs), 2045 (vs), 1605 (m, broad). UV-Vis: 356 nm, 364 nm, 421 nm.

3.5.15 Synthesis of $Co_2(CO)_6$(1c)

Dicobalt octacarbonyl (1.06 g, 3.10 mmol) was weighed out in a Schlenk flask in the glovebox and transferred to the Schlenk line. **1c** (1.01 g, 2.26 mmol) was then added as a solid followed by dichloromethane (40 mL). The reaction was stirred at room temperature and tracked by ESI-MS. After about 4 hours, the reaction was stopped. Solvent was evaporated under vacuum, and the remaining solid was washed successively with 10 mL portions of dry diethyl ether until washings were colorless. The dark product was dried under vacuum overnight then collected in air (0.996 g, 1.36 mmol, 60.1 %). X-ray quality crystals were grown by solvent diffusion of dichloromethane and diethyl ether at -10°C; a thin layer of 1-butanol was put between the two solvents to slow diffusion. This product decomposed quickly in the solid state, and was only characterized by X-ray crystallography.

3.5.16 Synthesis of $Co_2(CO)_6$(2b)

Dicobalt octacarbonyl (0.0917 g, 0.268mmol) was weighed out in a Schlenk flask in a glovebox then transferred to the Shlenk line, to which **2b** (0.0435 g, 0.147 mmol) was added as a solid. Dry dichloromethane was then added against a stream of nitrogen and the mixture was stirred at room temperature for two hours. The solvent was then evacuated, and the remaining solid was washed with dry diethyl ether (4 × 6 mL). The remaining solid was then dried under vacuum for two hours and collected (0.0595 g, 0.102 mmol, 69.4 %). X-ray quality crystals were grown by layering diethyl ether over a dichloromethane solution of the complex and allowing for diffusion at -10°C. Decomposes above 80°C. ^{1}H NMR (CD_2Cl_2): δ (ppm) 6.36 (s, 1H); 5.79 (m, 3H); 4.67 (s, 2H); 3.96 (d, 2H); 3.56 (m, 4H); 2.21 (m, 4H). ^{13}C NMR (CD_2Cl_2): δ (ppm) 130.42, 124.09, 63.87, 62.56, 62.14, 22.35. ^{31}P NMR (CD_2Cl_2): δ (ppm) -143.83 (septet for PF_6^-). IR (cm^{-1}, CH_2Cl_2); 2105 (st), 2067 (vs), 2045 (vs), 2034 (shoulder). UV-Vis: 356 nm, 365 nm, 421 nm.

3.5.17 Synthesis of $Co_2(CO)_6$(3b)

Dicobalt octacarbonyl (0.15 g, 0.439 mmol) and **3b** (0.087 g, 0.281 mmol) were added to a Schlenk flask as solids against a dry nitrogen atmosphere. Dry dichloromethane (10 mL) was then added and the mixture was allowed to react for two hours. The solvent was then evaporated, and the red solid was washed with ether (3 x 8 mL) then dried under vacuum for 2 hours. The dark red product (0.131 g, 0.220 mmol, 78.3 %) was collected and X-ray quality crystals were grown by dichloromethane and ether solvent diffusion in the freezer, with a small layer of 1-butanol between them. Decomposes above 90°C. ^{1}H NMR (CD_2Cl_2): δ (ppm) 6.38 (s, 1H); 5.74 (m, 3H); 4.70 (s, 2H); 4.00 (d, 2H); 3.42 (m, 4H); 1.88 (m, 4H); 1.72 (m, 2H). ^{13}C NMR (CD_2Cl_2): δ (ppm) 130.91, 122.91, 75.25, 74.03, 62.69, 62.10, 58.86, 20.96, 20.32. ^{31}P NMR (CD_2Cl_2) δ (ppm) -143.79 (septet for PF_6^-). IR (cm^{-1}, CH_2Cl_2): 2105 (st), 2066 (vs), 2045 (vs). UV-Vis: 356 nm, 364 nm, 421 nm.

3.5.18 Synthesis of $Co_2(CO)_5$(4b)

Dicobalt octacarbonyl (0.0405 g, 0.118 mmol) and **4b** (0.0391g, 0.127 mmol) were mixed as solids in a Schlenk flask. Dry dichloromethane (8 mL) was added at 0°C, and the mixture was allowed to stir for 1 hour at this temperature before warming to room temperature. The solution was stirred overnight at room temperature then refluxed for 1 hour. The solvent was then evacuated and the solid was washed once with hexane (8 mL) and then ether (2 x 8 mL) followed by drying under vacuum. The red product was then collected in air (0.0523 g, 0.0926 mmol, 78.5 %). X-ray quality crystals of $(Co_2(CO)_6)_2$(**4b**) were grown by layering diethyl ether over a dichloromethane solution of the complex and allowing for diffusion at -10°C. Decomposes above 130°C. ^{1}H NMR (CD_2Cl_2): δ (ppm) 7.20 (s, 2H); 4.40 (m, 4H); 4.05 (m, 2H); 3.58 (m, 2H); 1.85 (m, 4H); 1.70 (m, 2H). ^{13}C NMR (CD_2Cl_2): δ (ppm) 140.92, 129.13, 64.53, 64.23, 63.68, 28.93, 20.79, 20.24, 19.72, -0.01. ^{31}P NMR (CD_2Cl_2) δ (ppm) -143.75 (septet for PF_6^-). IR (cm^{-1}, CH_2Cl_2) 2099 (st), 2066 (m), 2044 (vs), 2027 (s), 1983 (m, broad). UV-Vis: 405 nm.

3.6 References

---

[1] a) Rylander, P.N., *Organic syntheses with noble metal catalysts,* Academic Press: New York, **1973,** *28*. b) Brandsma, L.; Vasilevsky, S.F.; Verkruijsse, H.D., *Application of transition metal catalysts in organic synthesis,* Springer: New York, **1999**. c) Jones, W.H. Ed. *Catalysis in organic synthesis,* Academic Press: Toronto, **1980**. d) Heaton, B. Ed. *Mechanisms in homogeneous catalysis,* Wiley-VCH: Weinheim, **2005**.

[2] Farrer, N.J.; McDonald, R.; McIndoe, J.S., *J. Chem. Soc. Dalton Trans.,* **2006**, 4570-4579.

[3] Farrer, N.J.; McDonald, R.; Piga, T.; McIndoe, J.S., *Polyhedron,* **2009**, in the press.

[4] Henderson, W.; Nicholson, B.K., *J. Chem. Soc., Chem. Commun.,* **1995**, 2531-2532.

[5] Decker, C.; Henderson, W.; Nicholson, B.K., *J. Chem. Soc. Dalton Trans.,* **1999**, 3507-3513.

[6] Henderson, W.; McIndoe, J.S.; Nicholson, B.K.; Dyson, P.J., *J. Chem. Soc., Dalton Trans.,* **1998**, 519-525.

[7] Santos, L.S.; Rosso, G.B.; Pilli, R.A.; Eberlin, M.N., *J. Org. Chem.,* **2007**, *72*, 5809-5812.

[8] Hinderling, C.; Adlhart, C.; Chen, P., *Angew. Chem. Int. Ed. Engl.,* **1998**, *37*, 2685-2689.

[9] Chisholm, D.M.; Oliver, A.G.; McIndoe, J.S., *Dalton Trans.,* **2009**, in the press.

[10] Ercolani, C.; Quagliano, J.V.; Vallarino, L.M., *Inorg. Chim. Acta,* **1969**, *3*, 421-425.

[11] Adlhart, C.; Chen, P., *Helv. Chim. Acta.* **2000**, *83*, 2192-2196.

[12] Khand, I.U.; Knox, G.R.; Pauson, P.L.; Watts, W.E., *Chem. Commun.,* **1971**, pg. 36.

[13] Khand, I.U.; Knox, G.R.; Pauson, P.L.; Watts, W.E., *J. Chem. Soc., Perkin I,* **1973**, 975-977.

[14] Pauson, P.L., *Tetrahedron Lett.,* **1985**, *41*, 5855-5860.

[15] Magnus, P.; Principe, L.M.; Slater, M.J., *J. Org. Chem.,* **1987**, *52*, 1483-1486.

[16] a) Blanco-Urgoiti, J.; Anorbe, L.; Perez-Serrano, L.; Dominguez, G.; Perez-Castells, J., *Chem. Soc. Rev.,* **2004**, *33*, 32-42. b) Fletcher, A.J; Christie, S.D.R., *J. Chem. Soc., Perkin Trans.,* **2000**, *1*, 1657-1668. c) Gibson, S.E.; Mainolfi, N., *Angew. Chem. Int. Ed. Engl.* **2005**, *44*, 3022-3037. d) Green, J.R., *Curr. Org. Chem.,* **2001**, *5*, 809-823.

[17] Khand, I.U.; Knox, G.R.; Pauson, P.L.; Watts, W.E.; Foreman, M.I., *J. Chem. Soc. Perkin Trans. 1,* **1973,** 977-981.

[18] Geis, O.; Schmalz, H.G., *Angew. Chem. Int. Ed. Engl.,* **1998,** *37,* 911-914.

[19] Sugihara, T.; Yamada, M.; Ban, H.; Yamaguchi, M.; Kaneko, C., *Angew. Chem. Int. Ed. Engl.,* **1997**, *36*, 2801-2804.

[20] Sugihara, T..; Yamada. M.; Yamaguchi, M.; Nishizawa, M., *Synlett.* **1999**, 771-773.

[21] Billington, D.C.; Helps, I.M.; Pauson, P.L.; Thomson, W.; Willison, D., *J. Organomet. Chem.* **1988**, *354*, 233-242.

[22] Sugihara, T.; Yamaguchi, M., *Synlett,* **1998**, 1384-1386.

[23] Hanson, B.E., *Comments Inorg. Chem.*, **2002**, *23*, 289-318.

[24] Morimoto,T.; Chatani, N.; Fukumoto,Y.; Murai, S., *J. Org. Chem.,* **1997**, *62*, 3762-3765.

[25] Kobayashi, T.; Koga, Y.; Narasaka, K., *J. Organomet. Chem.,* **2004**, *624*, 73-87.

[26] Jeong, N.; Ki Sung, B.; Sung Kim, J.; Bong Park, S.; Deok Seo, S.; Young Shin, J.; Yeol In, K.; KyungChoi, Y., *Pure App. Chem.,* **2001**, *74*, 85-91.

[27] Mukai, C.; Uchiyama, M.; Hanaoka, M., *J. Chem. Soc. Chem. Commun.,* **1992**, 1014-1015.

[28] Hoye, T.R.; Suriano, J.A., *J. Am. Chem. Soc.,* **1993**, *115*, 1154-1156.

[29] Pearson, A.J.; Dubbert, R.A., *J. Chem. Soc. Chem. Commun.,* **1991**, 202-203

[30] Pearson, A.J.; Dubbert, R.A., *Organometallics,* **1994**, *13*, 1656-1661.

[31] Negishi, E.; Holmes,S.J.; Tour, J.M.; Miller, J.A.; Cederbaum, F.E.; Swanson, D.R.; Takahashi, T., *J. Am. Chem. Soc.,* **1989**, *111*, 3336-3346.

[32] Mastrorilli, P.; Nobile, C.F.; Paolillo, R.; Suranna, G.P., *J. Mol. Catal. A: Chem.,* **2004**, *214*, 103-106.

[33] Magnus, P.; Exon, C.; Albaugh-Robertson, P., *Tetrahedron Lett.,* **1985**, *41*, 5861-5869.

[34] Bennett, M.A.; Donaldson, P.B., *Inorg. Chem.,* **1978**, *17*, 1995-2000.

[35] Rautenstrauch, V.; Megard, P.; Conesa, J.; Kuster, W., *Angew. Chem. Int. Ed. Engl.* **1990**, *29*, 1413-1416.

[36] Pagenkopf, B.L.; Livinghouse. T., *J. Am. Chem. Soc.,* **1996**, *118*, 2285-2286.

[37] Gordon, C.M.; Kiszka, M.; Dunkin, I.R.; Kerr, W.J.; Scott, J.S.; Gebicki, J., *J. Organomet. Chem.,* **1998**, *554*, 147-154.

[38] de Bruin, T.J.M.; Milet, A.; Greene, A.E.; Gimbert, Y., *J. Org. Chem.,* **2004**, *69*, 1075-1080.

[39] Banide, E.V.; Muller-Bunz, H.; Manning, A.R.; Evans, P.; McGlinchey, M.J., *Angew. Chem. Chem. Int. Ed. Engl.,* **2007**, *46*, 2907-2910.

[40] Pallerla, M. K.; Yap, G.P.A.; Fox, J.M., *J. Org. Chem.,* **2008**, *73*, 6137-6141.

[41] Krafft, M.E.; Scott, I.L.; Romero, R.H.; Feibelmann, S.; Van Pelt, C.E., *J. Am. Chem. Soc.,* **1993**, *115*, 7199-7207.

[42] Verdaguer, X.;Vazquez, J.; Fuster, G.; Bernardes-Genisson, V.; Greene, A.E.; Moyano, A.; Pericas, M.A.; Riera, A., *J. Org. Chem.*, **1998**, *63*, 7037-7052.

[43] Cabot, R.; Lledo, A.; Reves, M.; Riera, A.; Verdaguer, X., *Organometallics,* **2007,** *26*, 1134-1142.

[44] Blackmond, D.G., *Angew. Chem. Int. Ed. Engl.,* **2005**, *44*, 4302-4320.

[45] Wang, H.; Sawyer, J.R.; Evans, P.A.; Mu-Jyun Baik, *Angew. Chem. Int. Ed. Engl.,* **2008**, *47*, 342-345.

[46] Fei, Z.; Zhao, D.; Scopelliti, R.; Dyson, P.J., *Organometallics,* **2004**, *23*, 1622-1628.

[47] Gimbert, Y.; Lesage, D.; Milet, A.; Fournier, F.; Greene, A.E; Tabet, J.C., *Org. Lett.,* **2003**, *5*, 4073-4075.

[48] Cotton, F.A.; Jamerson, J.D.; Stults, B.R., *J. Am. Chem. Soc.,* **1976**, *98*, 1774-1779.

[49] Butcher, C.P.G.; Dyson, P.J.; Johnson, B.F.G.; Khimyak, T.; McIndoe, J.S., *Chem. Eur. J.,* **2003**, *9*, 944-950.

[50] Johnson, B.F.G.; McIndoe, J.S., *Coord. Chem. Rev.,* **2000**, *200-202*, 901-932.

[51] Baker, G.A.; Pandey, S.; Pandey, S.; Baker, S.N., *Analyst*, **2004**, *129*, 890-892.

[52] Yuan, L.X.; Feng, J.K.; Ai, X.P.; Cao, Y.L.; Chen, S.L.; Yang, H.X., *Electrochem. Commun.,* **2006**, *8*, 610-614.

[53] Schmidt A.M.; Eilbracht, P., *J. Org. Chem.,* **2005**, *70*, 5228-5535.

[54] Pearson, A.J.; Shively, R.J.Jr.; Dubbert, R.A., *Organometallics,* **1992**, *11,* 4096-4104.

[55] Maryanoff, B.E.; Zhang, H.C., **ARKIVOC**, **2007**, xii, 7-35.

[56] Rausch, B.J.; Gleiter, R.; Rominger, F., *J. Chem. Soc., Dalton Trans.,* **2002**, 2219-2226.

[57] Roy, S.K.; Basak, A., *Chem. Commun.,* **2006**, 1646-1648.

[58] Pearson, A.J.; Shively, R.J.Jr., *Organometallics,* **1994**, *13*, 578-584.

[59] Krafft, M.E.; Boñaga, L.V.R.; Hirosawa, C., *J. Org. Chem.,* **2001**, *66,* 3004-3020.

[60] Robert, F.; Milet, A.; Gimbert, Y.; Konya, D.; Greene, A.E., *J. Am. Chem. Soc.,* **2001**, *123*, 5396-5400.

[61] Billington, D.C.; Helps, M.I.; Pauson, P.L.; Thomson, W.; Willison, D., *J. Organomet. Chem.,* **1998**, *354*, 233-242.

[62] Dyson, P.J.; McIndoe, J.S., *Transition Metal Carbonyl Cluster Chemistry*, Gordon and Breach Science Publishers: Canada, **2000**.

[63] Krafft, M.E.; Boñaga, L.V.R.; Hirosawa, C., *J. Org. Chem.*, **2001**, *66*, 3004-3020.

[64] Shambayati, S.; Crowe, W.E.; Schreiber, S.L., *Tetrahedron*, **1990**, *31*, 5289-5290.

[65] Billington, D.C.; Helps, I.M.; Pauson, P.L.; Thomson, W.; Willson, D., *J. Organomet. Chem.*, **1988**, *354*, 233-242.

[66] Chung, Y.K.; Lee, B.Y.; Jeong, N.; Hudecek, M.; Pauson, P.L., *Organometallics*, **1993**, *12*, 220-223.

[67] Palagyi, J.; Marko, L., *J. Organomet. Chem.*, **1969**, *17*, 453-456.

[68] Yamanaka, M.; Nakamura, E., *J. Am. Chem. Soc.*, **2001**, *123*, 1703-1708.

[69] Predieri, G.; Tiripicchio, A.; Camellini, M.T., *J. Organomet. Chem.*, **1992**, *423*, 129-139.

[70] Battaglia, L.P.; Delledonne, D.; Nardelli, M.; Predieri, G.; Chiusoli, G.P.; Costa, M.; Pelizzi, C., *J. Organomet. Chem.*, **1989**, *363*, 209-222.

[71] O'Hair, R.A.J., *Chem. Commun.*, **2006**, 1469-1481.

[72] Marek, I.; Simaan, S.; Masarwa, A., *Angew. Chem. Int. Ed. Engl.*, **2007**, *46*, 7364-7376.

[73] Marchueta, I.; Verdaguer, X.; Moyano, A.; Pericàs, M.A.; Riera, A., *Org. Lett.*, **2001**, *3*, 3193-3196.

[74] De Vynck, V.; Goethals,E.J., *Macromol. Rapid Commun.*, **1997**, *18*, 149-156.

Chapter 4 Electrospray ionization mass spectrometry from non-polar solvents

4.1 Introduction

As mentioned section 1.3 the process of generating gas phase ions by ESI requires electrochemistry to occur in the capillary.[1] The separation of oppositely charged ions in solution by means of a high capillary voltage (~2-5kV) electrophoretically generates a fine mist of droplets with an excess of charge.[2] The gas phase ion evolves by either ion evaporation from the surface of these droplets or Coulombic explosion of the droplet itself (the relative importance of these two processes remains the subject of debate).[3] The excess charge on the droplets is generated by oxidation when in the positive ion mode (reduction in negative ion mode) of either the solution species or of the capillary itself[4] (i.e. $Zn \rightarrow Zn^{2+} + 2e^-$), but it is the most surface-active species which are represented in the actual spectrum.[5] For the purposes of ESI-MS of organometallic complexes, that species is also the analyte of interest.

The role of the solvent in this whole process is crucial. The solvent must sufficiently solvate each ion (both cation and anion) in solution so that charge separation in the capillary is possible. Reasonably, a solvent devoid of any electrolyte whatsoever will be unable to generate a fine mist of charged droplets, and it follows that a solvent unable to facilitate charge separation in the capillary will also be unable to generate a fine mist.

It is this last point that explains why moderately polar to polar solvents are typically used in ESI-MS; they are more able to stabilize and solvate ions making the ion pairs more responsive to the applied electric field in the capillary. Non-polar solvents such as hexane, toluene, benzene, etc do not facilitate charge separation of most salts in solution; ions remain strongly paired if even soluble at all. In the event that a salt *has* been dissolved in these solvents, the extent of ion pairing is usually such that the capillary voltage is not strong enough to separate them and a stable spray is not achieved. Adulterating these solvents with varying amounts of a more polar solvent

(dichloromethane/toluene,[6] acetonitrile/toluene,[7] etc) has resulted in the necessary stable sprays.

Considering the dielectric constants as a rough estimate of solvent polarity, a fairly large difference among the most common ESI-MS solvents is evident between acetone and dichloromethane (Table 4-1).[8]

Table 4-1: Dielectric constants for common solvents.

Polar solvents (ε)		**Non-polar solvents (ε)**	
Water	80.10	Fluorobenzene	5.47
Acetonitrile	36.64	Diethyl ether	4.27
Methanol	33.00	Toluene	2.38
Ethanol	25.30	Benzene	2.28
Acetone	21.01	Carbon tetrachloride	2.24
Dichloromethane	8.93	Hexane	1.89

Although generally considered to be a relatively non-polar solvent, dichloromethane (DCM) *can* be used for ESI-MS.[9] Its application is not as straight-forward as the more polar solvents though, and Figure 4-1 shows that at similar concentrations and identical instrumental conditions, DCM as solvent is considerably less sensitive than acetonitrile. It *is* possible to get high quality spectra from DCM but concentrations must be increased and instrument conditions tuned accordingly. Acetonitrile is one of the most commonly used solvents for ESI, and very high quality spectra of butylmethylimidazolium chloride (BMIM Cl) with an ion count (IC) of >35000 can be obtained at concentrations of $\sim 10^{-8}$ mol L^{-1} (Figure 4-1). The corresponding spectrum for dichloromethane is about two orders of magnitude less intense. As for toluene, it is obvious that no representative information can be obtained at all; it is this poor quality of spectrum that explains why toluene has never been used successfully for purposes of electrospray ionization.

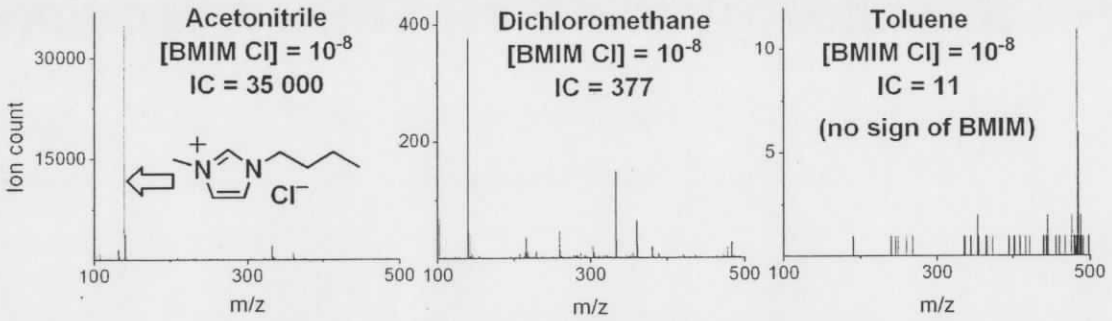

Figure 4-1: ESI-MS spectra of butylmethylimidazolium chloride dissolved to equal concentrations in three different solvents.

In the vein of organometallic chemistry, many polar solvents decompose the sensitive inorganic species even in small (but still significant) amounts, so the doping of non-polar solvents with acetonitrile, methanol, or acetone is unsuitable for purposes of characterizing highly sensitive species. The ability to spray toluene or hexane without the use of any decomposing solvents would significantly expand the scope and utility of ESI-MS to include those extremely sensitive compounds that cannot be run in polar solvents.

4.2 Ionic liquids

Research into ionic liquids (IL) is a rapidly expanding area of research.[10] Their low melting points (<100°C)[11] and ionic nature confer some unusual characteristics not present in conventional organic solvents. ILs have found direct applications[12] as lubricants[13] or surfactants[14] as well as somewhat indirect uses in separation chemistry,[15] biphasic catalysis,[16,17] recyclable solvents or reagents for organic synthesis,[16,18,19] photochemistry,[20] CO_2 capture,[21] liquid crystals,[22] and as electrolytes.[23,24] An important feature of ionic liquids is the ability to "tune" each IL for specific tasks.[25] By altering a side chain on the cation or by varying the anion,[26,27] the melting point, viscosity, basicity, conductivity, and solubility properties may all be altered. After accounting for all cationic derivatives, accessible alkyl chain lengths (synthetically facile or commercially available), the myriad of functional groups, and the variety of available anions, it has

been proposed that up to 10^{18} unique ILs may be accessible with at least one distinctive property or characteristic (Figure 4-2).[16]

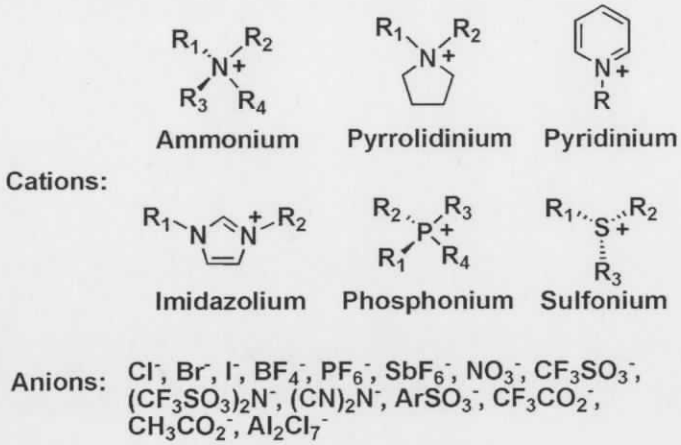

Figure 4-2: Common cation derivatives used in IL syntheses, as well as some common anions.[16]

Of particular interest to this project were the unique solubility properties of ILs and their role as supporting electrolytes in various electrochemical designs.[28,29] It was reasoned that if an IL could dissolve in a non-polar solvent such as hexane, then it might function as a supporting electrolyte in the ESI-MS characterization of another analyte that is stable only in the non-polar solvent. Since these non-polar solvents do not coordinate or decompose sensitive organometallic complexes,[30] this development would open the door to their application by ESI-MS, thereby extending the utility of the technique to nearly all of the routinely employed solvents. A related application of ILs to mass spectrometry has been accomplished for MALDI, whereby the IL functioned as a new matrix.[31] Scouring the literature found one related report of an ESI-MS spectrum of an imidazolium based ionic liquid dissolved in, and electrosprayed from benzene, but the report was investigating the IL-solvent interactions and the authors do not seem to have appreciated the significance of this observation in the vein of ESI-MS.[32]

4.3 Results and discussion

Phosphonium ILs have received less attention in recent years compared to their nitrogen based counterparts, but they have found various applications,[33] especially in industry.[34] One aspect of phosphonium ILs is their higher solubilities in more hydrophobic solvents as compared to ammonium ILs. For example, the salt tetradecyltrihexylphosphonium bis(trifluoromethyl)sulfonylamide[a] (**1**) is soluble in hexane. With the knowledge that ion separation in solution is important in generating a stable spray for electrospray ionization, it was reasoned that this hexane soluble IL might facilitate enough electrochemistry to generate the required stable spray of gas phase ions in the electrospray process.[35] Indeed, adding minimal amounts of **1** gave high quality spectra of the cation (or anion) along with at least one aggregate ($[C_2A]^+$ in Figure 4-3).[36] This represented the first ESI mass spectrum of any ion sprayed from neat hexane. Equally good spectra were obtained from pentane, cyclohexane, and toluene; none of which had ever been used for ESI-MS before.

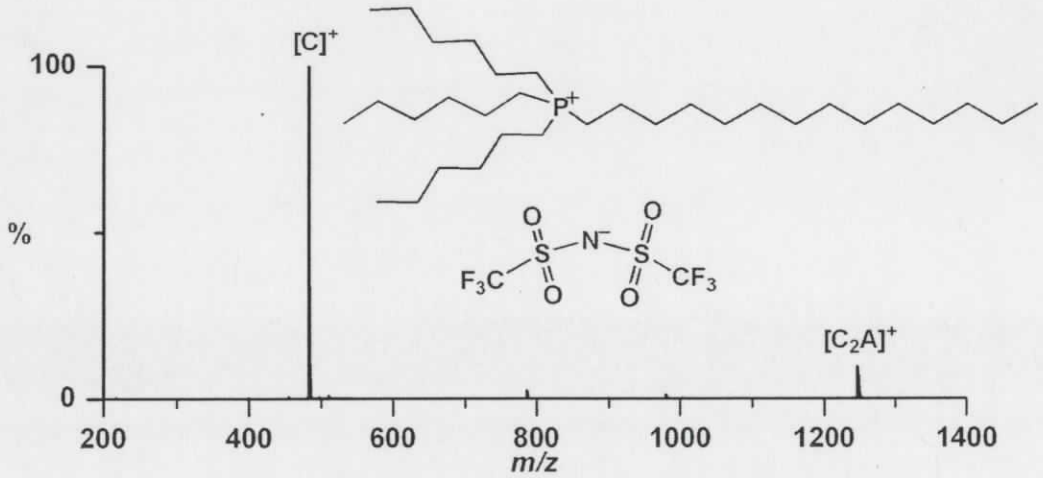

Figure 4-3: Positive ion ESI-MS of IL-**1** dissolved in hexane.

[a] The anion is abbreviated as: bistriflamide.

To probe this discovery further, a range of IL concentrations were analyzed. A relatively high threshold concentration of approximately 10^{-4} M was required for hexane, above which good quality data could be obtained (Figure 4-4). Comparing the concentrations for hexane to those for toluene and diethyl ether, it can be seen that moderately good spectra can be obtained at concentrations approximately 100 times lower in toluene and high quality spectra are attainable from diethyl ether at concentrations down to 10^{-11} mol L^{-1}.[37] Typical analyte concentrations for ESI-MS are around the nanomolar to micromolar levels, so concentrations of 10^{-4} mol L^{-1} for hexane represent poor sensitivity. This is probably due to the inherent insulating features of non-polar solvents which would require a higher concentration of electrolyte in order for the proper electrochemistry to occur.

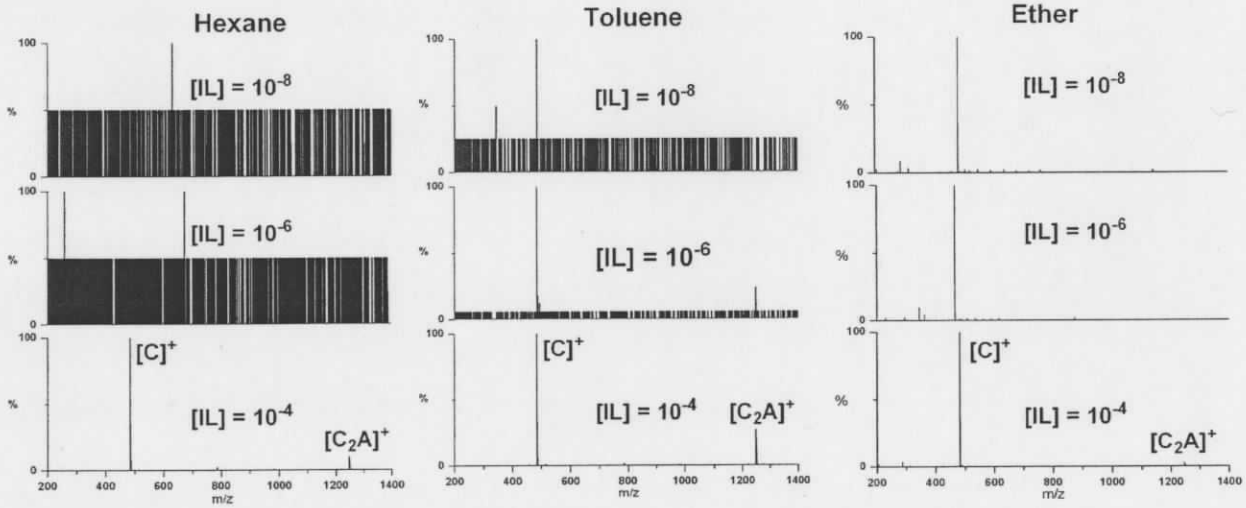

Figure 4-4: Increasing the concentration of **1** improves the spectra. The polarity of the solvent also plays an important role.[35] Spectra were collected for 90s each with an interscan time of 0.1s.

The role of the ionic liquid in this experiment is simply to act as a supporting electrolyte,[38] a role in which ILs are becoming more useful. In such a way the electrospray ionization process can function properly: electrochemical oxidation (reduction in the negative ion mode), charge separation of the electrolyte in the capillary, generation of a stable Taylor cone, and ion evaporation from charged droplets. The IL allows for another analyte, also soluble in hexane or non-polar solvents, to be dissolved

and sprayed from the same sample, with the requisite electrochemistry acting mainly on the IL. The very high sensitivity of ESI-MS means that only a minimum of the analyte needs to dissolve in order to be detected, and it has been previously shown that catalysts can unambiguously be characterized by ESI-MS despite being overwhelmed in a spectrum containing mainly IL aggregates.[39] Figure 4-5 shows that a common rhodium hydrogenation catalyst ($[RhCOD(PPh_3)_2]^+$)[40] is easily identified between the IL peak and its first aggregate.[41] As long as the IL does not chemically interfere with the analyte, this discovery significantly expands the scope of solvents available to ESI-MS.

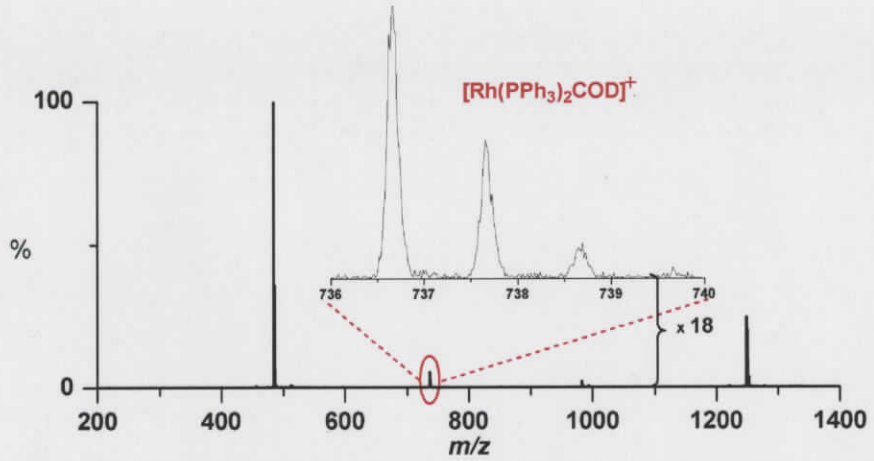

Figure 4-5: Dissolved catalysts are easily observed between aggregate peaks from cyclohexane. This spectrum was collected after vigorously shaking the mixture in attempts to improve dissolution. It was initially presumed that nothing dissolved at all, but the MS clearly shows enough is present to detect between the IL peaks. IL concentration was about 10^{-4} M.

One feature of this system was a marked improvement in analyte solubility for certain systems when the IL was present. This behavior is exemplified for an anionic iron carbonyl cluster (Figure 4-6), but this high degree of solubility is not necessary to obtain satisfactory spectra. Presumably ion exchange occurs to dissolve the normally insoluble salt, although not all salts exhibit this feature. It is important to note however, that due to the high sensitivity of ESI-MS, very little analyte needs to actually dissolve. Reasonable quality data may be obtained even if an unnoticeable amount of material has dissolved.

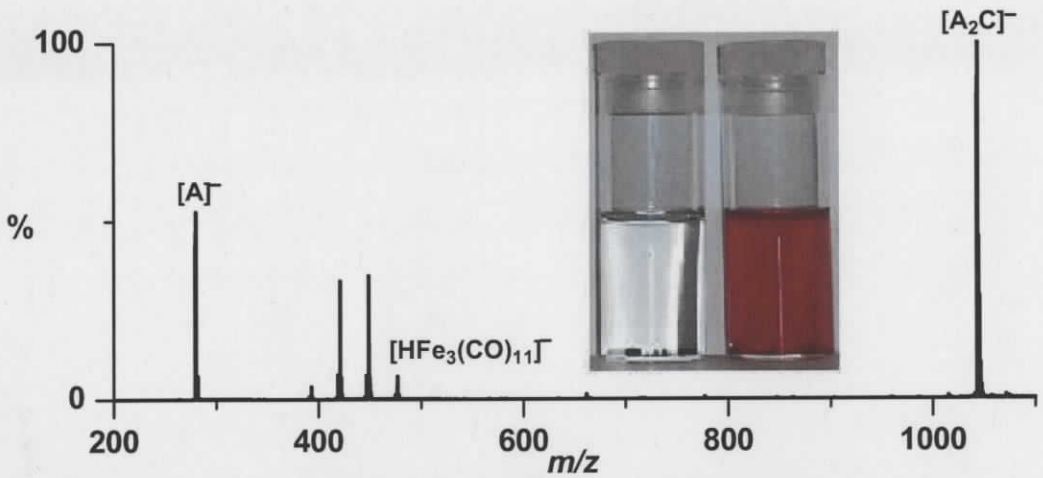

Figure 4-6: The ionic liquid improves the solubility of $[HNEt_3][HFe_3(CO)_{11}]$ in hexane.

Common to ESI-MS of ionic liquids are aggregate peaks, $[C_nA_{n-1}]^+$ in the positive ion mode, and $[A_nC_{n-1}]^-$ in the negative ion mode.[42] For **1,** molecular ion peaks are the prevalent peaks in both ion modes, but at least one aggregate is always observed. In attempts to reduce the extent of aggregation, a new ionic liquid (**2**) was synthesized (Equation 6) incorporating the tetra(3,5-bis(trifluoromethyl)phenyl)borate anion $[B(C_6H_3(CF_3)_2)]$.[43,44] This new IL (**2**) seems to have the largest overall molecular weight of known ILs, and its design considerably reduces the extent of cation-anion aggregation (Figure 4-7). Unexpectedly **2** was poorly soluble in hexane, though good quality spectra could be obtained from toluene.

$$PC_{32}H_{68}Cl + NaB(C_6H_3(CF_3)_2)_4 \longrightarrow \underset{B(C_6H_3(CF_3)_2)_4}{PC_{32}H_{68}} + NaCl$$

Equation 6

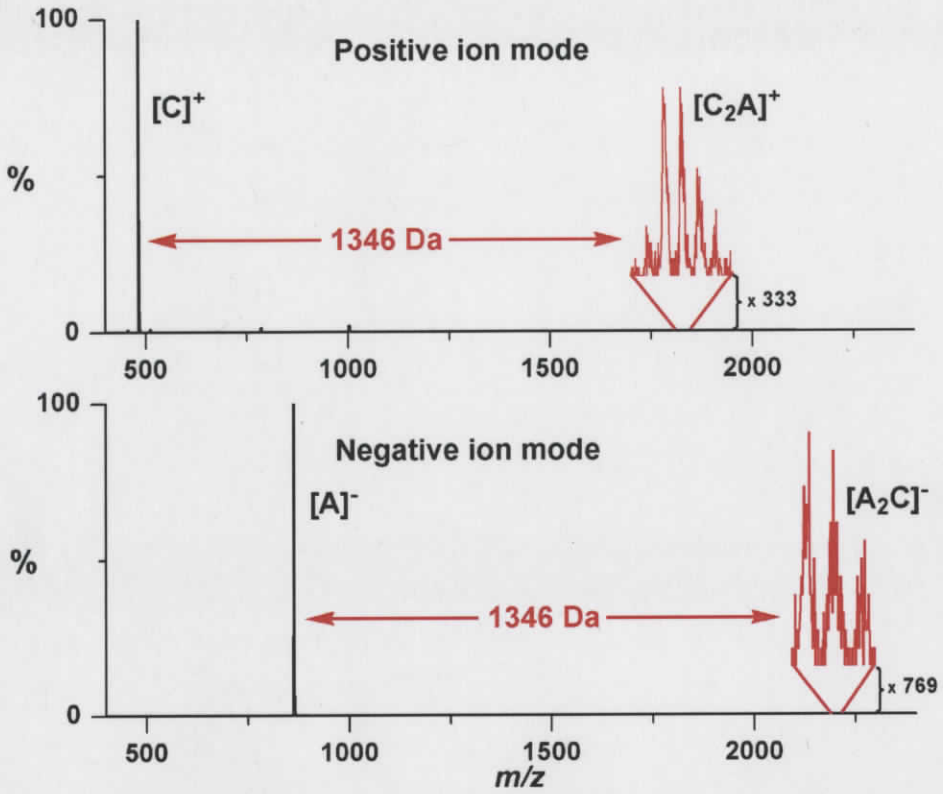

Figure 4-7: ESI-MS of **2** in toluene, showing the small extent of aggregation in both ion modes.

Given the surprising performance of these ILs for adulterating non-polar solvents, attempts were made to discover other cation/anion combinations that facilitated ESI-MS analysis. One salt combination that worked reasonably well was the crown ether salt of $NaB(C_6H_3(CF_3)_2)_4$. This ion allowed the use of toluene, and when applied to studying a sample of methylaluminoxane (MAO) in the positive ion mode, the very reactive $[18\text{-crown-6}\bullet AlMe_2]^+$ cation[45] was observed (Figure 4-8).[b] The ligation of the crown ether to $[Na]^+$ was sufficient to allow the requisite electrochemistry in the capillary.

[b] This result is probed in more detail in a later chapter.

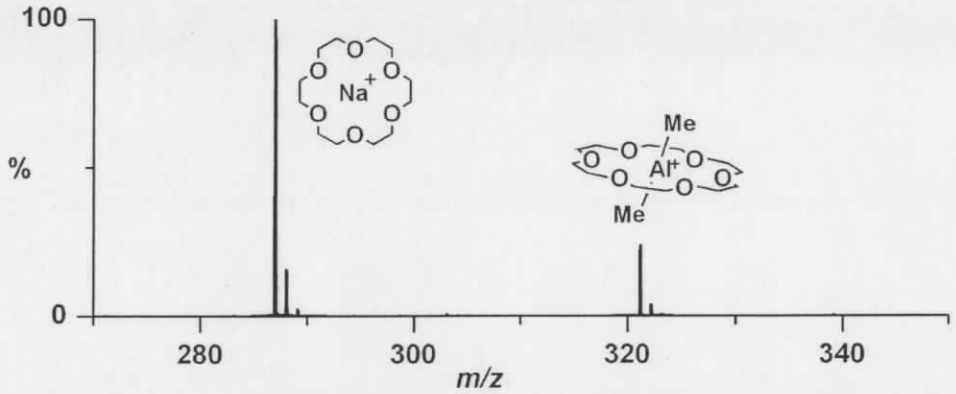

Figure 4-8: Compounds as sensitive as MAO have also been tried. This shows coordination of $[AlMe_2]^+$ within the crown ether.

4.4 Ionic liquid properties

Further attempts to expand this discovery by employing ILs with different anions and cations with alkyl chains of varying length led to the realization that not all ILs are equal in the task of enabling the use of non-polar solvents, especially hexane, for ESI-MS. To shed some light on this effect, it was desirable to probe different features of ILs that might correspond to their relative efficacy at enabling ESI-MS analysis.

4.4.1 Ionic liquid polarity

It was initially presumed that the polarity of an IL would depend largely on the lipophilicity of the cation's alkyl chains and the size of the anion. The polarity of an ionic liquid however, is very difficult to determine because, as for neutral solvents, there are a myriad of characteristics that contribute to polarity.[46] Solvatochromic probes (dyes) have been used to assign a qualitative measure of polarity,[47] with the idea of assisting practicing chemists to predict which solvents to use for various reactions. All solvent effects are accounted for together instead of simply measuring dipole moments, polarizabilities, or hydrogen-bonding sites and attempting to rationalize which solvent is best for a reaction based on one such measurement. The first application to ionic liquids appeared in a study of imidazolium ILs with the dye Nile Red (NR: Figure 4-9).[48] Other studies surfaced shortly thereafter[49,50] and upon analyzing trends employing different probes, the issue of complexity is noted.[51] Essentially, different dyes show different solvatochromic shifts in different ILs for different reasons. This is exemplified in one

study where 1-ethyl-3-methylimidazolium bistriflamide was determined to be nearly as polar as ethanol employing pyrene as the dye, but more akin to hexane when pyrenecarbaldehyde was used.[52]

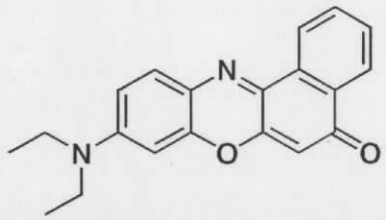

Figure 4-9: Molecular structure of Nile red.

Despite the wide use of phosphonium ILs only one study has analyzed the solvatochromic properties of a series of phosphonium ILs and sought to determine their relative polarity.[53] The ILs of that study all had shorter alkyl chains and halide or dimethylphosphate counterions, none of which would seem very lipophilic on inspection. As such, the following solvatochromic study is apparently done on the most lipophilic ILs that are known.

4.4.2 The ionic liquid/solvent combination

An initial experiment was to simply consider the effect of the IL on the solvent. At IL concentrations where high quality spectra are obtainable for all non-polar solvents, it was presumed that a solvatochromic shift would occur due to the "polarizing" effect of the IL, causing the hexane solvent to be more like that of a polar solvent. Polarity was measured by employing the dye NR and measuring the maximum UV-Vis absorption. Molar transition energies, determined in kJ mol^{-1}, were calculated from the equation $E_{NR} = ((hcN_A)/\lambda_{max}) \times 10^6$ where h is Planck's constant, c is the speed of light, N_A is Avagadro's number, and λ_{max} is the peak of maximum absorption; this protocol was followed as in Seddon's original polarity study of BMIM ILs.[48] **2** was not included in this study because it is not a room temperature IL (M.P. = 59-60 °C) and NR also displays a thermochromic shift;[54] as such the observed molar transition energy may not correspond to the polarity of **2**, but instead to the change in temperature. BMIM BF_4 was

included because it was the only IL with a literature reference, allowing a comparison to the known E_{NR} value of 217.2 kJ mol^{-1}.

The UV-Vis absorption spectrum of NR in a mixture of **1** dissolved in hexane (Figure 4-10) at a concentration of 10^{-3} M revealed that the polarity of the mixture is dominated by the bulk solvent, hexane. On the other hand, the spectrum of NR in the neat IL looks much more like that of methanol. The effect of the IL it seems then, is *not* to adjust the polarity of the bulk solvent.

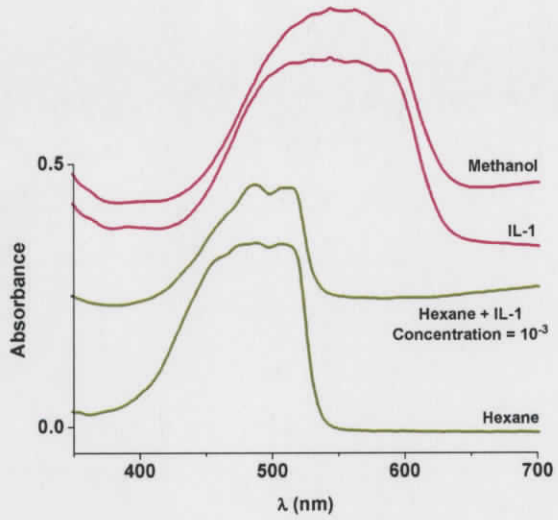

Figure 4-10: UV-Vis of NR dissolved in various solvents and IL/solvent combinations.

4.4.3 The effect of the anion

The above results prompted the analysis of a family of ILs in an attempt to understand more about their respective polarities and how they can be correlated to solubility and in turn to an improved ESI mass spectrum. The phosphonium ILs in Figure 4-11 allow an analysis of the effect of the anion across five ILs with an identical cation (ILs **1**-**5** in Figure 4-11) along with two other ILs (**6**,**7**); **6** and **7** cannot be correlated to the series with the same cation but are included because of their availability.

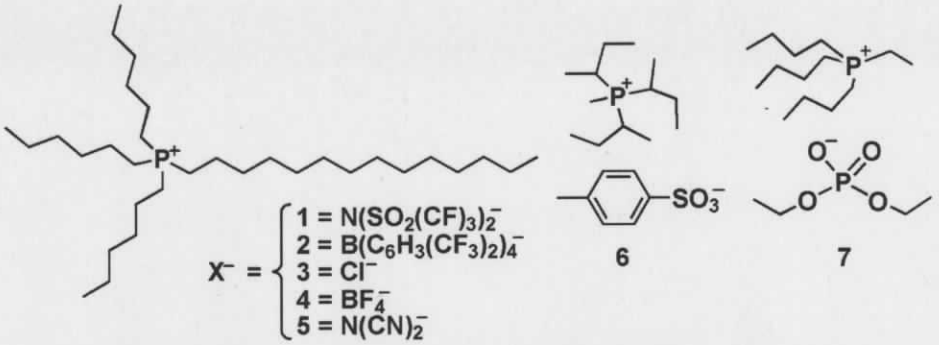

Figure 4-11: Phosphonium ILs studied to probe the effect of the anion.

The very broad absorption of NR was difficult to interpret but was a consistent feature for every IL studied. The peak of maximum absorption was taken in a region where all spectra had a definable hump (the region indicated by the black arrows in Figure 4-12). The λ_{max} for BMIM BF_4 from literature was 551 nm,[48] which is in the region of the red arrow, but this region was not consistent in spectra from other ILs.

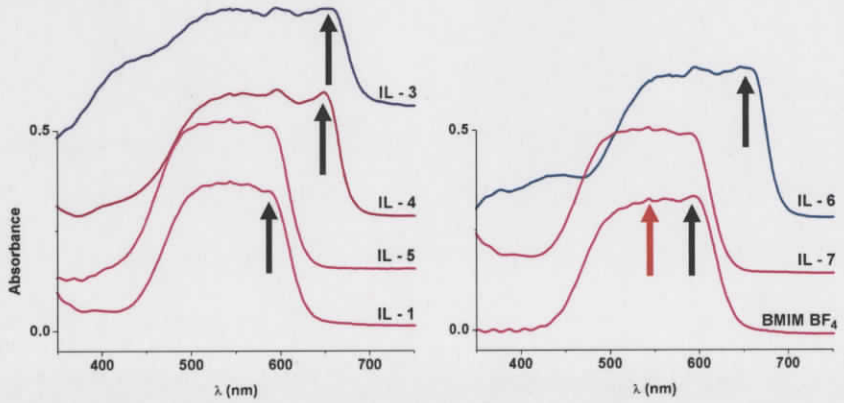

Figure 4-12: UV-Vis spectra of NR dissolved in neat phosphonium ILs and BMIM BF_4

Table 4-2 Molar transition energies for NR dissolved in ILs 1-7 and BMIM BF_4

Ionic Liquid	λ_{max} (nm)	E_{NR} (kJ mol^{-1})
BMIM BF_4	594	201.3
1	586	204.1
3	655	182.6
4	649	184.3
5	584	204.1
6	647	184.8
7	588	203.3

Table 4-3: Solubility of ILs 1-7 in hexane and toluene (misc. = miscible).

Ionic Liquid	Hexane (g L^{-1})	Toluene (g L^{-1})
1	15.0	misc.
3	16.5	misc.
4	1.9	misc.
5	1.2	misc.
6	0.5	29.9
7	3.6	60.6

The role of the anion was mentioned previously in Seddon's polarity study.[48] Seddon attributed IL polarity to "effective anion size", whereby the negative charge is very localized for both $[Cl]^-$ and $[BF_4]^-$, but becomes more diffuse for $[PF_6]^-$, making it less polar. The bistriflamide anion is a special case where the negative charge is spread across the S-N-S atoms,[55,56] significantly increasing the effective anion size and decreasing polarity. For the series analyzed here, **5** and **7** are also very non-polar, but their anion sizes do not fit with Seddon's interpretation. In terms of effective size, the negative charge for **5** is localized about the central nitrogen, and does not spread out onto the cyano carbons, making it a very small effective anion, so it should be more polar than **4**.[57] It was expected that for **7**, the negative charge would be localized primarily about the deprotonated oxygen center, although no reference could be found to support this suggestion. These anions are probably both smaller in effective size than the anion of **4**, and according to Seddon they should be more polar, but these NR results suggest they are *less* polar and approximately as polar as **1** with the very large effective anion.

The polarity of **1**, **5** and **7** appear to be quite close to that of methanol, a result that echoes previous studies with different cations but with the same anions.[58] The anion also has a very significant impact on polarity as can be seen by comparing E_{NR} (Table 4-2) for **1**-**5**. Importantly though, this measure of polarity does not predict the solubility of ILs in non-polar solvents, so the solubilities of each IL in hexane and toluene were then determined (Table 4-3). **1** and **3** were about ten times more soluble in hexane than the other ILs, but only **1** responded well by ESI-MS. Presumably the chloride ion of **3** was strongly paired

with the phosphonium cation so that its response to the applied capillary voltage decreased. The solubility of all ILs in toluene were markedly higher to the point that complete miscibility was presumed. ILs **3-7** all gave good spectra from toluene at concentrations of 10^{-6} mol L^{-1} (appendix 4: Appendix fig. 24).

4.4.4 The role of the alkyl chain length

The effect of the alkyl chain length on IL polarity was studied by investigating the series of pyrrolidinium ILs shown in Figure 4-13. This family of ILs was synthesized by Dr. Gary Baker (Oak Ridge) in a collaborative effort seeking to discover new ILs that would enable non-polar solvents in the electrospray process. An advantage of the N-based ILs was expected to be that the alpha protons would be unavailable for deprotonation in the presence of base, a noted detriment for the phosphonium ILs.[59] All ILs have the same anion to ensure that polarity will depend solely on the length of the alkyl chain. As for the series of phosphonium ILs, polarity was measured by the solvatochromic shift of NR (appendix 4). From Table 4-4, the molar transition energies suggest that for $n = 3$ and 9, the ILs are at their least polar. Notably, the series is incomplete and those ILs with $n = 4$, 6, 7, 8 and perhaps longer would be worth studying for a better picture of the situation. As with **2**, the polarity of **12** was not determined because it is not liquid at room temperature (m.p. 73-75°C) and the respective thermochromic shift of NR would exclude comparison in the series.

8: n = 2
9: n = 3
10: n = 5
11: n = 9
12: n = 21

Figure 4-13: Pyrrolidinium ILs investigated for chain length.

Table 4-4: Molar transition energies and solubilities in toluene for ILs 8-12.

Ionic Liquid	λ_{max} (nm)	E_{NR} (kJ mol^{-1})	Solubility in toluene (g L^{-1})
8	594	201.3	0.85
9	583	205.1	0.95
10	591	202.3	2.7
11	586	204.1	11.0
12	-	-	165.0

Attempts to dissolve **8-12** in hexane only resulted in emulsions for each IL, so toluene was used as a non-polar solvent instead. As before, an ideal concentration range was determined and found to be on the order of 10^{-5} mol L^{-1} in toluene (appendix 4: Appendix fig. 26). Spectra at concentrations an order of magnitude less than this were extremely weak and no stable ion current was obtained. This was observed for all ILs despite their very wide range of solubilities in toluene (Table 4-4). **8-10** were the least soluble in toluene, and at concentrations around 10^{-3} mol L^{-1} emulsions were observed (as in hexane). In order to dilute the sample in this state, an aliquot of this very fine emulsion was quickly diluted appropriately according to the dilution scheme. All ILs were soluble at concentrations of 10^{-4} mol L^{-1}.

On closer examination of the respective ESI-MS spectra of **8-12**, an interesting trend is noted.[c] As the alkyl chain on the IL shortens, the relative intensity of the first aggregate peak increases with respect to the monomer peak. In effect, the first aggregate for the smaller chain ILs is more lipophilic than the monomer; pairing up increases lipophilicity. This improves the spectral quality at this concentration. Moving to lower concentrations though, the ions are less paired from improved solvation, aggregation is therefore lessened, and spectra are much weaker. This occurs to a noticeable extent at concentrations of 10^{-6} mol L^{-1}. This type of pairing and aggregation is somewhat different than that seen for **3** because it is still possible to separate the aggregate from the

[c] See Appendix fig. 26 for ESI-MS of ILs 8-12 dissolved in toluene.

bistriflamide counter ion, whereas it was not possible to separate the first aggregate of **3** from the chloride conterion by simply increasing the capillary voltage.

4.5 Proposed explanation of the role of the ionic liquid

Two recent publications on ILs have described some features which may help explain why some ILs enable non-polar solvents while others do not. The first is by Seddon, who has demonstrated[60] that certain ILs can be purified by distillation while others cannot.[61] This is a feature that seems counterintuitive based on the assumption that distilling a salt would occur with anion and cation charge separation. The energy involved in Coulombic charge separation should alone be sufficient to totally inhibit such a process.[62] A second publication by Fraser seeks to characterize ILs along a continuum following the extent of ion pairing.[63] At one end were those ILs that strongly pair in the neat IL. They were described more as "molecular ion pairs," with the cation and anion closely associated with each other in the liquid, and their measured conductivities were very low. At the other end of Fraser's continuum were those ILs that do not pair much at all; the respective ions being quite separated from each other in the neat salt and their conductivities were much closer to a potassium chloride standard solution.

It seems reasonable to suggest that Fraser's "molecular ion pairs" may have accessible boiling points that facilitate distillation because the cation and anion would enter the gas phase together (although Seddon did not attempt to distill any of the ILs studied by Fraser). The molecular ion pairs are so strongly paired in the liquid form that they can enter the gas phase together and be distilled without charge separation. The latter ILs however, would be too separated from each other in the liquid form, that their boiling points would be inaccessible based on the Coulombic charge separation.

The logic which correlates the extent of ion pairing with conductivity and measured boiling points may help explain why not all ILs are equal in the task of enabling non-polar solvents for ESI-MS. Ionic liquids with the same lipophilic cation but with $[BF_4]^-$ or $[Cl]^-$ anions are either not soluble enough in the non-polar solvent, but more importantly they are so strongly paired in solution that the electrochemistry in the capillary is inhibited. These ILs may have accessible boiling points for this reason.

The ILs that effectively enabled the use of non-polar solvent would be less likely to have accessible boiling points. The respective charges on each ion are well shielded from their environments making them well removed from their counterion. This would raise their boiling points but also make them more responsive to the applied capillary voltage. The caveat for ESI-MS however, is that they must dissolve to a sufficient amount in the non-polar solvent.

From the literature on the conductivities of imidazolium ILs it appears that a variety of effects contribute to the bulk property.[64] An important aspect of conductivity is ion mobility, related to (but not solely dependent on) ion size. Conductivity was shown to increase with increasing size up to a limit (around the size of $[BF_4]^-$),[65] then decrease as size increases further, indicating that ion mobility was beginning to decline. Results from a different study suggest that conductivity maximizes at even smaller anion sizes (around the size of $[N(CN)_2]^-$).[66] This trend does not explain why the very large anion of **2** ($[B(C_6H_3(CF_3)_2)_4]^-$) with a mass of 863.2 *m/z* worked so well in enabling toluene, and it also does not explain why the bistriflamide anion facilitates the electrochemistry so well from hexane.

When considering all of the conflicting aspects of ionic liquids together (lipophilicity, solubility, size, polarity, ion pairing, etc) it is difficult to avoid the conclusion that the initial presumption that a sufficiently soluble IL is enough to facilitate high quality ESI-MS alone. Effectively, basing the ESI-MS response solely on the ability of **1** to dissolve in hexane was the right approach to the problem. Our advice to others is that any hexane-soluble ionic compound is suitable, and that beyond this stipulation, the exact combination chosen should be the one that is least likely to interfere with the solution chemistry of interest. Importantly, it may be necessary to increase the compound's concentration to levels that most experienced mass spectrometrists would avoid before beginning their experiments in the first place.

4.6 Experimental

4.6.1 Methods at the mass spectrometer

Ideal instrument settings for the most important parameters were optimized for each respective solvent and are summarized in Table 4-5. Optimized instrument parameters for selected solvents.

Table 4-5: Instrument parameter for different solvents.

Parameters	Pentane	Hexane	Diethyl Ether	Toluene
Flowrate (μL/min)	10	10	10	10
Capillary Voltage (V)	2900	2900	2900	2900
Cone Voltage (V)	20	20	20	20
Source Temp. (°C)	60	80	40	115
Desolvation gas Temp. (°C)	60	200	50	250
Desolvation gas flowrate (L/hr)	200	200	200	200
Collision Energy (V)	2	2	2	2

4.6.2 Solubility determination

For each IL, a saturated solution in the solvent of interest was prepared and shaken vigorously, generating a finely divided emulsion. The mixture was allowed to settle as long as necessary to separate, so the top solvent layer was clear on visible inspection. Exactly 2 mL of the top layer was pipetted into a preweighed flask with a vacuum adaptor (no grease). The solvent (hexane or toluene) was removed under vacuum, and the residue left under vacuum at room temperature for a further hour. The flask, adaptor and residue was reweighed with the difference corresponding to dissolved IL.

4.6.3 Polarity measurements

A solution of Nile Red in methanol was prepared (2.1 mol L^{-1}). A weighed amount of this solution was added to a preweighed amount of IL, swirled to facilitate homogeneity, and the methanol evaporated under vacuum. The maximum absorbance of Nile Red in each IL solution was determined by UV/Vis spectroscopy on a Varian Cary 5 UV-Vis-NIR spectrophotometer, in the region of 200-800 nm. The solution was run against a background of neat IL.

4.6.4 Synthesis of 2

Trihexyltetradecylphosphonium chloride (0.143 g, 0.28 mmol) and sodium tetra-(3,5-bis(trifluoromethyl)phenyl)borate (0.243 g, 0.28 mmol) were separately dissolved in toluene (4 mL and 6 mL plus 2 drops acetonitrile respectively). The solutions were combined and stirred for one hour. The mixture was then filtered through a Celite plug and washed with toluene. Solvent was then removed under vacuum and the residue dried under vacuum at 50 °C for 3 hours to provide a light brown liquid (42%). ^{1}H NMR ($CDCl_3$): δ (ppm) 7.68 (s, 8H, *ortho*-H); 7.51 (s, 4H, *para*-H); 1.92, 1.56, 1.42, 1.23, 0.87, 0.85 (all multiplets, 68H, CH_2 and CH_3). ESI-MS: (+ve) 483.5 *m/z* $[PC_{32}H_{68}]^+$; ESI-MS (–ve) 863.1 $[BC_{32}H_{12}F_{24}]^-$. M.P.: 59-60°C.

4.6.5 *N*-docosylmethylpyrrolidinium bromide[67]

N-methylpyrrolidine (0.35 mL, 3.37mmol) was dissolved in isopropanol (10 mL) in a 100 mL 3-neck round bottom flask with a reflux condenser and dropping funnel under an inert nitrogen atmosphere. 1-Bromodocosane (1.5 g, 3.85 mmol) was dissolved in an equal mixture of hexane and dichloromethane until dissolved then taken up to 50 mL with isopropanol. This was transferred into the dropping funnel with DCM wash, and added to the amine solution dropwise at a temperature of 50°C. Once added the solution was stirred for a further 48 hours. Solvent removed by rotovap and vacuum to give a brownish solid (1.56 g, 98 %yield). ^{1}H NMR ($CDCl_3$): δ (ppm) 3.83 (m, 4H, CH_2); 3.63 (m, 2H, CH_2); 3.30 (s, 3H, CH_3); 2.30 (m, 4H, CH_2); 1.76 (m, 2H, CH_2); 1.24 (m, 38H, CH_2); 0.86 (t, 3H, CH_3). M.P.: 82-88°C.

4.6.6 Synthesis of 12

N-docosylmethylpyrrolidinium bromide (0.312 g, 0.657 mmol) was dissolved in dichloromethane (4 mL). Lithium bis(trifluoromethyl)sulfonylamide (0.193 g, 0.672 mmol) was dissolved in water (4 mL) and added to the organic fraction. The mixture was stirred vigorously for 30 minutes. The mixture was then transferred to a separatory funnel and the organic fraction separated from the aqueous fraction. The organic phase was then extracted with water (5 × 2 mL), followed by a single aqueous phase extraction of 20 mL dichloromethane. All organic fractions were combined, dried with $MgSO_4$, filtered (CH_2Cl_2 wash), and vacuum pumped to dryness. The final product was an off white solid (0.214 g, 48 %). ^{1}H NMR ($CDCl_3$) refer to Figure 4-14: δ (ppm) 3.55 (m, 4H, CH_2-b); 3.31 (m, 2H, CH_2-d); 3.08 (s, 3H, CH_3-a); 2.28 (m, 4H, CH_2-c); 1.76 (m, 2H, CH_2-e); 1.35 (m, 2H, CH_2-f), 1.25 (m, 36H, CH_2-g to x); 0.90 (t, 3H, CH_3-y). ^{13}C NMR ($CDCl_3$): δ (ppm) 120.5-z, 64.85-d, 64.62-b, 48.57-a, 31.92 to 29.02-g to x , 26.19-f, 23.89-e, 21.57-c, 14.10-y. M.P.:73-75°C.

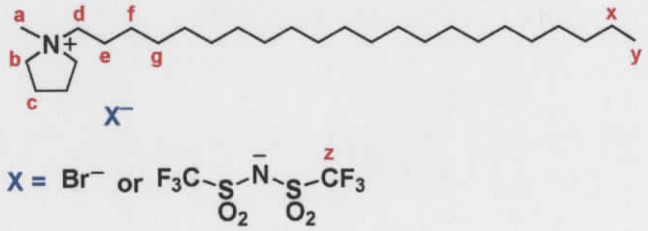

Figure 4-14: Structure of **2** for NMR assignment.

4.7 References

---

[1] de la Mora, J.F.; Van Berkel, G. J.; Enke, C.G.; Cole, R. B.; Martinez-Sanchez, M.; Fenn, J.B., *J. Mass Spectrom.*, **2000**, *35*, 939-952.

[2] Cech, N.B.; Enke, C.G., *Mass Spectrom. Rev.*, **2001**, *20*, 362-387.

[3] Tang, L.; Kebarle, P., *Anal. Chem.*, **1991**, *63*, 2709-2715.

[4] Blades, A.T.; Ikonomou, M.G.; Kebarle, P., *Anal. Chem.*, **1991**, *63*, 2109-2114.

[5] Richardson, D.E.; Plattner, D.A., *Comprehensive organometallic chemistry: Organometallic chemistry in the gas phase.* **2007**, *1*, 801-822.

[6] Chen, P., *Angew. Chem. Int. Ed. Engl.*, **2003**, *43*, 2832-2847.

[7] Santos, L.S.; Metzger, J.O., *Angew. Chem. Int. Ed. Engl.* **2006**, *45*, 977-981.

[8] Lide, D.R., *82nd Handbook of chemistry and physics.* 2001-2002, CRC Press Ltd. **2001**. New York.

[9] Brayshaw, S.K.; Ingleson, M.J.; Green, J.C.; McIndoe, J.S.; Raithby, P.R.; Kociok-Köhn, G.; Weller, A.S., *J. Am. Chem. Soc.*, **2006**, *128*, 6247-6263.

[10] Seddon, K.R., *J. Chem. Tech. Biotechnol.*, **1997**, *68*, 351-356.

[11] Welton, T., *Coord. Chem. Rev.*, **2004**, *248*, 2459-2477.

[12] Plechkova, N.V.; Seddon, K.R., *Chem. Soc. Rev.*, **2008**, *37*, 123-150.

[13] Mu. Z.; Liu, W.; Zhang, S.; Zhou, F., *Chem. Commun.*, **2004**, *33*, 524-525.

[14] Merrigan, T.L.; Bates, E.D.; Dorman, S.C.; Davis, J.H.Jr., *Chem. Commun.*, **2000**, 2051-2052.

[15] Liu, F.; Abrams, M.B.; Baker, R.T.; Tumas, W., *Chem. Commun.*, **2001**, 433-434.

[16] Dyson, P.J.; Geldbach, T.J., *Metal catalysed reactions in ionic liquids,* Springer: Amsterdam, **2005**.

[17] Dyson, P.J.; Ellis, D.J.; Welton, T., *Can. J. Chem.*, **2001**, *79*, 705-708.

[18] McNulty, J.; Capretta, A.; Wilson, J.; Dyck, J.; Adjabeng, G.; Robertson, A., *Chem. Commun.*, **2002**, 1986-1987.

[19] Ramnial, R.; Ino, D.D.; Clyburne, J.A.C., *Chem. Commun.*, **2005**, 325-327.

[20] Gordon, C.M.; McLean, A.J., *Chem. Commun.*, **2000**, 1395-1396.

[21] Bates, E.D.; Mayton, R.D.; Ntai, I.; Davis, J.H., *J. Am. Chem. Soc.*, **2002**, *124*, 926-927.

[22] Gordon, C.M.; Holbrey, J.D.; Kennedy, A.R.; Seddon, K.R., *J. Mater. Chem.*, **1998**, *8*, 2627-2636.

[23] Mazille, F.; Fei, Z.; Kuang, D.; Zhao, D.; Zakeeruddin, S.M.; Gratzel, M.; Dyson, P.J., *Inorg. Chem.*, **2006**, *45*, 1585-1590.

[24] Villagran, C.; Banks, C.E.; Hardacre, C.; Compton, R.G., *Anal. Chem.,* **2004**, *76*, 1998-2003.

[25] Branco, L.C.; Rosa, J.N.; Moura Ramos, J.J.; Afonso, C.A.M., *Chem. Eur. J.,* **2002**, *8*, 3671-3677.

[26] Welton, T., *Chem. Rev.,* **1999**, *99*, 2071-2083.

[27] Deetlefs, M.; Seddon, K.R., *Green Chem.,* **2003**, *5*, 181-186.

[28] Ohno, H., *Electrochemical Aspects of Ionic Liquids,* Hoboken, John Wiley & Sons, Inc., **2005**.

[29] Domanska, U., *Pure Appl. Chem.,* **2005**, *77*, 543-557.

[30] Lubben, A.T.; McIndoe, J.S.; Weller, A.S., *Organometallics,* **2008**, *27*, 3303-3306.

[31] Armstrong, D.W.; Zhang, L.K.; He, L.; Gross, M.L., *Anal. Chem.,* **2001**, *73*, 3679-3686.

[32] Łachwa, J.; Szydłowski, J.; Makowska, A.; Seddon, K.R.; Esperanca, J.M.S.S.; Guedes, H.J.R.; Rebelo, L.P.N., *Green Chem.,* **2006**, *8*, 262-267.

[33] Gerritsma, D.A.; Robertson, A.; McNulty, J.; Capretta, A., *Tetrahedron. Lett.,* **2004**, *45*, 7629-7631.

[34] Bradaric, C.J.; Downard, A.; Kennedy, C.; Robertson, A.J.; Zhou, Y., *Green Chem.,* **2003**, *5*, 143-152.

[35] Henderson, M.A.; McIndoe, J.S., *Chem Comm.*, **2006**, 2872-2874.

[36] Gozzo, G. C.; Santos, L. S.; Augusti, R.; Consorti, C. S.; Dupont, J., Eberlin, M. N., *Chem. Eur. J.*, **2004**, *10,* 6187-6193.

[37] Henderson, M.A.; McIndoe, J.S; Dyson, P.J., *Ionic liquids: From knowledge to application*; Solutions for electrospray ionization mass spectrometry, Rogers, R.D.; Plechkova, N.V.; Seddon, K.R., ACS Symposium Series, American Chemical Society.

[38] Zhu, Q.; Song, Y.; Zhu, X.; Wang, X., *J. Electroanal. Chem.,* **2007**, *601*, 229-236.

[39] Zhao, D.; Dyson, P.J.; McIndoe, J.S., *Chem. Commun.,* **2003**, 508-509.

[40] Halpern, J.; *SCIENCE*, **1982**, *217*, 401-407.

[41] Schrock, R.R.; Osborn, J.A., *J. Am. Chem. Soc.,* **1971**, *93*, 2397-2407.

[42] Dyson, P.J.; Khalaila, I.; Luettgen, S.; McIndoe, J.S.; Zhao, D., *Chem. Commun.*, **2004**, 2204-2205.

[43] van den Broeke, J.; Stam, M.; Lutz, M.; Kooijman, H.; Spek, A.L.; Deelman, B.J.; van Koten, G., *Eur. J. Inorg. Chem.*, **2003**, 2798-2811.

[44] Finden, J.; Beck, G.; Lantz, A,; Walsh, R.; Zawarotko, M.J.; Singer, R.D., *J. Chem. Crystallogr.*, **2003**, *33*, 287-295.

[45] Bott, S.G.; Alvanipour, A.; Morley, S.D.; Atwood, D.A.; Means, C.M.; Coleman, A.W.; Atwood, J.L., *Angew. Chem.*, **1987**, *99*, 476-478.

[46] Reichardt, C., *Green Chem.*, **2005**, *7*, 339-351.

[47] Deye, J.F.; Berger, T.A., *Anal. Chem.*, **1990**, *62*, 615-622.

[48] Carmichael, A.J.; Seddon, K.R., *J. Phys. Org. Chem.*, **2000**, *13*, 591-595.

[49] Oehlke, A.; Hofmann, K.; Spange, S., *New J. Chem.*, **2006**, *30*, 533-536.

[50] Fletcher, K.A.; Storey, I.A.; Hendricks, A.E.; Pandey, S.; Pandey, S., *Green Chem.*, **2001**, *3*, 210-215.

[51] Chiappe, C.; Pieraccini, D., *J. Phys. Org. Chem.*, **2005**, *18*, 275-297.

[52] Sudhir, M.V.K.A.; Brennecke, J.F.; Samanta, A., *Chem. Commun.*, **2001**, 413-414.

[53] Harrod, W.B.; Pienta, N.J., *J. Phys. Org. Chem.*, **1990**, *3*, 534-544.

[54] Golini, C.M; Williams, B.W.; Foresman, J.B., *J. Fluorescence,* **1998**, *8*, 395-404.

[55] Golding, J.J.; MacFarlane, D.R.; Spiccia, L.; Forsyth, M.; Skelton, B.W.; White, A.H., *Chem. Commun.*, **1998**, 1593-1594.

[56] Bonhote, P.; Dias, A.P.; Papageorgiou, N.; Kalyanasundaram, K.; Gratzel, M., *Inorg. Chem.*, **1996**, *35*, 1168-1178.

[57] Shkrob, I.A.; Wishart, J.F., *J. Phys. Chem. B.*, **2009**, *113*, 5582-5592.

[58] Mandal, P.K.; Saha, S.; Karmakar, R.; Samanta, A., *CURRENT SCIENCE,* **2006**, *90*, 301-310.

[59] Bailey, P.J.; Barrett, T.; Parsons, S., *J. Organomet. Chem.*, **2001**, *625*, 236-244.

[60] Earle, M.J.; Esperanca, M.S.S.; Gilea, M.A.; Canongia Lopes, J.N.; Rebelo, L.P.N.; Magee, J.W.; Seddon, K.R.; Widegren, J.A., *Nature,* **2006**, *439(7078)*, 831-834.

[61] Leal, J.P.; Esperanca, J.M.S.S.; Minas da Piedade, M.E.; Canongia Lopes, J.N.; Rebelo, L.P.N.; Seddon, K.R., *J. Phys. Chem. A.,* **2007**, *111*, 6176-6182.

[62] Chen, H.; Ouyang, Z.; Cooks, R.G., *Angew. Chem. Int. Ed.*, **2006**, *45,* 3656-3660.

[63] Fraser, K.J.; Izgorodina, E.I.; Forsyth, M.; Scott, J.L.; MacFarlane, D.R., *Chem. Commun.,* **2007**, 3817-3819.

[64] Ya-Hung Yu; Soriano, A.N.; Meng-Hui Li, *Thermochim. Acta,* **2009**, *482*, 42-48.

[65] Vila, J.; Varela, L.M.; Cabeza, O., *Electrochim. Acta.,* **2007**, *52*, 7413-7417.

[66] Ya-Hung Yu; Soriano, A.N.; Meng-Hui Li, *J. Chem. Thermodynamics,* **2009**, *41*, 103-108.

[67] Abdallah, D.J.; Weiss, R.G., *Chem. Mater.,* **2000**, *12*, 406-413.

Chapter 5 ESI-MS of methylaluminoxane

5.1 Introduction

In order for the discovery of the ESI-MS enabling features of ILs in lipophilic solvents to be of use, it must be applied to the study of sensitive compounds that would otherwise degrade in polar solvents. Consideration of the organometallic catalysis literature suggested that Ziegler-Natta polymerization would be an ideal system to study. Although initially developed as a heterogeneous system[1] with a $TiCl_4$ catalyst and $Al(Et)_3$ activator,[2] group 4 metallocenes were introduced in 1976 by Kaminsky as the first single site homogeneous systems.[3]

These homogeneous systems have proven their worth with a number of advantages.[4] Unlike heterogeneous systems, every metal center is in the same chemical environment and has the potential to be catalytically active, each growing a separate polymer chain.[5] A very narrow polydispersity results, probably a consequence of the fact that almost every metal center is active at the same time.[6] The ligands of these homogeneous catalysts present another advantage,[7] in that their modification can tune the regiospecificity of polypropylene (PP) in a way that was not possible before. Finally, molecular weights can be controlled by varying time and temperature of reaction.[3]

The cyclopentadienyl ligand can be substituted in a variety of ways to tune the metal center (Figure 5-1). Kaminsky's work initially focused on the dichlorometallocene, but further research yielded complexes with slightly different properties. Chiral *ansa* metallocene catalysts were developed by Ewen,[8] which gave isotactic PP with melting points much higher than the atactic analogues. Shortly thereafter constrained geometry catalysts were developed,[9] where the bulk of the two ligands was held back by linking them with a small angle linker.[10,11] The active site on the metal center is more open to attack by incoming olefin, and insertion reactions are less influenced by the ligand bulk. Along these lines the Stephan group discovered that phosphinimide ligands function similar to cyclopentadienyl, and in certain cases much better.[12]

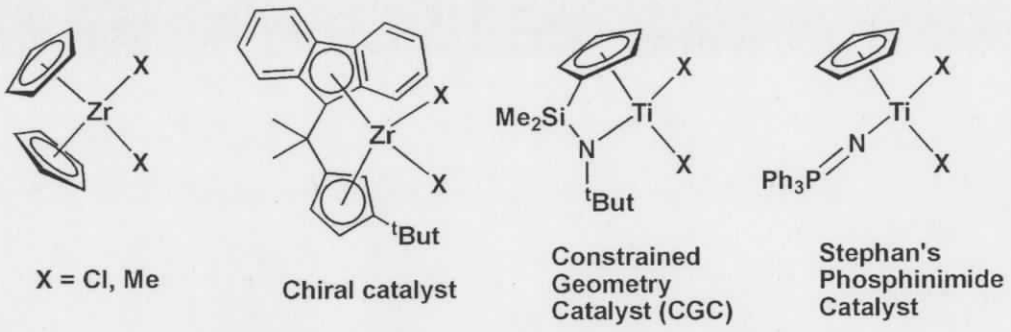

Figure 5-1: Precatalyst for single site olefin polymerization

Important to the activity of all of these pre-catalysts is an activating agent that will generate the true catalyst for polymerization.[4] This cocatalyst performs an important duty in generating the active species, and a variety of Lewis bases have been found to achieve this end.[13,14] Fluorinated boron cocatalysts (Figure 5-2) in conjunction with pre-catalysts in Figure 5-1 result in a very effective catalytic system. Trace amounts of any impurity is enough to completely shut down catalytic activity, which adds considerable handling difficulty. So far the only industrially viable cocatalyst is methylaluminoxane (MAO), and it is this unusual species that constitutes the bulk of research in this chapter.

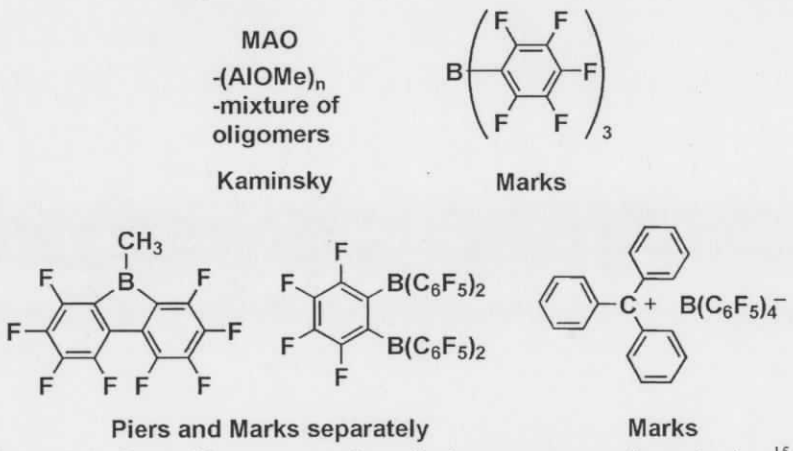

Figure 5-2: Several known cocatalysts for homogeneous polymerization.[15,16]

5.2 The importance of MAO

The significance of Kaminsky's discovery stems as much if not more from the discovery of the cocatalytic nature of (MAO) than the actual metallocene catalyst. Trimethyl aluminum (TMA), along with other trialkyl alanes, were known alkylators beforehand, with triethylaluminum as the cocatalyst of choice for heterogeneous systems with $TiCl_4$.[17] Kaminsky discovered that adding a small amount of water to TMA generated a vastly more potent activator for the homogeneous system.[18] This was a serendipitous discovery made when an NMR tube for the study of the reaction between $TiCp_2Me_2$ and TMA at low temperature, was simply closed with a plastic cap instead of flamed-sealed.[5] Comparing the spectrum of the plastic cap sample with that of the flame sealed sample revealed a new peak in the CH_2 region. Scaling up the reaction in the presence of ethylene, with periodic opening for NMR analysis, revealed that the pressure of ethylene dropped faster and faster with successive samplings. In essence every time the experimenter exposed the autoclave to air then closed it again for another ethylene pressurization, the polymerization was faster than before. It did not take long to realize the role of water in the system, and control experiments confirmed the importance of TMA hydrolysis.[5] When the hydrolysis of TMA was carried out before the precatalyst was added, an unknown aluminum, oxygen, and methyl containing oligomer was obtained that could be isolated and used with the catalyst. Thus, MAO was discovered.

5.3 Function of MAO

MAO participates in a number of reactions with the precatalyst, exemplified here by bis(cyclopentadienyl) zirconium dichloride (**1:** Equation 5-1).[19] A simple and reversible complexation/decomplexation (Equation 5-1) generates the short lived intermediate **1a**. This intermediate can alkylate the metal in a ligand exchange reaction (Equation 5-2) to make the monomethylated precatalyst **2** and a monohalogenated MAO complex **2a**. Complex **2** then reacts again with MAO to abstract the remaining chloride ligand (Equation 5-3) via the bridging intermediate **2b**, to generate the active catalyst **3**.

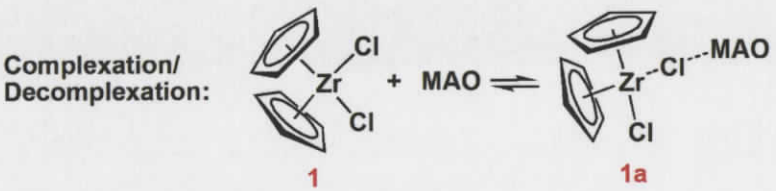

Equation 5-1

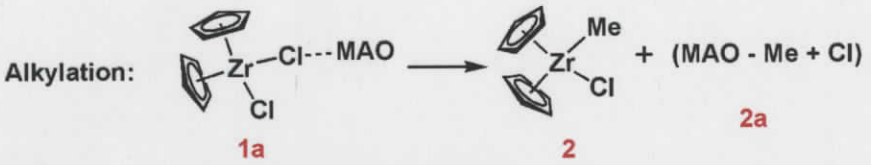

Equation 5-2

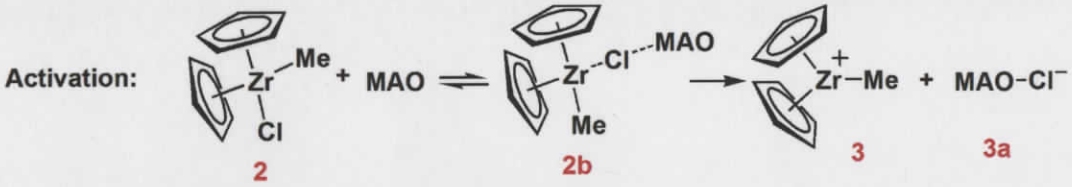

Equation 5-3

This activation process has undergone intense scrutiny over the years. Most species containing zirconium are reasonably straightforward to characterize by standard NMR techniques, but those of MAO are very difficult. Studies by Marks, with the highly Lewis acidic tris(pentafluorophenyl) borane (BAr^F), revealed the nature by which the active catalyst is generated from the dimethyl zirconocene complex (Equation 5-4). Intermediate **4a** was characterized crystalographically and shown to polymerize ethylene without any induction period.[20] In this manner BAr^F behaves as a stoichiometric cocatalyst. On exposure to propylene, at a temperature of -25°C, NMR studies revealed that over 70% of **4a** underwent olefin insertion and polymerization. This study quite conclusively demonstrated that the active catalyst was generated by methyl abstraction by a Lewis acid, not from small concentrations of an impurity, and it also proved the catalyst was cationic.[20]

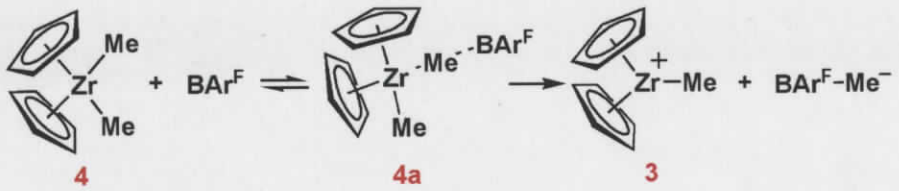

4 4a 3

Equation 5-4

Stoichiometric addition of MAO does not work at all. In fact, no catalytic activity is observed until Al:Zr ratios of approximately 100:1 are reached, with optimal performance around 1000:1, while certain systems require up to 20,000:1.[6] Kaminsky's initial kinetic investigations determined that the reaction rate depended linearly on Zr concentration, but quadratically on aluminoxane.[4] Furthermore, for every zirconium atom there are between six and twenty aluminum atoms and the ideal ratio of Al:H_2O to generate the most active aluminoxane is between 2:1 and 5:1.[3]

The system is extremely sensitive to reaction conditions, and the excess MAO is puzzling. A number of explanations have been put forth in attempts to explain the enormous excess:

1. The cationic catalyst (**3**) is extremely active, and therefore any impurities may rapidly lead to its decomposition. The excess of MAO scavenges trace amounts of deactivating halide, oxygen, or water.[21]

2. Catalyst **3** can deactivate by α-hydrogen transfer from a zirconium methyl group to a methyl group on a separate zirconium or aluminum atom (**5**) to generate an equivalent of methane and a methylene bridged metal dimer (**5a**: Equation 5-5).[22] In order to reactivate the metal center a dimethyl aluminum end group (**5b**) is required (Equation 5-6); these end groups are expected to be in small concentration, so the large MAO excess would be needed for a sufficient amount of them to be present.[5]

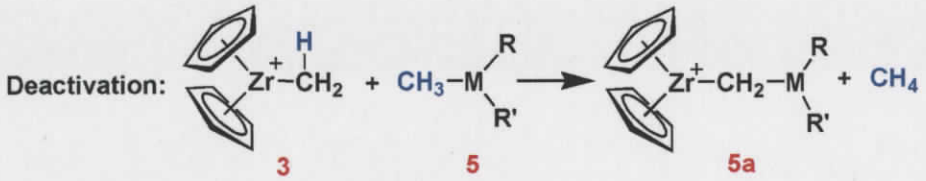

Equation 5-5

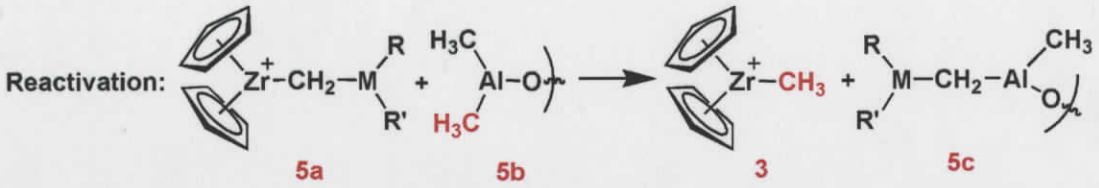

M = Al, R = Me, R' = MAO
M = Zr, R = Me, R' = Cp_2

Equation 5-6

3. The actual activating agent, or the true cocatalyst, would be the most reactive species and therefore present in very small concentration after scavenging and drying of the environment. The large excess ensures enough is present to activate all metal centers. It has always been found that a small amount of TMA exists in MAO,[23] even at Al:H_2O ratios of 1:1. Furthermore, it has been found that the TMA coordinates to MAO, and it has been suggested that it is this feature which activates the metal center.[24] The concentration of TMA is always small, so the excess is important.

4. MAO is not a very strong Lewis acid (LA). Calculations have shown that for methyl abstraction in generating the active catalyst, K_{eq} is about 2×10^3 (Equation 5-7). This means that at millimolar levels, only about 20% of the precatalyst has been activated; the excess MAO raises the amount of activated catalyst to an acceptable level.[25]

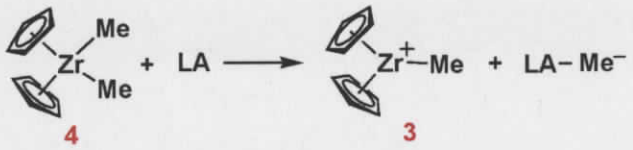

Equation 5-7

5.4 MAO structure

Specifically, an alkylaluminoxane (or alkylalumoxane) is a molecule with at least one O^{2-} group bridging two aluminum atoms,[26] a definition which does not apply to any molecule where oxygen bridges anything other than aluminum, such as alkoxides. The alkyl group from the trialkyl aluminum reactant completes the name: methylaluminoxane (from trimethyl aluminum), ethylaluminoxane (from triethylaluminum), and so on. Alkylaluminoxanes are made from the hydrolysis of pyrophoric trialkylaluminum compounds (Equation 5-8) in an extremely exothermic reaction (ΔH = -1090 kJ/mol for hydrolysis of TMA).[26]

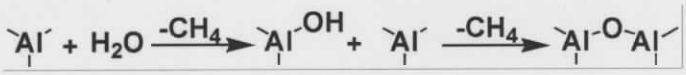

Equation 5-8

Given the exothermicity of this reaction and the tendency for explosions if not carried out with due care, other methods have been developed:

1. Addition of water in the form of a hydrated salt (Equation 5-9).[4]

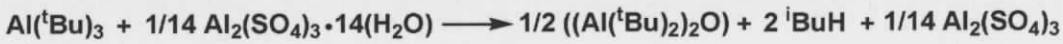

Equation 5-9

2. Oxygen transfer reactions from other oxygen sources such as CO_2 (Equation 5-10),[27] PbO (Equation 5-11),[28] or siloxanes (Equation 5-12).[29]

$$2AlEt_3 \xrightarrow[-Et_2C=O]{+\ CO_2} Et_2AlOAlEt_2$$

Equation 5-10

$$2AlR_3 + PbO \longrightarrow R_2AlOAlR_2 + PbR_2$$

Equation 5-11

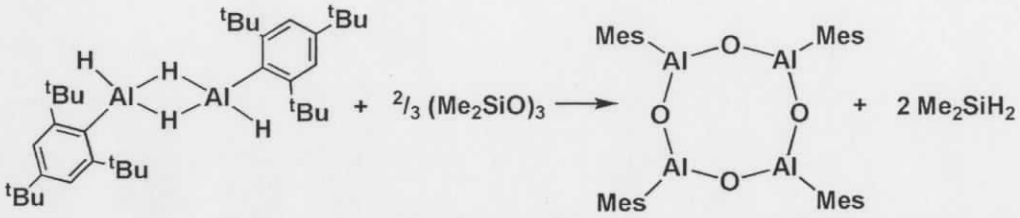

Equation 5-12

MAO has proven to be an incredibly elusive compound to structurally characterize. Much work has been devoted to understand this "ghost".[26,30] It has been determined that MAO is a complex mixture of oligomers with the empirical formula $(AlOMe)_n$, where n is any integer between one and twenty. Proton NMR studies have narrowed the empirical formula to $[AlO_{0.75\text{-}0.8}Me_{1.4\text{-}1.5}]_n$, for the most active MAO cocatalysts.[31]

Before Kaminsky's discovery in 1976, interest in understanding the nature of MAO was limited as results proved highly ambiguous and inconclusive. After the discovery of the effective cocatalytic nature of MAO, research picked up again with early proposals of the simple linear and cyclic structures (Figure 5-3).[30] In 1983 the first crystal structure of an aluminoxane of molecular formula $K(Al_7O_6Me_{16})$ was reported by Atwood (Figure 5-3).[32] Other crystal structures by Barron revealed the significance of cage compounds such as $[AlO^tBu]_n$ (where n = 6-9 and 12),[33] which were also shown to act themselves as cocatalysts (Equation 5-13). Recent theoretical work by Linnolahti[34] has suggested that nanotubular structures may also be components of MAO, and theoretical work from the Ziegler group found that cage structures are computationally plausible co-catalysts.[35]

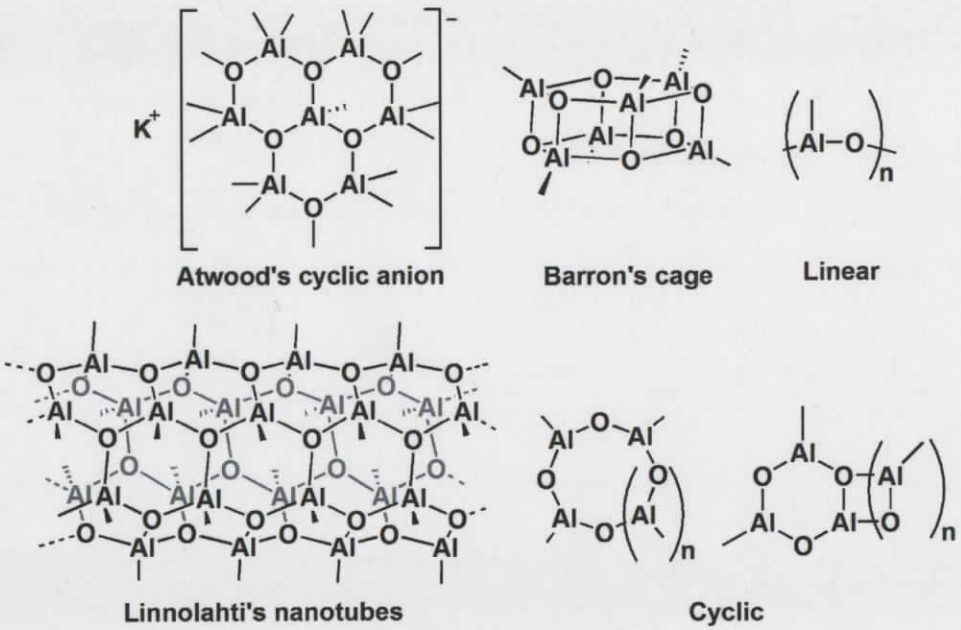

Figure 5-3: Several proposed structures of MAO

Barron's group focused on the more crystalline *t*-butyl aluminoxanes and observed evidence to suggest the inherent Lewis acidity responsible for catalyst activation lies in the ring strain of the cage compounds.[36] The reactivity associated with such strained cage compounds was attributed to the "latent Lewis acidity" of the cage bonds (red bonds of **6**; Equation 5-13), and opening the cage in the activation process relieved the strained bonds. The reactivity is present when the cage is closed, but diminishes on activation of the catalyst.

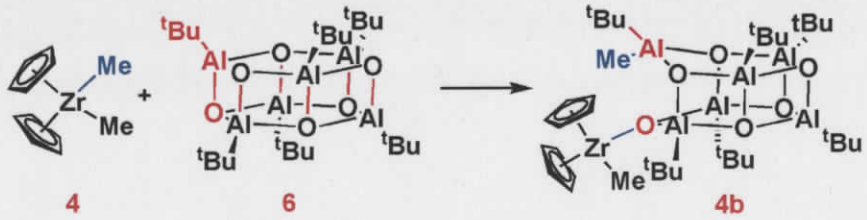

Equation 5-13

It is possible that *all* structures from Figure 5-3 are present in a commercial sample, albeit at varying concentrations. Any of these species are likely to be reactive enough to react

with traces of water that would otherwise deactivate the catalyst. Calculations have shown that certain structures are far more stable than others and are therefore less likely to interconvert or randomize in solution. Arguably, these structures would be less likely to activate the metal center, and would therefore be less useful. Their stability would however, favor their abundance. Correspondingly, other structures are more labile and able to coordinate any free TMA, or undergo comproportionation and disproportionation reactions with other species via their available Lewis acidic sites (empty *p*-orbital on Al) and basic sites (available lone pairs on O). It would be these more reactive species that would be expected to perform the desired cocatalytic functions.

A number of factors contribute to the experimental challenges associated with analysis of MAO:

1. The lack of spectroscopic handles makes it difficult to know what is in solution. ^{1}H and ^{13}C NMR have only methyl groups to examine; when all methyl groups are in similar environments very little structural evidence is obtained.[37] As for aluminum and oxygen, NMR evidence exists,[38] but again, the trouble of ambiguity associated with poor NMR signals, quadrupolar nuclei, low isotopic abundances of those nuclei, or concentration problems confound attempts to understand the system. Other spectroscopic methods such as IR[39] and UV-VIS are also poorly tailored to the study of MAO.

2. Alkyl alanes, aluminoxanes, and haloalanes rapidly associate to give dimers, trimers, and larger oligomers. The Lewis acidic sites on aluminum easily accept any available lone pair, even if it means sharing two electrons between two bonds. This makes such species highly fluxional with multiple NMR signals despite very similar environments.

3. Aluminoxanes rapidly and easily undergo disproportionation whenever their equilibrium is disrupted. Adjusting temperature or pressure, in an attempt to distill or precipitate one component of the mixture, shifts the equilibrium and drastically changes the composition.

4. Different methods of synthesis and product isolation produce different alkylaluminoxanes. The preferred structure will depend on the amount of water added, the temperature at which it was added, how quickly it was added, the solvent used, the alkyl side chain, and the stirring rate.

5.5 Previous ESI-MS studies of this system

There are almost no mass spectrometric studies of MAO.[40] After an extensive search, the only published mass spectrum of MAO appears to be in Kaminsky's original patent application of 1983.[41] This spectrum had a molecular ion at 290 *m/z*, corresponding to a molecular formula of $(AlOMe)_5$. It seems the majority of work towards determining a molecular mass has been done by line width NMR analysis[42] or ebullioscopic and cryoscopic measurements.[24] These studies are confounded with ambiguity and reliable molar masses have not yet been determined.

A couple of groups have separately done high quality gas phase ESI-MS studies[43,44] of the active zirconium catalyst. Chen[45] and Metzger[46] have shown that mass selecting catalyst **3** for collision with a reactive olefin in a separate chamber, results in the coordination, insertion, and chain propagation reactions characteristic of the Cossee-Arlman mechanism.[47] Chen observed propagation of four butene equivalents, while Metzger observed propagation of five ethene moieties. Rates were calculated to be slower than diffusion-controlled in the gas phase but were several orders of magnitude faster than the solution phase reaction.

The first ESI-MS study to mention aluminum-containing species appeared in 2005 when Repo used MAO to activate an iron catalyst for polymerization of various acrylate species. This study focused mainly on the iron center responsible for catalysis, but the authors make a cursory observation of a series of peaks separated by 73-75 *m/z* in the positive ion mode.[48] They reasoned them to be associated with the interaction of TMA with moisture present in the instrument, but made no attempt to assign any structures. They also neglected any study of the negative ion mode, although they do mention that studying MAO by ESI-MS is not possible due to the non-polar nature of toluene.

Perhaps the most impressive work towards understanding the nature by which the catalytic zirconium/MAO ion pair interact with each other has come from the group of Chen in a pair of communications.[49,50] Following a series of control experiments, two polymeric species were observed to have formed with different rates. It was suggested that the polymer chain grew on the zirconium center following the Cossee-Arlman mechanism as expected, but the chain can be transferred to an aluminum center on MAO in a thermoneutral transmetallation reaction with a rate that exceeds the rate of propagation on zirconium. Polymerization then continues in a slower "Aufbau"[51] type reaction on MAO. The faster series was said to have not yet undergone the transmetallation reaction, while the slower series had. Their result was supported by a series of calculations as well as by comparison to the BAr^F activated system. The conclusion was that the rate of transmetallation to MAO was faster than propagation on the transition metal catalyst, thereby functioning to slow the overall rate of reaction. Transmetallation from zirconium to MAO continues until all methyl groups are consumed on MAO, at which point the two series converge and the polymer chains jump back and forth between the zirconium center and MAO in competing polymerization and transmetallation reactions.[50] The observed rate has contributions from both reactions.

Given the amount of research that has been done on designing more active or more specific transition metal polymerization catalysts,[52,53] it was decided that the negative ion mode provided an opportunity for research that was largely unexplored. In a well-cited review that covers many activating agents for numerous polymerization catalysts, Marks described MAO as a "black box," although it was presumed that the function of the true MAO cocatalyst performed similarly to the BAr^F cocatalysts.[21]

5.6 Precedent for further study of the cocatalyst

The slowing effect of the transmetallation reaction on the rate of polymerization is a serious detriment to the polymerization. As evidenced by the high rates observed for the BAr^F activated system, it would be ideal to have a stoichiometric cocatalyst that could function to maintain the necessary dry environment, but which would also not slow catalysis as described by Chen.[49] This, along with the fact that MAO is cheaper to make

than BAr^F, would considerably reduce the cost of the added cocatalyst and the amount of aluminum impurities present in the final product.

Although the work by Barron has shed valuable light on potential structures, differences between the *tert*-butyl aluminoxane and the methyl aluminoxane system are significant. The methyl system is far more reactive, due to less hindrance about the metal. Ziegler has performed calculations on structure **4b** (Equation 5-13) and suggests this is more likely a dormant species that does not function to activate the metal, but instead to deactivate it.[54] The more active species, which was not crystallized, was proposed to have the Zr bound to the Al center instead. This dilemma however, only adds to the uncertainty surrounding the mechanism by which MAO activates the catalyst.

Attempts to employ mass spectrometry to study the composition of MAO have never come to fruition, probably because common ionization methods have some mechanism that would produce artefacts. Electron impact is too energetic, producing fragment ions; MALDI requires a suitable matrix that would likely react with MAO; the same would be true for FAB and LSIMS. Electrospray ionization mass spectrometry has never been used – at least not successfully – probably because of its dependence on polar solvents. The ability to inject a genuine catalytic sample has only just been introduced with the ability to employ lipophilic ionic liquids for ESI-MS in the electrospray ionization process.[55] The active catalyst is cationic, and the cocatalyst is anionic, making this an ideal system for study by ESI-MS without the need for synthesis. Furthermore, the few ESI-MS studies that have been undertaken seem to have neglected to investigate the negative ion mode.

5.7 Results and Discussion

5.7.1 The MAO system

Preliminary experiments focused on identifying the most efficient way to obtain high quality data. A range of ionic liquids in toluene were investigated but all proved to be reactive with either MAO or the metallocene in a way that was fatal to the experiment; IL-**2** (in chapter 4) was essentially useless as the BAr^F anion exchanged phenyl groups

for methyl or chloride from MAO.[56] However, it was found that fluorobenzene (PhF) was an excellent solvent for ESI-MS, and did not require an IL adulterant so long as sufficient quantities of the catalyst and cocatalyst were used. Some studies have used bromobenzene as solvent in olefin polymerization without noted detriment,[57] and as such fluorobenzene was used as the solvent for all subsequent studies.

5.7.1.1 First results from both ion modes

To understand how MAO activates the zirconium center a mixture of Cp_2ZrCl_2/MAO in fluorobenzene was examined. In the positive ion mode, some easily identified peaks were seen (Figure 5-4). The zirconocene dimerizes after dehalogenation, but peaks are easily assigned (Table 5-1), and varying amounts of methylation were observed. This was an encouraging result that has been previously observed.[58]

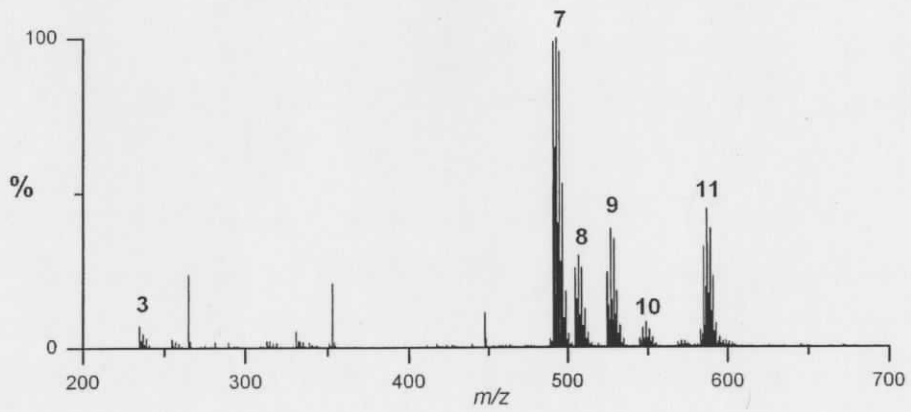

Figure 5-4: Positive ion spectrum of MAO activated $ZrCp_2Cl_2$ system in PhF.

Table 5-1: Peak assignments for Figure 5-4.

Peak: *m/z*	Assignment
3: 234.9	$[ZrCp_2Me]^+$
7: 492.9	$[Zr_2Cp_4ClMeH]^+$
8: 506.9	$[Zr_2Cp_4ClMe_2]^+$
9: 526.9	$[Zr_2Cp_4Cl_2Me]^+$
10: 548.8	$[Zr_2Cp_4Cl_3]^+$
11: 586.9	$[Zr_2Cp_4Cl(Tol.)(H_2O)]^+$ [a]

Switching ion modes gave some insight to the fate of the MAO anion generated in the same reaction (Figure 5-5). At first glance this is a painfully complicated spectrum, but there are some points of interest:

[a] It is presumed that the toluene of this ion came from the initial reaction mixture which was prepared in toluene, before dilution in PhF for ESI-MS analysis.

1. There appears to be a favored mass range in the region of 1750 - 1900 *m/z* and 2100 - 2250 *m/z*. Based on the known structural diversity of aluminoxanes and the potential to form a wide range of oligomers, it was a surprise that two regions seem preferred instead of the entire mass range. Furthermore, these masses are of considerably higher nominal mass than what has previously been determined.

2. Favored peaks in the regions of interest are separated by about 20 *m/z*. Because the precatalyst was Cp_2ZrCl_2, it is reasonable to suggest that the differences correspond to the loss of CH_3^- with concurrent addition of Cl^-. The presence of a series of peaks, and not merely two peaks implies that one MAO molecule can dehalogenate and methylate multiple zirconocene precatalysts (ie: the active cocatalyst has more than one active site).

3. Close inspection of the isotopic distributions confirm that multiple chlorides are present in one peak, but the peak still does not match an expected isotope pattern. The elements Al, O, C, and H are all basically monoisotopic, with the only significant other isotope being ^{13}C at ~1.1% abundance.[59] If there are up to 70 methyl groups in one MAO species the $[M + 1]^-$ peak should be about 80% intensity with respect to the 100% peak, but that is not the case here. The $[M + 1]^-$ and $[M + 2]^-$ peaks cannot be rationalized solely on the probability distributions of the isotopes of chloride and carbon.

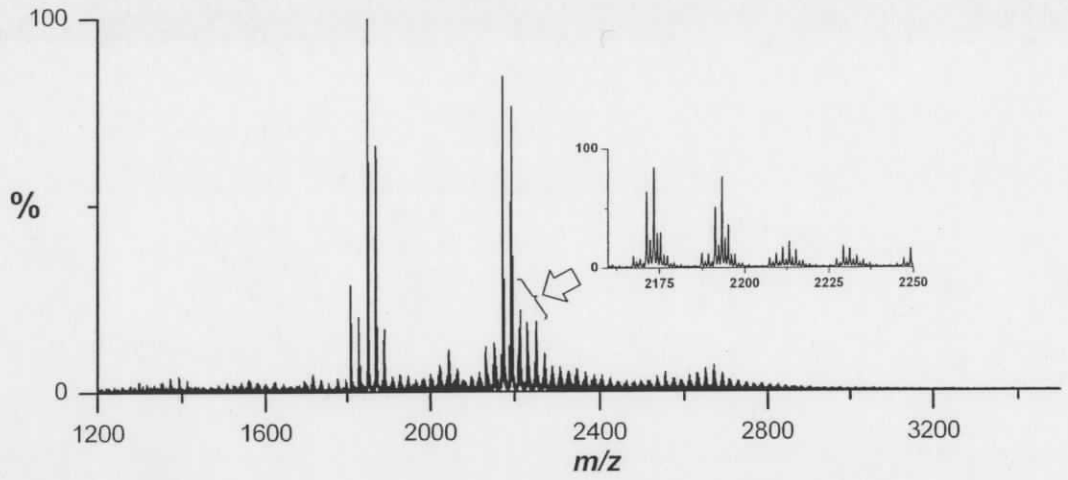

Figure 5-5: Negative ion spectrum generated from the activation of $ZrCp_2Cl_2$ in PhF.

After these first results, it was desirable to understand how the system was different at varying Al:Zr ratios. To rule out the isotopic contribution of chloride and to simplify the spectrum somewhat, Cp_2ZrMe_2 was used instead of the dichloride precatalyst. It was very difficult to interpret results from the positive ion mode at high ratios because there were no zirconium containing species observed. The negative ion mode was, however, more telling. The spectrum was isotopically simpler, but again only two regions were favored; this time peaks were easily distinguished and separated from each other. At lower Al:Zr ratios around 100:1, the pattern begins to look similar to the distribution in Figure 5-5. Close inspection of the isotope pattern reveals again considerable contributions from $[M + 1]^-$, $[M + 2]^-$, and $[M + 3]^-$. The absence of chloride from this system but the same general distribution of peaks, suggests that the ionization path is perhaps independent of the Zr complex.

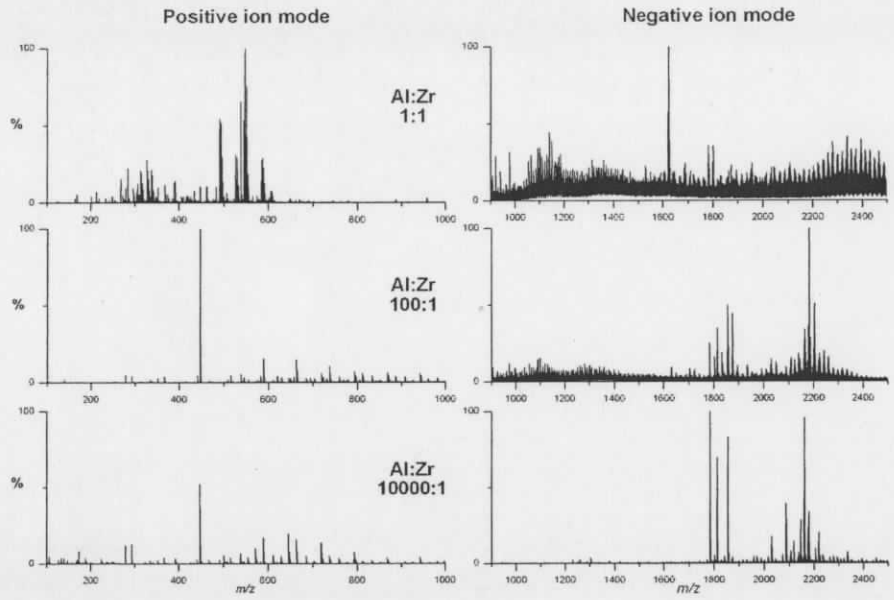

Figure 5-6: Spectra of the catalyst/cocatalyst at successively decreasing ratios of MAO:Zr.[b]

Kaminsky's efforts in elucidating the mechanisms of MAO offer the first explanation of the unusual isotope pattern. As described earlier (Equation 5-5), one deactivating path is by α-hydrogen transfer from the methyl group on zirconium to the methyl group of another metal atom (either zirconium or aluminum); this generates a methylene bridged dimer (**5b**) and an equivalent of methane (Equation 5-5). Reactivation of the zirconium occurs by transferring a methyl group from another aluminum atom to zirconium (Equation 5-6). If however, the methylene-bridged dimer is reactivated by a methyl group from an aluminum center on the same aluminoxane, then the result would be a net change of -1 *m/z*. Perhaps then, a better assignment of each peak in a given pattern is $[M]^-$, $[M-1]^-$, $[M-2]^-$.

Another contributor to this would be the exchange of oxygen for methyl. An oxidized catalyst can be reactivated with a methyl group from MAO resulting in an overall gain of 1 *m/z*. This method of reactivation counters any loss from the methylene-bridged dimer,

[b] A more complete series of ratios can be found in Appendix 5: Appendix fig. 27.

but in a strictly dried environment its contribution would be significantly less and the pattern dominated by the reactivation of the methylene dimers.

To simplify the study further, a commercial MAO solution was analyzed without any added catalyst. It was expected that ionization would occur in a similar fashion as with the Zr/MAO system; that is, methyl abstraction from an aluminum center to make either a cationic MAO species with the charge localized about two coordinate Al, or an anionic MAO complex with charge localized on a four coordinate aluminum center. From the positive ion mode, two strong series are evident (Figure 5-7). Each peak in the respective series is separated by 74 *m/z* which corresponds to a monomer unit of AlO_2Me (Table 5-2), matching previous observations of Repo who attributed this trend to the oxidation of MAO in the source.[48] These oligomeric series were never observed in experiments involving the zirconium catalyst, so it seems reasonable to suggest that a different mode of ionization is responsible for their appearance in its absence.

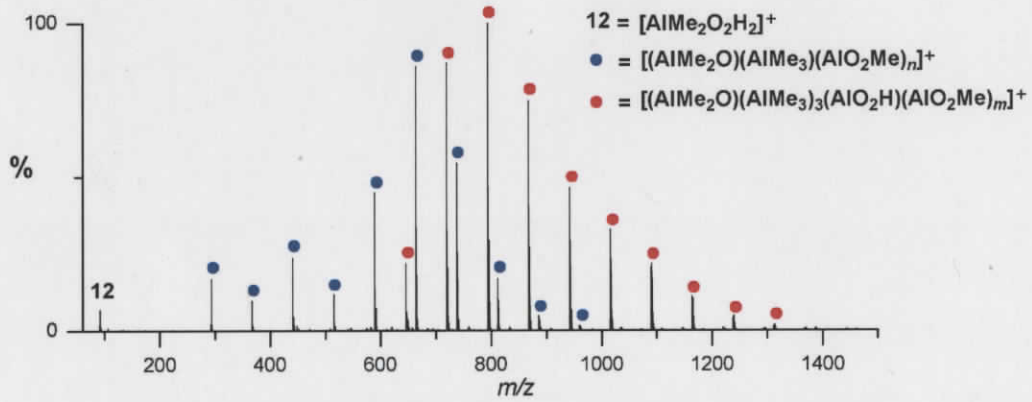

Figure 5-7: Positive ion spectrum of commercial MAO in toluene/PhF.

Table 5-2: Assignment of Figure 5-7

Series	Assignment
Blue	n = 2-10
Red	m = 4-11

In the negative ion mode, a surprisingly simple spectrum was again observed, and more importantly it matched the spectrum of MAO in the presence of the zirconium precatalyst. Presumably, ionization of the MAO alone in this mode occurs similarly to the ionization from the Zr/MAO system. In consideration of the exothermicity of Equation 5-8 and the known fluxionality of MAO structures, one would expect to observe a far more complicated spectrum with peaks across the entire range of *m/z* values. The simplicity observed in Figure 5-8 suggests that certain MAO structures are favored over

others. Importantly though, those structures that do not ionize easily would go unnoticed by mass spectrometry, so this spectrum is of course only representative of the most easily ionized structures.

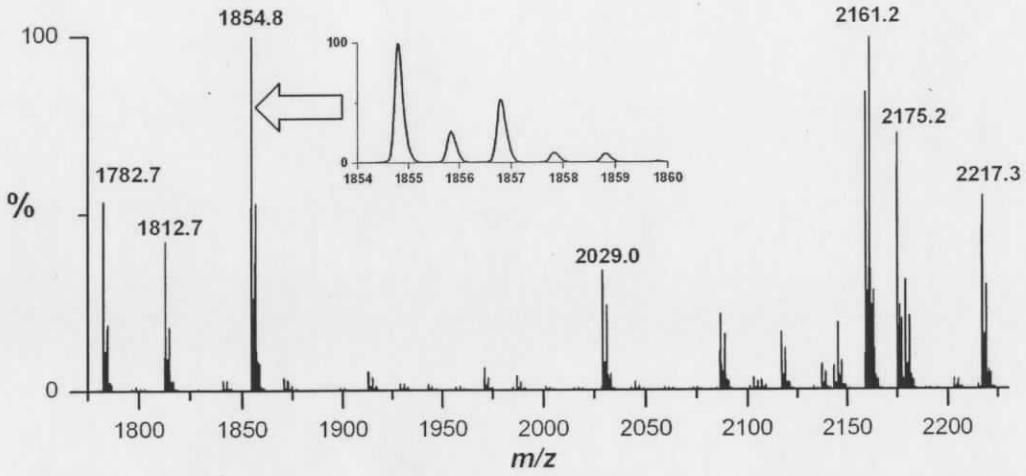

Figure 5-8: Negative ion spectrum of MAO in toluene/PhF.

5.7.1.2 MS/MS structural analysis

Assigning the negative ion spectrum was a very difficult task for a number of reasons. The various combinations of aluminum (26.9815 g/mol), oxygen (15.9994 g/mol), carbon (12.0107 g/mol), and hydrogen (1.0079 g/mol) that can be created to generate a molecule with molecular masses as large as the ones in Figure 5-8 is daunting. Several Python programs were written to assist in the task, and as an example of challenge at hand, the peak at 1855 *m/z* has 53 different molecular formulae within 0.1 *m/z*,[c] even assuming all C and H are present as methyl groups, i.e. a C:H ratio of 1:3.

Structural information can be obtained by analyzing the respective MS/MS spectra. At lower collision energies, loss of a fragment with a mass of 72 *m/z* was dominant for all peaks (Figure 5-9). This corresponds to an equivalent of trimethylaluminum (TMA), a further confirmation of its presence in solution. What is unusual however, is the sheer

---

[c] This program is called "MAO_MolecularFormula1.py" and is included in the appendix.

amount of TMA present. MS/MS of the species at 1854.8 *m/z* loses up to *eleven* equivalents of TMA; other peaks lose similar amounts of TMA (1812: 8 TMA equivalents; 1870: >9 eqs.; 2161: >10 eqs.; 2175: 13 eqs.; 2279: >9 eqs.). This extensive coordination of TMA was noted for all peaks in the region, even for samples of MAO that were evacuated for prolonged periods at high vacuum to remove any traces of free TMA (b.p. 127°C).[d]

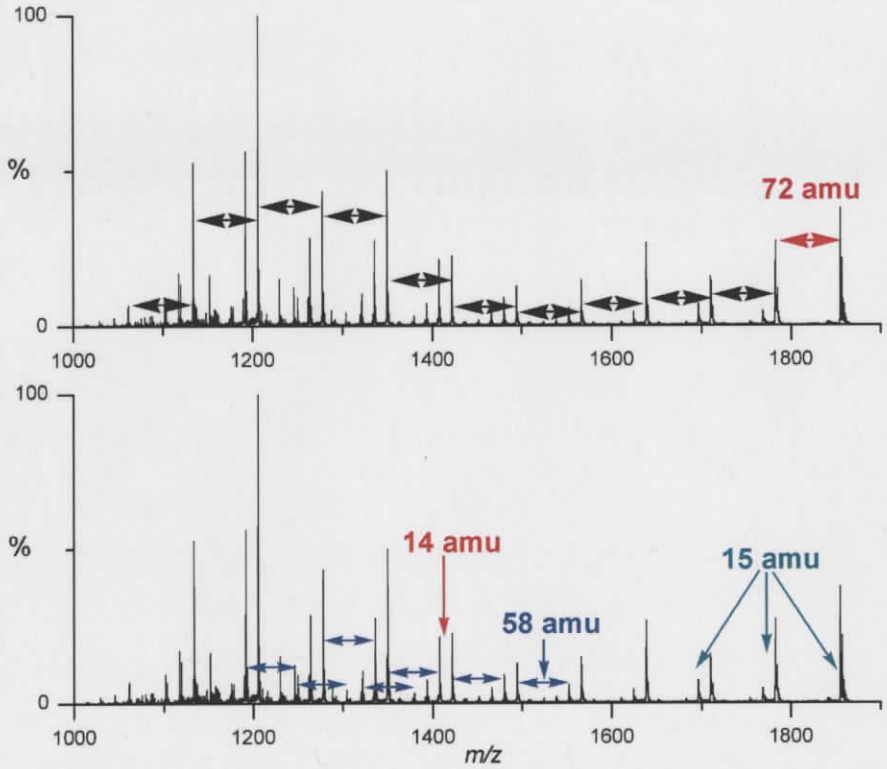

Figure 5-9: MS/MS spectra of 1854.7 *m/z* reveal the presence of both TMA (72 *m/z*) and AlOMe (58 *m/z*) groups.

Another feature that is present in the MS/MS patterns of all peaks was that at higher collision energies, the differences between the dominant peak (which resulted from sequential loss of several TMA moieties) and the next lowest peak shifted from 15 *m/z* to

---

[d] See appendix 5: Appendix fig. 28, Appendix fig. 29, and Appendix fig. 30 for MS/MS spectra of other peaks in Figure 5-8.

14 *m/z*. At low collision energies, loss of 15 *m/z* was easily attributed to a methyl group, but shifting this loss to a methylene does not seem reasonable. The most logical explanation for this is that after a few TMA groups have been lost a new fragment may be lost as well. As it happens 14 *m/z* corresponds to the difference in mass between TMA and the repeating MAO monomer AlOMe which has a mass of 58 *m/z*, hence both structural moieties are present.

A third feature of the MS/MS patterns is that some product ions are common between spectra. This was best illustrated by comparing the fragmentation patterns of the peak at 1812 *m/z* and 2175 *m/z* (Figure 5-10). This means that some of the higher mass structures are related to the lower mass structures in a chemically sensible way. Assignment of one peak in the spectrum should lead to another's assignment very easily.

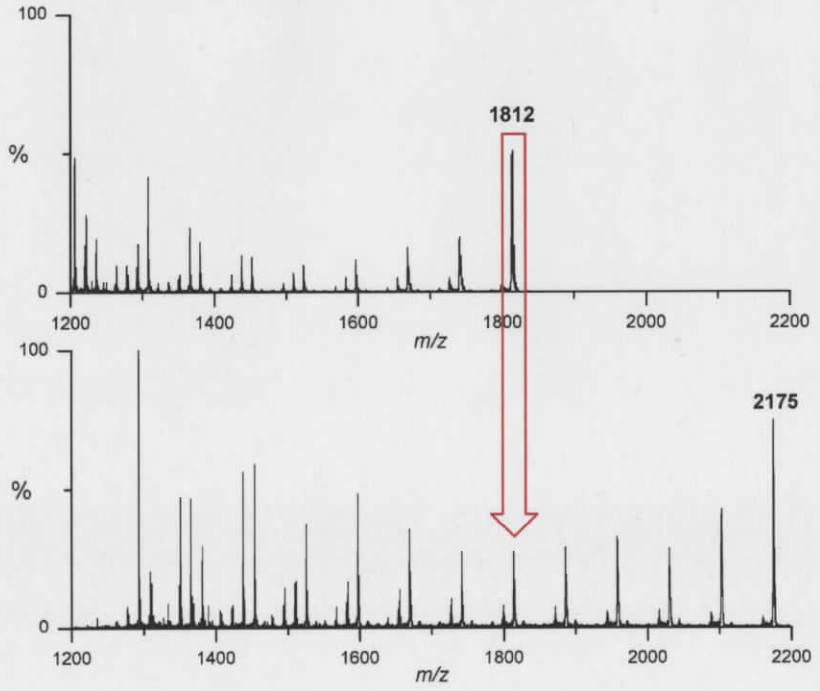

Figure 5-10: MS/MS of peaks at 2175 *m/z* and 1812 *m/z*.

Although the MS/MS data is helpful and informative, assignment is still difficult. Sinn was able to rationalize certain MAO cage structures similar to Barron's *t*-butyl aluminoxane structures, but his assignments had very low molecular masses.[60] In

essence, after the hydrolysis of one Al-CH_3 bond on a TMA group, the resulting Al-OH group will condense with another TMA molecule to give an Al-O-Al dimer (Equation 5-8). Sinn followed this logic with successive hydrolyses and condensations to generate the tetramer and then aggregated several tetramers by forming Al-O coordinate bonds to generate a cage structure analogous to Barron's crystalline cages. Rationalizing the large masses in this system requires extending the condensation reactions further to make larger oligomers, and then aggregating these oligomers to give molecular masses closer to those observed in Figure 5-8.

In order for Sinn's methodology to work here though, certain criteria must be met for each assignment:

1. There must be a good match between the calculated mass and spectral mass. This requires a well calibrated spectrum in order to compare with calculations, so the instrument must be calibrated every time before use.

2. The calculated isotope pattern must match that of the observed spectrum. This is a characteristic tool commonly employed when analyzing inorganic mass spectra, and the inset of Figure 5-8 reveals a definable pattern.

3. For any proposed structure, the valencies of all atoms must be considered and accounted for.

4. The entire structure must carry the appropriate overall negative charge.

5. The expected fragmentation pattern must reasonably match that of the MS/MS fragmentation pattern. The appropriate numbers of TMA groups must be present in all structures.

6. The sum molecular formulae for the dominant peaks should match reasonably well with the NMR data determined by Atwood. This point allows for some variability in Al:O:Me ratios for structures of different peaks, but the net ratios must come close to $Al_1O_{0.75\text{-}0.8}Me_{1.4\text{-}1.5}$. It may be that the most easily ionized species may not have this ratio (so this criterion is the least strict), but the NMR data provides a useful means of restricting the parameter space.

5.7.1.3 Assignment difficulties

Aluminum, oxygen and methyl are all relatively small atoms/groups, and the data show that these three elements combine to form very high molecular weight ions. To expedite the peak assignment process, various Python[61] programs were written. There was an evolution in this programming, and each program approached the problem with different constraints. In the end however, every program fell short of satisfying all criteria described above at the same time. It was possible to come up with molecular formulae that matched the spectral masses very closely, but did not meet the valency requirements of all atoms in the molecule, or carry an appropriate charge (Table 5-3). The corollary was also possible, whereby the valencies of all atoms are satisfied and the structure carries the negative charge, but the calculated mass does not match very closely with the spectral mass (Table 5-4). Finally, it was possible that both the calculated mass and the charge matched the spectrum within reason, but the number of TMA fragments (Table 5-5) was not consistent with MS/MS fragmentation.

Table 5-3: Good mass match, but the charge does not match: 2175.2 *m/z*.[e]

(*m/z*)	Formula	**Charge**
2175.2139	$Al_{12}O_{96}Me_{21}$	**-177**
2175.1984	$Al_{19}O_{41}Me_{67}$	**-92**
2175.2226	$Al_{30}O_{14}Me_{76}$	**-14**
2175.2055	$Al_{40}O_{30}Me_{41}$	**+19**
2175.2168	$Al_{47}O_{52}Me_{5}$	**+32**

[e] This output was obtained from the program: MAO_MolecularFormula1.py in Appendix 5.

Table 5-4: The charge matches, but the mass does not: 1854.7 *m/z*.[f]

(*m/z*)	Formula	Charge
1853.7639	$Al_{17}O_{15}Me_{20}(OMe)_2(AlMe_3)_{11}$	-1
1853.9017	$Al_{18}O_{11}Me_{30}(OMe)_3(AlMe_3)_9$	-1
1855.5778	$Al_{18}O_{20}Me_{13}(OMe)_2(AlMe_3)_{11}$	-1
1855.4400	$Al_{19}O_{24}Me_9OMe(AlMe_3)_{11}$	-1
1855.3022	$Al_{20}O_{28}Me_5(AlMe_3)_{11}$	-1

Table 5-5: Mass and charge (of -1) both match, but the number of TMA's does not match: 1782.7 *m/z*[f] (MS/MS data in Appendix 5 shows that at least 9 TMA groups are present on this ion).

(*m/z*)	Formula	# $AlMe_3$
1782.8655	$Al_{26}O_{36}(OMe)_7(AlMe_3)_4$	**4**
1782.8941	$Al_{27}O_{32}Me(OMe)_{17}$	**0**
1782.8657	$Al_{29}O_{36}Me_9(OMe)_7(AlMe_3)$	**1**
1782.8659	$Al_{27}O_{36}Me_3(OMe)_7(AlMe_3)_3$	**3**

There is also the issue of a good isotopic signature. Aluminum, oxygen, carbon, and hydrogen are all dominated by a single isotope (with significant contributions from ^{13}C), but each peak in Figure 5-8 has a distinctive pattern wherein the $[M + 2]^-$ peak is significantly higher than the $[M + 1]^-$ peak. At first this pattern implicated chlorine, but when chlorine is included in the molecular formula, the very large abundance of methyl group (with ^{13}C abundance of 1.1%) leads to the dominance of $[M + 1]^-$ over $[M + 2]^-$. This effectively means that the contribution of one ^{37}Cl is not enough to significantly alter the effect of ^{13}C. If the observed pattern is in fact an isotopic signature (as opposed to an overlapping ion), the polyisotopic atom that is dominating the pattern must be accompanied by sufficient exclusively monoisotopic atoms to overwhelm the effect of ^{13}C. Possible contaminants include whatever proprietary hydrated metal salt was used to make the MAO.

[f] This output was obtained from the program: MAO_MolecularFormula2.py in Appendix 5.

5.7.1.4 Experimental challenges

A final difficulty in studying this system was the extreme sensitivity to trace amounts of moisture or oxygen. In order to obtain a reasonable spectrum, the ESI source had to be rinsed for several hours with dry, oxygen-free solvent at high temperatures to get rid of any moisture within the ESI source housing that could potentially degrade the sample. Between samples, when the syringe and tubing setup were transferred back into the glovebox to recharge the syringe, an alternate syringe with clean and dry solvent had to be injected in its place. This was done to prevent air and moisture from diffusing into the capillary while no tubing was attached. All samples were handled in the glovebox and taken directly to the instrument while in the syringe to be analyzed, where they replaced the original syringe and solvent. Furthermore, all solvents were strictly dried and both sets of syringes, PEEK tubing, and injection ports were first rinsed with dilute MAO and toluene, then evacuated for up to 48 hours in the glovebox antechamber to remove trace water. If any of these steps was skipped or not given due diligence, the chances of MAO reacting with water in the tubing or capillary significantly increased; the result was the PEEK tubing, syringe, or capillary became blocked with pyrophoric material and the experiment was at an end.

At times, even *with* a thorough preparation the tip of the capillary became blocked within the source. It has recently been determined by other group members that the ESI source chamber is at a slightly negative pressure under normal operating conditions, which means oxygen and moisture from the atmosphere can slowly leak into the source. This finding presents a considerable source of artefacts. If atmospheric oxygen and moisture is constantly leaking into the source housing, then it has the potential to react with the electrosprayed MAO sample. This will certainly clog the tip of the capillary but will also affect the observed spectrum. It is not possible to know whether speciation is representative of what is in solution or if it is a result of a gas phase reaction with atmospheric water.

5.7.1.5 Adding a halide to MAO

In attempts to understand the ionization mechanism of MAO, and reduce the effect of methyl abstraction from another aluminum (which effectively reduces the concentration of negatively charged MAO), halides were added. Salts of both chloride and bromide were added at much lower concentrations than MAO with the hope that a halide would coordinate a Lewis acidic aluminum center in a Lewis acid-base reaction and charge the complex non-destructively by forming an 'ate complex. Both chloride and bromide appeared to have a very similar effect on the system, and they were considerably more reactive than expected. Even at concentrations 100-fold more dilute than MAO (i.e. X : Al < 1:100), considerable changes in the mass spectra were observed (Figure 5-11).

From the MS/MS patterns[g] certain expected features are present:

1. The presence of one or more TMAs are observed in several fragments.
2. The MAO monomer (AlOMe) is also observed, along with loss of methane.
3. Multiple halides are observed in several instances, although all species are singly charged. This implies that some exchange between a coordinated halide and an adjacent Al-CH_3 group has occurred, with no net change in charge.

---

[g] MS/MS spectra are included in the appendix: Appendix fig. 32 and Appendix fig. 33.

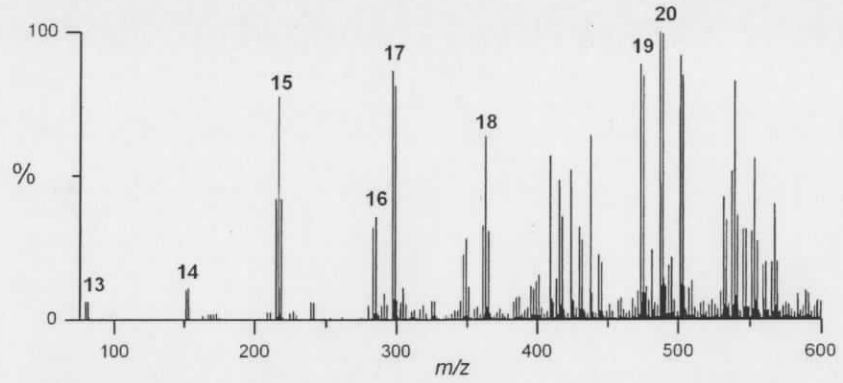

Figure 5-11: Negative ion spectrum of MAO with 1/100th molar equivalent of Br^-.

Table 5-6: Assignment of Figure 5-11

Peak: *m/z*	Assignment
13: 80.94	$[Br]^-$
14: 153.03	$[AlMe_3Br]^-$
15: 216.96	$[AlMe_2Br_2]^-$
16: 285.14	$[Al_3Me_5(OMe)HOBr]^-$
17: 197.17	$[Al_3Me_6(OMe)OBr]^-$
18: 363.09	$[Al_3Me_5(OMe)OBr_2]^-$
19: 473.29	$[Al_5Me_{11}(OMe)_3HBr]^-$
20: 487.31	$[Al_5Me_{12}(OMe)_3Br]^-$

Assigning these spectra was relatively simple and could be done according to the criteria described in 5.7.1.2. A feature of these ions that does not seem to have much literature support is the presence of methoxide ligands. This was discovered in studying the tri-*iso*-butyl aluminum system (and is described in section 5.7.2.1), and subsequently employed in assigning these peaks. Often at least one methoxide group will be required, but all structures have a good match between calculated and spectral masses, a well defined isotopic fingerprint, the valencies of all atoms is met, and there is a net negative charge on each molecule.

5.7.2 The triisobutyl aluminum system

After discovering that MAO could be studied by ESI-MS, other less reactive systems were also studied. TMA is extremely reactive with water, but bulking up the alkyl group has the effect of protecting the aluminum center from incoming water thereby decreasing the aggressiveness of the reaction. The increased bulk also acts to protect the empty *p*-orbital and reduces the tendency of alkyl alanes to dimerize by forming electron deficient bonds. As a result alkyl alanes such as tri *t*-butyl or tri*iso*butyl aluminum are monomers in solution. Results from the MAO system suggested that turning this study towards these monomers may provide insight into the reaction of these compounds with water as they occur. Furthermore, certain systems have shown cocatalytic activity,[62,63] suggesting their cocatalytic nature might be simpler to study than the MAO system.

Triisobutyl aluminum (TiBA) is one such monomer in solution that has reported cocatalytic activity.[16,64] As with MAO, a first experiment was simply to analyze a commercial sample. Only noise was observed in the positive ion mode, but the spectrum of the negative ion mode was very clean and showed two distinct peaks (Figure 5-12). These peaks were much smaller in mass than those of the MAO sample and they both lacked characteristic isotope patterns of halides or other metal contaminants. Furthermore, they appeared high enough in mass to exclude the possibility of a deprotonated aluminum dimer or trimer.

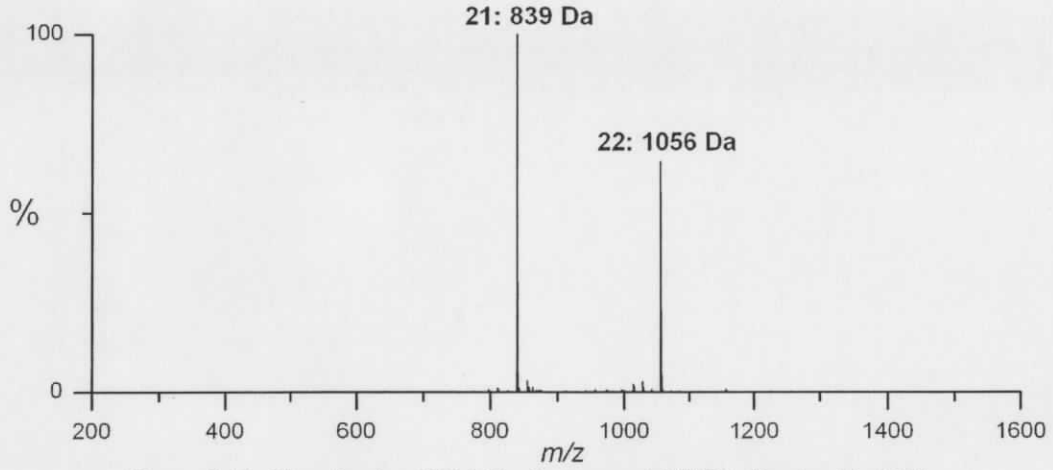

Figure 5-12: Negative ion ESI-MS of commercial TiBA dissolved in PhF.

The intensity of this spectrum was poor, which hindered high quality MS/MS spectra. It was therefore difficult to assign these peaks with the information at hand, but under the assumption that oxygen (from water) was involved somehow, a very small amount of water was added (mole ratio of Al:H_2O of ~10:1) in an attempt to change the spectrum. This resulted in the overwhelming dominance of peak **21** at 839 *m/z* (Figure 5-13a). Peak **22** at 1056 *m/z* was still present in the baseline, but it was clear from this spectrum, that most reactivity occurred to generate **21**. Titrating more water into the same sample resulted in the gradual increase in the relative peak height of **22** (Figure 5-13 B-E), which seemed to maximize around an Al:H_2O ratio of 4:3. Further increasing the ratio up to 1:1 completely eliminated **21** from the spectrum, and peak **22** suffered with the appearance of

some lower mass decomposition products. As was observed for MAO, it appears that the hydrolysis of TiBA favors certain structures over others.

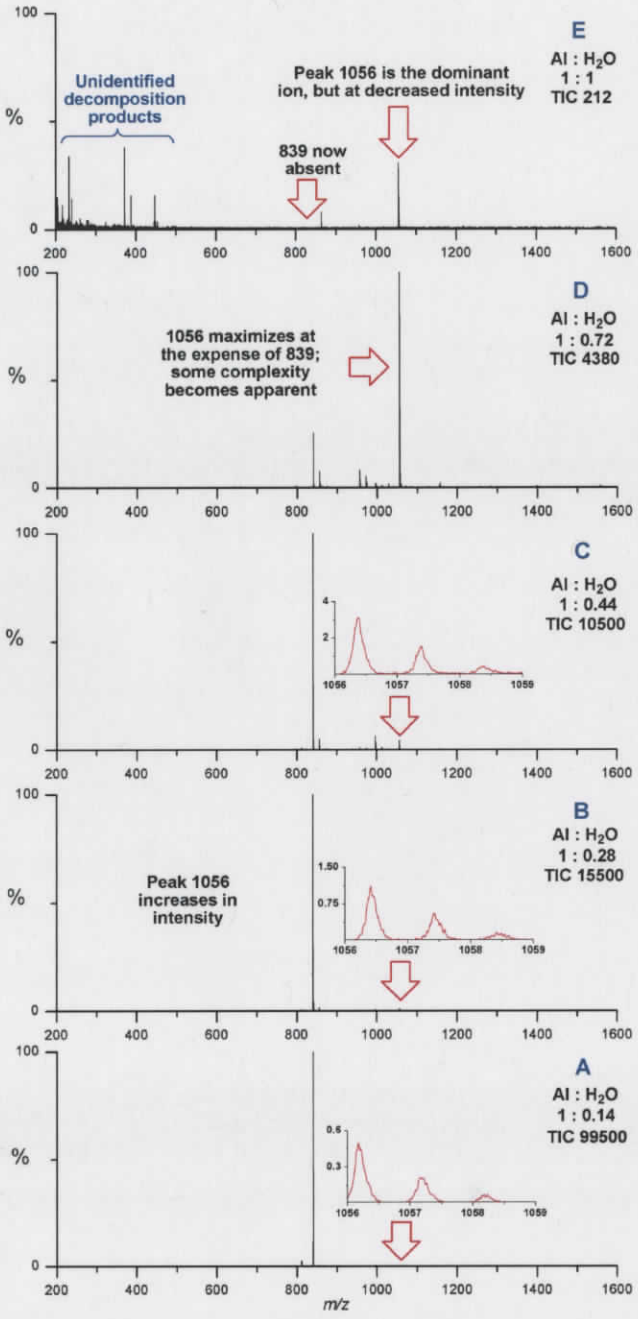

Figure 5-13: Partially hydrolyzed TiBA. A) $1/10^{th}$ equivalent H_2O:Al. As water is titrated into the sample of TiBA (B-E), and the ratio of H_2O: Al approaches 1:1, peak **21** seems to decrease in intensity while peak **22** appears to grow in.

An important note for the spectra of Figure 5-13 is the issue of ion current. Although it appears that **21** decreases and **22** grows in at higher Al:H_2O ratios, a possibility is that **22** is less reactive towards hydrolysis than **21**. Considering the total ion current (TIC), and that it decreases sequentially (only 100 scans were combined for each spectrum) as the ratio of Al:H_2O approaches 1:1, it is possible that most reactivity is occurring to generate **21** (which undergoes a different reaction at higher Al:H_2O ratios), and that **22** only *appears* to grow in because **21** is decomposing.

5.7.2.1 The Positive Ion Mode

From the positive ion mode of the same experiment (Al:H_2O of 1:0.14), a spectrum of similar simplicity was observed (Figure 5-14), although the intensity was considerably lower. Notably no oligomeric repeat corresponding to $AlO_2{}^iBu$ was observed in the positive ion spectrum (recall the repeat unit of AlO_2Me in Figure 5-7 from the MAO system). A couple of peaks seemed most prominent, and MS/MS was performed on the most intense of these.

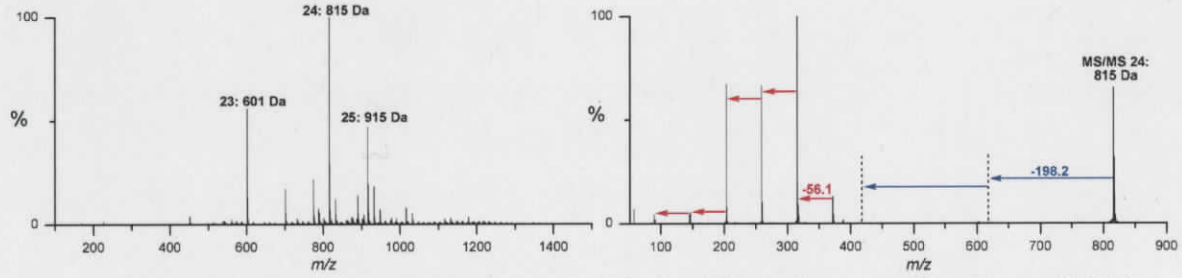

Figure 5-14: Positive ion ESI-MS of the hydrolysis of TiBA taken at an Al:H_2O rato of 1:0.14.

Peak assignment was not trivial, but an adapted Python program from the MAO system was again useful.[h] The program returned the number of aluminum atoms, oxygen atoms, and butyl groups, but by carefully considering the output most options could be eliminated and reasonable structures determined. The methodology for peak assignment went as follows:

---

[h] This program is called TIBA_MolecularFormula.py. It is included in Appendix 5.

1. Each aluminum atom was associated with a 3^+ charge. Multiplying the number of aluminum atoms by its charge gives the total positive charge.

2. Each oxygen center can be associated with a 2^- charge. Accounting for all oxygen atoms, then adding this number to the total positive charge gives the new total charge.

3. Each butyl group can have a 1^- charge. The total negative charge for all butyl groups can then be added to the previous total.

4. It is also possible for there to be butoxide groups which would account for one butyl group and one oxygen atom, but only carry a charge of 1^-.

5. The sum of all charges for all aluminum, oxygen, butyl, and/or butoxide groups must be the same as the charge observed on the ion in the spectrum (either +1 for the positive ion mode or -1 for the negative ion mode).

Following this protocol and using the positive ion spectrum as an example, the only plausible output for peak **24** (Figure 5-15) is at 815.69 *m/z* with a molecular formula of $[Al_4O_5{}^iBu_{11}]^+$, which matches closely the observed mass of 815.76 *m/z*.

```
>>>
What is the peak mass?
815.5
What is an acceptable error tolerance in the mass?
.5
815.47734 Al 0 O 26 Bu 7
815.9694 Al 0 O 51 Bu 0
815.24218 Al 1 O 35 Bu 4
815.00702 Al 2 O 44 Bu 1
815.69762 Al 4 O 5 Bu 11
815.46246 Al 5 O 14 Bu 8
815.95452 Al 5 O 39 Bu 1
815.2273 Al 6 O 23 Bu 5
815.44758 Al 10 O 2 Bu 9
815.93964 Al 10 O 27 Bu 2
815.21242 Al 11 O 11 Bu 6
815.92476 Al 15 O 15 Bu 3
815.6896 Al 16 O 24 Bu 0
815.90988 Al 20 O 3 Bu 4
815.67472 Al 21 O 12 Bu 1
815.65984 Al 26 O 0 Bu 2
>>>
```

Figure 5-15: Sample output for the Python program: TIBA_MolecFormula.py

In order to create a reasonable structure, all oxygen atoms must be bound as butoxide moieties. This means there are 5 butoxide groups and 6 butyl groups, but from the MS/MS (Figure 5-14) there are two $Al(^{i}Bu)_3$ groups, so all remaining butyls are bound to two aluminum centers. A more representative molecular formula is then $[Al_2(O^{i}Bu)_5(Al^{i}Bu_3)_2]^+$. The simplest structure that can then be determined is structure **24** in Figure 5-16. The valencies of all atoms are accounted for, all fragments from the MS/MS experiment are reasonably present, the positive charge is present, and there is a good match with the *m/z* value. Peaks **23** and **25** in the spectrum were assigned without MS/MS data, but reasonable structures could also be drawn following this logic.

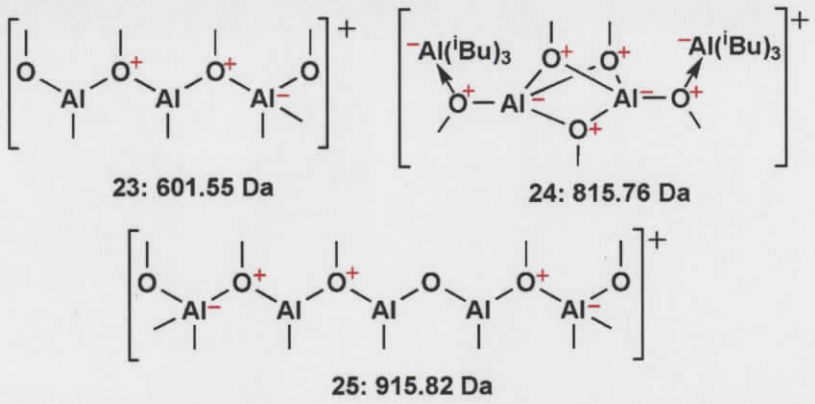

Figure 5-16: Potential structures for three prominent ions in Figure 5-14. Other plausible isomers can likely be drawn. Isobutyl groups are represented by a single bond for simplicity.

5.7.2.2 Back to the Negative Ion Mode

For some reason the protocol described above for peak assignment did not work in assigning a reasonable structure for peak **21** in the negative ion mode. Even after obtaining a high quality and relatively simple looking MS/MS spectrum, conclusive assignment still proved difficult. More information was required (Figure 5-17; clearly present are the loss of 3 $Al^{i}Bu_3$ groups to yield a product ion at 245 *m/z*).

With the knowledge that water could significantly improve the intensity of peak **21**, an isotopic labeling experiment was tried in an attempt to change the spectrum. Labeling

the hydrogen atom by hydrolysis with deuterium oxide yielded no change indicating an absence of hydroxyl groups. Moving the label to oxygen however, employing O^{18} labeled water, was more informative. As shown in Figure 5-17, peak **21** quite clearly has three oxygen atoms. What was more interesting was that all three oxygen atoms were also present in the product ion at 245 *m/z* in the MS/MS experiment of the species at 846 *m/z* (ie: all oxygen atoms were bound to the same aluminum center).

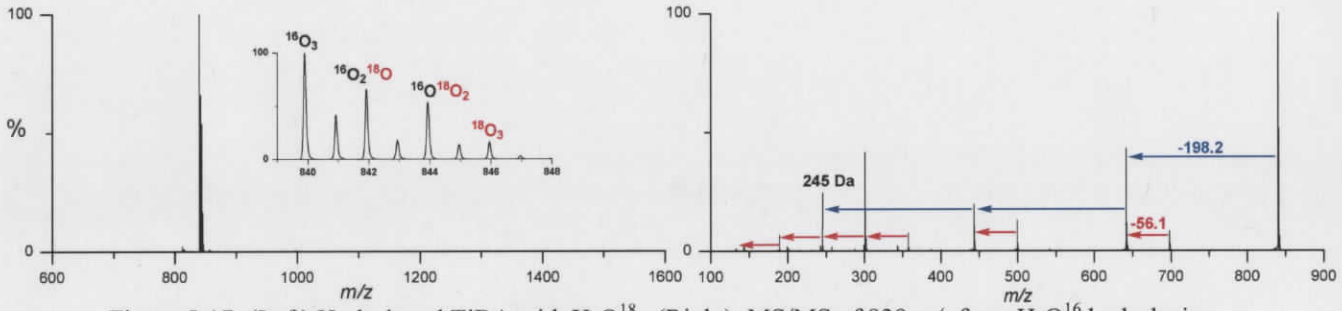

Figure 5-17: (Left) Hydrolyzed TiBA with H_2O^{18}. (Right) MS/MS of 839 *m/z* from H_2O^{16} hydrolysis.

The fragment at 245 *m/z* which contained all three oxygen atoms is only 47 *m/z* higher in mass than TiBA (M.Wt.: 198.3 g/mol), i.e. 1 *m/z* less than TiBA + 3O. It was reasoned then that the product ion at 245 *m/z* corresponded to a deprotonated aluminum tri-*iso*-butoxide center; this would account for its presence as well as the occurrence of three oxygen atoms on the same aluminum atom. From this complex, the most reasonable structure to be drawn that included the three TiBA groups is structure **21** in Figure 5-18. This structure has the three oxygen atoms bound to one Al atom, three TiBA groups, the correct *m/z* value, it includes the requisite negative charge, and satisfies the valency requirements for all atoms.

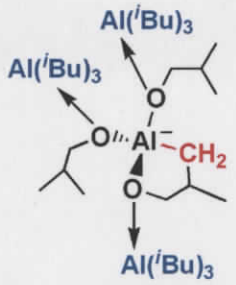

Structure 21

Figure 5-18: Structure **21** corresponding to peak **21**.

5.7.2.3 Discussion of structure 21

The most reasonable working reaction that would lead to structure **21** is Equation 5-14. Not accounted for in this equation is the intramolecular C-H activation that would generate a proton, but this does not have to occur exclusively in solution; the C-H activation may be something that occurs in the capillary with the reduction of $2H^+$ to H_2, yielding structure **21** in the negative ion mode.

$$4\ Al^iBu_3 + 3H_2O \longrightarrow Al(O^iBu)_3(Al^iBu_3)_3 + 3\ H_2$$

Equation 5-14

The reason the peak assignment protocol (and the Python program) described in 5.7.2.1 did not work for assigning structure **21** was because the method of ionization was different than for those ions in the positive ion mode; structure **21** had performed an intramolecular C-H activation with subsequent deprotonation. This is an unusual reaction for such a Lewis acid that would normally seek to react with the most Lewis basic species present: namely an oxygen atom. There is something about the structure of this molecule that confers upon the central aluminum atom the preference to form a bond to carbon instead of a fourth bond to oxygen. What is even more unusual is that this preference dominates the bulk reactivity of the complex in solution when there is obviously a multitude of other phenomena that might also occur.

An unusual feature of this reaction is that it appears that the reactivity occurs on one aluminum center instead of all metal centers as though they were equivalent. This implies that once a trialkyl aluminum center has exchanged an alkyl for an alkoxy group, it is activated to successive hydrolyses with a second and third water molecule. This raises some further questions:

1. How (and why) do the isobutoxide groups originate? There does not appear to be much knowledge of this reaction in the literature; most suggestions are that Al-O bonds form while expelling an alkane. There is no known evidence of alkyl/hydride exchange between the aluminum and oxygen centers.

2. If the central Al atom has three isobutoxide groups, then why does aluminum triisobutoxide not undergo this same intramolecular activation? It would be expected to dimerize with another aluminum oxide species, creating a very stable Al_2O_2 ring.

3. Why does this complex activate a C-H bond, but other structures within the same system, such as those assigned from the positive ion mode, do not activate a C-H bond?

It was reasoned that this unusual reactivity was due in part to the excess of TiBA still present in solution. Upon hydrolysis of one Al-C bond, the other two alkyl groups become activated, but it is unclear exactly how the alkyl groups find their way to the oxygen atom.[i] This process would consume most of the water relatively quickly. These hydrolyses occurred at -78 °C, and the added water is effectively an ice cube, so the reaction is slowed, which may hinder some more vigorous reactions while allowing others to proceed. Excluding the presence of the three TiBA groups, the central aluminum atom should be quite electron deficient: 1) it has an available empty *p*-orbital and 2) it is bound to three very electronegative oxygen atoms. However, these oxygen atoms are able to donate electron density back to the aluminum through overlap of filled

---

[i] This phenomenon has not been observed before, so the mechanism of migration, or exchange of alkyl groups and hydrides is only a proposal and was not investigated further.

p-orbitals on O with the empty *p*-orbital on Al. Further diminishment of Lewis acidity could come about through dimerization, and it undoubtedly would if there were significant quantities of other aluminum triisobutoxide molecules available. TiBA is still in large excess though, and it is a monomer in this solution, making coordination of TiBA to the oxygen atoms more likely than dimerization of the aluminum trialkoxy species.

The effect of the coordination can be speculated upon; it is imagined that the Lewis acidity of the central aluminum is reduced due to π-back donation from available lone pairs on oxygen into the empty *p*-orbital on aluminum. However, countering this electronic effect is a steric one from the coordination of 3 TiBA molecules to these electronegative oxygen atoms. It is unlikely that the molecule could remain planar (a prerequisite for π overlap), so the central Al would feel the full (albeit somewhat diminished) inductive effect of three directly bound oxygen atoms (Figure 5-19). This would put the aluminum in a similar environment to the boron atoms in the well-known BAr^F ligands: unable to dimerize due to steric factors, and no π overlap with nearby electronegative atoms. The result is a very strong Lewis acid, seemingly strong enough to activate a C-H bond to release H^+, and forming the anion observed in the mass spectrum.

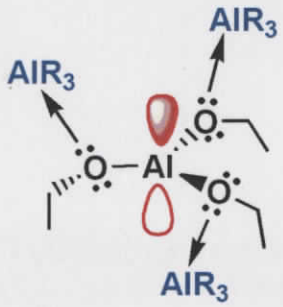

Figure 5-19: Structure of potential cocatalyst in a mixture of aluminoxanes.

This reactivity is only observed when there is a very large excess of TiBA around. On decreasing the concentration of TiBA (with more H_2O: Figure 5-13) more Al-C bonds would be activated on more TiBA molecules, thereby reducing the competition between the electronic and steric effects.

Analogous compounds to structure **21** would be in very low concentration in a mixture of MAO oligomers that has been hydrolyzed with an excess of water (greater than a ratio of 1:1, Al:H_2O), and their very high reactivity would not be complicated by intramolecular C-H activation. The very high Lewis acidity of the central aluminum atom could instead extract a methyl group from dimethyl zirconocene, thereby activating the metallocene for catalysis. In essence, these species may be closely related to the highly reactive, short lived cocatalysts that function to demethylate the zirconocene center. The balance between the increased Lewis acidity from the oxygen atoms and the coordinating effects of the three TiBA groups makes this molecule well suited to demethylating (and hence activating) the zirconium center.

5.7.3 Different routes to structure 21

Once structure **21** had been reasonably assigned it was desirable to further understand its chemistry. Although structure **21** was identified in solution, it would likely not be an active cocatalyst itself because it can simply form an intramolecular Al-C bond. If derivatives of **21** could be isolated and purified in high yield, then they may be subsequently added to dimethyl zirconocene in a stoichiometric reaction, thereby greatly reducing the cost associated with the vast excess of MAO required in this reaction. Its plausibility as a synthetic target (in situ or even isolating it) stems from its electronic and steric similarity to BAr^F ligands and its low molecular weight.

5.7.3.1 Alcoholysis

A second route to structure **21** was discovered by alcoholysis of TiBA. This time a substoichiometric amount of isobutyl alcohol was added under similar conditions as the hydrolysis experiment. The mixture was allowed to react for fifteen minutes at -78°C then allowed to warm and the spectrum shown in Figure 5-20 was collected. Peak **21** was again the dominant ion, but there were some new peaks of interest.

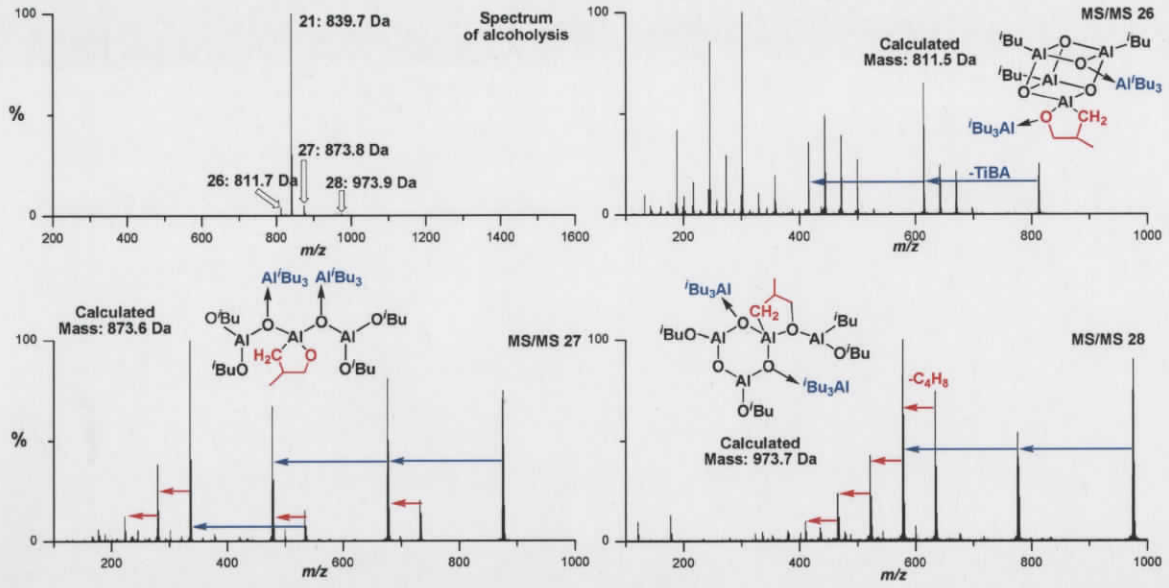

Figure 5-20: Spectrum of the alcoholysis of TiBA, along with the MS/MS spectra of the three extra peaks.

Peaks **26**, **27**, and **28** were subjected to MS/MS to investigate their structural features. For each peak, reasonable structures could be drawn that had also undergone an intramolecular C-H activation reaction. Although their structures were somewhat different to **21**, there exists the similar competition between steric and electronic effects that leads to C-H activation.

5.7.3.2 Mixtures of aluminum trialkoxides and trialkyl aluminums

Another method of acquiring analogues to structure **21** would be to simply mix an aluminum trialkoxide with a trialkyl aluminum[65] complex in the proper stoichiometry (Equation 5-15). Unfortunately aluminum tri-*iso*-butoxide is not commercially available, and had to be made by ligand exchange in a reaction with aluminum tri-*sec*-butoxide. It was noted however, that aluminum tri-*sec*-butoxide had a structure that would allow for the backbiting of the alkyl chain in the same fashion as the isobutoxide group, forming the same five-membered ring, so a first experiment involving simply aluminum tri-*sec*-butoxide and triisobutyl aluminum was attempted.

$$3AlR_3 + Al(OR)_3 \longrightarrow Al(OR_3)(AlR_3)_3$$

Equation 5-15

Surprisingly, instead of the overwhelming dominance of structure **21**, (or the *sec*-butoxide analogue at 839.7 *m/z*), peak **22** at 1056 *m/z* was the favored compound (Figure 5-21). With the help of the Python program, the molecular formula of $[Al_9O_8Bu_{12}]^-$ was determined most reasonable for which one possible structure (of many) is shown in Figure 5-21.

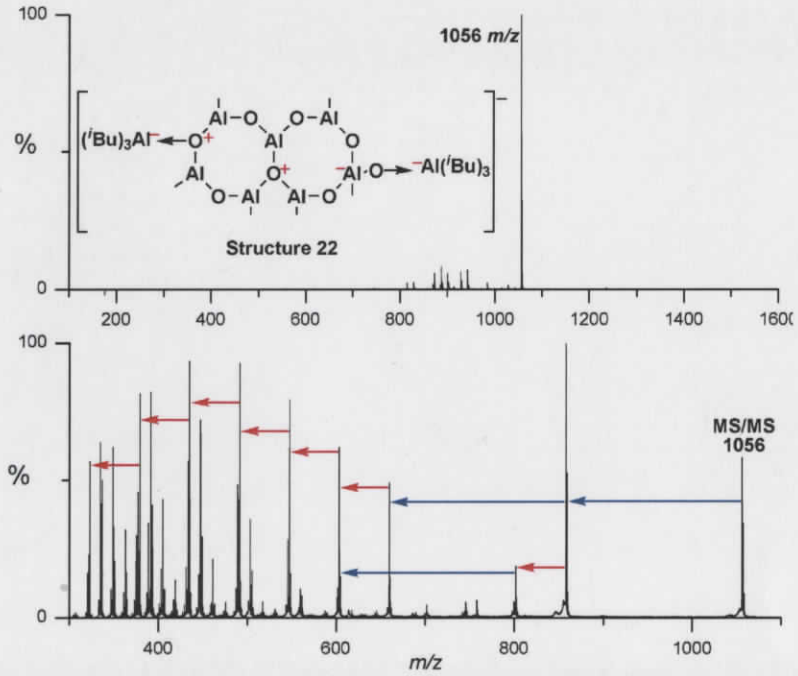

Figure 5-21: (Top) Spectrum of the mixture of triisobutyl aluminum with aluminum tri-sec-butoxide. (Bottom) MS/MS of peak 1056 *m/z*.

As before, structure **22** satisfies the valency requirements of all atoms, has an overall negative charge, good match with *m/z* values, and is consistent with the MS/MS fragmentation pattern. What is obvious from this assignment is that no intramolecular C-H activation has occurred; structure **22** ionizes due to the sum valencies on all atoms.

This means there is no special Lewis acidity conferred upon any aluminum atom that gives it the preference to bond to carbon instead of oxygen.

Mixing aluminum tri-*iso*-butoxide with triisobutyl aluminum according to Equation 5-15 yielded the spectrum shown in Figure 5-22. The dominant ion (peak **29**) was at 767.9 *m/z*, and had an MS/MS fragmentation pattern revealing the presence of three intact TiBA groups. The smallest product ion in this process was at 173.1 *m/z*, which corresponded to an empirical formula of $[AlO_2{}^iBu_2]^-$. The most reasonable structure to be drawn then was structure **29**. It seems that there may be a trace of **21**, but the inset of Figure 5-22 seems to be poorly calibrated; peak **22** was notably absent.

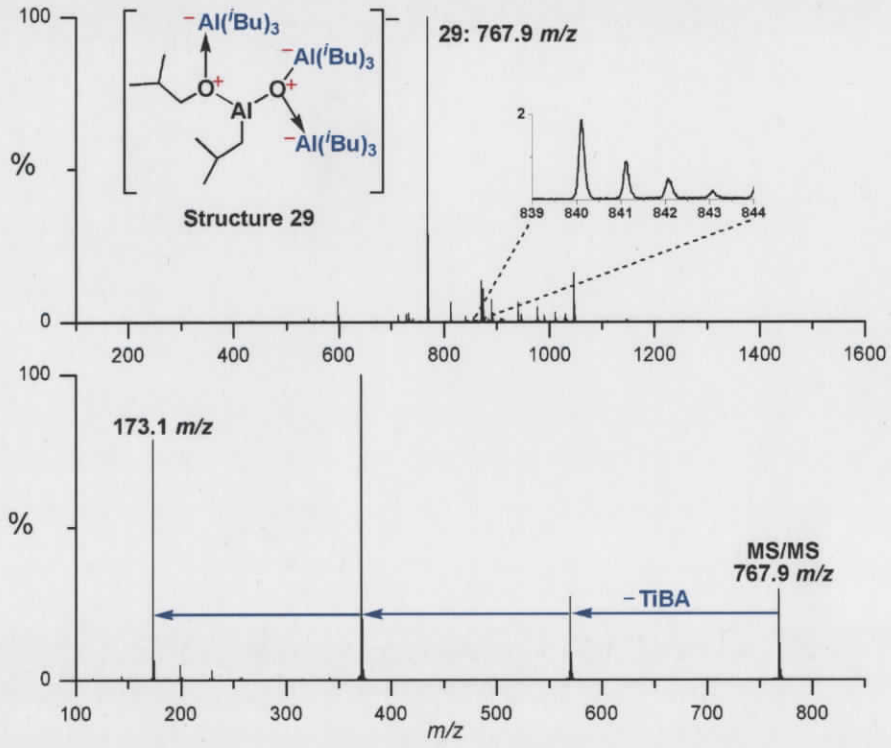

Figure 5-22: (Top) Spectrum of the mixture of aluminum tri-*iso*-butoxide and tri-isobutyl aluminum. (Bottom) MS/MS of peak **29**.

5.8 Future Work

Present and future work towards the goal of studying MAO specifically, should involve improving the experimental challenges of obtaining good quality data. To this end a glovebox has been purchased[j] that will be attached to the front of the instrument[66]. A hole will be cut in the side to allow PEEK tubing to pass through and attach to the instrument. In this way, all samples, syringes, ports, and tubing can be handled constantly under an inert atmosphere. Once attached to the instrument, the tubing and capillary can be flushed with dry and de-aerated solvent from this inert atmosphere without ever coming in contact with the outer atmosphere. At the source, a modified housing is being designed that will ensure a firm and air-tight seal around all joints that may leak to the atmosphere. This housing will include pressure gauges to ensure the ESI process occurs at or slightly above atmospheric pressure, thus ensuring that no moisture enters the ESI-source. If there is a leak, then it will be flowing out of the source housing. These modifications will limit the amount of artefacts present in these mass spectrometry experiments, and this will improve the quality and reproducibility of these spectra.

This project is effectively in its infancy. The study of alkylaluminoxanes has been fraught with ambiguity for a long time, but this work presents a new possible avenue by which their analysis may be approached. Because ESI-MS is a solution based technique, and the ionization method is very gentle, the potential to study aluminoxane ions from solution without structural changes will give insight into this difficult problem.

Although the system will undoubtedly be custom built, similar setups have been successful for ESI[66] as well as MALDI[67] mass spectrometry. Once the ability to obtain high quality spectra from an inert atmosphere is obtained, study of the MAO system can be performed again. The question of how much decomposition may have occurred can be addressed, and whether there has been any reactivity in the gas phase at all.

---

[j] The funds for the glovebox were raised through the ACS PRF *New Directions* program, based on a proposal called "Prising open the black box: probing the nature of methylaluminoxane using mass spectrometry". All the preliminary results for this proposal came from this chapter. The funds will also support a postdoctoral research fellow for one year and a PhD student.

Furthermore, solution phase speciation can be probed without the troublesome issue of clogging either the capillary or the PEEK tubing.

Studies that will seek to discover the actual MAO cocatalyst will direct laboratory work, but it will be important to elucidate the manner in which MAO forms as well. Once potential candidates are identified by ESI-MS, their syntheses may be attempted. An obvious target is $Al(O^tBu)_3(Al^tBu_3)_3$: the *tert*-butyl group is bulky, provides simple NMR spectra, enhances sample crystallinity, and is incapable of the intramolecular C-H activation that yields the anion.

Monitoring and tracking the hydrolysis of TMA throughout very careful titration experiments, and properly understanding the solution phase speciation as more water is added will be critical in addressing the very reactive chemistry of this system. The reactivity of other tri-alkyl aluminum systems may prove insightful as they are less vigorous.

Simply establishing the extent to which **21** is formed in solution is important; it is entirely possible that this ion represents only a tiny proportion of the total sample. It is, however, the one that has certainly undergone the most interesting chemistry, and deserves active pursuit. That endeavor will be much more feasible once the appropriate equipment for handling this reactive system is in place.

5.9 Experimental

5.9.1 Methods at the mass spectrometer

Fluorobenzene was purified by refluxing over phosphorous pentoxide followed by distillation. Syringes and PEEK tubing were vacuum pumped for at least 48 hours in a glovebox antechamber.

For each experiment, two sets of PEEK tubing and two syringes were first rinsed with a slightly diluted sample of MAO in the glovebox, followed by several rinsings of neat fluorobenzene. The ESI-MS source was thoroughly cleaned with any solvent necessary, followed by detailed rinsing with sodium dried toluene. The capillary was also changed

to a new capillary. One syringe and PEEK tubing set was removed from the glovebox and attached to the mass spectrometer. Dry fluorobenzene was then flushed through the instrument for three hours with the source temperature set to 100°C and desolvation gas temperature set to 300°C. When an experiment was being run, the source temperature was reduced to 80°C and desolvation temperature to 200°C. The cone voltage was set to 20 V and collision energy set to 2 V.

A pre-weighed amount of precatalyst was weighed in a vial and dissolved in fluorobenzene (10 mL). Based on the desired stoichiometry between Zr and AlOMe, a calculated and measured amount of MAO was then added to this mixture and allowed to stir for at least ten minutes. Ten drops of this solution were then diluted with 1.5 mL fluorobenzene. The second PEEK tubing was then filled with neat fluorobenzene, and the diluted reaction mixture was taken up in the syringe and the syringe inserted into the needle port. This entire assembly was then removed from the glovebox and quickly taken to the instrument. The first set of syringe and PEEK tubing was removed from the instrument, and the second set attached in its place. The sample was then infused at a rate of about 20 μL per minute, and the spectrum was acquired in continuum mode immediately. If consistent ion intensity was not obtained shortly, the capillary voltage was increased by 50 V every few seconds to observe any improvements in spectra. Once a stable ion current was obtained the flow rate was slowly decreased by 1 μL/min so as to maximize the available time on the instrument. Once a threshold was reached, the flow rate was never reduced beyond this point until the syringe was empty, at which point the first syringe + PEEK tubing was reattached and dry fluorobenzene again flushed through the capillary.

5.9.2 Hydrolysis and ESI-MS of TiBA[33]

Tri-isobutyl aluminum (10 mL of 1 M toluene solution) was added to a Schlenk flask in the glove box then transferred to the Schlenk line under N_2. The sample was cooled to -78°C and allowed to stir. Water in the desired amount was added directly to the reaction mixture with a micro-syringe. The reaction was stirred at -78°C until the ice had completely reacted, then allowed to warm to room temperature. This could take up to a

couple of hours depending on how much water was added. Once at room temperature, the flask was transferred back into the glovebox. The instrument was prepared as described in 5.9.1. About 5 drops of the reaction mixture were diluted in fluorobenzene (1.5 mL) and taken up in a dry syringe. The sample was then taken to the instrument for ESI-MS.

5.10 References

[1] Ziegler, K.; Holzkamp, E.; Breil, H.; Martin, H., *Angew. Chem.*,**1955**, *67*, 541.

[2] Natta, G., *Angew.Chem.*, **1956**, *68*, 393.

[3] Andresen, A.; Cordes, H.G.; Herwig, J.; Kaminsky, W.; Merck, A.; Mottweiler, R.; Pein, J.; Sinn, H.; Vollmer, H.J., *Angew. Chem. Int. Ed. Engl.*, **1976**, *15*, 630-632.

[4] Sinn, H.; Kaminsky, W.; Vollmer, H.J.; Woldt, R., *Angew. Chem. Int. Ed. Engl.*, **1980**, *19*, 390-392.

[5] Kaminsky, W., *J. Polym. Sci., Part A: J. Polym. Chem.*, **2004**, *42*, 3911-3921.

[6] Alt, H.G.; Koppl, A., *Chem. Rev.*, **2000**, *100*, 1205-1221.

[7] Hlatky, G.G.,*Coord. Chem. Rev.*, **2000**, *199*, 235-329.

[8] Ewen, J.A.; Jones, R.L.; Razavi, A.; Ferrera, J.D., *J. Am. Chem. Soc.*, **1988**, *110*, 6255-6256.

[9] Shapiro, P.J.; Bunel, E.; Schaefer, W.P.; Bercaw, J.E., *Organometallics*, **1990**, *9*, 867-869.

[10] Deck, P.A.; Beswick, C.L.; Marks, T.J., *J. Am. Chem. Soc.*, **1998**, *120*, 1772-1784.

[11] Chen, Y.X.; Marks,T.J., *Organometallics*, **1997**, *16*, 3649-3652.

[12] a) Stephan, D.W.; Stewart, J.C.; Guerin, F.; Spence, R.E.H.; Wei Xu, Harrison, D.G., *Organometallics.*, **1999**, *18*, 116-118. b) Stephan, D.W.; Stewart, C.; Guerin, F.; Courtnay, S.; Kickham, J.; Hollink, E.; Beddie, C.; Hoskin, W.; Graham, T.; Wei. P.; Spence, R.E.H.; Xu, W.; Koch, L.Gao, W.; Harrison, D.G., *Organometallics*, **2003**, *22*, 1937-1947. c) Spencer, L.P.; Altwer, R.; Wei, P.; Gelmini, L.; Gauld, J.; Stephan, D.W., *Organometallics*, **2003**, *22*, 3841-3854.

[13] Chase, P.A.; Piers, W.E.; Patrick, B.O., *J. Am. Chem. Soc.*, **2000**, *122*, 12911-12912.

[14] Metz, M.V.; Schwartz, D.J.; Stern, C.L.; Nickias, P.N.; Marks, T.J., *Angew. Chem. Int. Ed. Engl.,* **2000**, *39*, 1312-1316.

[15] Williams, V.C.; Piers, W.E.; Clegg, W.; Elsegood, M.R.J.; Collins, S.; Marder, T.B., *J. Am. Chem. Soc.,* **1999**, *121*, 3244-3245.

[16] Naga, N.; Shiono, T.; Ikeda, T., *J. Molec. Catal. A,* **1999**, *150*, 155-162.

[17] Ziegler, K., *Angew. Chem.,* **1964**, *76*, 545-553.

[18] Sinn, H.; Kaminsky, W., *Adv. Organomet. Chem.,* **1980**, *18*, 99-149.

[19] Babushkin, D.E.; Semikolenova, N.V.; Zakharov, V.A.; Talsi, E.P., *Macromol. Chem. Phys.,* **2000**, *201*, 558-567.

[20] Yang, X.; Stern, C.L.; Marks, T.J., *J. Am. Chem. Soc.* **1991**, *113*, 3623-3625.

[21] Chen. E.; Marks, T.J., *Chem. Rev.,* **2000**, *100*, 1391-1434.

[22] Kaminsky, W.; Bark, A.; Steiger, R., *J. Molec. Catal. A.,* **1992**, *74*, 109-119.

[23] Barron, A.R., *Organometallics,* **1995**, *14*, 3581-3583.

[24] Sinn. H., *Macromol. Symp.* **1995**, *97*, 27-52.

[25] Luo, L.; Marks, T.J., *Top. Catal.* **1999**, *7*, 97-106.

[26] Barron, A.R., *Metallocene-based Polyolefins*, **2000**, *1*, 33-67.

[27] Harnew, D.W.; Meisters, A.; Mole, T., *Aust. J. Chem.,* **1974**, *27*, 1639-1653.

[28] Boleslawski, M.; Pasynkiewicz, S., *J. Organomet. Chem.,* **1972**, *43*, 75-80.

[29] Wehmschulte, R.J.; Power, P.P., *J. Am. Chem. Soc.,* **1997**, *119*, 8387.

[30] Pasynkiewics, S., *Polyhedron,* **1990**, *9*, 429-453.

[31] Imhoff, D.W.; Simeral, L.S.; Sangokoya, S.A.; Peel, J.H., *Organometallics,* **1998**, *17*, 1941-1945.

[32] Atwood, J.L.;Hrncir, D.C.; Priester, R.D.; Rogers,R.D., *Organometallics,* **1983**, *2*, 985-989.

[33] a) Mason,M.R.; Smith, J.M.; Bott,S.G.; Barron,A.R., *J. Am. Chem. Soc.,* **1993**, *115*, 4971-4984. b) Harlan, C.J.; Mason, M.R.; Barron, A.R., *Organometallics,* **1994**, *13*, 2957-2969.

[34] Linnolahti, M.; Severn, J.R.; Pakkanen, T.A., *Angew, Chem. Int. Ed. Engl.,* **2006**, *45*, 3331-3334.

[35] a) Zurek, E.; Woo, T.K.; Firman, T.K.; Ziegler, T., *Inorg. Chem.,* **2001**, *40*, 361-370.
b) Zurek, E.; Ziegler, T., *Inorg. Chem.,* **2001**, *40*, 3279-3292.

[36] Harlan, C.J.; Bott, S.G.; Barron, A.R., *J. Am. Chem. Soc.,* **1995**, *117*, 6465-6474.

[37] Babushkin, D.E.; Brintzinger, H.H., *J. Am. Chem. Soc.,* **2002**, *124*, 12869-12873.

[38] Zakharov, V.A.; Talzi, E.P.; Zakharov, I.I.; Babushkin, D.E.; Semikolenova, N.V., *Kinet. Catat.,* **1999**, *40*, 836-850.

[39] Eilertsen, J.L.; Stovneng, J.A.; Ystenes, M.; Rytter, E., *Inorg. Chem.,* **2005**, *44*, 4843-4851.

[40] Ziegler, T., *Faraday Discuss.,* **2003**, *124*, 145-153.

[41] Sinn, H.W.; Kaminsky, W.O.; Vollmer, H.J.C.; Woldt, R.O.H.H., *US. 4,404,344*, **1983**.

[42] Babushkin, D.E.; Semikolenova, N.V.; Panchenko, V.N..; Sobolev, A.P.; Zakharov, V.A.; Talsi, E.P., *Macromol. Chem. Phys.,* **1997**, *198*, 3845

[43] Christ, C.S. Jr.; Eyler, J.R.; Richardson, D.E., *J. Am. Chem. Soc.,* **1990**, *112*, 596-607.

[44] Richardson, D. E.; Alameddin, N. G.; Ryan, M. F.; Hayes, T.; Eyler, J. R.; Siedle, A.R., *J. Am. Chem. Soc.*, **1996**, *118*, 11244-11253.

[45] Feichtinger, D.; Plattner, D.A.; Chen, P., *J. Am. Chem. Soc.,* **1998**, *120*, 7125-7126.

[46] Santos, L.S.; Metzger, J.O., *Angew. Chem. Int. Ed.* **2006**, *45*, 977-981.

[47] Tritto, I.; San Xi Li; Boggioni, L.; Sacchi, M.C.; Locatelli, P.; Oniell, A., *Macromol. Chem. Phys.,* **1997**, *198*, 1347-1361.

[48] Castro, P.M.; Lahtinen, P.; Axenov, K.; Viidanoja, J.; Kotiaho, T.; Leskela, M.; Repo. T., *Organometallics,* **2005**, *24*, 3664-3670.

[49] Di Lena, F.; Quintanilla, E.; Chen, P., *Chem Commun.,* **2005**, 5757-5759.

[50] Di Lena, F.; Quintanilla, E.; Chen, P., *Chem Commun.,* **2006**, 4309-4311.

[51] Budzelaar, P.H.M.; Talarico, G.; Insertion and β-hydrogen transfer at aluminum. In *Group 13 chemistry III: Industrial applications.* Roesky, H.W.; Atwood, D.A., Eds.; Springer: New York, **2003**, 141-165.

[52] Kawai, K.; Fujita, T., *Top. Organomet. Chem.,* **2009**, *26*, 3-46.

[53] Odian, G., *Principles of polymerization;* Wiley-Interscience: Hoboken, **2004**, 665-725.

[54] Zurek, E.; Ziegler, T., *Faraday Discuss.*, **2003**, *124*, 93-109.

[55] Henderson, M.A.; McIndoe, J.S., *Chem Comm.*, **2006**, 2872-2874.

[56] Piers, W.E.; Chivers, T., *Chem. Soc. Rev.*, **1997**, *26*, 345-354.

[57] Horton, A.D., *Organometallics,* **1996**, *15*, 2675-2677.

[58] Bochmann, M.; Lancaster, S.J., *Angew. Chem. Int. Ed. Engl.*, **1994**, *33*, 1634-1637.

[59] Henderson, W.; McIndoe, J.S., *Mass spectrometry of inorganic and organometallic compounds.* John Wiley and Sons, Ltd. **2005**.

[60] Sinn, H., *Macromol. Symp.*, **1995**, *97*, 27-52.

[61] Python programming official website: http://www.python.org/

[62] Parfenova, L.V.; Gabdrakhmanov, V.Z.; Khalilov, L.M.; Dzhemilev, U.M., *J. Organomet. Chem.*, **2009**, doi: 10.1016/j.jorganchem.2009.07.037

[63] Ejfler, J.; Kobyłka, M.; Hojniak, M.; Sobota, P., *J. Molec. Catal. A.*, **2004**, *224*, 93-96.

[64] Nomura, K.; Komatsu, T.; Nakamura, M.; Imanishi, Y., *J. Molec. Catal. A.*, **2000**, *164*, 131-135.

[65] Obrey, S.J.; Bott, S.G.; Barron, A.R., *Organometallics,* **2001**, *20*, 5162-5170.

[66] Lubben, A.T.; McIndoe, J.S.; Weller, A.S., *Organometallics*, **2008**, *27*, 3303-3306

[67] Eelman, M.D.; Blacquiere, J.M.; Moriarty, M.M.; Fogg, D.E., *Angew. Chem. Int. Ed. Engl.*, **2008**, *47*, 303-306.

Appendix 1: EDESI and peak assignments for gas phase reactivity

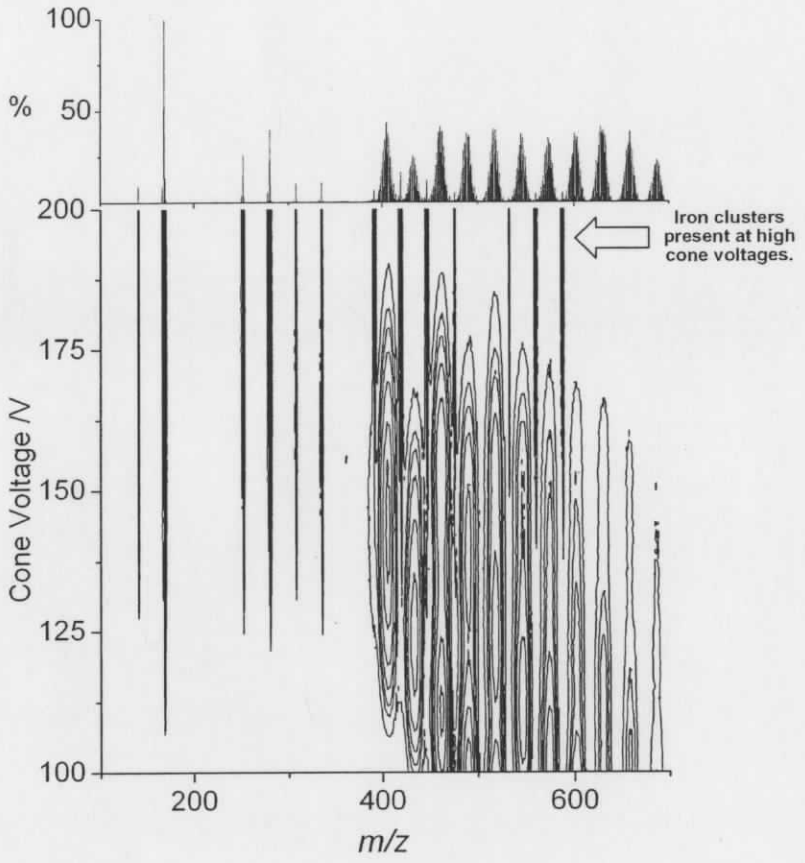

Appendix fig. 1: EDESI-MS of $[H_3Ru_4(CO)_{12}]^-$ in the presence of $Fe(CO)_{5\,(g)}$.

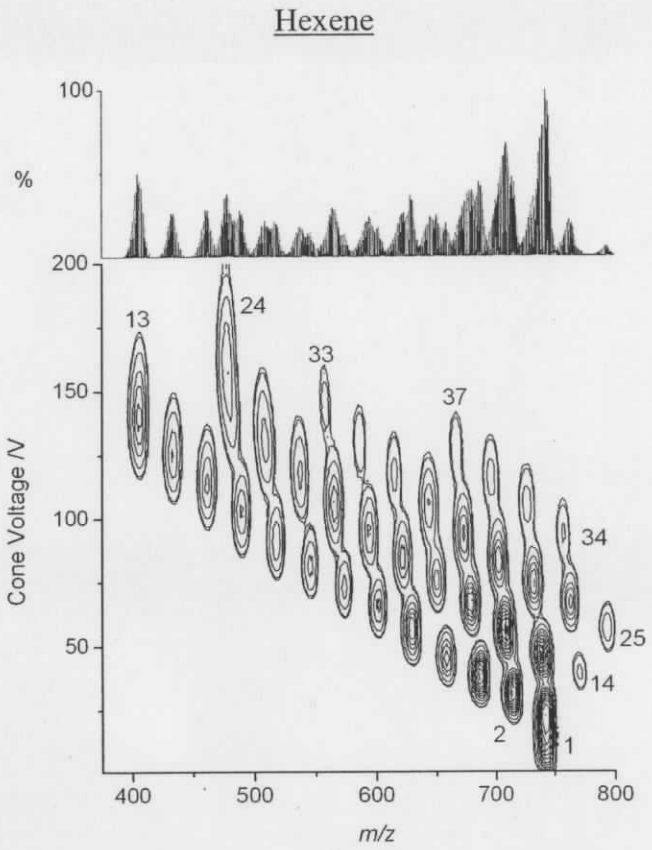

Appendix fig. 2: EDESI-MS of $[H_3Ru_4(CO)_{12}]^-$ collected in the presence of 1-hexene gas.

	no. of Hexene moieties											
	0			1			2			3		
no. of COs	Cmpd #	Assignment	Avg. Mol. Wt.	Cmpd #	Assignment	Avg. Mol. Wt.	Cmpd #	Assignment	Avg. Mol. Wt.	Cmpd #	Assignment	Avg. Mol. Wt.
12	1	$[H_3Ru_4(CO)_{12}]^-$	746.58									
11	2	$[H_3Ru_4(CO)_{11}]^-$	718.59									
10	3	$[H_3Ru_4(CO)_{10}]^-$	690.6	14	$[H_3Ru_4(CO)_{10}(C_6H_{10})]^-$	772.67						
9	4	$[H_3Ru_4(CO)_9]^-$	662.61	15	$[H_3Ru_4(CO)_9(C_6H_{10})]^-$	744.68						
8	5	$[HRu_4(CO)_8]^-$	634.62	16	$[H_3Ru_4(CO)_8(C_6H_{10})]^-$	716.69	25	$[H_3Ru_4(CO)_8(C_{12}H_{16})]^-$	794.72			
7	6	$[HRu_4(CO)_7]^-$	606.63	17	$[H_3Ru_4(CO)_7(C_6H_{10})]^-$	688.7	26	$[H_3Ru_4(CO)_7(C_{12}H_{14})]^-$	764.73			
6	7	$[HRu_4(CO)_6]^-$	578.64	18	$[H_3Ru_4(CO)_6(C_6H_6)]^-$	656.65	27	$[H_3Ru_4(CO)_6(C_{12}H_{14})]^-$	736.74			
5	8	$[HRu_4(CO)_5]^-$	550.65	19	$[H_3Ru_4(CO)_5(C_6H_4)]^-$	626.66	28	$[H_3Ru_4(CO)_5(C_{12}H_{14})]^-$	708.75			
4	9	$[HRu_4(CO)_4]^-$	522.66	20	$[HRu_4(CO)_4(C_6H_2)]^-$	594.67	29	$[H_3Ru_4(CO)_4(C_{12}H_{14})]^-$	680.76			
3	10	$[HRu_4(CO)_3]^-$	494.67	21	$[HRu_4(CO)_3(C_6)]^-$	564.61	30	$[H_3Ru_4(CO)_3(C_{12}H_{12})]^-$	650.77	34	$[H_3Ru_4(CO)_3(C_{18}H_{22})]^-$	732.8
2	11	$[HRu_4(CO)_2]^-$	466.68	22	$[HRu_4(CO)_2(C_6)]^-$	536.62	31	$[HRu_4(CO)_2(C_{12}H_{12})]^-$	620.78	35	$[HRu_4(CO)_2(C_{18}H_{22})]^-$	702.81
1	12	$[HRu_4(CO)]^-$	438.69	23	$[HRu_4(CO)(C_6)]^-$	508.63	32	$[HRu_4(CO)(C_{12}H_{10})]^-$	590.79	36	$[HRu_4(CO)(C_{18}H_{20})]^-$	672.82
0	13	$[HRu_4]^-$	410.7	24	$[HRu_4C_6]^-$	478.64	33	$[HRu_4(C_{12}H_6)]^-$	558.8	37	$[HRu_4(C_{18}H_{18})]^-$	642.83

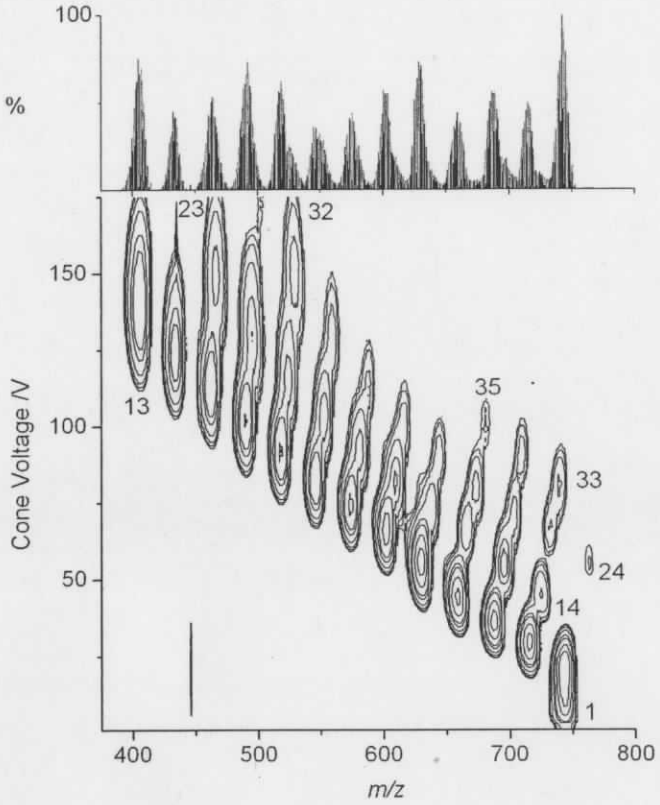

Appendix fig. 3: EDESI-MS of $[H_3Ru_4(CO)_{12}]^-$ collected in the presence of cyclopentene gas.

		no. of Cyclopentene moieties										
		0			1			2			3	
no. of COs	Cmpd #	Assignment	Avg. Mol. Wt.	Cmpd #	Assignment	Avg. Mol. Wt.	Cmpd #	Assignment	Avg. Mol. Wt.	Cmpd #	Assignment	Avg. Mol. Wt.
12	1	$[H_3Ru_4(CO)_{12}]^-$	746.58									
11	2	$[H_3Ru_4(CO)_{11}]^-$	718.59									
10	3	$[H_3Ru_4(CO)_{10}]^-$	690.6									
9	4	$[H_3Ru_4(CO)_9]^-$	662.61	14	$[H_2Ru_4(CO)_9(C_5H_5)]^-$	726.63						
8	5	$[HRu_4(CO)_8]^-$	634.62	15	$[H_2Ru_4(CO)_8(C_5H_5)]^-$	698.64	24	$[H_3Ru_4(CO)_8(C_{10}H_{14})]^-$	768.71			
7	6	$[HRu_4(CO)_7]^-$	606.63	16	$[H_2Ru_4(CO)_7(C_5H_5)]^-$	670.65	25	$[HRu_4(CO)_7(C_{10}H_{10})]^-$	734.72			
6	7	$[HRu_4(CO)_6]^-$	578.64	17	$[H_2Ru_4(CO)_6(C_5H_3)]^-$	640.66	26	$[HRu_4(CO)_6(C_{10}H_{10})]^-$	706.73			
5	8	$[HRu_4(CO)_5]^-$	550.65	18	$[H_2Ru_4(CO)_5(C_5H_3)]^-$	612.67	27	$[HRu_4(CO)_5(C_{10}H_{10})]^-$	678.74	33	$[HRu_4(CO)_5(C_{15}H_{16})]^-$	744.72
4	9	$[HRu_4(CO)_4]^-$	522.66	19	$[HRu_4(CO)_4(C_5H_2)]^-$	582.68	28	$[HRu_4(CO)_4(C_{10}H_{10})]^-$	650.75	34	$[HRu_4(CO)_4(C_{15}H_{16})]^-$	716.73
3	10	$[HRu_4(CO)_3]^-$	494.67	20	$[HRu_4(CO)_3C_5]^-$	552.69	29	$[HRu_4(CO)_3(C_{10}H_8)]^-$	620.76	35	$[HRu_4(CO)_3(C_{15}H_{16})]^-$	688.74
2	11	$[HRu_4(CO)_2]^-$	466.68	21	$[HRu_4(CO)_2C_5]^-$	524.7	30	$[HRu_4(CO)_2(C_{10}H_6)]^-$	590.77			
1	12	$[HRu_4(CO)]^-$	438.69	22	$[HRu_4(CO)C_5]^-$	496.71	31	$[HRu_4(CO)(C_{10}H_4)]^-$	560.78			
0	13	$[HRu_4]^-$	410.7	23	$[HRu_4C_5]^-$	468.72	32	$[HRu_4(C_{10}H_2)]^-$	530.79			

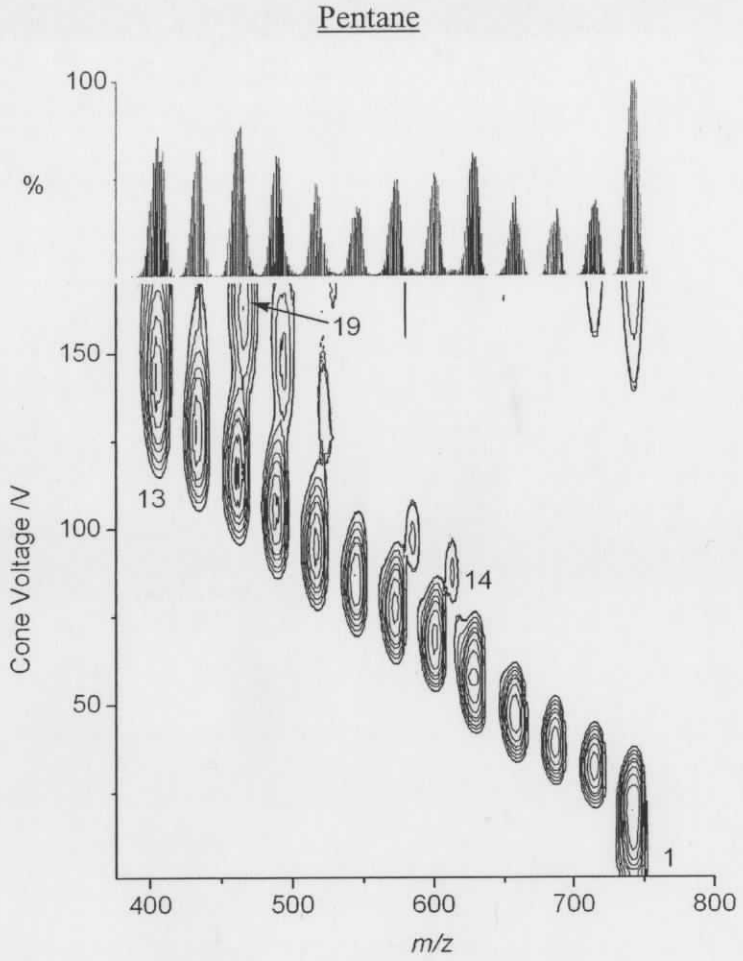

Appendix fig. 4: EDESI-MS of $[H_3Ru_4(CO)_{12}]^-$ collected in the presence of pentane gas.

	no. of Pentane moieties					
	0			1		
no. of COs	Cmpd #	Assignment	Avg. Mol. Wt.	Cmpd #	Assignment	Avg. Mol. Wt.
12	1	$[H_3Ru_4(CO)_{12}]^-$	746.58			
11	2	$[H_3Ru_4(CO)_{11}]^-$	718.59			
10	3	$[H_3Ru_4(CO)_{10}]^-$	690.6			
9	4	$[H_3Ru_4(CO)_9]^-$	662.61			
8	5	$[HRu_4(CO)_8]^-$	634.62			
7	6	$[HRu_4(CO)_7]^-$	606.63			
6	7	$[HRu_4(CO)_6]^-$	578.64			
5	8	$[HRu_4(CO)_5]^-$	550.65	14	$[H_3Ru_4(CO)_5(C_5H_6)]^-$	616.66
4	9	$[HRu_4(CO)_4]^-$	522.66	15	$[H_3Ru_4(CO)_4(C_5H_6)]^-$	588.67
3	10	$[HRu_4(CO)_3]^-$	494.67	16	$[HRu_4(CO)_3(C_5H_6)]^-$	558.68
2	11	$[HRu_4(CO)_2]^-$	466.68	17	$[HRu_4(CO)_2(C_5H_4)]^-$	528.69
1	12	$[HRu_4(CO)]^-$	438.69	18	$[HRu_4(CO)(C_5H_2)]^-$	498.7
0	13	$[HRu_4]^-$	410.7	19	$[HRu_4C_5]^-$	468.71

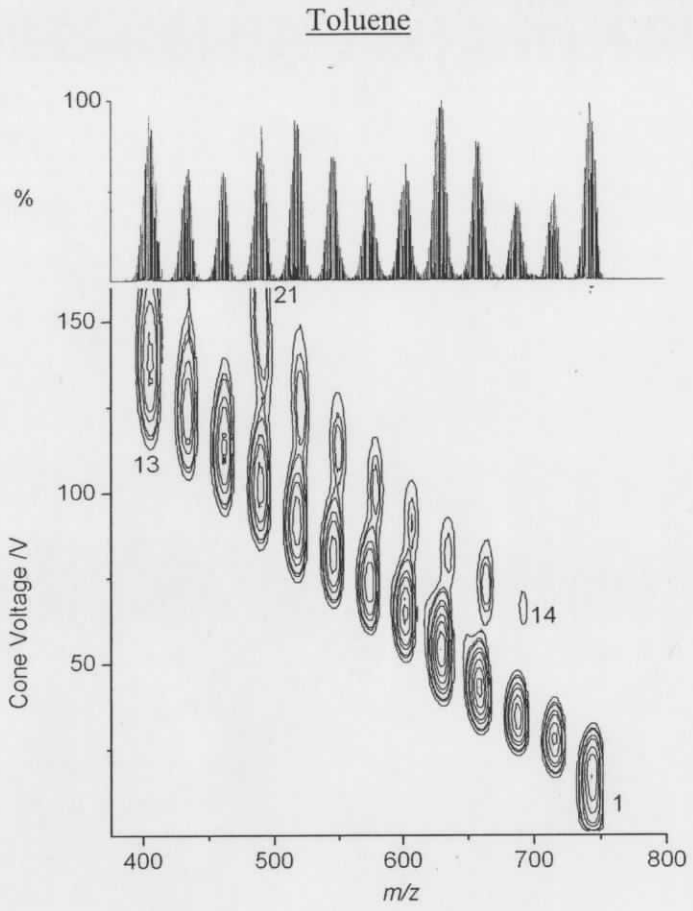

Appendix fig. 5: EDESI-MS of $[H_3Ru_4(CO)_{12}]^-$ collected in the presence of toluene gas.

		no. of Toluene moieties 0			1	
no. of COs	Cmpd #	Assignment	Avg. Mol. Wt.	Cmpd #	Assignment	Avg. Mol. Wt.
12	1	$[H_3Ru_4(CO)_{12}]^-$	746.58			
11	2	$[H_3Ru_4(CO)_{11}]^-$	718.59			
10	3	$[H_3Ru_4(CO)_{10}]^-$	690.6			
9	4	$[H_3Ru_4(CO)_9]^-$	662.61			
8	5	$[HRu_4(CO)_8]^-$	634.62			
7	6	$[HRu_4(CO)_7]^-$	606.63	14	$[H_3Ru_4(CO)_7(C_7H_4)]^-$	694.63
6	7	$[HRu_4(CO)_6]^-$	578.64	15	$[H_3Ru_4(CO)_6(C_7H_4)]^-$	666.64
5	8	$[HRu_4(CO)_5]^-$	550.65	16	$[H_3Ru_4(CO)_5(C_7H_4)]^-$	638.65
4	9	$[HRu_4(CO)_4]^-$	522.66	17	$[HRu_4(CO)_4(C_7H_4)]^-$	608.66
3	10	$[HRu_4(CO)_3]^-$	494.67	18	$[HRu_4(CO)_3(C_7H_4)]^-$	580.67
2	11	$[HRu_4(CO)_2]^-$	466.68	19	$[HRu_4(CO)_2(C_7H_4)]^-$	552.68
1	12	$[HRu_4(CO)]^-$	438.69	20	$[HRu_4(CO)(C_7H_2)]^-$	522.69
0	13	$[HRu_4]^-$	410.7	21	$[HRu_4C_7]^-$	492.7

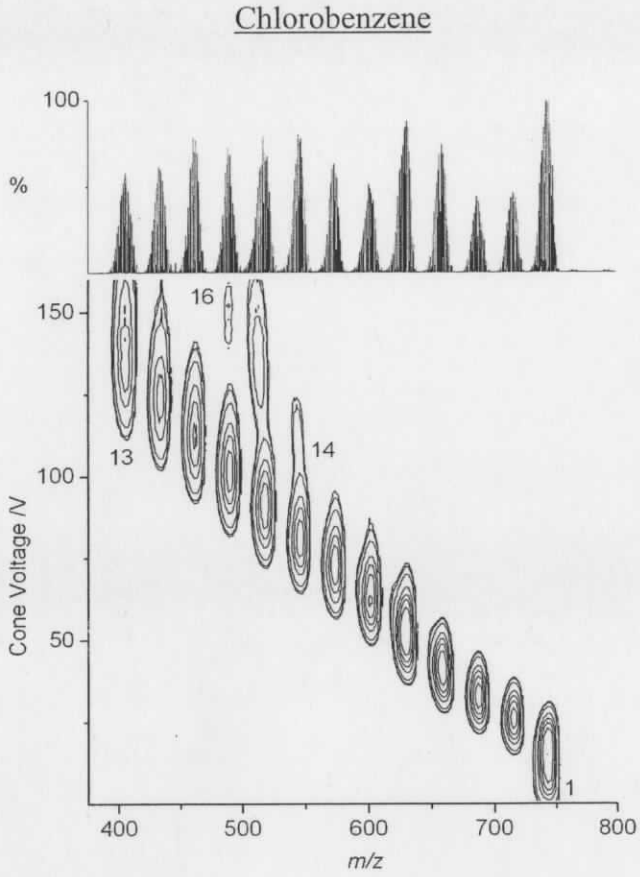

Appendix fig. 6: EDESI-MS of $[H_3Ru_4(CO)_{12}]^-$ collected in the presence of chlorobenzene gas.

		no. of Chlorobenzene moieties				
		0			1	
no. of COs	Cmpd #	Assignment	Avg. Mol. Wt.	Cmpd #	Assignment	Avg. Mol. Wt.
12	1	$[H_3Ru_4(CO)_{12}]^-$	746.58			
11	2	$[H_3Ru_4(CO)_{11}]^-$	718.59			
10	3	$[H_3Ru_4(CO)_{10}]^-$	690.6			
9	4	$[H_3Ru_4(CO)_9]^-$	662.61			
8	5	$[HRu_4(CO)_8]^-$	634.62			
7	6	$[HRu_4(CO)_7]^-$	606.63			
6	7	$[HRu_4(CO)_6]^-$	578.64			
5	8	$[HRu_4(CO)_5]^-$	550.65			
4	9	$[HRu_4(CO)_4]^-$	522.66			
3	10	$[HRu_4(CO)_3]^-$	494.67			
2	11	$[HRu_4(CO)_2]^-$	466.68			
1	12	$[HRu_4(CO)]^-$	438.69	14	$[HRu_4(CO)(C_6H_3Cl)]^-$	546.62
0	13	$[HRu_4]^-$	410.7	15	$[Ru_4C_6Cl]^-$	514.64
0				16	$[Ru_4C_4Cl]^-$	490.65

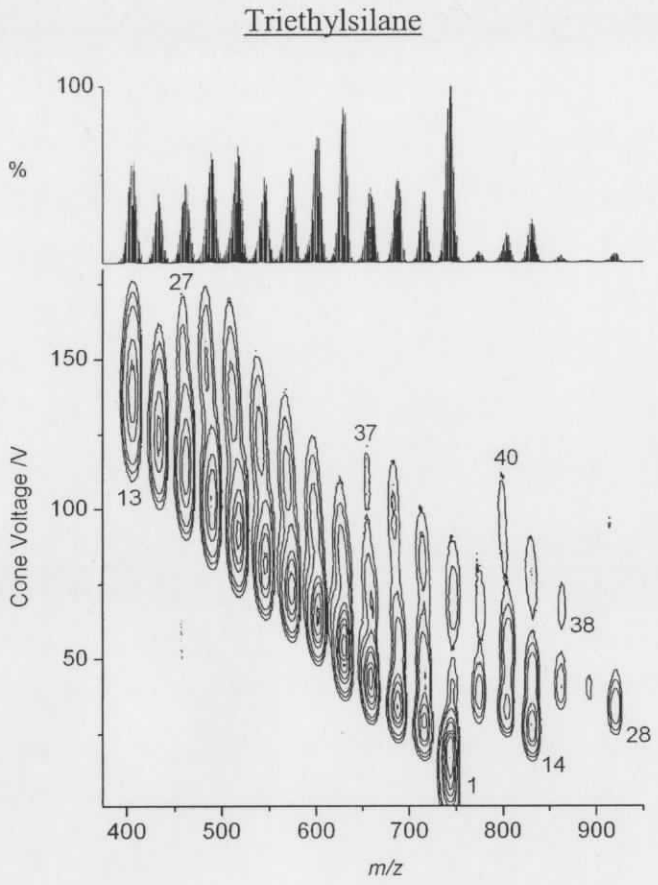

Appendix fig. 7: EDESI-MS of $[H_3Ru_4(CO)_{12}]^-$ collected in the presence of triethylsilane gas.

no. of Triethylsilane moieties

	0			1			2			3		
no. of COs	Cmpd #	Assignment	Avg. Mol. Wt.	Cmpd #	Assignment	Avg. Mol. Wt.	Cmpd #	Assignment	Avg. Mol. Wt.	Cmpd #	Assignment	Avg. Mol. Wt.
12	1	$[H_3Ru_4(CO)_{12}]^-$	746.58									
11	2	$[H_3Ru_4(CO)_{11}]^-$	718.59	14	$[H_4Ru_4(CO)_{11}(SiC_6H_{15})]^-$	834.69						
10	3	$[H_3Ru_4(CO)_{10}]^-$	690.6	15	$[H_4Ru_4(CO)_{10}(SiC_6H_{15})]^-$	806.7	28	$[H_5Ru_4(CO)_{10}(Si_2C_{12}H_{30})]^-$	922.79			
9	4	$[H_3Ru_4(CO)_9]^-$	662.61	16	$[H_4Ru_4(CO)_9(SiC_6H_{15})]^-$	778.71	29	$[H_5Ru_4(CO)_9(Si_2C_{12}H_{30})]^-$	894.8			
8	5	$[HRu_4(CO)_8]^-$	634.62	17	$[H_4Ru_4(CO)_8(SiC_6H_{15})]^-$	750.72	30	$[H_3Ru_4(CO)_8(Si_2C_{12}H_{30})]^-$	864.81			
7	6	$[HRu_4(CO)_7]^-$	606.63	18	$[HRu_4(CO)_7(SiC_6H_{14})]^-$	718.73	31	$[HRu_4(CO)_7(Si_2C_{12}H_{30})]^-$	834.82			
6	7	$[HRu_4(CO)_6]^-$	578.64	19	$[HRu_4(CO)_6(SiC_6H_{14})]^-$	690.74	32	$[HRu_4(CO)_6(Si_2C_{12}H_{28})]^-$	804.83			
5	8	$[HRu_4(CO)_5]^-$	550.65	20	$[HRu_4(CO)_5(SiC_6H_{12})]^-$	660.75	33	$[HRu_4(CO)_5(Si_2C_{12}H_{28})]^-$	776.84			
4	9	$[HRu_4(CO)_4]^-$	522.66	21	$[HRu_4(CO)_4(SiC_6H_{10})]^-$	630.76	34	$[HRu_4(CO)_4(Si_2C_{12}H_{26})]^-$	746.84	38	$[H_4Ru_4(CO)_4(Si_3C_{18}H_{45})]^-$	868.91
3	10	$[HRu_4(CO)_3]^-$	494.67	22	$[HRu_4(CO)_3(SiC_6H_8)]^-$	600.77	35	$[HRu_4(CO)_3(Si_2C_{12}H_{22})]^-$	714.85	39	$[HRu_4(CO)_3(Si_3C_{18}H_{40})]^-$	832.92
2	11	$[HRu_4(CO)_2]^-$	466.68	23	$[HRu_4(CO)_2(SiC_6H_6)]^-$	570.78	36	$[HRu_4(CO)_2(Si_2C_{12}H_{20})]^-$	684.86	40	$[HRu_4(CO)_2Si_3C_{18}H_{36})]^-$	800.93
1	12	$[HRu_4(CO)]^-$	438.69	24	$[HRu_4(CO)(SiC_6H_6)]^-$	542.79	37	$[HRu_4(CO)(Si_2C_{12}H_{20})]^-$	656.87			
0	13	$[HRu_4]^-$	410.7	25	$[HRu_4Si(C_6H_4)]^-$	512.63						
0				26	$[HRu_4(SiC_4H_2)]^-$	486.61						
0				27	$[HRu_4(SiC_2)]^-$	460.6						

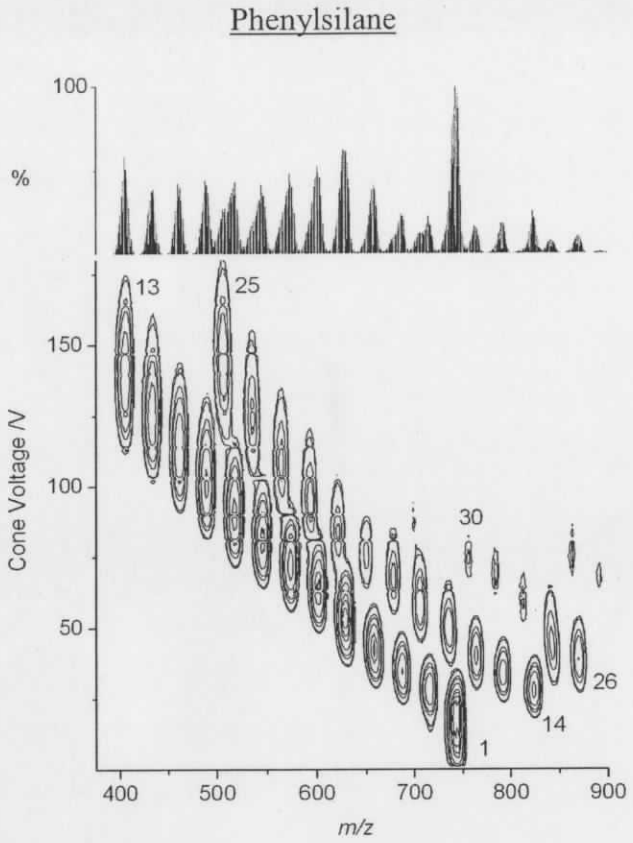

Appendix fig. 8: EDESI-MS of $[H_3Ru_4(CO)_{12}]^-$ collected in the presence of phenylsilane gas.

	no. of Phenylsilane moieties								
	0			1			2		
no. of COs	Cmpd #	Assignment	Avg. Mol. Wt.	Cmpd #	Assignment	Avg. Mol. Wt.	Cmpd #	Assignment	Avg. Mol. Wt.
12	1	$[H_3Ru_4(CO)_{12}]^-$	746.58						
11	2	$[H_3Ru_4(CO)_{11}]^-$	718.59	14	$[H_6Ru_4(CO)_{11}(SiC_6H_5)]^-$	826.62			
10	3	$[H_3Ru_4(CO)_{10}]^-$	690.6	15	$[H_2Ru_4(CO)_{10}(SiC_6H_5)]^-$	794.63	26	$[H_3Ru_4(CO)_{10}(Si_2C_{12}H_{10})]^-$	900.62
9	4	$[H_3Ru_4(CO)_9]^-$	662.61	16	$[H_2Ru_4(CO)_9(SiC_6H_5)]^-$	766.64	27	$[H_3Ru_4(CO)_9(Si_2C_{12}H_{10})]^-$	872.63
8	5	$[HRu_4(CO)_8]^-$	634.62	17	$[HRu_4(CO)_8(SiC_6H_4)]^-$	736.65	28	$[H_3Ru_4(CO)_8(Si_2C_{12}H_{10})]^-$	844.64
7	6	$[HRu_4(CO)_7]^-$	606.63	18	$[HRu_4(CO)_7(SiC_6H_4)]^-$	708.66	29	$[HRu_4(CO)_7(Si_2C_{12}H_{10})]^-$	814.65
6	7	$[HRu_4(CO)_6]^-$	578.64	19	$[HRu_4(CO)_6(SiC_6H_4)]^-$	680.67	30	$[HRu_4(CO)_6(Si_2C_{12}H_{10})]^-$	786.66
5	8	$[HRu_4(CO)_5]^-$	550.65	20	$[HRu_4(CO)_5(SiC_6H_4)]^-$	652.68			
4	9	$[HRu_4(CO)_4]^-$	522.66	21	$[HRu_4(CO)_4(SiC_6H_2)]^-$	632.69			
3	10	$[HRu_4(CO)_3]^-$	494.67	22	$[HRu_4(CO)_3(SiC_6H_2)]^-$	604.7			
2	11	$[HRu_4(CO)_2]^-$	466.68	23	$[HRu_4(CO)_2(SiC_6H_2)]^-$	576.71			
1	12	$[HRu_4(CO)]^-$	438.69	24	$[HRu_4(CO)(SiC_6)]^-$	546.72			
0	13	$[HRu_4]^-$	410.7	25	$[HRu_4(SiC_6)]^-$	518.73			

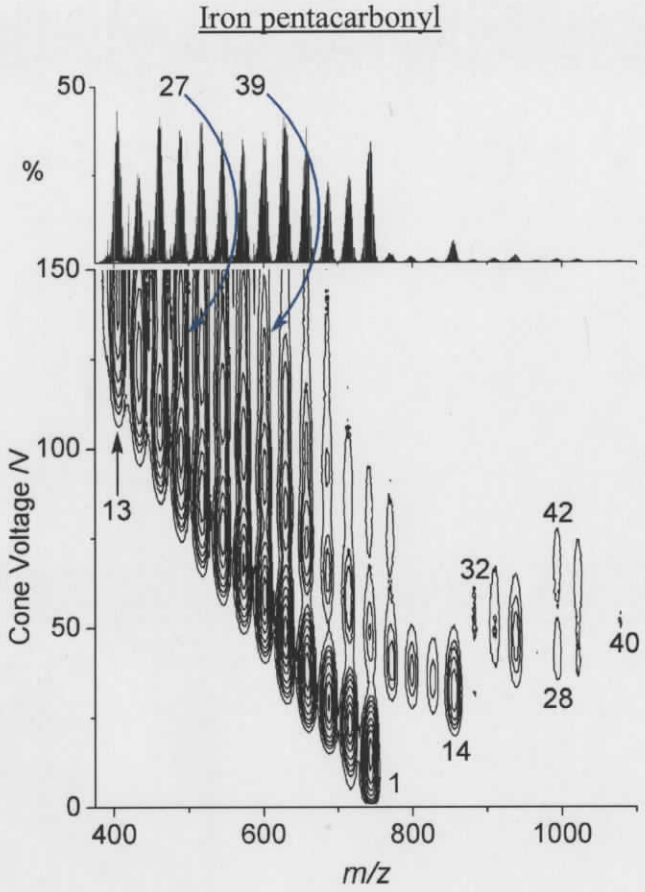

Appendix fig. 9: EDESI-MS of $[H_3Ru_4(CO)_{12}]^-$ collected in the presence of iron pentacarbonyl gas.

	no. of Iron pentacarbonyl moieties											
	0			1			2			3		
no. of COs	Cmpd #	Assignment	Avg. Mol. Wt.	Cmpd #	Assignment	Avg. Mol. Wt.	Cmpd #	Assignment	Avg. Mol. Wt.	Cmpd #	Assignment	Avg. Mol. Wt.
18										40	$[HRu_4Fe_3(CO)_{18}]^-$	1077.00
17							28	$[HRu_4Fe_2(CO)_{17}]^-$	993.15			
16							29	$[HRu_4Fe_2(CO)_{16}]^-$	965.14	41	$[HRu_4Fe_3(CO)_{16}]^-$	1020.98
15							30	$[HRu_4Fe_2(CO)_{15}]^-$	937.13	42	$[HRu_4Fe_3(CO)_{15}]^-$	992.97
14				14	$[HRu_4Fe(CO)_{14}]^-$	853.27	31	$[HRu_4Fe_2(CO)_{14}]^-$	909.12			
13				15	$[HRu_4Fe(CO)_{13}]^-$	825.26	32	$[HRu_4Fe_2(CO)_{13}]^-$	881.11			
12	1	$[H_3Ru_4(CO)_{12}]^-$	746.58	16	$[HRu_4Fe(CO)_{12}]^-$	797.25						
11	2	$[H_3Ru_4(CO)_{11}]^-$	718.59	17	$[HRu_4Fe(CO)_{11}]^-$	769.24						
10	3	$[H_3Ru_4(CO)_{10}]^-$	690.6	18	$[HRu_4Fe(CO)_{10}]^-$	741.23						
9	4	$[H_3Ru_4(CO)_9]^-$	662.61	19	$[HRu_4Fe(CO)_9]^-$	713.22	33	$[HRu_4Fe_2(CO)_9]^-$	769.07			
8	5	$[HRu_4(CO)_8]^-$	634.62	20	$[HRu_4Fe(CO)_8]^-$	685.21	34	$[HRu_4Fe_2(CO)_8]^-$	741.06			
7	6	$[HRu_4(CO)_7]^-$	606.63	21	$[HRu_4Fe(CO)_7]^-$	657.2	35	$[HRu_4Fe_2(CO)_7]^-$	713.05			
6	7	$[HRu_4(CO)_6]^-$	578.64	22	$[HRu_4Fe(CO)_6]^-$	629.19	36	$[HRu_4Fe_2(CO)_6]^-$	685.04			
5	8	$[HRu_4(CO)_5]^-$	550.65	23	$[HRu_4Fe(CO)_5]^-$	601.18	37	$[HRu_4Fe_2(CO)_5]^-$	657.03			
4	9	$[HRu_4(CO)_4]^-$	522.66	24	$[HRu_4Fe(CO)_4]^-$	573.17	38	$[HRu_4Fe_2(CO)_4]^-$	629.02			
3	10	$[HRu_4(CO)_3]^-$	494.67	25	$[HRu_4Fe(CO)_3]^-$	545.16	39	$[HRu_4Fe_2(CO)_3]^-$	601.01			
2	11	$[HRu_4(CO)_2]^-$	466.68	26	$[HRu_4Fe(CO)_2]^-$	517.15						
1	12	$[HRu_4(CO)]^-$	438.69	27	$[HRu_4Fe(CO)_1]^-$	489.14						
0	13	$[HRu_4]^-$	410.7									

Appendix 2: EDESI and breakdown plots for the Pauson-Khand reaction

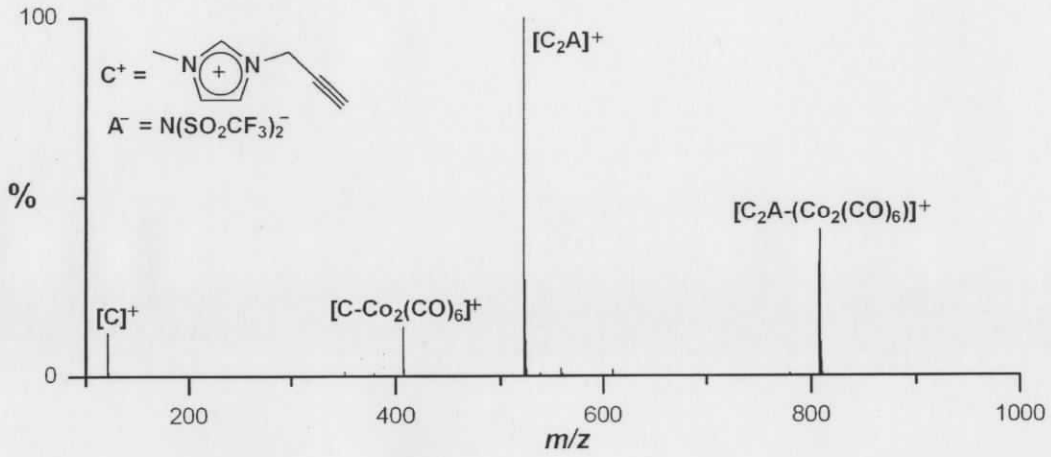

Appendix fig. 10: First spectrum from the dichloromethane solution of the ionic liquid methyl propargylimidazolium bis(trifluoromethyl)sulfonylamide and $Co_2(CO)_8$. Clearly present is the charged dicobalt hexacarbonyl-alkyne complex.

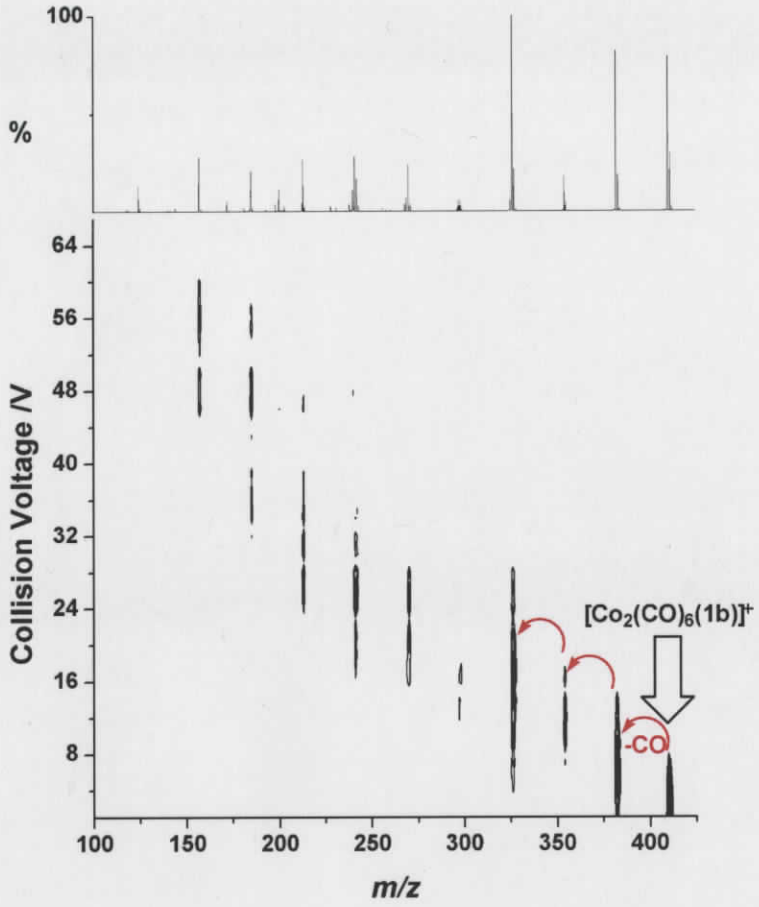

Appendix fig. 11: MS/MS of $[Co_2(CO)_6(\mathbf{1b})]^+$.

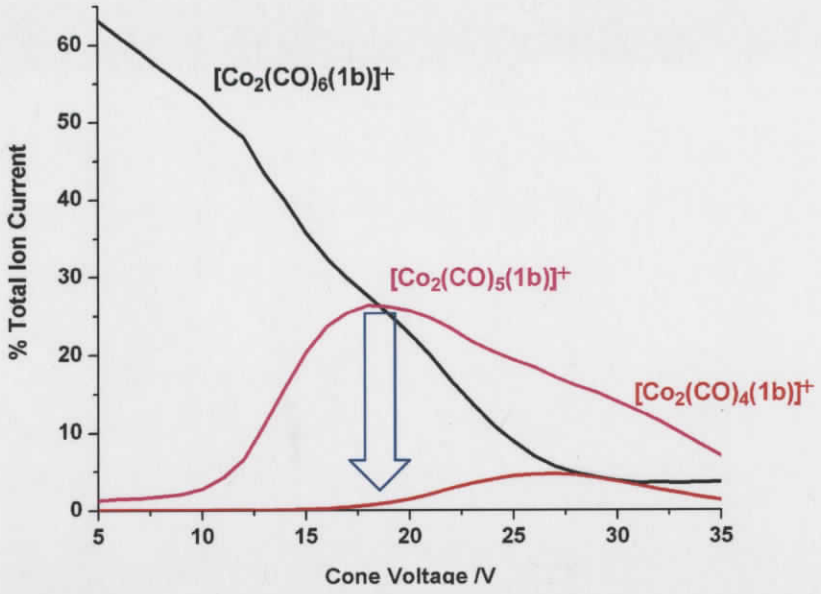

Appendix fig. 12: Breakdown plot of the EDESI-MS spectrum of $[Co_2(CO)_6(\mathbf{1b})]^+$ in the absence of any reactive gas. Only the first two fragment ions are shown in this picture for clarity. For a more complete representation of this experiment, refer to the EDESI-MS contour plot.

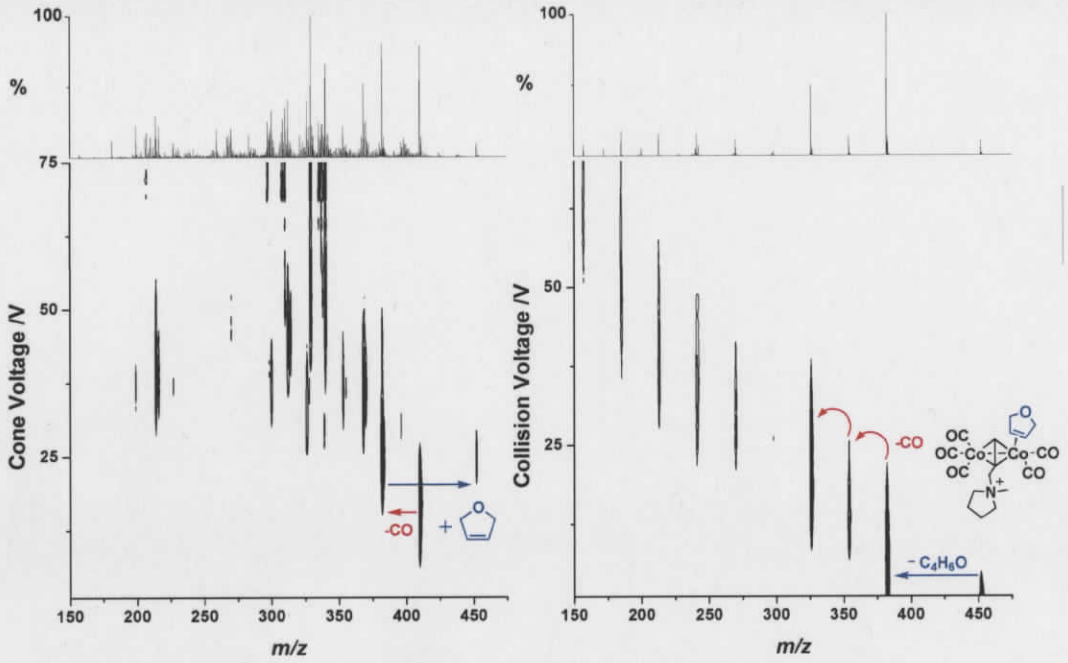

Appendix fig. 13: (Left) EDESI-MS contour plot of the reaction of $[Co_2(CO)_6(\mathbf{1b})]^+$ with 2,3-dihydrofuran gas. (Right) MS/MS spectrum of the only product ion showing that the alkene is the first fragment to fall off the complex.

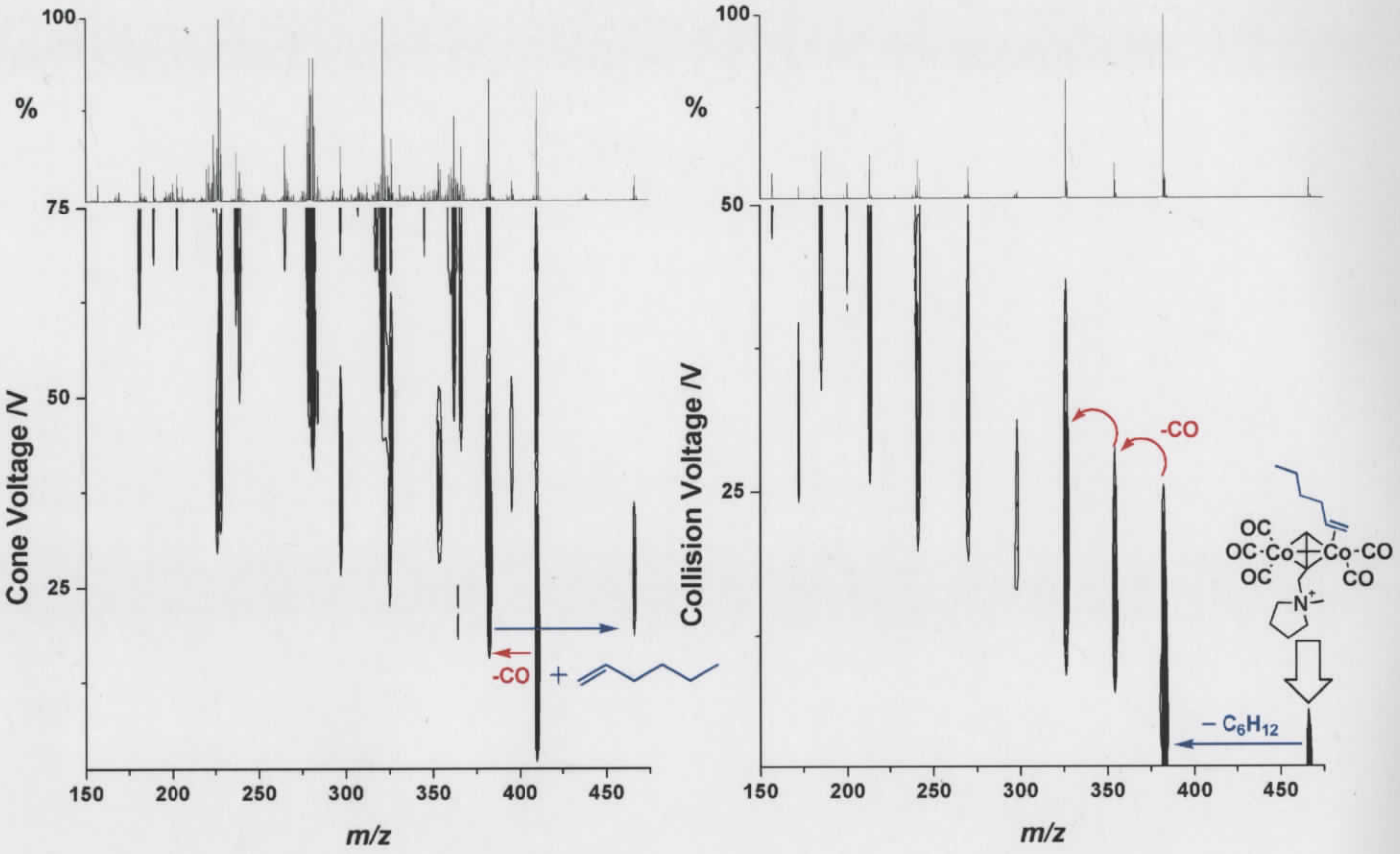

Appendix fig. 14: (Left) EDESI-MS contour plot of the reaction of $[Co_2(CO)_6(\mathbf{1b})]^+$ with 1-hexene gas. (Right) MS/MS spectrum of the only product ion showing that the alkene is the first fragment to fall off the complex.

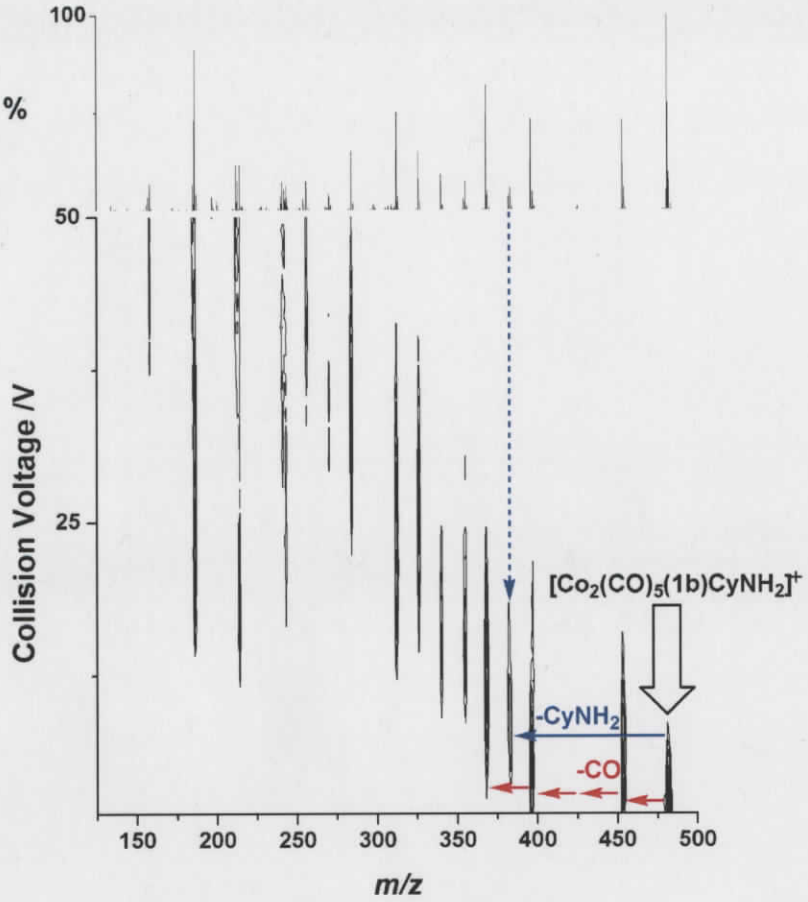

Appendix fig. 15: EDESI-MS/MS of the first addition product in the reaction of $[Co_2(CO)_6(\mathbf{1b})]^+$ with cyclohexylamine.

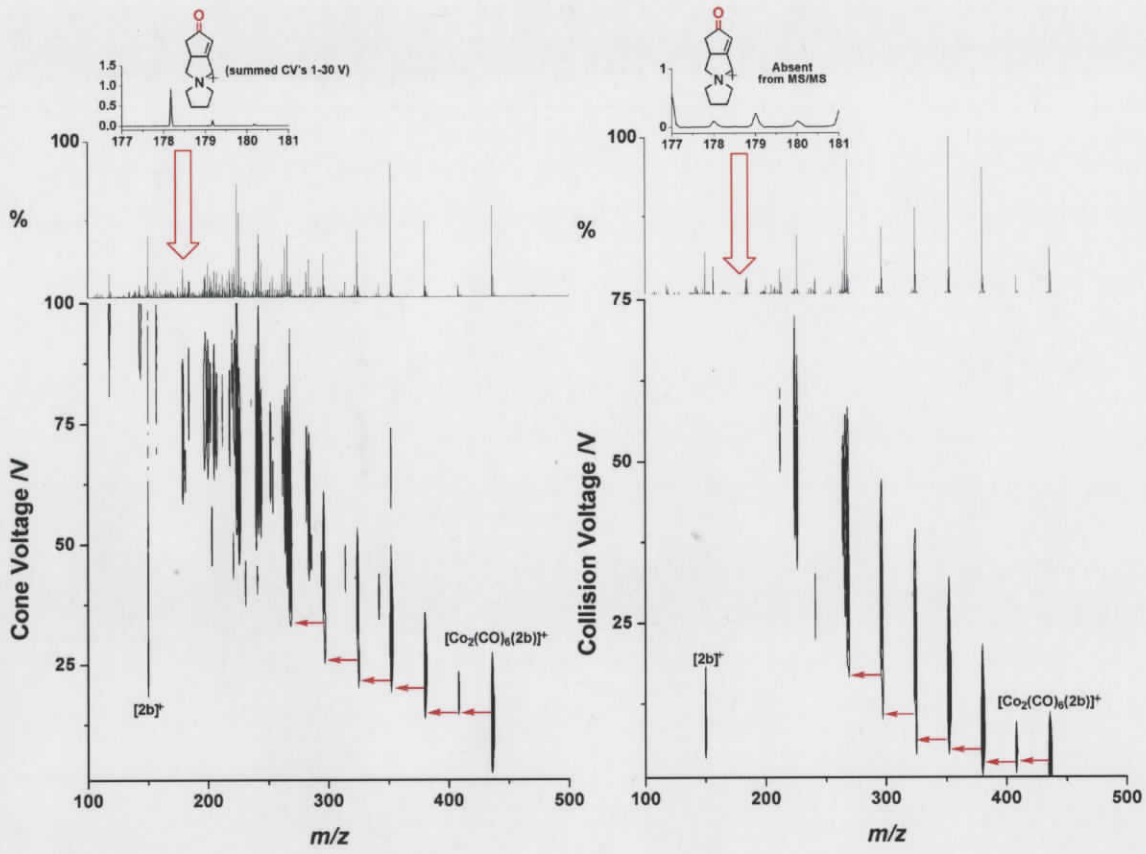

Appendix fig. 16: (Left) EDESI-MS of $[Co_2(CO)_6(\mathbf{2b})]^+$; inset shows the presence of cyclic product. (Right) EDESI-MS/MS of $[Co_2(CO)_6(\mathbf{2b})]^+$; inset shows the notable absence of cyclic product.

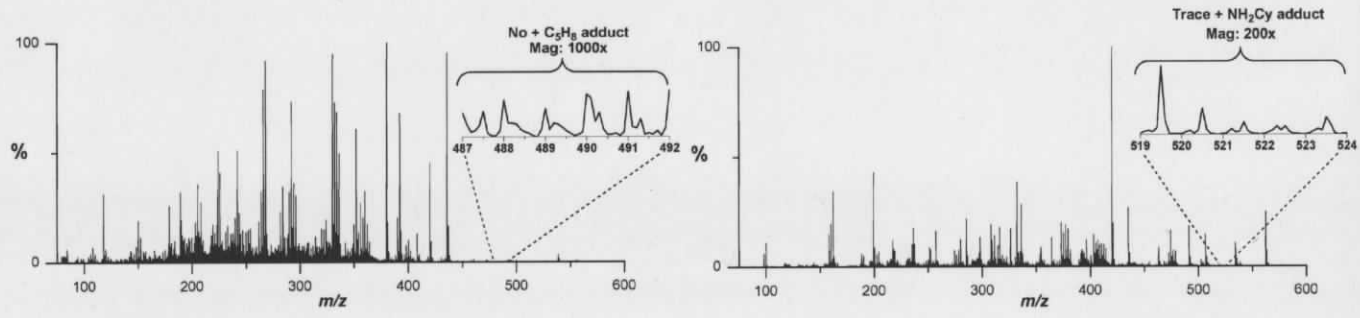

Appendix fig. 17: Summed EDESI-MS of the gas phase reactions of $[Co_2(CO)_6(\mathbf{2b})]^+$ with cyclopentene (left) and cyclohexylamine (right). No coordination of either species occurs upon loss of a CO ligand from the parent compound.

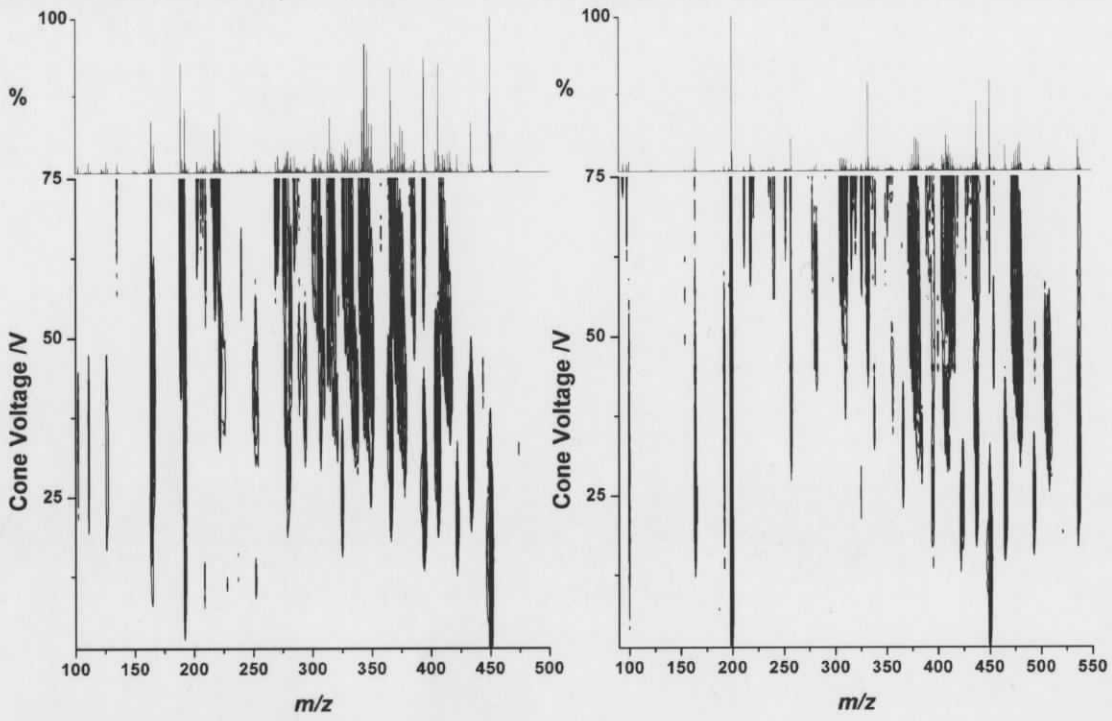

Appendix fig. 18: Gas phase reaction of $[Co_2(CO)_6(\mathbf{2b})]^+$ with cyclopentene (left) and cyclohexylamine (right).

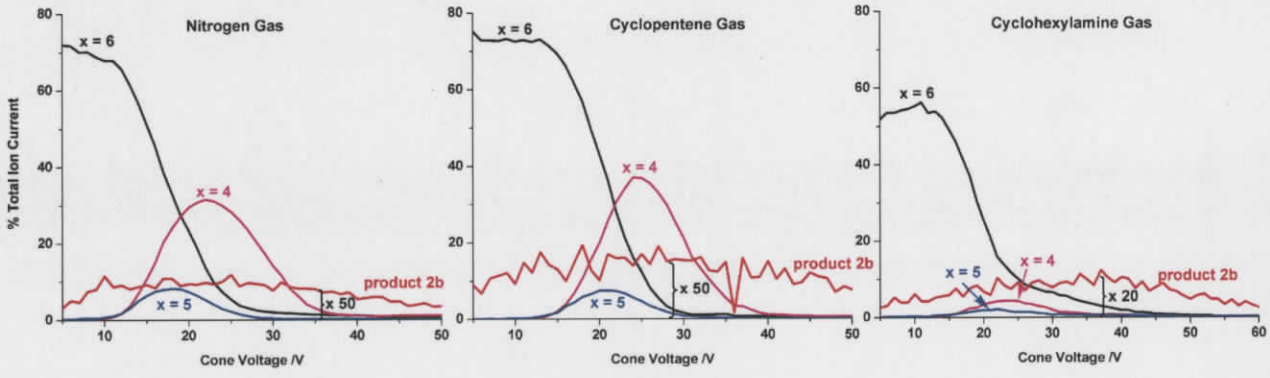

Appendix fig. 19: Breakdown plots of $[Co_2(CO)_6(\mathbf{2b})]^+$ from EDESI experiments with nitrogen, cyclopentene, and cyclohexylamine.

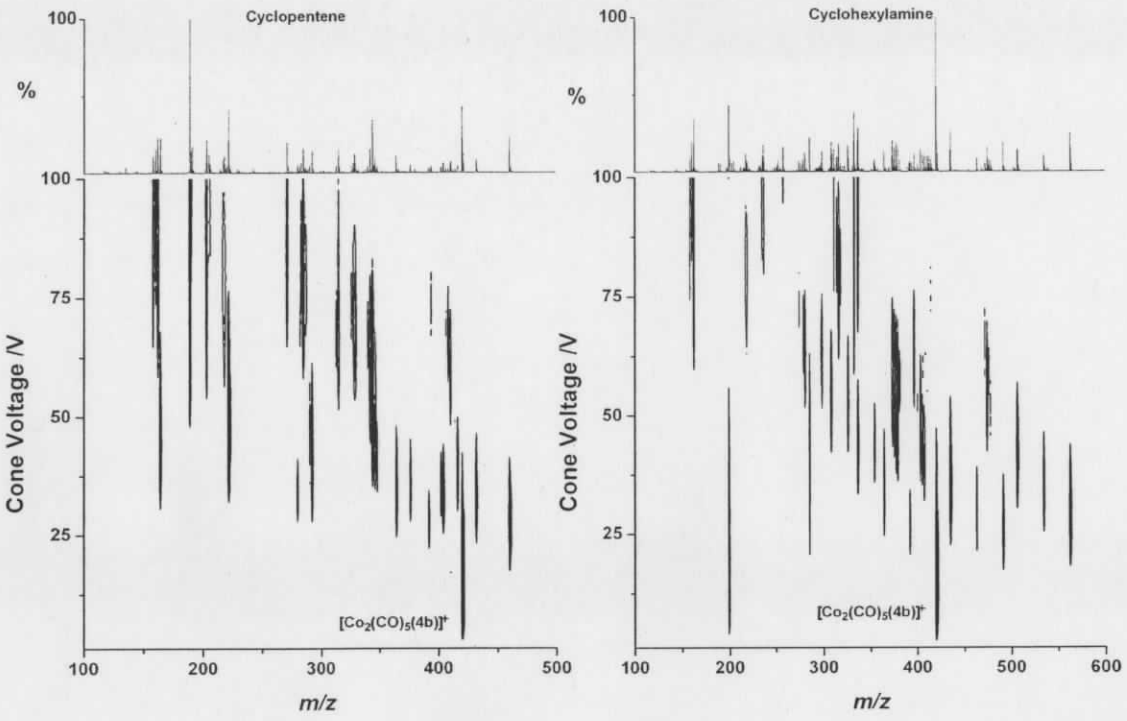

Appendix fig. 20: Gas phase reaction of $[Co_2(CO)_5(\mathbf{4b})]^+$ with (left) cyclopentene gas and (right) cyclohexylamine gas.

Appendix 3: Crystal structure data for Pauson-Khand complexes

All crystal structures were solved by Dr. Allen Oliver from the University of Notre Dame.

4c:

The compound crystallizes as colourless blade-like/tablet-like crystals. There are four molecules of the pyrollidinium cation and associated BPh4 counterion in the unit cell of the primitive, monoclinic space group $P2_1/c$.

The structure of the compound is as expected. The acetylinic hydrogens were observed in a difference Fourier map but were included in calculated positions. The C7-C8 and C10-C11 bond distances (1.715(2) and 1.718(2) Å, respectively) and nearly linear C6-C7-C8 and C9-C10-C11 bond angles (179.50(17 and 179.26(16)°) reflect the triple bond nature.

The bond distances and angles are otherwise as expected.

Crystal data for $C_{35}H_{36}BN$; M_r = 481.46; monoclinic; space group $P2_1/c$; a = 9.5882(4) Å; b = 15.8802(5) Å; c = 18.7956(7) Å; α = 90°; β = 104.463(2)°; γ = 90°; V = 2771.17(18) $Å^3$; Z = 4; T = 100(2) K; λ(Mo-Kα) = 0.71073 Å; μ(Mo-Kα) = 0.065 mm^{-1}; d_{calc} = 1.154g.cm^{-3}; 21465 reflections collected; 5670 unique (R_{int} = 0.0341); giving R_1 = 0.0399, wR_2 = 0.0915 for 4315 data with [I>2σ(I)] and R_1 = 0.0587, wR_2 = 0.1005 for all 5670 data. Residual electron density ($e^-.Å^{-3}$) max/min: 0.267/-0.210.

An arbitrary sphere of data were collected on a colourless tablet-like crystal, having approximate dimensions of 0.30 × 0.27 × 0.12 mm, on a Bruker Kappa X8-APEX-II diffractometer using a combination of ω- and φ-scans of 0.3°. Data were corrected for absorption and polarization effects and analyzed for space group determination. The structure was solved by direct methods and expanded routinely. The model was refined by full-matrix least-squares analysis of F^2 against all reflections. All non-hydrogen atoms were refined with anisotropic thermal displacement parameters. Unless otherwise noted,

hydrogen atoms were included in calculated positions. Thermal parameters for the hydrogens were tied to the isotropic thermal parameter of the atom to which they are bonded (1.5 × for methyl, 1.2 × for all others).

Appendix Table 1: Crystal data and structure refinement for 4c.

Identification code	**4c**
Empirical formula	$C_{35}H_{36}BN$
Formula weight	481.46
Temperature	100(2) K
Wavelength	0.71073 Å
Crystal system	monoclinic
Space group	$P2_1/c$
Unit cell dimensions	a = 9.5882(4) Å α = 90° b = 15.8802(5) Å β = 104.463(2)° c = 18.7956(7) Å
Volume	2771.17(18) $Å^3$
Z	4
Density (calculated)	1.154 $g.cm^{-3}$
Absorption coefficient (μ)	0.065 mm^{-1}
F(000)	1032
Crystal size	0.30 × 0.27 × 0.12 mm^3
ω range for data collection	1.70 to 26.45°
Index ranges	$-12 \leq h \leq 11$, $-19 \leq k \leq 17$, $-22 \leq l \leq 23$
Reflections collected	21465
Independent reflections	5670 [R_{int} = 0.0341]
Completeness to θ = 26.45°	99.4 %
Absorption correction	numerical
Max. and min. transmission	1.0000 and 0.8804
Refinement method	Full-matrix least-squares on F^2
Data / restraints / parameters	5670 / 0 / 334
Goodness-of-fit on F^2	1.048
Final R indices [I>2σ(I)]	R_1 = 0.0399, wR_2 = 0.0915
R indices (all data)	R_1 = 0.0587, wR_2 = 0.1005
Largest diff. peak and hole	0.267 and -0.210 $e^-.Å^{-3}$

Appendix Table 2: Atomic coordinates and equivalent isotropic displacement parameters ($Å^2$) for **4c**. U(eq) is defined as one third of the trace of the orthogonalized U_{ij} tensor.

	x	y	z	U(eq)
N(1)	0.72706(11)	0.12029(6)	0.23303(6)	0.018(1)
C(1)	0.85020(14)	0.09787(9)	0.19940(7)	0.022(1)
C(2)	0.80866(15)	0.03495(9)	0.13743(8)	0.028(1)
C(3)	0.67860(15)	0.06461(10)	0.07849(8)	0.030(1)
C(4)	0.55466(14)	0.08456(9)	0.11250(7)	0.025(1)
C(5)	0.59763(13)	0.14848(8)	0.17358(7)	0.021(1)
C(6)	0.69076(14)	0.04553(8)	0.27471(7)	0.022(1)
C(7)	0.57321(15)	0.06361(9)	0.30825(7)	0.026(1)
C(8)	0.47839(17)	0.07886(10)	0.33555(8)	0.035(1)

C(9)	0.77174(14)	0.19406(8)	0.28459(7)	0.023(1)
C(10)	0.89340(15)	0.17381(8)	0.34561(7)	0.025(1)
C(11)	0.99123(16)	0.15661(9)	0.39522(8)	0.031(1)
B(1)	0.16870(15)	0.29121(9)	0.14945(8)	0.018(1)
C(21)	0.17305(13)	0.19327(8)	0.12177(7)	0.019(1)
C(22)	0.21504(14)	0.12535(8)	0.16942(8)	0.022(1)
C(23)	0.21782(15)	0.04312(9)	0.14470(8)	0.029(1)
C(24)	0.17607(15)	0.02498(9)	0.07112(9)	0.030(1)
C(25)	0.13318(15)	0.09016(9)	0.02197(8)	0.029(1)
C(26)	0.13246(14)	0.17184(8)	0.04725(7)	0.024(1)
C(31)	0.00318(13)	0.31769(8)	0.14900(7)	0.019(1)
C(32)	-0.11503(14)	0.28929(8)	0.09485(7)	0.022(1)
C(33)	-0.25404(14)	0.31755(9)	0.08909(8)	0.026(1)
C(34)	-0.28136(14)	0.37582(9)	0.13825(8)	0.028(1)
C(35)	-0.16790(16)	0.40615(9)	0.19206(8)	0.031(1)
C(36)	-0.02915(15)	0.37715(9)	0.19725(8)	0.026(1)
C(41)	0.27490(13)	0.30272(8)	0.23201(7)	0.018(1)
C(42)	0.23262(15)	0.27787(9)	0.29509(7)	0.026(1)
C(43)	0.31884(16)	0.28691(9)	0.36549(8)	0.031(1)
C(44)	0.45477(16)	0.32142(9)	0.37623(8)	0.031(1)
C(45)	0.50221(15)	0.34585(8)	0.31574(8)	0.027(1)
C(46)	0.41328(14)	0.33663(8)	0.24548(7)	0.021(1)
C(51)	0.22017(13)	0.35390(8)	0.09111(7)	0.017(1)
C(52)	0.33190(13)	0.33194(8)	0.05891(7)	0.020(1)
C(53)	0.37902(13)	0.38454(8)	0.01105(7)	0.022(1)
C(54)	0.31665(14)	0.46255(8)	-0.00653(7)	0.022(1)
C(55)	0.20569(14)	0.48670(8)	0.02357(7)	0.021(1)
C(56)	0.15863(13)	0.43309(8)	0.07089(7)	0.018(1)
H(1A)	0.8855	0.1498	0.1806	0.026
H(1B)	0.9303	0.0744	0.2381	0.026
H(2A)	0.7863	-0.0198	0.1573	0.033
H(2B)	0.8910	0.0264	0.1153	0.033
H(3A)	0.7043	0.1155	0.0541	0.035
H(3B)	0.6491	0.0202	0.0408	0.035
H(4A)	0.4726	0.1068	0.0741	0.030
H(4B)	0.5227	0.0322	0.1323	0.030
H(5A)	0.5154	0.1581	0.1956	0.026
H(5B)	0.6202	0.2026	0.1528	0.026
H(6A)	0.6639	-0.0027	0.2407	0.027
H(6B)	0.7770	0.0292	0.3134	0.027
H(8)	0.4017	0.0912	0.3576	0.042
H(9A)	0.7976	0.2421	0.2569	0.028
H(9B)	0.6892	0.2115	0.3040	0.028
H(11)	1.0701	0.1427	0.4352	0.038
H(22A)	0.2428	0.1358	0.2208	0.027
H(23A)	0.2490	-0.0010	0.1791	0.034
H(24A)	0.1766	-0.0314	0.0543	0.036
H(25A)	0.1041	0.0789	-0.0292	0.035
H(26A)	0.1029	0.2156	0.0123	0.029
H(32A)	-0.0994	0.2488	0.0604	0.026
H(33A)	-0.3310	0.2967	0.0510	0.031
H(34A)	-0.3768	0.3947	0.1350	0.034
H(35A)	-0.1845	0.4471	0.2258	0.037

H(36A)	0.0472	0.3987	0.2353	0.031
H(42A)	0.1399	0.2536	0.2891	0.031
H(43A)	0.2847	0.2694	0.4064	0.037
H(44A)	0.5147	0.3282	0.4244	0.037
H(45A)	0.5959	0.3690	0.3222	0.032
H(46A)	0.4482	0.3542	0.2048	0.025
H(52A)	0.3772	0.2787	0.0704	0.024
H(53A)	0.4548	0.3668	-0.0098	0.026
H(54A)	0.3497	0.4991	-0.0389	0.027
H(55A)	0.1614	0.5402	0.0119	0.025
H(56A)	0.0812	0.4508	0.0905	0.022

Appendix Table 3: Anisotropic displacement parameters $(Å)^2$ for **4c**. The anisotropic displacement factor exponent takes the form: $-2\pi^2[h^2 a^{*2} U_{11} + ... + 2 h k a^* b^* U_{12}]$

	U_{11}	U_{22}	U_{33}	U_{23}	U_{13}	U_{12}
N(1)	0.0193(6)	0.0160(6)	0.0194(6)	0.0014(4)	0.0051(4)	-0.0001(4)
C(1)	0.0170(7)	0.0257(7)	0.0245(7)	0.0007(5)	0.0073(5)	0.0004(5)
C(2)	0.0243(7)	0.0313(8)	0.0287(8)	-0.0060(6)	0.0096(6)	0.0010(6)
C(3)	0.0275(8)	0.0367(9)	0.0241(7)	-0.0063(6)	0.0060(6)	-0.0029(6)
C(4)	0.0214(7)	0.0293(8)	0.0235(7)	0.0010(6)	0.0030(6)	-0.0020(6)
C(5)	0.0175(7)	0.0219(7)	0.0236(7)	0.0056(5)	0.0035(5)	0.0019(5)
C(6)	0.0239(7)	0.0190(7)	0.0248(7)	0.0052(5)	0.0069(6)	-0.0002(5)
C(7)	0.0274(8)	0.0281(8)	0.0209(7)	0.0060(6)	0.0041(6)	-0.0019(6)
C(8)	0.0324(9)	0.0506(10)	0.0241(8)	0.0064(7)	0.0111(7)	0.0009(7)
C(9)	0.0273(7)	0.0174(7)	0.0238(7)	-0.0008(5)	0.0049(6)	-0.0014(5)
C(10)	0.0300(8)	0.0221(7)	0.0239(7)	-0.0012(6)	0.0079(6)	-0.0040(6)
C(11)	0.0341(8)	0.0295(8)	0.0270(8)	0.0009(6)	0.0015(7)	-0.0054(6)
B(1)	0.0171(7)	0.0184(8)	0.0190(7)	0.0003(6)	0.0048(6)	-0.0005(5)
C(21)	0.0125(6)	0.0220(7)	0.0228(7)	-0.0009(5)	0.0067(5)	-0.0019(5)
C(22)	0.0195(7)	0.0230(7)	0.0264(7)	0.0019(5)	0.0104(6)	0.0004(5)
C(23)	0.0285(8)	0.0218(8)	0.0406(9)	0.0054(6)	0.0190(7)	0.0032(6)
C(24)	0.0275(8)	0.0212(8)	0.0467(9)	-0.0083(6)	0.0200(7)	-0.0038(6)
C(25)	0.0254(7)	0.0317(8)	0.0310(8)	-0.0107(6)	0.0080(6)	-0.0035(6)
C(26)	0.0231(7)	0.0236(7)	0.0253(7)	-0.0013(6)	0.0051(6)	0.0005(5)
C(31)	0.0204(7)	0.0175(7)	0.0196(7)	0.0055(5)	0.0083(5)	-0.0003(5)
C(32)	0.0210(7)	0.0195(7)	0.0259(7)	0.0038(5)	0.0067(6)	0.0001(5)
C(33)	0.0179(7)	0.0252(8)	0.0339(8)	0.0096(6)	0.0035(6)	-0.0018(5)
C(34)	0.0189(7)	0.0305(8)	0.0387(9)	0.0155(6)	0.0142(6)	0.0048(6)
C(35)	0.0329(8)	0.0330(9)	0.0326(8)	0.0019(6)	0.0189(7)	0.0075(6)
C(36)	0.0229(7)	0.0300(8)	0.0254(7)	-0.0014(6)	0.0087(6)	0.0001(6)
C(41)	0.0199(7)	0.0155(7)	0.0198(7)	-0.0005(5)	0.0053(5)	0.0027(5)
C(42)	0.0267(7)	0.0275(8)	0.0237(7)	0.0024(6)	0.0081(6)	-0.0014(6)
C(43)	0.0402(9)	0.0333(9)	0.0196(7)	0.0031(6)	0.0093(6)	0.0042(7)
C(44)	0.0383(9)	0.0283(8)	0.0212(7)	-0.0026(6)	-0.0035(6)	0.0042(6)
C(45)	0.0237(7)	0.0201(7)	0.0323(8)	-0.0039(6)	-0.0009(6)	0.0001(5)
C(46)	0.0227(7)	0.0162(7)	0.0227(7)	-0.0006(5)	0.0056(5)	0.0017(5)
C(51)	0.0144(6)	0.0197(7)	0.0155(6)	-0.0019(5)	0.0013(5)	-0.0025(5)
C(52)	0.0165(6)	0.0214(7)	0.0206(7)	0.0025(5)	0.0035(5)	0.0028(5)
C(53)	0.0162(7)	0.0291(8)	0.0209(7)	0.0020(5)	0.0064(5)	0.0009(5)
C(54)	0.0212(7)	0.0263(8)	0.0196(7)	0.0035(5)	0.0050(5)	-0.0047(5)
C(55)	0.0209(7)	0.0187(7)	0.0215(7)	0.0014(5)	0.0026(5)	-0.0001(5)

C(56)	0.0161(6)	0.0201(7)	0.0176(6)	-0.0023(5)	0.0038(5)	-0.0007(5)

Appendix Table 4: Bond lengths [Å] for **4c**.

Atom-atom	Distance	Atom-atom	Distance
N(1)-C(6)	1.5102(16)	N(1)-C(9)	1.5124(16)
N(1)-C(1)	1.5143(16)	N(1)-C(5)	1.5153(15
C(1)-C(2)	1.5106(19)	C(2)-C(3)	1.5213(19)
C(3)-C(4)	1.5168(19)	C(4)-C(5)	1.5106(18)
C(6)-C(7)	1.4508(19)	C(7)-C(8)	1.175(2)
C(9)-C(10)	1.4530(19)	C(10)-C(11)	1.178(2)
B(1)-C(31)	1.6398(19)	B(1)-C(41)	1.6398(18)
B(1)-C(21)	1.6438(19)	B(1)-C(51)	1.6454(19)
C(21)-C(22)	1.3955(18)	C(21)-C(26)	1.3990(18)
C(22)-C(23)	1.3885(19)	C(23)-C(24)	1.371(2)
(24)-C(25)	1.380(2)	C(25)-C(26)	1.3820(19)
C(31)-C(32)	1.3956(18)	C(31)-C(36)	1.3965(19)
C(32)-C(33)	1.3848(18)	C(33)-C(34)	1.378(2)
C(34)-C(35)	1.374(2)	C(35)-C(36)	1.3881(19)
C(41)-C(46)	1.3952(18)	C(41)-C(42)	1.4020(18
C(42)-C(43)	1.3815(19)	C(43)-C(44)	1.381(2)
C(44)-C(45)	1.381(2)	C(45)-C(46)	1.3893(18)
C(51)-C(52)	1.3998(17)	C(51)-C(56)	1.4006(17)
C(52)-C(53)	1.3836(18)	C(53)-C(54)	1.3794(18)
C(54)-C(55)	1.3783(18)	C(55)-C(56)	1.3856(18)
C(1)-H(1A)	0.99	C(1)-H(1B)	0.99
C(2)-H(2A)	0.99	C(2)-H(2B)	0.99
C(3)-H(3A)	0.99	C(3)-H(3B)	0.99
C(4)-H(4A)	0.99	C(4)-H(4B)	0.99
C(5)-H(5A)	0.99	C(5)-H(5B)	0.99
C(6)-H(6A)	0.99	C(6)-H(6B)	0.99
C(8)-H(8)	0.95	C(9)-H(9A)	0.99
C(9)-H(9B)	0.99	C(11)-H(11)	0.95
C(22)-H(22A)	0.95	C(23)-H(23A)	0.95
C(24)-H(24A)	0.95	C(25)-H(25A)	0.95
C(26)-H(26A)	0.95	C(32)-H(32A)	0.95
C(33)-H(33A)	0.95	C(34)-H(34A)	0.95
C(35)-H(35A)	0.95	C(36)-H(36A)	0.95
C(42)-H(42A)	0.95	C(43)-H(43A)	0.95
C(44)-H(44A)	0.95	C(45)-H(45A)	0.95
C(46)-H(46A)	0.95	C(52)-H(52A)	0.95
C(53)-H(53A)	0.95	C(54)-H(54A)	0.95
C(55)-H(55A)	0.95	C(56)-H(56A)	0.95

Symmetry transformations used to generate equivalent atoms:

Appendix Table 5: Bond angles [°] for **4c**.

Atom-atom-atom	Angle	Atom-atom-atom	Angle
C(6)-N(1)-C(9)	109.97(10)	C(6)-N(1)-C(1)	109.66(10)
C(9)-N(1)-C(1)	108.90(10)	C(6)-N(1)-C(5)	111.24(10)
C(9)-N(1)-C(5)	107.00(9)	C(1)-N(1)-C(5)	110.00(10)
C(1)-C(2)-C(3)	111.53(11)	C(2)-C(1)-N(1)	113.23(10)
C(4)-C(3)-C(2)	110.11(12)	C(5)-C(4)-C(3)	111.53(11)
C(4)-C(5)-N(1)	112.31(10)	C(7)-C(6)-N(1)	112.00(11)
C(8)-C(7)-C(6)	179.50(17)	C(10)-C(9)-N(1)	112.18(11)
C(2)-C(1)-H(1A)	108.9	N(1)-C(1)-H(1A)	108.9
C(2)-C(1)-H(1B)	108.9	N(1)-C(1)-H(1B)	108.9
H(1A)-C(1)-H(1B)	107.7	C(1)-C(2)-H(2A)	109.3
C(3)-C(2)-H(2A)	109.3	C(1)-C(2)-H(2B)	109.3
C(3)-C(2)-H(2B)	109.3	H(2A)-C(2)-H(2B)	108
C(4)-C(3)-H(3A)	109.6	C(2)-C(3)-H(3A)	109.6
C(4)-C(3)-H(3B)	109.6	C(2)-C(3)-H(3B)	109.6
H(3A)-C(3)-H(3B)	108.2	C(5)-C(4)-H(4A)	109.3
C(3)-C(4)-H(4A)	109.3	C(5)-C(4)-H(4B)	109.3
C(3)-C(4)-H(4B)	109.3	H(4A)-C(4)-H(4B)	108
C(4)-C(5)-H(5A)	109.1	N(1)-C(5)-H(5A)	109.1
C(4)-C(5)-H(5B)	109.1	N(1)-C(5)-H(5B)	109.1
H(5A)-C(5)-H(5B)	107.9	C(7)-C(6)-H(6A)	109.2
N(1)-C(6)-H(6A)	109.2	C(7)-C(6)-H(6B)	109.2
N(1)-C(6)-H(6B)	109.2	H(6A)-C(6)-H(6B)	107.9
C(7)-C(8)-H(8)	180	C(10)-C(9)-H(9A)	109.2
N(1)-C(9)-H(9A)	109.2	C(10)-C(9)-H(9B)	109.2
N(1)-C(9)-H(9B)	109.2	H(9A)-C(9)-H(9B)	107.9
C(10)-C(11)-H(11)	180	C(11)-C(10)-C(9)	179.26(16
C(31)-B(1)-C(41)	110.35(10)	C(31)-B(1)-C(21)	110.00(10)
C(41)-B(1)-C(21)	110.25(10)	C(31)-B(1)-C(51)	107.00(10)
C(41)-B(1)-C(51)	110.15(10)	C(21)-B(1)-C(51)	109.03(10)
C(22)-C(21)-C(26)	114.72(12)	C(22)-C(21)-B(1)	123.66(11)
C(26)-C(21)-B(1)	121.62(11)	C(23)-C(22)-C(21)	122.59(13)
C(24)-C(23)-C(22)	120.67(13)	C(23)-C(24)-C(25)	118.73(13)
C(24)-C(25)-C(26)	120.02(14)	C(25)-C(26)-C(21)	123.26(13)
C(32)-C(31)-C(36)	114.87(12)	C(32)-C(31)-B(1)	121.98(11)
C(36)-C(31)-B(1)	122.79(11)	C(33)-C(32)-C(31)	122.88(13)
C(34)-C(33)-C(32)	120.36(13)	C(35)-C(34)-C(33)	118.73(13)
C(34)-C(35)-C(36)	120.27(14)	C(35)-C(36)-C(31)	122.89(13)
C(46)-C(41)-C(42)	114.70(12)	C(46)-C(41)-B(1)	123.53(11)
C(42)-C(41)-B(1)	121.77(11)	C(43)-C(42)-C(41)	123.40(13)
C(44)-C(43)-C(42)	119.88(13)	C(43)-C(44)-C(45)	118.93(13)
C(44)-C(45)-C(46)	120.17(13)	C(45)-C(46)-C(41)	122.90(13)
C(52)-C(51)-C(56)	114.99(11)	C(52)-C(51)-B(1)	121.78(11)
C(56)-C(51)-B(1)	123.22(11)	C(53)-C(52)-C(51)	122.70(12)
C(54)-C(53)-C(52)	120.36(12)	C(55)-C(54)-C(53)	118.98(12)
C(54)-C(55)-C(56)	120.07(12)	C(55)-C(56)-C(51)	122.89(12)
C(23)-C(22)-H(22A)	118.7	C(21)-C(22)-H(22A)	118.7
C(24)-C(23)-H(23A)	119.7	C(22)-C(23)-H(23A)	119.7
C(23)-C(24)-H(24A)	120.6	C(25)-C(24)-H(24A)	120.6
C(24)-C(25)-H(25A)	120	C(26)-C(25)-H(25A)	120
C(25)-C(26)-H(26A)	118.4	C(21)-C(26)-H(26A)	118.4

C(33)-C(32)-H(32A)	118.6	C(31)-C(32)-H(32A)	118.6
C(34)-C(33)-H(33A)	119.8	C(32)-C(33)-H(33A)	119.8
C(35)-C(34)-H(34A)	120.6	C(33)-C(34)-H(34A)	120.6
C(34)-C(35)-H(35A)	119.9	C(36)-C(35)-H(35A)	119.9
C(35)-C(36)-H(36A)	118.6	C(31)-C(36)-H(36A)	118.6
C(43)-C(42)-H(42A)	118.3	C(41)-C(42)-H(42A)	118.3
C(44)-C(43)-H(43A)	120.1	C(42)-C(43)-H(43A)	120.1
C(43)-C(44)-H(44A)	120.5	C(45)-C(44)-H(44A)	120.5
C(44)-C(45)-H(45A)	119.9	C(46)-C(45)-H(45A)	119.9
C(45)-C(46)-H(46A)	118.5	C(41)-C(46)-H(46A)	118.5
C(53)-C(52)-H(52A)	118.7	C(51)-C(52)-H(52A)	118.7
C(54)-C(53)-H(53A)	119.8	C(52)-C(53)-H(53A)	119.8
C(55)-C(54)-H(54A)	120.5	C(53)-C(54)-H(54A)	120.5
C(54)-C(55)-H(55A)	120	C(56)-C(55)-H(55A)	120
C(55)-C(56)-H(56A)	118.6	C(51)-C(56)-H(56A)	118.6

Symmetry transformations used to generate equivalent atoms:

Appendix Table 6: Torsion angles [°] for **4c**.

Atom-atom-atom-atom	Angle	Atom-atom-atom-atom	angle
C(6)-N(1)-C(1)-C(2)	69.49(13)	C(9)-N(1)-C(1)-C(2)	-170.14(11)
C(5)-N(1)-C(1)-C(2)	-53.16(14)	N(1)-C(1)-C(2)-C(3)	54.50(16
C(1)-C(2)-C(3)-C(4)	-54.62(16)	C(2)-C(3)-C(4)-C(5)	55.89(15)
C(3)-C(4)-C(5)-N(1)	-56.60(15)	C(6)-N(1)-C(5)-C(4)	-67.79(14)
C(9)-N(1)-C(5)-C(4)	172.08(11)	C(1)-N(1)-C(5)-C(4)	53.92(13)
C(9)-N(1)-C(6)-C(7)	60.20(13)	C(1)-N(1)-C(6)-C(7)	179.92(11)
C(5)-N(1)-C(6)-C(7)	-58.17(14)	N(1)-C(6)-C(7)-C(8)	-39(20)
C(6)-N(1)-C(9)-C(10)	57.41(14)	C(1)-N(1)-C(9)-C(10)	-62.77(14)
C(5)-N(1)-C(9)-C(10)	178.36(11)	N(1)-C(9)-C(10)-C(11)	-50(14)
C(31)-B(1)-C(21)-C(22)	-99.99(13)	C(41)-B(1)-C(21)-C(22)	21.93(16)
C(51)-B(1)-C(21)-C(22)	142.97(12)	C(31)-B(1)-C(21)-C(26)	79.27(14)
C(41)-B(1)-C(21)-C(26)	-158.81(11)	C(51)-B(1)-C(21)-C(26)	-37.77(16)
C(26)-C(21)-C(22)-C(23)	0.69(18)	B(1)-C(21)-C(22)-C(23)	180.00(12)
C(21)-C(22)-C(23)-C(24)	-1.2(2)	C(22)-C(23)-C(24)-C(25)	0.9(2)
C(23)-C(24)-C(25)-C(26)	-0.2(2)	C(24)-C(25)-C(26)-C(21)	-0.3(2)
C(22)-C(21)-C(26)-C(25)	0.07(19)	B(1)-C(21)-C(26)-C(25)	-179.25(12)
C(41)-B(1)-C(31)-C(32)	-158.75(11)	C(21)-B(1)-C(31)-C(32)	-36.89(16)
C(51)-B(1)-C(31)-C(32)	81.41(14)	C(41)-B(1)-C(31)-C(36)	28.60(17)
C(21)-B(1)-C(31)-C(36)	150.46(12)	C(51)-B(1)-C(31)-C(36)	-91.24(14)
C(36)-C(31)-C(32)-C(33)	-0.05(19)	B(1)-C(31)-C(32)-C(33)	-173.24(12)
C(31)-C(32)-C(33)-C(34)	-0.5(2)	C(32)-C(33)-C(34)-C(35)	1.1(2)
C(33)-C(34)-C(35)-C(36)	-1.2(2)	C(34)-C(35)-C(36)-C(31)	0.7(2)
C(32)-C(31)-C(36)-C(35)	-0.1(2)	B(1)-C(31)-C(36)-C(35)	173.07(12)
C(31)-B(1)-C(41)-C(46)	-138.48(12)	C(21)-B(1)-C(41)-C(46)	99.81(14)
C(51)-B(1)-C(41)-C(46)	-20.55(16)	C(31)-B(1)-C(41)-C(42)	42.21(16)
C(21)-B(1)-C(41)-C(42)	-79.50(15)	C(51)-B(1)-C(41)-C(42)	160.13(12)
C(46)-C(41)-C(42)-C(43)	0.92(19)	B(1)-C(41)-C(42)-C(43)	-179.71(13)
C(41)-C(42)-C(43)-C(44)	-0.5(2)	C(42)-C(43)-C(44)-C(45)	-0.4(2)
C(43)-C(44)-C(45)-C(46)	0.8(2)	C(44)-C(45)-C(46)-C(41)	-0.3(2)
C(42)-C(41)-C(46)-C(45)	-0.50(18)	B(1)-C(41)-C(46)-C(45)	-179.86(12)

C(31)-B(1)-C(51)-C(52)	-157.66(11)	C(41)-B(1)-C(51)-C(52)	82.38(14)
C(21)-B(1)-C(51)-C(52)	-38.72(15)	C(31)-B(1)-C(51)-C(56)	23.54(15)
C(41)-B(1)-C(51)-C(56)	-96.43(13)	C(21)-B(1)-C(51)-C(56)	142.47(11)
C(56)-C(51)-C(52)-C(53)	0.42(18)	B(1)-C(51)-C(52)-C(53)	-178.48(12)
C(51)-C(52)-C(53)-C(54)	0.50(19)	C(52)-C(53)-C(54)-C(55)	-0.81(19)
C(53)-C(54)-C(55)-C(56)	0.21(18)	C(54)-C(55)-C(56)-C(51)	0.76(19)
C(52)-C(51)-C(56)-C(55)	-1.04(17)	B(1)-C(51)-C(56)-C(55)	177.84(11)

Symmetry transformations used to generate equivalent atoms:

$Co_2(CO)_6$**1c:**

Crystal data for $C_{38}H_{34}BCo_2NO_6$; M_r = 729.33; monoclinic; space group $P2_1/c$; a = 19.100(2) Å; b = 10.9572(11) Å; c = 17.5214(18) Å; $\alpha = 90°$; $\beta = 113.705(2)°$; $\gamma = 90°$; V = 3357.5(6) $Å^3$; Z = 4; T = 120(2) K; λ(Mo-Kα) = 0.71073 Å; μ(Mo-Kα) = 1.036 mm^{-1}; d_{calc} = 1.443g.cm^{-3}; 48069 reflections collected; 6896 unique (R_{int} = 0.0339); giving R_1 = 0.0279, wR_2 = 0.0766 for 5985 data with [I>2σ(I)] and R_1 = 0.0351, wR_2 = 0.0866 for all 6896 data. Residual electron density ($e^-.Å^{-3}$) max/min: 0.374/-0.315.

An arbitrary sphere of data were collected on a red plate-like crystal, having approximate dimensions of 0.30 × 0.21 × 0.07 mm, on a Bruker APEX-II diffractometer using a combination of ω- and φ-scans of 0.3°. Data were corrected for absorption and polarization effects and analyzed for space group determination. The structure was solved by direct methods and expanded routinely. The model was refined by full-matrix least-squares analysis of F^2 against all reflections. All non-hydrogen atoms were refined with anisotropic thermal displacement parameters. Unless otherwise noted, hydrogen atoms were included in calculated positions. Thermal parameters for the hydrogens were tied to the isotropic thermal parameter of the atom to which they are bonded (1.5 × for methyl, 1.2 × for all others).

Appendix Table 7: Crystal data and structure refinement for $Co_2(CO)_6$**1c**.

Identification code	$Co_2(CO)_6$1c
Empirical formula	$C_{38}H_{34}BCo_2NO_6$
Formula weight	729.33
Temperature	120(2) K
Wavelength	0.71073 Å
Crystal system	monoclinic

Space group	$P2_1/c$
Unit cell dimensions	$a = 19.100(2)$ Å $\alpha = 90°$ $b = 10.9572(11)$ Å $\beta = 113.705(2)°$ $c = 17.5214(18)$ Å $\gamma = 90°$
Volume	3357.5(6) Å^3
Z	4
Density (calculated)	1.443 g.cm^{-3}
Absorption coefficient (μ)	1.036 mm^{-1}
F(000)	1504
Crystal size	0.30 × 0.21 × 0.07 mm^3
ω range for data collection	1.16 to 26.45°
Index ranges	$-23 \leq h \leq 23$, $-13 \leq k \leq 13$, $-21 \leq l \leq 21$
Reflections collected	48069
Independent reflections	6896 [$R_{int} = 0.0339$]
Completeness to $\theta = 26.45°$	99.8 %
Absorption correction	Numerical
Max. and min. transmission	0.9310 and 0.7462
Refinement method	Full-matrix least-squares on F^2
Data / restraints / parameters	6896 / 0 / 433
Goodness-of-fit on F^2	1.108
Final R indices [$I>2\sigma(I)$]	$R_1 = 0.0279$, $wR_2 = 0.0766$
R indices (all data)	$R_1 = 0.0351$, $wR_2 = 0.0866$
Largest diff. peak and hole	0.374 and -0.315 e$^-$.Å^{-3}

Appendix Table 8: Atomic coordinates and equivalent isotropic displacement parameters (Å^2) for $Co_2(CO)_6$**1c**. U(eq) is defined as one third of the trace of the orthogonalized U_{ij} tensor.

	x	y	z	U(eq)
Co(1)	0.40850(1)	0.45992(2)	0.13508(2)	0.019(1)
Co(2)	0.34969(1)	0.27263(2)	0.05871(2)	0.020(1)
O(1)	0.45964(9)	0.36904(16)	0.30787(9)	0.037(1)
O(2)	0.40056(9)	0.71837(14)	0.17534(10)	0.034(1)
O(3)	0.54645(10)	0.46139(18)	0.09899(12)	0.050(1)
O(4)	0.21189(8)	0.12071(13)	-0.01175(9)	0.029(1)
O(5)	0.42602(9)	0.24996(18)	-0.05727(11)	0.045(1)
O(6)	0.42264(10)	0.10616(16)	0.20046(11)	0.048(1)
N(1)	0.21262(8)	0.52320(13)	-0.10461(9)	0.016(1)
B(1)	0.18059(11)	0.95239(18)	-0.24573(12)	0.015(1)
C(1)	0.44124(11)	0.40331(19)	0.24181(12)	0.025(1)
C(2)	0.40373(11)	0.61890(19)	0.15854(12)	0.025(1)
C(3)	0.49345(12)	0.4622(2)	0.11268(13)	0.031(1)
C(4)	0.26509(11)	0.17919(17)	0.01280(12)	0.023(1)
C(5)	0.39839(11)	0.2533(2)	-0.01104(13)	0.028(1)
C(6)	0.39510(12)	0.1706(2)	0.14598(13)	0.030(1)
C(7)	0.30142(10)	0.41008(16)	0.09182(11)	0.019(1)
C(8)	0.31876(10)	0.44313(16)	0.02820(11)	0.017(1)
C(9)	0.29724(10)	0.51953(17)	-0.04810(11)	0.019(1)
C(10)	0.16690(10)	0.59041(16)	-0.06327(11)	0.019(1)
C(11)	0.09234(10)	0.52073(17)	-0.09124(12)	0.021(1)
C(12)	0.11899(11)	0.38896(16)	-0.08791(12)	0.021(1)
C(13)	0.17635(10)	0.39631(15)	-0.12726(11)	0.017(1)
C(14)	0.20539(11)	0.58889(17)	-0.18275(11)	0.021(1)
C(21)	0.25737(10)	0.91459(15)	-0.16312(11)	0.016(1)
C(22)	0.25614(10)	0.88767(16)	-0.08545(11)	0.018(1)
C(23)	0.32196(11)	0.86001(18)	-0.01529(12)	0.025(1)

C(24)	0.39214(12)	0.8573(2)	-0.02032(13)	0.030(1)
C(25)	0.39613(11)	0.8832(2)	-0.09582(13)	0.029(1)
C(26)	0.33027(11)	0.91146(17)	-0.16483(12)	0.021(1)
C(31)	0.10688(10)	0.95811(15)	-0.21973(10)	0.015(1)
C(32)	0.08543(10)	1.06533(16)	-0.19089(11)	0.017(1)
C(33)	0.02769(10)	1.06823(17)	-0.16147(11)	0.019(1)
C(34)	-0.01153(10)	0.96243(17)	-0.15958(11)	0.020(1)
C(35)	0.00749(10)	0.85414(17)	-0.18816(11)	0.019(1)
C(36)	0.06499(10)	0.85349(16)	-0.21754(11)	0.018(1)
C(41)	0.16319(10)	0.85169(15)	-0.32191(11)	0.016(1)
C(42)	0.21692(11)	0.76740(16)	-0.32623(11)	0.019(1)
C(43)	0.19919(12)	0.68041(17)	-0.38958(12)	0.024(1)
C(44)	0.12659(13)	0.67412(18)	-0.45221(12)	0.027(1)
C(45)	0.07206(12)	0.75650(18)	-0.45093(12)	0.025(1)
C(46)	0.09031(11)	0.84259(17)	-0.38709(11)	0.021(1)
C(51)	0.19365(10)	1.08991(16)	-0.27678(11)	0.016(1)
C(52)	0.25506(11)	1.16582(17)	-0.22965(11)	0.020(1)
C(53)	0.26395(12)	1.28339(17)	-0.25476(12)	0.023(1)
C(54)	0.21061(12)	1.33108(17)	-0.32804(12)	0.023(1)
C(55)	0.14866(11)	1.25960(17)	-0.37629(12)	0.022(1)
C(56)	0.14069(10)	1.14184(16)	-0.35107(11)	0.019(1)
H(7A)	0.2573	0.4214	0.1081	0.022
H(9A)	0.3254	0.4890	-0.0809	0.022
H(9B)	0.3147	0.6041	-0.0308	0.022
H(10A)	0.1941	0.5888	-0.0018	0.023
H(10B)	0.1579	0.6764	-0.0821	0.023
H(11A)	0.0572	0.5441	-0.1484	0.025
H(11B)	0.0666	0.5342	-0.0529	0.025
H(12A)	0.1433	0.3593	-0.0297	0.025
H(12B)	0.0759	0.3344	-0.1201	0.025
H(13A)	0.1506	0.3867	-0.1885	0.020
H(13B)	0.2157	0.3318	-0.1048	0.020
H(14A)	0.2346	0.5451	-0.2091	0.032
H(14B)	0.2254	0.6720	-0.1687	0.032
H(14C)	0.1514	0.5924	-0.2214	0.032
H(22A)	0.2084	0.8883	-0.0805	0.022
H(23A)	0.3185	0.8429	0.0362	0.030
H(24A)	0.4371	0.8379	0.0273	0.036
H(25A)	0.4441	0.8816	-0.1003	0.034
H(26A)	0.3346	0.9296	-0.2158	0.026
H(32A)	0.1114	1.1390	-0.1915	0.021
H(33A)	0.0151	1.1430	-0.1426	0.023
H(34A)	-0.0507	0.9639	-0.1391	0.024
H(35A)	-0.0188	0.7808	-0.1876	0.023
H(36A)	0.0767	0.7786	-0.2372	0.021
H(42A)	0.2675	0.7696	-0.2843	0.023
H(43A)	0.2375	0.6250	-0.3896	0.029
H(44A)	0.1143	0.6147	-0.4951	0.032
H(45A)	0.0219	0.7544	-0.4937	0.030
H(46A)	0.0516	0.8976	-0.3877	0.025
H(52A)	0.2921	1.1358	-0.1785	0.024
H(53A)	0.3069	1.3310	-0.2213	0.028
H(54A)	0.2162	1.4115	-0.3451	0.028
H(55A)	0.1115	1.2912	-0.4268	0.026
H(56A)	0.0978	1.0946	-0.3853	0.023

Appendix Table 9: Anisotropic displacement parameters $(Å)^2$ for $Co_2(CO)_6$**1c**. The anisotropic displacement factor exponent takes the form: $-2\pi^2[h^2 a^{*2} U_{11} + ... + 2 h k a^* b^* U_{12}]$

	U_{11}	U_{22}	U_{33}	U_{23}	U_{13}	U_{12}
Co(1)	0.0134(1)	0.0278(2)	0.0147(1)	-0.0003(1)	0.0042(1)	-0.0019(1)
Co(2)	0.0169(1)	0.0227(1)	0.0175(1)	0.0010(1)	0.0045(1)	0.0034(1)
O(1)	0.0361(9)	0.0518(10)	0.0196(8)	0.0078(7)	0.0078(7)	0.0098(7)
O(2)	0.0337(9)	0.0295(8)	0.0349(9)	-0.0007(7)	0.0098(7)	-0.0037(6)
O(3)	0.0284(9)	0.0755(14)	0.0570(12)	-0.0047(10)	0.0278(9)	-0.0072(8)
O(4)	0.0301(8)	0.0240(7)	0.0290(8)	-0.0055(6)	0.0086(6)	-0.0026(6)
O(5)	0.0314(9)	0.0734(13)	0.0344(9)	-0.0112(8)	0.0173(8)	0.0058(8)
O(6)	0.0467(10)	0.0424(10)	0.0393(10)	0.0153(8)	0.0021(8)	0.0134(8)
N(1)	0.0169(8)	0.0160(7)	0.0143(7)	-0.0003(6)	0.0059(6)	0.0005(6)
B(1)	0.0146(9)	0.0163(9)	0.0155(10)	0.0001(7)	0.0066(8)	0.0002(7)
C(1)	0.0177(9)	0.0319(11)	0.0234(11)	-0.0020(8)	0.0062(8)	0.0008(8)
C(2)	0.0188(9)	0.0338(12)	0.0181(9)	0.0032(8)	0.0039(8)	-0.0044(8)
C(3)	0.0244(11)	0.0436(13)	0.0245(11)	-0.0034(9)	0.0090(9)	-0.0041(9)
C(4)	0.0274(11)	0.0207(9)	0.0187(9)	0.0014(7)	0.0072(8)	0.0060(8)
C(5)	0.0190(10)	0.0357(11)	0.0239(10)	-0.0048(8)	0.0036(8)	0.0067(8)
C(6)	0.0253(11)	0.0303(11)	0.0295(11)	0.0017(9)	0.0050(9)	0.0045(9)
C(7)	0.0141(8)	0.0217(9)	0.0174(9)	-0.0008(7)	0.0038(7)	0.0002(7)
C(8)	0.0121(8)	0.0209(9)	0.0170(9)	-0.0020(7)	0.0045(7)	-0.0009(7)
C(9)	0.0142(9)	0.0237(9)	0.0172(9)	0.0007(7)	0.0055(7)	-0.0020(7)
C(10)	0.0198(9)	0.0178(9)	0.0200(9)	-0.0042(7)	0.0090(8)	0.0013(7)
C(11)	0.0166(9)	0.0235(9)	0.0229(10)	-0.0037(7)	0.0073(8)	0.0011(7)
C(12)	0.0197(9)	0.0200(9)	0.0221(9)	-0.0020(7)	0.0087(8)	-0.0027(7)
C(13)	0.0181(9)	0.0138(8)	0.0169(9)	-0.0013(6)	0.0046(7)	-0.0005(7)
C(14)	0.0290(10)	0.0183(9)	0.0151(9)	0.0032(7)	0.0077(8)	0.0010(7)
C(21)	0.0163(9)	0.0130(8)	0.0192(9)	-0.0009(7)	0.0066(7)	0.0001(6)
C(22)	0.0185(9)	0.0171(8)	0.0178(9)	-0.0013(7)	0.0068(7)	0.0010(7)
C(23)	0.0269(10)	0.0286(10)	0.0170(9)	0.0013(8)	0.0067(8)	0.0044(8)
C(24)	0.0207(10)	0.0399(12)	0.0224(10)	0.0029(9)	0.0006(8)	0.0073(9)
C(25)	0.0169(9)	0.0396(12)	0.0293(11)	0.0015(9)	0.0087(8)	0.0034(8)
C(26)	0.0193(9)	0.0256(10)	0.0200(9)	0.0010(7)	0.0086(8)	0.0003(7)
C(31)	0.0123(8)	0.0179(8)	0.0121(8)	0.0018(6)	0.0028(7)	0.0006(6)
C(32)	0.0163(9)	0.0172(8)	0.0176(9)	0.0003(7)	0.0058(7)	-0.0015(7)
C(33)	0.0207(9)	0.0191(9)	0.0194(9)	-0.0020(7)	0.0094(8)	0.0016(7)
C(34)	0.0146(9)	0.0270(10)	0.0183(9)	0.0025(7)	0.0077(7)	0.0010(7)
C(35)	0.0164(9)	0.0202(9)	0.0196(9)	0.0026(7)	0.0062(7)	-0.0035(7)
C(36)	0.0170(9)	0.0172(8)	0.0182(9)	0.0006(7)	0.0066(7)	0.0008(7)
C(41)	0.0194(9)	0.0155(8)	0.0166(9)	0.0021(7)	0.0100(7)	-0.0018(7)
C(42)	0.0220(9)	0.0193(9)	0.0186(9)	0.0027(7)	0.0109(8)	0.0004(7)
C(43)	0.0358(11)	0.0187(9)	0.0262(10)	0.0014(7)	0.0214(9)	0.0009(8)
C(44)	0.0438(12)	0.0211(10)	0.0219(10)	-0.0056(8)	0.0196(9)	-0.0102(8)
C(45)	0.0270(11)	0.0284(10)	0.0182(9)	-0.0010(8)	0.0073(8)	-0.0101(8)
C(46)	0.0207(9)	0.0212(9)	0.0208(9)	0.0005(7)	0.0090(8)	-0.0023(7)
C(51)	0.0169(9)	0.0172(8)	0.0181(9)	-0.0005(7)	0.0108(7)	0.0011(7)
C(52)	0.0213(9)	0.0199(9)	0.0189(9)	-0.0009(7)	0.0093(8)	-0.0008(7)
C(53)	0.0272(10)	0.0204(9)	0.0257(10)	-0.0068(7)	0.0144(8)	-0.0062(7)
C(54)	0.0338(11)	0.0147(9)	0.0284(10)	0.0006(7)	0.0204(9)	0.0005(8)
C(55)	0.0236(10)	0.0222(9)	0.0224(10)	0.0051(7)	0.0129(8)	0.0070(7)
C(56)	0.0163(9)	0.0204(9)	0.0219(9)	0.0003(7)	0.0099(7)	0.0017(7)

Appendix Table 10: Bond lengths [Å] for $Co_2(CO)_6$**1c**.

Atom-atom	Distance	Atom-atom	Distance	Atom-atom	Distance
Co(1)-C(2)	1.800(2)	Co(1)-C(3)	1.816(2)	Co(1)-C(1)	1.826(2)
Co(1)-C(7)	1.9518(18)	Co(1)-C(8)	1.9743(18)	Co(1)-Co(2)	2.4607(4
Co(2)-C(4)	1.806(2)	Co(2)-C(6)	1.809(2)	Co(2)-C(5)	1.822(2)
Co(2)-C(8)	1.9675(18)	Co(2)-C(7)	1.9710(18)	O(1)-C(1)	1.130(2)
O(2)-C(2)	1.137(3)	O(3)-C(3)	1.130(3)	O(4)-C(4)	1.130(2)
O(5)-C(5)	1.131(3)	O(6)-C(6)	1.133(3)	N(1)-C(14)	1.503(2)
N(1)-C(9)	1.519(2)	N(1)-C(10)	1.529(2)	N(1)-C(13)	1.533(2)
B(1)-C(31)	1.646(3)	B(1)-C(21)	1.646(3)	B(1)-C(51)	1.655(3)
B(1)-C(41)	1.659(3)	C(7)-C(8)	1.334(3)	C(8)-C(9)	1.488(2)
C(10)-C(11)	1.513(3)	C(11)-C(12)	1.524(3)	C(12)-C(13)	1.513(2)
C(21)-C(22)	1.402(2)	C(21)-C(26)	1.405(3)	C(22)-C(23)	1.393(3)
C(23)-C(24)	1.379(3)	C(24)-C(25)	1.385(3)	C(25)-C(26)	1.385(3)
C(31)-C(32)	1.403(2)	C(31)-C(36)	1.407(2)	C(32)-C(33)	1.393(2)
C(33)-C(34)	1.388(3)	C(34)-C(35)	1.392(3)	C(35)-C(36)	1.388(3)
C(41)-C(46)	1.405(3)	C(41)-C(42)	1.405(2)	C(42)-C(43)	1.398(3)
C(43)-C(44)	1.381(3)	C(44)-C(45)	1.385(3)	C(45)-C(46)	1.396(3)
C(51)-C(52)	1.404(3)	C(51)-C(56)	1.408(2)	C(52)-C(53)	1.394(3)
C(53)-C(54)	1.381(3)	C(54)-C(55)	1.387(3)	C(55)-C(56)	1.392(3)

Symmetry transformations used to generate equivalent atoms:

Appendix Table 11: Bond angles [°] for $Co_2(CO)_6$**1c**.

Atom-atom-atom	Angle	Atom-atom-atom	angle
C(2)-Co(1)-C(3)	99.65(10)	C(2)-Co(1)-C(1)	97.05(9)
C(3)-Co(1)-C(1)	104.96(9)	C(2)-Co(1)-C(7)	102.59(8)
C(3)-Co(1)-C(7)	143.86(9)	C(1)-Co(1)-C(7)	100.18(8)
C(2)-Co(1)-C(8)	101.68(8)	C(3)-Co(1)-C(8)	107.86(9)
C(1)-Co(1)-C(8)	138.52(8)	C(7)-Co(1)-C(8)	39.73(7)
C(2)-Co(1)-Co(2)	151.29(6)	C(3)-Co(1)-Co(2)	98.41(7)
C(1)-Co(1)-Co(2)	99.62(7)	C(7)-Co(1)-Co(2)	51.50(5)
C(8)-Co(1)-Co(2)	51.25(5)	C(4)-Co(2)-C(6)	93.74(9)
C(4)-Co(2)-C(5)	104.01(9)	C(6)-Co(2)-C(5)	107.13(10)
C(4)-Co(2)-C(8)	107.47(8)	C(6)-Co(2)-C(8)	143.69(9)
C(5)-Co(2)-C(8)	96.13(9)	C(4)-Co(2)-C(7)	97.10(8)
C(6)-Co(2)-C(7)	110.21(9)	C(5)-Co(2)-C(7)	135.39(9)
C(8)-Co(2)-C(7)	39.60(7)	C(4)-Co(2)-Co(1)	147.80(6)
C(6)-Co(2)-Co(1)	95.55(7)	C(5)-Co(2)-Co(1)	102.55(7)
C(8)-Co(2)-Co(1)	51.49(5)	C(7)-Co(2)-Co(1)	50.80(5)
C(14)-N(1)-C(9)	106.89(13)	C(14)-N(1)-C(10)	109.88(14)
C(9)-N(1)-C(10)	111.38(13)	C(14)-N(1)-C(13)	109.40(13)
C(9)-N(1)-C(13)	113.35(13)	C(10)-N(1)-C(13)	105.95(13)
C(31)-B(1)-C(21)	108.96(14)	C(31)-B(1)-C(51)	108.36(14)
C(21)-B(1)-C(51)	108.64(14)	C(31)-B(1)-C(41)	109.33(14)
C(21)-B(1)-C(41)	111.08(14)	C(51)-B(1)-C(41)	110.43(14)
O(1)-C(1)-Co(1)	178.14(18)	O(2)-C(2)-Co(1)	178.11(18)
O(3)-C(3)-Co(1)	178.7(2)	O(4)-C(4)-Co(2)	176.18(17)
O(5)-C(5)-Co(2)	174.4(2)	O(6)-C(6)-Co(2)	179.1(2)
C(8)-C(7)-Co(1)	71.04(11)	C(8)-C(7)-Co(2)	70.06(11)

Co(1)-C(7)-Co(2)	77.70(7)	C(7)-C(8)-C(9)	146.24(17)
C(7)-C(8)-Co(2)	70.34(11)	C(9)-C(8)-Co(2)	136.26(13)
C(7)-C(8)-Co(1)	69.23(11)	C(9)-C(8)-Co(1)	128.36(13)
Co(2)-C(8)-Co(1)	77.26(7)	C(8)-C(9)-N(1)	115.96(14)
C(11)-C(10)-N(1)	104.24(14)	C(10)-C(11)-C(12)	102.08(14)
C(13)-C(12)-C(11)	102.94(14)	C(12)-C(13)-N(1)	105.36(14)
C(22)-C(21)-C(26)	114.78(16)	C(22)-C(21)-B(1)	123.36(15)
C(26)-C(21)-B(1)	121.83(16)	C(23)-C(22)-C(21)	122.76(17)
C(24)-C(23)-C(22)	120.25(18)	C(23)-C(24)-C(25)	119.02(18)
C(24)-C(25)-C(26)	120.02(18)	C(25)-C(26)-C(21)	123.16(18)
C(32)-C(31)-C(36)	114.87(16)	C(32)-C(31)-B(1)	122.51(15)
C(36)-C(31)-B(1)	122.37(15)	C(33)-C(32)-C(31)	122.79(16)
C(34)-C(33)-C(32)	120.33(17)	C(33)-C(34)-C(35)	118.82(17)
C(36)-C(35)-C(34)	119.86(16)	C(35)-C(36)-C(31)	123.32(16)
C(46)-C(41)-C(42)	114.58(16)	C(46)-C(41)-B(1)	120.91(16)
C(42)-C(41)-B(1)	124.47(16)	C(43)-C(42)-C(41)	122.82(18)
C(44)-C(43)-C(42)	120.68(18)	C(43)-C(44)-C(45)	118.41(18)
C(44)-C(45)-C(46)	120.40(19)	C(45)-C(46)-C(41)	123.09(18)
C(52)-C(51)-C(56)	115.10(16)	C(52)-C(51)-B(1)	123.15(16)
C(56)-C(51)-B(1)	121.65(16)	C(53)-C(52)-C(51)	122.76(18)
C(54)-C(53)-C(52)	120.34(18)	C(53)-C(54)-C(55)	118.86(17)
C(54)-C(55)-C(56)	120.35(18)	C(55)-C(56)-C(51)	122.58(17)

Symmetry transformations used to generate equivalent atoms:

$Co_2(CO)_6$ 3b

The complex crystallizes as red block-like crystals. There are two crystallographically independent molecules of the $Co_2(CO)_6$ cation and associated PF_6 anion in the unit cell of the primitive, centric, monoclinic space group $P2_1/c$. The two independent molecules are chemically identical and only differ in derived metrics (primarily torsion angles and thermal motion of one counterion).

Each $Co_2(CO)_6$ cluster is coordinated by the acetylinic moiety of the pyrollidinium ligand. The ethylinic functionality does not coordinate the Co-Co center. The hydrogens on the ethylene and acetylene groups were observed in a difference Fourier map (confirming their identity) and were subsequently included in calculated positions.

CRYSTAL SUMMARY

Crystal data for $C_{17}H_{18}Co_2F_6NO_6$ P; M_r = 595.15; monoclinic; space group $P2_1/c$; a = 17.5879(5) Å; b = 13.7820(4) Å; c = 20.6662(6) Å; $\alpha = 90°$; $\beta = 112.8570(10)°$; $\gamma = 90°$; V = 4616.1(2) $Å^3$; Z = 8; T = 100(2) K; λ(Mo-Kα) = 0.71073 Å; μ(Mo-Kα) = 1.588 mm^-

[1]; d_{calc} = 1.713g.cm^{-3}; 66581 reflections collected; 9424 unique (R_{int} = 0.0342); giving R_1 = 0.0375, wR_2 = 0.1027 for 7600 data with [I>2σ(I)] and R_1 = 0.0505, wR_2 = 0.1141 for all 9424 data. Residual electron density (e$^-$.Å^{-3}) max/min: 1.079/-0.733.

An arbitrary sphere of data were collected on a red block-like crystal, having approximate dimensions of 0.29 × 0.19 × 0.15 mm, on a Bruker APEX-II diffractometer using a combination of ω- and φ-scans of 0.3°. Data were corrected for absorption and polarization effects and analyzed for space group determination. The structure was solved by direct methods and expanded routinely. The model was refined by full-matrix least-squares analysis of F^2 against all reflections. All non-hydrogen atoms were refined with anisotropic thermal displacement parameters. Unless otherwise noted, hydrogen atoms were included in calculated positions. Thermal parameters for the hydrogens were tied to the isotropic thermal parameter of the atom to which they are bonded (1.2 × for all H).

Appendix Table 12: Crystal data and structure refinement for $Co_2(CO)_6$**3b**.

Identification code	$Co_2(CO)_6$**3b**
Empirical formula	$C_{17}H_{18}Co_2F_6NO_6P$
Formula weight	595.15
Temperature	100(2) K
Wavelength	0.71073 Å
Crystal system	monoclinic
Unit cell dimensions	a = 17.5879(5) Å α = 90° b = 13.7820(4) Å β = 112.8570(10)° c = 20.6662(6) Å γ = 90°
Volume	4616.1(2) Å^3
Z	8
Density (calculated)	1.713 g.cm^{-3}
Absorption coefficient (μ)	1.588 mm^{-1}
F(000)	2384
Crystal size	0.29 × 0.19 × 0.15 mm^3
θ range for data collection	1.26 to 26.44°
Index ranges	-21 ≤ h ≤ 21, -15 ≤ k ≤ 17, -25 ≤ l ≤ 25
Reflections collected	66581
Independent reflections	9424 [R_{int} = 0.0342]
Completeness to θ = 26.44°	99.40%
Absorption correction	numerical
Max. and min. transmission	0.8763 and 0.6851
Refinement method	Full-matrix least-squares on F^2
Data / restraints / parameters	9424 / 0 / 596
Goodness-of-fit on F^2	1.065
Final R indices [I>2σ(I)]	R_1 = 0.0375, wR_2 = 0.1027

R indices (all data)	$R_1 = 0.0505$, $wR_2 = 0.1141$
Largest diff. peak and hole	1.079 and -0.733 $e^-.Å^{-3}$

Appendix Table 13: Atomic coordinates and equivalent isotropic displacement parameters ($Å^2$) for $Co_2(CO)_6$**3b**. U(eq) is defined as one third of the trace of the orthogonalized U_{ij} tensor.

	x	y	z	U(eq)
Co(1)	0.19455(2)	1.19147(3)	0.16158(2)	0.019(1)
Co(2)	0.08559(2)	1.31080(3)	0.09938(2)	0.019(1)
O(12)	0.33133(13)	1.06698(16)	0.16286(12)	0.033(1)
O(13)	0.27716(16)	1.30922(17)	0.28909(12)	0.043(1)
O(14)	0.08933(15)	1.04166(16)	0.18762(12)	0.034(1)
O(15)	-0.01391(13)	1.40328(15)	-0.03530(11)	0.030(1)
O(16)	-0.04549(13)	1.21425(16)	0.13219(11)	0.031(1)
O(17)	0.14472(17)	1.48593(17)	0.18757(12)	0.043(1)
N(1)	0.14368(14)	1.13791(16)	-0.05078(11)	0.018(1)
C(1)	0.09348(19)	1.0683(2)	-0.10851(15)	0.023(1)
C(2)	0.1364(2)	1.0440(2)	-0.15743(15)	0.028(1)
C(3)	0.2212(2)	1.0010(3)	-0.11757(17)	0.036(1)
C(4)	0.2733(2)	1.0674(2)	-0.05771(17)	0.033(1)
C(5)	0.22882(17)	1.0955(2)	-0.01024(15)	0.024(1)
C(6)	0.09773(16)	1.1468(2)	-0.00183(14)	0.018(1)
C(7)	0.13576(17)	1.2112(2)	0.06019(14)	0.018(1)
C(8)	0.18864(17)	1.2840(2)	0.08767(14)	0.020(1)
C(9)	0.15269(17)	1.2365(2)	-0.07960(14)	0.020(1)
C(10)	0.07363(18)	1.2784(2)	-0.13136(15)	0.023(1)
C(11)	0.0692(2)	1.3135(2)	-0.19167(17)	0.031(1)
C(12)	0.27942(18)	1.1149(2)	0.16346(15)	0.024(1)
C(13)	0.24547(19)	1.2615(2)	0.24069(16)	0.028(1)
C(14)	0.13150(19)	1.0985(2)	0.17914(15)	0.024(1)
C(15)	0.02315(18)	1.3689(2)	0.01731(16)	0.023(1)
C(16)	0.00384(18)	1.2527(2)	0.11887(15)	0.024(1)
C(17)	0.1201(2)	1.4183(2)	0.15502(16)	0.027(1)
Co(3)	0.72308(2)	1.29602(3)	0.15343(2)	0.023(1)
Co(4)	0.78248(2)	1.42516(3)	0.10473(2)	0.024(1)
O(32)	0.64386(17)	1.4271(2)	0.22194(15)	0.059(1)
O(33)	0.87108(15)	1.20511(19)	0.26082(13)	0.042(1)
O(34)	0.61592(16)	1.12709(19)	0.13482(15)	0.050(1)
O(35)	0.82715(16)	1.49757(18)	-0.00941(15)	0.047(1)
O(36)	0.95177(14)	1.41198(18)	0.21349(13)	0.041(1)
O(37)	0.70293(16)	1.59803(19)	0.13570(14)	0.051(1)
N(2)	0.58454(15)	1.31617(19)	-0.07062(13)	0.026(1)
C(21)	0.49518(18)	1.3432(3)	-0.11612(17)	0.034(1)
C(22)	0.4705(2)	1.3220(4)	-0.1920(2)	0.054(1)
C(23)	0.5263(2)	1.3801(4)	-0.2209(2)	0.056(1)
C(24)	0.6176(2)	1.3558(4)	-0.1778(2)	0.054(1)
C(25)	0.6407(2)	1.3675(3)	-0.10054(19)	0.044(1)
C(26)	0.60167(17)	1.3569(2)	0.00147(15)	0.025(1)
C(27)	0.68626(17)	1.3415(2)	0.05576(15)	0.021(1)
C(28)	0.75588(17)	1.2902(2)	0.07375(15)	0.021(1)
C(29)	0.5968(2)	1.2086(2)	-0.0685(2)	0.041(1)
C(30)	0.5361(3)	1.1516(3)	-0.0543(2)	0.056(1)

C(31)	0.4981(4)	1.0769(4)	-0.0944(3)	0.091(2)
C(32)	0.6746(2)	1.3757(3)	0.19683(18)	0.036(1)
C(33)	0.8145(2)	1.2432(3)	0.22190(17)	0.031(1)
C(34)	0.6564(2)	1.1933(2)	0.14205(18)	0.031(1)
C(35)	0.80944(19)	1.4701(2)	0.03471(19)	0.034(1)
C(36)	0.8866(2)	1.4188(2)	0.17220(18)	0.031(1)
C(37)	0.7342(2)	1.5321(2)	0.12371(18)	0.034(1)
P(1)	0.15967(5)	0.84014(6)	0.07309(4)	0.023(1)
F(1)	0.09562(11)	0.81216(14)	0.10730(10)	0.036(1)
F(2)	0.22263(12)	0.86934(13)	0.03679(11)	0.040(1)
F(3)	0.14317(12)	0.73957(13)	0.03169(10)	0.039(1)
F(4)	0.17598(13)	0.94279(15)	0.11120(12)	0.050(1)
F(5)	0.08610(12)	0.88854(15)	0.00767(10)	0.040(1)
F(6)	0.23287(12)	0.79274(17)	0.13703(11)	0.049(1)
P(2)	0.41328(5)	1.32647(7)	0.07416(6)	0.041(1)
F(7)	0.37622(13)	1.23786(18)	0.10097(13)	0.059(1)
F(8)	0.44986(16)	1.41559(16)	0.0466(2)	0.087(1)
F(9)	0.50157(16)	1.2916(2)	0.1205(3)	0.128(2)
F(10)	0.32455(15)	1.3644(3)	0.02763(17)	0.112(1)
F(11)	0.4188(3)	1.2648(2)	0.0134(2)	0.133(2)
F(12)	0.4084(3)	1.3898(2)	0.1352(2)	0.119(1)
H(1A)	0.0839	1.0077	-0.087	0.028
H(1B)	0.0391	1.0977	-0.136	0.028
H(2A)	0.1419	1.1036	-0.182	0.034
H(2B)	0.1024	0.9971	-0.1933	0.034
H(3A)	0.2494	0.9911	-0.1502	0.043
H(3B)	0.2153	0.937	-0.0983	0.043
H(4A)	0.3255	1.034	-0.0294	0.039
H(4B)	0.2873	1.1269	-0.0776	0.039
H(5A)	0.2233	1.0374	0.0158	0.029
H(5B)	0.2626	1.1438	0.0246	0.029
H(6A)	0.0414	1.1708	-0.0295	0.022
H(6B)	0.0923	1.0811	0.0152	0.022
H(8A)	0.2288	1.3219	0.0743	0.035(9)
H(9A)	0.1763	1.2823	-0.0399	0.023
H(9B)	0.1925	1.2309	-0.1026	0.023
H(10A)	0.0261	1.2794	-0.1202	0.028
H(11A)	0.1164	1.3127	-0.2032	0.037
H(11B)	0.0187	1.3397	-0.2238	0.037
H(21A)	0.458	1.3075	-0.0988	0.041
H(21B)	0.4874	1.4134	-0.1104	0.041
H(22A)	0.412	1.3403	-0.218	0.065
H(22B)	0.476	1.2516	-0.1988	0.065
H(23A)	0.5121	1.3632	-0.2709	0.067
H(23B)	0.517	1.4505	-0.218	0.067
H(24A)	0.6284	1.2881	-0.1877	0.065
H(24B)	0.6527	1.3989	-0.1928	0.065
H(25A)	0.6412	1.4376	-0.09	0.053
H(25B)	0.6975	1.3428	-0.0758	0.053
H(26A)	0.5909	1.4276	-0.0033	0.029
H(26B)	0.5617	1.328	0.0189	0.029
H(28A)	0.7783	1.2398	0.0512	0.025
H(29A)	0.5971	1.1878	-0.1143	0.049

H(29B)	0.6519	1.1938	-0.0321	0.049
H(30A)	0.5231	1.168	-0.0152	0.068
H(31A)	0.5106	1.0596	-0.1337	0.109
H(31B)	0.4585	1.0407	-0.0838	0.109

Appendix Table 14: Anisotropic displacement parameters $(Å)^2$ for $Co_2(CO)_6$**3b**. The anisotropic displacement factor exponent takes the form: $-2\pi^2[h^2 a^{*2} U_{11} + \ldots + 2 h k a^* b^* U_{12}]$.

	U_{11}	U_{22}	U_{33}	U_{23}	U_{13}	U_{12}
Co(1)	0.0175(2)	0.0218(2)	0.0151(2)	-0.0004(1)	0.0047(2)	-0.0005(2)
Co(2)	0.0182(2)	0.0206(2)	0.0190(2)	-0.0005(2)	0.0082(2)	0.0009(2)
O(12)	0.0234(12)	0.0382(13)	0.0334(13)	0.0075(10)	0.0070(10)	0.0086(10)
O(13)	0.0476(16)	0.0410(14)	0.0274(13)	-0.0091(11)	0.0019(12)	-0.0018(11)
O(14)	0.0453(14)	0.0263(12)	0.0421(14)	-0.0010(10)	0.0281(12)	-0.0060(11)
O(15)	0.0314(12)	0.0275(12)	0.0258(12)	0.0037(9)	0.0046(10)	0.0027(9)
O(16)	0.0222(11)	0.0426(13)	0.0298(12)	0.0056(10)	0.0131(10)	-0.0004(10)
O(17)	0.0662(17)	0.0294(13)	0.0323(13)	-0.0079(11)	0.0191(12)	-0.0065(12)
N(1)	0.0159(11)	0.0206(12)	0.0153(11)	0.0014(9)	0.0045(9)	0.0010(9)
C(1)	0.0279(16)	0.0239(15)	0.0163(14)	-0.0028(11)	0.0072(12)	-0.0045(12)
C(2)	0.0384(18)	0.0273(16)	0.0194(15)	-0.0036(12)	0.0112(14)	0.0022(14)
C(3)	0.044(2)	0.0373(19)	0.0306(18)	0.0032(15)	0.0197(16)	0.0158(16)
C(4)	0.0285(17)	0.0430(19)	0.0281(17)	0.0067(14)	0.0126(14)	0.0173(14)
C(5)	0.0192(15)	0.0302(16)	0.0211(15)	0.0049(12)	0.0060(12)	0.0079(12)
C(6)	0.0155(13)	0.0232(14)	0.0159(13)	-0.0012(11)	0.0064(11)	-0.0026(11)
C(7)	0.0155(13)	0.0237(14)	0.0160(13)	0.0027(11)	0.0077(11)	0.0028(11)
C(8)	0.0185(14)	0.0225(14)	0.0186(14)	0.0005(11)	0.0079(12)	-0.0011(11)
C(9)	0.0194(14)	0.0209(14)	0.0185(14)	0.0020(11)	0.0076(12)	-0.0020(11)
C(10)	0.0224(15)	0.0247(15)	0.0244(15)	0.0031(12)	0.0109(13)	0.0030(12)
C(11)	0.0210(16)	0.0412(19)	0.0268(17)	0.0082(14)	0.0059(13)	0.0008(13)
C(12)	0.0211(15)	0.0306(16)	0.0169(14)	0.0048(12)	0.0022(12)	-0.0015(13)
C(13)	0.0285(17)	0.0294(17)	0.0231(16)	0.0017(13)	0.0073(14)	0.0025(13)
C(14)	0.0295(16)	0.0255(16)	0.0195(15)	-0.0010(12)	0.0114(13)	0.0039(13)
C(15)	0.0207(15)	0.0186(14)	0.0302(17)	-0.0043(12)	0.0114(13)	-0.0013(11)
C(16)	0.0225(15)	0.0280(16)	0.0198(15)	0.0026(12)	0.0071(13)	0.0079(12)
C(17)	0.0346(18)	0.0250(16)	0.0232(16)	0.0025(13)	0.0125(14)	0.0049(13)
Co(3)	0.0166(2)	0.0289(2)	0.0222(2)	-0.0043(2)	0.0069(2)	0.0000(2)
Co(4)	0.0161(2)	0.0229(2)	0.0308(2)	-0.0059(2)	0.0058(2)	-0.0027(2)
O(32)	0.0456(16)	0.077(2)	0.0551(17)	-0.0289(15)	0.0220(14)	0.0118(14)
O(33)	0.0279(13)	0.0601(17)	0.0331(13)	0.0040(12)	0.0051(11)	0.0100(12)
O(34)	0.0375(15)	0.0379(15)	0.0747(19)	0.0033(13)	0.0231(14)	-0.0075(12)
O(35)	0.0402(15)	0.0434(15)	0.0609(17)	0.0110(13)	0.0235(13)	-0.0073(12)
O(36)	0.0208(12)	0.0484(15)	0.0434(14)	-0.0200(12)	0.0011(11)	-0.0001(10)
O(37)	0.0412(15)	0.0402(15)	0.0593(17)	-0.0195(13)	0.0073(13)	0.0094(12)
N(2)	0.0147(12)	0.0356(15)	0.0231(13)	-0.0017(11)	0.0020(10)	0.0020(10)
C(21)	0.0162(15)	0.047(2)	0.0313(18)	0.0022(15)	0.0012(13)	0.0029(14)
C(22)	0.026(2)	0.087(3)	0.037(2)	-0.003(2)	-0.0002(17)	0.007(2)
C(23)	0.040(2)	0.085(3)	0.037(2)	0.011(2)	0.0089(18)	0.013(2)
C(24)	0.037(2)	0.080(3)	0.044(2)	0.011(2)	0.0144(18)	0.010(2)
C(25)	0.0227(18)	0.068(3)	0.039(2)	-0.0002(18)	0.0092(15)	-0.0041(16)
C(26)	0.0171(14)	0.0242(15)	0.0286(16)	-0.0045(12)	0.0048(12)	0.0021(12)
C(27)	0.0177(14)	0.0216(15)	0.0234(15)	-0.0038(11)	0.0074(12)	-0.0027(11)

C(28)	0.0155(14)	0.0238(15)	0.0219(14)	-0.0055(11)	0.0064(12)	-0.0044(11)
C(29)	0.0289(18)	0.0317(18)	0.044(2)	-0.0115(15)	-0.0040(16)	0.0066(14)
C(30)	0.051(3)	0.042(2)	0.066(3)	-0.002(2)	0.012(2)	-0.0039(19)
C(31)	0.094(4)	0.060(3)	0.108(5)	-0.025(3)	0.028(4)	-0.035(3)
C(32)	0.0280(18)	0.047(2)	0.0323(18)	-0.0079(15)	0.0104(15)	0.0004(15)
C(33)	0.0273(17)	0.0420(19)	0.0247(17)	-0.0031(14)	0.0110(14)	-0.0020(15)
C(34)	0.0228(17)	0.0360(19)	0.0353(18)	0.0019(14)	0.0126(14)	0.0043(14)
C(35)	0.0228(16)	0.0287(17)	0.047(2)	0.0022(15)	0.0114(16)	-0.0037(13)
C(36)	0.0248(17)	0.0296(17)	0.0414(19)	-0.0138(14)	0.0146(16)	-0.0035(13)
C(37)	0.0261(17)	0.0318(18)	0.0381(19)	-0.0086(15)	0.0042(15)	-0.0032(14)
P(1)	0.0170(4)	0.0237(4)	0.0294(4)	-0.0027(3)	0.0093(3)	-0.0008(3)
F(1)	0.0240(10)	0.0537(13)	0.0347(10)	0.0143(9)	0.0146(8)	0.0036(8)
F(2)	0.0370(11)	0.0307(10)	0.0694(14)	-0.0071(9)	0.0381(11)	-0.0054(8)
F(3)	0.0452(12)	0.0264(10)	0.0450(12)	-0.0080(8)	0.0177(10)	-0.0099(9)
F(4)	0.0452(12)	0.0426(12)	0.0697(15)	-0.0310(11)	0.0304(12)	-0.0082(10)
F(5)	0.0333(11)	0.0470(12)	0.0409(11)	0.0207(9)	0.0149(9)	0.0101(9)
F(6)	0.0237(10)	0.0731(15)	0.0387(12)	0.0035(10)	0.0003(9)	0.0159(10)
P(2)	0.0213(4)	0.0333(5)	0.0744(7)	0.0054(5)	0.0251(5)	0.0011(4)
F(7)	0.0377(12)	0.0630(15)	0.0798(17)	0.0192(13)	0.0265(12)	-0.0117(11)
F(8)	0.0634(17)	0.0332(13)	0.199(3)	0.0280(17)	0.088(2)	0.0095(11)
F(9)	0.0227(14)	0.103(3)	0.241(5)	0.082(3)	0.032(2)	0.0105(14)
F(10)	0.0312(14)	0.187(4)	0.109(2)	0.099(3)	0.0194(15)	0.0082(18)
F(11)	0.260(5)	0.0582(19)	0.163(4)	-0.029(2)	0.170(4)	-0.045(3)
F(12)	0.196(4)	0.067(2)	0.113(3)	-0.0188(19)	0.081(3)	0.011(2)

Appendix Table 15: Bond lengths [Å] for $Co_2(CO)_6$**3b**.

atom-atom	distance	atom-atom	distance
Co(1)-C(13)	1.808(3)	Co(1)-C(12)	1.816(3)
Co(1)-C(14)	1.821(3)	Co(1)-C(8)	1.962(3)
Co(1)-C(7)	1.962(3)	Co(1)-Co(2)	2.4731(5)
Co(2)-C(15)	1.810(3)	Co(2)-C(16)	1.822(3)
Co(2)-C(17)	1.828(3)	Co(2)-C(8)	1.955(3)
Co(2)-C(7)	1.968(3)	O(12)-C(12)	1.131(4)
O(13)-C(13)	1.145(4)	O(14)-C(14)	1.138(4)
O(15)-C(15)	1.132(3)	O(16)-C(16)	1.138(3)
O(17)-C(17)	1.132(4)	N(1)-C(9)	1.517(3)
N(1)-C(1)	1.518(3)	N(1)-C(5)	1.520(3)
N(1)-C(6)	1.525(3)	C(1)-C(2)	1.515(4)
C(2)-C(3)	1.516(4)	C(3)-C(4)	1.525(5)
C(4)-C(5)	1.523(4)	C(6)-C(7)	1.487(4)
C(7)-C(8)	1.336(4)	C(9)-C(10)	1.502(4)
C(10)-C(11)	1.311(4)	Co(3)-C(34)	1.794(3)
Co(3)-C(32)	1.825(3)	Co(3)-C(33)	1.830(3)
Co(3)-C(28)	1.946(3)	Co(3)-C(27)	1.967(3)
Co(3)-Co(4)	2.4676(6)	Co(4)-C(35)	1.799(4)
Co(4)-C(37)	1.818(3)	Co(4)-C(36)	1.822(3)
Co(4)-C(28)	1.963(3)	Co(4)-C(27)	1.972(3)
O(32)-C(32)	1.133(4)	O(33)-C(33)	1.136(4)
O(34)-C(34)	1.132(4)	O(35)-C(35)	1.137(4)
O(36)-C(36)	1.137(4)	O(37)-C(37)	1.138(4)

N(2)-C(29)	1.496(4)	N(2)-C(26)	1.509(4)
N(2)-C(25)	1.526(4)	N(2)-C(21)	1.531(4)
C(21)-C(22)	1.485(5)	C(22)-C(23)	1.555(6)
C(23)-C(24)	1.539(5)	C(24)-C(25)	1.496(5)
C(26)-C(27)	1.490(4)	C(27)-C(28)	1.335(4)
C(29)-C(30)	1.445(6)	C(30)-C(31)	1.328(6)
P(1)-F(6)	1.584(2)	P(1)-F(4)	1.590(2)
P(1)-F(1)	1.5926(18)	P(1)-F(3)	1.5951(19)
P(1)-F(5)	1.609(2)	P(1)-F(2)	1.6112(19)
P(2)-F(9)	1.551(3)	P(2)-F(11)	1.551(3)
P(2)-F(12)	1.563(3)	P(2)-F(10)	1.571(3)
P(2)-F(7)	1.582(2)	P(2)-F(8)	1.591(2)
C(1)-H(1A)	0.99	C(1)-H(1B)	0.99
C(2)-H(2A)	0.99	C(2)-H(2B)	0.99
C(3)-H(3A)	0.99	C(3)-H(3B)	0.99
C(4)-H(4A)	0.99	C(4)-H(4B)	0.99
C(5)-H(5A)	0.99	C(5)-H(5B)	0.99
C(6)-H(6A)	0.99	C(6)-H(6B)	0.99
C(8)-H(8A)	1	C(9)-H(9A)	0.99
C(9)-H(9B)	0.99	C(10)-H(10A)	0.95
C(11)-H(11A)	0.95	C(11)-H(11B)	0.95
C(21)-H(21A)	0.99	C(21)-H(21B)	0.99
C(22)-H(22A)	0.99	C(22)-H(22B)	0.99
C(23)-H(23A)	0.99	C(23)-H(23B)	0.99
C(24)-H(24A)	0.99	C(24)-H(24B)	0.99
C(25)-H(25A)	0.99	C(25)-H(25B)	0.99
C(26)-H(26A)	0.99	C(26)-H(26B)	0.99
C(28)-H(28A)	1	C(29)-H(29A)	0.99
C(29)-H(29B)	0.99	C(30)-H(30A)	0.95
C(31)-H(31A)	0.95	C(31)-H(31B)	0.95

Symmetry transformations used to generate equivalent atoms:

Appendix Table 16: Bond angles [°] for $Co_2(CO)_6$**3b**.

atom-atom-atom	angle	atom-atom-atom	angle
C(13)-Co(1)-C(12)	100.15(14)	C(13)-Co(1)-C(14)	108.75(13)
C(12)-Co(1)-C(14)	98.40(13)	C(13)-Co(1)-C(8)	102.41(13)
C(12)-Co(1)-C(8)	100.89(12)	C(14)-Co(1)-C(8)	139.52(13)
C(13)-Co(1)-C(7)	139.66(13)	C(12)-Co(1)-C(7)	101.02(12)
C(14)-Co(1)-C(7)	101.60(12)	C(8)-Co(1)-C(7)	39.82(11)
C(13)-Co(1)-Co(2)	97.29(10)	C(12)-Co(1)-Co(2)	149.54(9)
C(14)-Co(1)-Co(2)	99.36(10)	C(8)-Co(1)-Co(2)	50.71(8)
C(7)-Co(1)-Co(2)	51.12(8)	C(15)-Co(2)-C(16)	99.08(13)
C(15)-Co(2)-C(17)	99.40(13)	C(16)-Co(2)-C(17)	108.35(14)
C(15)-Co(2)-C(8)	102.81(12)	C(16)-Co(2)-C(8)	142.54(12)
C(17)-Co(2)-C(8)	97.65(13)	C(15)-Co(2)-C(7)	97.39(12)
C(16)-Co(2)-C(7)	107.64(12)	C(17)-Co(2)-C(7)	136.99(13)
C(8)-Co(2)-C(7)	39.82(11)	C(15)-Co(2)-Co(1)	147.86(9)
C(16)-Co(2)-Co(1)	96.42(9)	C(17)-Co(2)-Co(1)	102.17(10)
C(8)-Co(2)-Co(1)	50.96(8)	C(7)-Co(2)-Co(1)	50.90(8)

C(9)-N(1)-C(1)	112.1(2)	C(9)-N(1)-C(5)	109.3(2)
C(1)-N(1)-C(5)	109.7(2)	C(9)-N(1)-C(6)	110.6(2)
C(1)-N(1)-C(6)	106.0(2)	C(5)-N(1)-C(6)	109.1(2)
C(2)-C(1)-N(1)	112.0(2)	C(1)-C(2)-C(3)	111.3(2)
C(2)-C(3)-C(4)	111.2(3)	C(5)-C(4)-C(3)	112.2(3)
N(1)-C(5)-C(4)	112.6(2)	C(7)-C(6)-N(1)	116.3(2)
C(8)-C(7)-C(6)	145.1(3)	C(8)-C(7)-Co(1)	70.07(17)
C(6)-C(7)-Co(1)	135.4(2)	C(8)-C(7)-Co(2)	69.53(17)
C(6)-C(7)-Co(2)	130.3(2)	Co(1)-C(7)-Co(2)	77.98(10)
C(7)-C(8)-Co(2)	70.65(17)	C(7)-C(8)-Co(1)	70.12(17)
Co(2)-C(8)-Co(1)	78.32(10)	C(10)-C(9)-N(1)	114.5(2)
C(11)-C(10)-C(9)	121.1(3)	O(12)-C(12)-Co(1)	178.3(3)
O(13)-C(13)-Co(1)	177.1(3)	O(14)-C(14)-Co(1)	177.1(3)
O(15)-C(15)-Co(2)	177.1(3)	O(16)-C(16)-Co(2)	177.8(3)
O(17)-C(17)-Co(2)	175.9(3)	C(34)-Co(3)-C(32)	97.64(15)
C(34)-Co(3)-C(33)	96.96(15)	C(32)-Co(3)-C(33)	107.28(15)
C(34)-Co(3)-C(28)	104.48(13)	C(32)-Co(3)-C(28)	142.10(14)
C(33)-Co(3)-C(28)	100.22(13)	C(34)-Co(3)-C(27)	100.29(14)
C(32)-Co(3)-C(27)	106.40(14)	C(33)-Co(3)-C(27)	139.45(13)
C(28)-Co(3)-C(27)	39.89(12)	C(34)-Co(3)-Co(4)	150.94(11)
C(32)-Co(3)-Co(4)	96.84(12)	C(33)-Co(3)-Co(4)	102.58(10)
C(28)-Co(3)-Co(4)	51.17(8)	C(27)-Co(3)-Co(4)	51.29(8)
C(35)-Co(4)-C(37)	100.70(16)	C(35)-Co(4)-C(36)	97.58(15)
C(37)-Co(4)-C(36)	106.77(14)	C(35)-Co(4)-C(28)	99.64(14)
C(37)-Co(4)-C(28)	140.02(13)	C(36)-Co(4)-C(28)	104.19(13)
C(35)-Co(4)-C(27)	103.31(13)	C(37)-Co(4)-C(27)	101.86(13)
C(36)-Co(4)-C(27)	140.47(13)	C(28)-Co(4)-C(27)	39.67(11)
C(35)-Co(4)-Co(3)	149.54(11)	C(37)-Co(4)-Co(3)	100.93(11)
C(36)-Co(4)-Co(3)	96.41(11)	C(28)-Co(4)-Co(3)	50.56(8)
C(27)-Co(4)-Co(3)	51.13(8)	C(29)-N(2)-C(26)	111.7(3)
C(29)-N(2)-C(25)	111.2(3)	C(26)-N(2)-C(25)	108.4(2)
C(29)-N(2)-C(21)	111.2(2)	C(26)-N(2)-C(21)	106.2(2)
C(25)-N(2)-C(21)	108.0(2)	C(22)-C(21)-N(2)	114.2(3)
C(21)-C(22)-C(23)	109.6(3)	C(24)-C(23)-C(22)	109.7(3)
C(25)-C(24)-C(23)	112.6(3)	C(24)-C(25)-N(2)	115.6(3)
C(27)-C(26)-N(2)	116.6(2)	C(28)-C(27)-C(26)	145.6(3)
C(28)-C(27)-Co(3)	69.21(17)	C(26)-C(27)-Co(3)	130.7(2)
C(28)-C(27)-Co(4)	69.82(17)	C(26)-C(27)-Co(4)	135.2(2)
Co(3)-C(27)-Co(4)	77.57(10)	C(27)-C(28)-Co(3)	70.90(17)
C(27)-C(28)-Co(4)	70.51(17)	Co(3)-C(28)-Co(4)	78.26(10)
C(30)-C(29)-N(2)	115.8(3)	C(31)-C(30)-C(29)	121.9(5)
O(32)-C(32)-Co(3)	177.7(3)	O(33)-C(33)-Co(3)	174.8(3)
O(34)-C(34)-Co(3)	178.3(3)	O(35)-C(35)-Co(4)	179.2(3)
O(36)-C(36)-Co(4)	177.8(3)	O(37)-C(37)-Co(4)	178.8(3)
F(6)-P(1)-F(4)	91.25(13)	F(6)-P(1)-F(1)	90.89(11)
F(4)-P(1)-F(1)	91.04(11)	F(6)-P(1)-F(3)	90.50(12)
F(4)-P(1)-F(3)	177.40(13)	F(1)-P(1)-F(3)	90.86(11)
F(6)-P(1)-F(5)	179.29(12)	F(4)-P(1)-F(5)	88.79(12)
F(1)-P(1)-F(5)	89.81(10)	F(3)-P(1)-F(5)	89.44(11)
F(6)-P(1)-F(2)	90.49(12)	F(4)-P(1)-F(2)	89.09(11)
F(1)-P(1)-F(2)	178.61(12)	F(3)-P(1)-F(2)	88.97(10)
F(5)-P(1)-F(2)	88.81(11)	F(9)-P(2)-F(11)	88.1(3)
F(9)-P(2)-F(12)	91.8(3)	F(11)-P(2)-F(12)	179.2(2)

F(9)-P(2)-F(10)	178.6(2)	F(11)-P(2)-F(10)	92.7(3)
F(12)-P(2)-F(10)	87.4(2)	F(9)-P(2)-F(7)	89.68(15)
F(11)-P(2)-F(7)	91.39(16)	F(12)-P(2)-F(7)	89.39(18)
F(10)-P(2)-F(7)	91.42(14)	F(9)-P(2)-F(8)	90.76(16)
F(11)-P(2)-F(8)	88.40(17)	F(12)-P(2)-F(8)	90.82(19)
F(10)-P(2)-F(8)	88.15(15)	F(7)-P(2)-F(8)	179.51(19)
C(2)-C(1)-H(1A)	109.2	N(1)-C(1)-H(1A)	109.2
C(2)-C(1)-H(1B)	109.2	N(1)-C(1)-H(1B)	109.2
H(1A)-C(1)-H(1B)	107.9	C(1)-C(2)-H(2A)	109.4
C(3)-C(2)-H(2A)	109.4	C(1)-C(2)-H(2B)	109.4
C(3)-C(2)-H(2B)	109.4	H(2A)-C(2)-H(2B)	108
C(2)-C(3)-H(3A)	109.4	C(4)-C(3)-H(3A)	109.4
C(2)-C(3)-H(3B)	109.4	C(4)-C(3)-H(3B)	109.4
H(3A)-C(3)-H(3B)	108	C(5)-C(4)-H(4A)	109.2
C(3)-C(4)-H(4A)	109.2	C(5)-C(4)-H(4B)	109.2
C(3)-C(4)-H(4B)	109.2	H(4A)-C(4)-H(4B)	107.9
N(1)-C(5)-H(5A)	109.1	C(4)-C(5)-H(5A)	109.1
N(1)-C(5)-H(5B)	109.1	C(4)-C(5)-H(5B)	109.1
H(5A)-C(5)-H(5B)	107.8	C(7)-C(6)-H(6A)	108.2
N(1)-C(6)-H(6A)	108.2	C(7)-C(6)-H(6B)	108.2
N(1)-C(6)-H(6B)	108.2	H(6A)-C(6)-H(6B)	107.4
C(7)-C(8)-H(8A)	136.5	Co(2)-C(8)-H(8A)	136.5
Co(1)-C(8)-H(8A)	136.5	C(10)-C(9)-H(9A)	108.6
N(1)-C(9)-H(9A)	108.6	C(10)-C(9)-H(9B)	108.6
N(1)-C(9)-H(9B)	108.6	H(9A)-C(9)-H(9B)	107.6
C(11)-C(10)-H(10A)	119.5	C(9)-C(10)-H(10A)	119.5
C(10)-C(11)-H(11A)	120	C(10)-C(11)-H(11B)	120
H(11A)-C(11)-H(11B)	120	C(22)-C(21)-H(21A)	108.7
N(2)-C(21)-H(21A)	108.7	C(22)-C(21)-H(21B)	108.7
N(2)-C(21)-H(21B)	108.7	H(21A)-C(21)-H(21B)	107.6
C(21)-C(22)-H(22A)	109.8	C(23)-C(22)-H(22A)	109.8
C(21)-C(22)-H(22B)	109.8	C(23)-C(22)-H(22B)	109.8
H(22A)-C(22)-H(22B)	108.2	C(24)-C(23)-H(23A)	109.7
C(22)-C(23)-H(23A)	109.7	C(24)-C(23)-H(23B)	109.7
C(22)-C(23)-H(23B)	109.7	H(23A)-C(23)-H(23B)	108.2
C(25)-C(24)-H(24A)	109.1	C(23)-C(24)-H(24A)	109.1
C(25)-C(24)-H(24B)	109.1	C(23)-C(24)-H(24B)	109.1
H(24A)-C(24)-H(24B)	107.8	C(24)-C(25)-H(25A)	108.4
N(2)-C(25)-H(25A)	108.4	C(24)-C(25)-H(25B)	108.4
N(2)-C(25)-H(25B)	108.4	H(25A)-C(25)-H(25B)	107.4
C(27)-C(26)-H(26A)	108.1	N(2)-C(26)-H(26A)	108.1
C(27)-C(26)-H(26B)	108.1	N(2)-C(26)-H(26B)	108.1
H(26A)-C(26)-H(26B)	107.3	C(27)-C(28)-H(28A)	136.3
Co(3)-C(28)-H(28A)	136.3	Co(4)-C(28)-H(28A)	136.3
C(30)-C(29)-H(29A)	108.3	N(2)-C(29)-H(29A)	108.3
C(30)-C(29)-H(29B)	108.3	N(2)-C(29)-H(29B)	108.3
H(29A)-C(29)-H(29B)	107.4	C(31)-C(30)-H(30A)	119.1
C(29)-C(30)-H(30A)	119.1	C(30)-C(31)-H(31A)	120
C(30)-C(31)-H(31B)	120	H(31A)-C(31)-H(31B)	120

Symmetry transformations used to generate equivalent atoms:

Appendix Table 17: Torsion angles [°] for $Co_2(CO)_6$**3b**.

atom-atom-atom-atom	angle	atom-atom-atom-atom	angle
C(13)-Co(1)-Co(2)-C(15)	141.2(2)	C(12)-Co(1)-Co(2)-C(15)	16.6(3)
C(14)-Co(1)-Co(2)-C(15)	-108.37(19)	C(8)-Co(1)-Co(2)-C(15)	41.1(2)
C(7)-Co(1)-Co(2)-C(15)	-11.0(2)	C(13)-Co(1)-Co(2)-C(16)	-100.32(14)
C(12)-Co(1)-Co(2)-C(16)	135.1(2)	C(14)-Co(1)-Co(2)-C(16)	10.14(13)
C(8)-Co(1)-Co(2)-C(16)	159.59(14)	C(7)-Co(1)-Co(2)-C(16)	107.55(14)
C(13)-Co(1)-Co(2)-C(17)	10.06(14)	C(12)-Co(1)-Co(2)-C(17)	-114.5(2)
C(14)-Co(1)-Co(2)-C(17)	120.53(13)	C(8)-Co(1)-Co(2)-C(17)	-90.03(14)
C(7)-Co(1)-Co(2)-C(17)	-142.06(14)	C(13)-Co(1)-Co(2)-C(8)	100.09(14)
C(12)-Co(1)-Co(2)-C(8)	-24.5(2)	C(14)-Co(1)-Co(2)-C(8)	-149.45(14)
C(7)-Co(1)-Co(2)-C(8)	-52.04(14)	C(13)-Co(1)-Co(2)-C(7)	152.13(14)
C(12)-Co(1)-Co(2)-C(7)	27.5(2)	C(14)-Co(1)-Co(2)-C(7)	-97.41(14)
C(8)-Co(1)-Co(2)-C(7)	52.04(14)	C(9)-N(1)-C(1)-C(2)	65.2(3)
C(5)-N(1)-C(1)-C(2)	-56.4(3)	C(6)-N(1)-C(1)-C(2)	-174.1(2)
N(1)-C(1)-C(2)-C(3)	57.4(3)	C(1)-C(2)-C(3)-C(4)	-54.3(4)
C(2)-C(3)-C(4)-C(5)	52.2(4)	C(9)-N(1)-C(5)-C(4)	-69.2(3)
C(1)-N(1)-C(5)-C(4)	54.1(3)	C(6)-N(1)-C(5)-C(4)	169.8(2)
C(3)-C(4)-C(5)-N(1)	-52.9(3)	C(9)-N(1)-C(6)-C(7)	-59.0(3)
C(1)-N(1)-C(6)-C(7)	179.4(2)	C(5)-N(1)-C(6)-C(7)	61.3(3)
N(1)-C(6)-C(7)-C(8)	20.0(6)	N(1)-C(6)-C(7)-Co(1)	-107.3(3)
N(1)-C(6)-C(7)-Co(2)	134.6(2)	C(13)-Co(1)-C(7)-C(8)	26.6(3)
C(12)-Co(1)-C(7)-C(8)	-93.84(19)	C(14)-Co(1)-C(7)-C(8)	165.09(18)
Co(2)-Co(1)-C(7)-C(8)	72.36(16)	C(13)-Co(1)-C(7)-C(6)	177.7(2)
C(12)-Co(1)-C(7)-C(6)	57.2(3)	C(14)-Co(1)-C(7)-C(6)	-43.9(3)
C(8)-Co(1)-C(7)-C(6)	151.1(4)	Co(2)-Co(1)-C(7)-C(6)	-136.6(3)
C(13)-Co(1)-C(7)-Co(2)	-45.8(2)	C(12)-Co(1)-C(7)-Co(2)	-166.20(11)
C(14)-Co(1)-C(7)-Co(2)	92.73(11)	C(8)-Co(1)-C(7)-Co(2)	-72.36(16)
C(15)-Co(2)-C(7)-C(8)	101.16(18)	C(16)-Co(2)-C(7)-C(8)	-156.83(18)
C(17)-Co(2)-C(7)-C(8)	-11.2(3)	Co(1)-Co(2)-C(7)-C(8)	-72.99(16)
C(15)-Co(2)-C(7)-C(6)	-45.2(3)	C(16)-Co(2)-C(7)-C(6)	56.8(3)
C(17)-Co(2)-C(7)-C(6)	-157.5(2)	C(8)-Co(2)-C(7)-C(6)	-146.3(3)
Co(1)-Co(2)-C(7)-C(6)	140.7(3)	C(15)-Co(2)-C(7)-Co(1)	174.15(11)
C(16)-Co(2)-C(7)-Co(1)	-83.84(12)	C(17)-Co(2)-C(7)-Co(1)	61.77(19)
C(8)-Co(2)-C(7)-Co(1)	72.99(16)	C(6)-C(7)-C(8)-Co(2)	132.3(4)
Co(1)-C(7)-C(8)-Co(2)	-84.20(8)	C(6)-C(7)-C(8)-Co(1)	-143.5(4)
Co(2)-C(7)-C(8)-Co(1)	84.20(8)	C(15)-Co(2)-C(8)-C(7)	-86.18(18)
C(16)-Co(2)-C(8)-C(7)	38.1(3)	C(17)-Co(2)-C(8)-C(7)	172.31(18)
Co(1)-Co(2)-C(8)-C(7)	72.81(16)	C(15)-Co(2)-C(8)-Co(1)	-158.99(10)
C(16)-Co(2)-C(8)-Co(1)	-34.7(2)	C(17)-Co(2)-C(8)-Co(1)	99.49(11)
C(7)-Co(2)-C(8)-Co(1)	-72.81(16)	C(13)-Co(1)-C(8)-C(7)	-162.73(18)
C(12)-Co(1)-C(8)-C(7)	94.20(18)	C(14)-Co(1)-C(8)-C(7)	-22.8(3)
Co(2)-Co(1)-C(8)-C(7)	-73.43(16)	C(13)-Co(1)-C(8)-Co(2)	-89.30(12)
C(12)-Co(1)-C(8)-Co(2)	167.63(11)	C(14)-Co(1)-C(8)-Co(2)	50.6(2)
C(7)-Co(1)-C(8)-Co(2)	73.43(16)	C(1)-N(1)-C(9)-C(10)	47.7(3)
C(5)-N(1)-C(9)-C(10)	169.6(2)	C(6)-N(1)-C(9)-C(10)	-70.3(3)
N(1)-C(9)-C(10)-C(11)	-131.2(3)	C(13)-Co(1)-C(12)-O(12)	-157(9)
C(14)-Co(1)-C(12)-O(12)	92(9)	C(8)-Co(1)-C(12)-O(12)	-52(9)
C(7)-Co(1)-C(12)-O(12)	-11(9)	Co(2)-Co(1)-C(12)-O(12)	-33(9)
C(12)-Co(1)-C(13)-O(13)	116(6)	C(14)-Co(1)-C(13)-O(13)	-141(6)
C(8)-Co(1)-C(13)-O(13)	13(6)	C(7)-Co(1)-C(13)-O(13)	-4(6)

Co(2)-Co(1)-C(13)-O(13)	-38(6)	C(13)-Co(1)-C(14)-O(14)	129(5)
C(12)-Co(1)-C(14)-O(14)	-127(5)	C(8)-Co(1)-C(14)-O(14)	-9(5)
C(7)-Co(1)-C(14)-O(14)	-24(5)	Co(2)-Co(1)-C(14)-O(14)	28(5)
C(16)-Co(2)-C(15)-O(15)	-126(5)	C(17)-Co(2)-C(15)-O(15)	124(5)
C(8)-Co(2)-C(15)-O(15)	24(5)	C(7)-Co(2)-C(15)-O(15)	-16(5)
Co(1)-Co(2)-C(15)-O(15)	-8(5)	C(15)-Co(2)-C(16)-O(16)	152(7)
C(17)-Co(2)-C(16)-O(16)	-105(7)	C(8)-Co(2)-C(16)-O(16)	26(7)
C(7)-Co(2)-C(16)-O(16)	51(7)	Co(1)-Co(2)-C(16)-O(16)	0(7)
C(15)-Co(2)-C(17)-O(17)	-76(4)	C(16)-Co(2)-C(17)-O(17)	-179(100)
C(8)-Co(2)-C(17)-O(17)	29(4)	C(7)-Co(2)-C(17)-O(17)	36(4)
Co(1)-Co(2)-C(17)-O(17)	80(4)	C(34)-Co(3)-Co(4)-C(35)	-24.2(3)
C(32)-Co(3)-Co(4)-C(35)	-143.6(2)	C(33)-Co(3)-Co(4)-C(35)	106.9(2)
C(28)-Co(3)-Co(4)-C(35)	13.8(2)	C(27)-Co(3)-Co(4)-C(35)	-38.1(2)
C(34)-Co(3)-Co(4)-C(37)	110.4(2)	C(32)-Co(3)-Co(4)-C(37)	-9.07(15)
C(33)-Co(3)-Co(4)-C(37)	-118.54(15)	C(28)-Co(3)-Co(4)-C(37)	148.38(15)
C(27)-Co(3)-Co(4)-C(37)	96.49(15)	C(34)-Co(3)-Co(4)-C(36)	-141.1(2)
C(32)-Co(3)-Co(4)-C(36)	99.44(14)	C(33)-Co(3)-Co(4)-C(36)	-10.03(14)
C(28)-Co(3)-Co(4)-C(36)	-103.11(14)	C(27)-Co(3)-Co(4)-C(36)	-155.00(14)
C(34)-Co(3)-Co(4)-C(28)	-38.0(2)	C(32)-Co(3)-Co(4)-C(28)	-157.45(15)
C(33)-Co(3)-Co(4)-C(28)	93.08(15)	C(27)-Co(3)-Co(4)-C(28)	-51.89(15)
C(34)-Co(3)-Co(4)-C(27)	13.9(2)	C(32)-Co(3)-Co(4)-C(27)	-105.56(15)
C(33)-Co(3)-Co(4)-C(27)	144.97(15)	C(28)-Co(3)-Co(4)-C(27)	51.89(15)
C(29)-N(2)-C(21)-C(22)	-66.9(4)	C(26)-N(2)-C(21)-C(22)	171.4(3)
C(25)-N(2)-C(21)-C(22)	55.3(4)	N(2)-C(21)-C(22)-C(23)	-60.2(4)
C(21)-C(22)-C(23)-C(24)	56.2(5)	C(22)-C(23)-C(24)-C(25)	-52.0(5)
C(23)-C(24)-C(25)-N(2)	51.0(5)	C(29)-N(2)-C(25)-C(24)	72.3(4)
C(26)-N(2)-C(25)-C(24)	-164.6(3)	C(21)-N(2)-C(25)-C(24)	-49.9(4)
C(29)-N(2)-C(26)-C(27)	59.7(3)	C(25)-N(2)-C(26)-C(27)	-63.1(3)
C(21)-N(2)-C(26)-C(27)	-179.0(3)	N(2)-C(26)-C(27)-C(28)	-17.7(6)
N(2)-C(26)-C(27)-Co(3)	-133.0(2)	N(2)-C(26)-C(27)-Co(4)	109.4(3)
C(34)-Co(3)-C(27)-C(28)	-100.30(19)	C(32)-Co(3)-C(27)-C(28)	158.50(18)
C(33)-Co(3)-C(27)-C(28)	13.4(3)	Co(4)-Co(3)-C(27)-C(28)	72.89(16)
C(34)-Co(3)-C(27)-C(26)	46.5(3)	C(32)-Co(3)-C(27)-C(26)	-54.7(3)
C(33)-Co(3)-C(27)-C(26)	160.2(3)	C(28)-Co(3)-C(27)-C(26)	146.8(4)
Co(4)-Co(3)-C(27)-C(26)	-140.3(3)	C(34)-Co(3)-C(27)-Co(4)	-173.20(11)
C(32)-Co(3)-C(27)-Co(4)	85.60(14)	C(33)-Co(3)-C(27)-Co(4)	-59.5(2)
C(28)-Co(3)-C(27)-Co(4)	-72.89(16)	C(35)-Co(4)-C(27)-C(28)	89.1(2)
C(37)-Co(4)-C(27)-C(28)	-166.74(19)	C(36)-Co(4)-C(27)-C(28)	-30.9(3)
Co(3)-Co(4)-C(27)-C(28)	-72.17(17)	C(35)-Co(4)-C(27)-C(26)	-62.2(3)
C(37)-Co(4)-C(27)-C(26)	42.0(3)	C(36)-Co(4)-C(27)-C(26)	177.9(3)
C(28)-Co(4)-C(27)-C(26)	-151.3(4)	Co(3)-Co(4)-C(27)-C(26)	136.6(3)
C(35)-Co(4)-C(27)-Co(3)	161.27(12)	C(37)-Co(4)-C(27)-Co(3)	-94.57(13)
C(36)-Co(4)-C(27)-Co(3)	41.3(2)	C(28)-Co(4)-C(27)-Co(3)	72.17(17)
C(26)-C(27)-C(28)-Co(3)	-132.9(5)	Co(4)-C(27)-C(28)-Co(3)	83.93(8)
C(26)-C(27)-C(28)-Co(4)	143.2(5)	Co(3)-C(27)-C(28)-Co(4)	-83.93(8)
C(34)-Co(3)-C(28)-C(27)	88.79(19)	C(32)-Co(3)-C(28)-C(27)	-34.9(3)
C(33)-Co(3)-C(28)-C(27)	-171.20(19)	Co(4)-Co(3)-C(28)-C(27)	-73.22(16)
C(34)-Co(3)-C(28)-Co(4)	162.01(12)	C(32)-Co(3)-C(28)-Co(4)	38.3(2)
C(33)-Co(3)-C(28)-Co(4)	-97.98(13)	C(27)-Co(3)-C(28)-Co(4)	73.22(16)
C(35)-Co(4)-C(28)-C(27)	-99.27(19)	C(37)-Co(4)-C(28)-C(27)	20.4(3)
C(36)-Co(4)-C(28)-C(27)	160.31(19)	Co(3)-Co(4)-C(28)-C(27)	73.68(16)
C(35)-Co(4)-C(28)-Co(3)	-172.94(12)	C(37)-Co(4)-C(28)-Co(3)	-53.2(2)
C(36)-Co(4)-C(28)-Co(3)	86.63(13)	C(27)-Co(4)-C(28)-Co(3)	-73.68(16)

C(26)-N(2)-C(29)-C(30)	70.5(4)	C(25)-N(2)-C(29)-C(30)	-168.3(3)
C(21)-N(2)-C(29)-C(30)	-47.9(4)	N(2)-C(29)-C(30)-C(31)	129.7(5)
C(34)-Co(3)-C(32)-O(32)	-116(8)	C(33)-Co(3)-C(32)-O(32)	144(8)
C(28)-Co(3)-C(32)-O(32)	10(8)	C(27)-Co(3)-C(32)-O(32)	-13(8)
Co(4)-Co(3)-C(32)-O(32)	39(8)	C(34)-Co(3)-C(33)-O(33)	60(3)
C(32)-Co(3)-C(33)-O(33)	160(3)	C(28)-Co(3)-C(33)-O(33)	-46(3)
C(27)-Co(3)-C(33)-O(33)	-55(3)	Co(4)-Co(3)-C(33)-O(33)	-98(3)
C(32)-Co(3)-C(34)-O(34)	-155(11)	C(33)-Co(3)-C(34)-O(34)	-47(11)
C(28)-Co(3)-C(34)-O(34)	56(11)	C(27)-Co(3)-C(34)-O(34)	96(11)
Co(4)-Co(3)-C(34)-O(34)	85(11)	C(37)-Co(4)-C(35)-O(35)	160(26)
C(36)-Co(4)-C(35)-O(35)	51(26)	C(28)-Co(4)-C(35)-O(35)	-55(26)
C(27)-Co(4)-C(35)-O(35)	-95(26)	Co(3)-Co(4)-C(35)-O(35)	-65(26)
C(35)-Co(4)-C(36)-O(36)	-84(9)	C(37)-Co(4)-C(36)-O(36)	172(100)
C(28)-Co(4)-C(36)-O(36)	18(9)	C(27)-Co(4)-C(36)-O(36)	38(9)
Co(3)-Co(4)-C(36)-O(36)	69(9)	C(35)-Co(4)-C(37)-O(37)	138(16)
C(36)-Co(4)-C(37)-O(37)	-121(16)	C(28)-Co(4)-C(37)-O(37)	18(16)
C(27)-Co(4)-C(37)-O(37)	32(16)	Co(3)-Co(4)-C(37)-O(37)	-21(16)

Symmetry transformations used to generate equivalent atoms:

$(Co_2(CO)_6)_2$ 4b:

The compound crystallizes as dark red block-like crystals. There are four molecules of the cation and associated PF_6 anion in the unit cell of the primitive, centric, monoclinic space group P21/c.

The cation consists of two $Co_2(CO)_6$ moieties, each of which is coordinated by a separate acetylinic arm of the pyrollidinium. In each case, the acetylene group is coordinated in a μ-2 fashion to both cobalt centers of the $Co_2(CO)_6$. The acetylinic hydrogens, H8a and H11a, were located from a difference Foruier map and included with refined coordinates and a thermal parameter tied to that of the carbon to which they are bonded.

The C7-C8 and C10-C11 bond distances [1.328(4) and 1.336(4) Å] are somewhat longer than a typical C-C triple bond (around 1.19 Å) and are more close to a C-C double bond (on average 1.35 Å). The other bond distances are as expected.

Crystal data for $C_{23}H_{16}Co_4F_6NO_{12}P$; M_r = 879.06; monoclinic; space group $P2_1/c$; a = 12.7182(5) Å; b = 14.5661(6) Å; c = 18.0495(7) Å; α = 90°; β = 106.797(2)°; γ = 90°; V = 3201.1(2) $Å^3$; Z = 4; T = 100(2) K; λ(Mo-Kα) = 0.71073 Å; μ(Mo-Kα) = 2.180 mm^{-1}; d_{calc} = 1.824g.cm^{-3}; 43584 reflections collected; 6521 unique (R_{int} = 0.0567); giving R_1 =

0.0345, wR_2 = 0.0799 for 4905 data with [I>2σ(I)] and R_1 = 0.0553, wR_2 = 0.0883 for all 6521 data. Residual electron density ($e^-.Å^{-3}$) max/min: 0.562/-0.486.

An arbitrary sphere of data were collected on a red block-like crystal, having approximate dimensions of 0.18 × 0.11 × 0.10 mm, on a Bruker APEX-II diffractometer using a combination of ω- and φ-scans of 0.3°. Data were corrected for absorption and polarization effects and analyzed for space group determination. The structure was solved by direct methods and expanded routinely. The model was refined by full-matrix least-squares analysis of F^2 against all reflections. All non-hydrogen atoms were refined with anisotropic thermal displacement parameters. Unless otherwise noted, hydrogen atoms were included in calculated positions. Thermal parameters for the hydrogens were tied to the isotropic thermal parameter of the atom to which they are bonded (1.5 × for methyl, 1.2 × for all others).

Appendix Table 18: Crystal data and structure refinement for $(Co_2(CO)_6)_2$ **4b**.

Identification code	$(Co_2(CO)_6)_2$ **4b**
Empirical formula	$C_{23}H_{16}Co_4F_6NO_{12}P$
Formula weight	879.06
Temperature	100(2) K
Wavelength	0.71073 Å
Crystal system	monoclinic
Space group	$P2_1/c$
Unit cell dimensions	a = 12.7182(5) Å α = 90° b = 14.5661(6) Å β = 106.797(2)° c = 18.0495(7) Å γ = 90°
Volume	3201.1(2) $Å^3$
Z	4
Density (calculated)	1.824 $g.cm^{-3}$
Absorption coefficient (μ)	2.180 mm^{-1}
F(000)	1736
Crystal size	0.18 × 0.11 × 0.10 mm^3
ω range for data collection	1.67 to 26.40°
Index ranges	$-15 \le h \le 15$, $-16 \le k \le 18$, $-22 \le l \le 22$
Reflections collected	43584
Independent reflections	6521 [R_{int} = 0.0567]
Completeness to θ = 26.40°	99.6 %
Absorption correction	Numerical
Max. and min. transmission	0.8510 and 0.6416
Refinement method	Full-matrix least-squares on F^2
Data / restraints / parameters	6521 / 0 / 430
Goodness-of-fit on F^2	1.014
Final R indices [I>2σ(I)]	R_1 = 0.0345, wR_2 = 0.0799

R indices (all data)	$R_1 = 0.0553$, $wR_2 = 0.0883$
Largest diff. peak and hole	0.562 and -0.486 $e^-.Å^{-3}$

Appendix Table 19: Atomic coordinates and equivalent isotropic displacement parameters ($Å^2$) for $(Co_2(CO)_6)_2$ **4b**. U(eq) is defined as one third of the trace of the orthogonalized U_{ij} tensor.

	x	y	z	U(eq)
Co(1)	0.70533(3)	0.20934(3)	0.18249(2)	0.021(1)
Co(2)	0.63187(3)	0.31714(3)	0.07539(2)	0.022(1)
Co(3)	0.09001(3)	0.26019(3)	-0.00897(2)	0.026(1)
Co(4)	0.19880(3)	0.39074(3)	0.05933(2)	0.023(1)
O(1)	0.69380(18)	0.12816(16)	0.32830(13)	0.041(1)
O(2)	0.90860(17)	0.31373(16)	0.25325(13)	0.038(1)
O(3)	0.77569(18)	0.05827(16)	0.09729(13)	0.037(1)
O(4)	0.7277(2)	0.22297(17)	-0.03501(13)	0.044(1)
O(5)	0.76256(17)	0.48163(15)	0.14077(13)	0.035(1)
O(6)	0.44968(17)	0.40983(14)	-0.03810(12)	0.034(1)
O(7)	0.05347(17)	0.08493(16)	-0.09343(14)	0.043(1)
O(8)	-0.0321(2)	0.21726(19)	0.10306(16)	0.056(1)
O(9)	-0.0500(2)	0.37601(17)	-0.13355(15)	0.052(1)
O(10)	0.41627(17)	0.47050(14)	0.12868(13)	0.036(1)
O(11)	0.09836(17)	0.55095(16)	-0.03523(13)	0.036(1)
O(12)	0.10126(18)	0.40400(17)	0.19046(13)	0.041(1)
N(1)	0.37845(17)	0.13029(16)	0.11244(13)	0.019(1)
C(1)	0.3058(2)	0.06016(19)	0.06012(16)	0.021(1)
C(2)	0.2216(2)	0.0179(2)	0.09458(17)	0.026(1)
C(3)	0.2774(2)	-0.0275(2)	0.17167(17)	0.032(1)
C(4)	0.3531(2)	0.0410(2)	0.22673(17)	0.029(1)
C(5)	0.4339(2)	0.0864(2)	0.19039(16)	0.024(1)
C(6)	0.3138(2)	0.2134(2)	0.12658(16)	0.021(1)
C(7)	0.2434(2)	0.2616(2)	0.05786(16)	0.022(1)
C(8)	0.2364(2)	0.3009(2)	-0.00978(18)	0.024(1)
C(9)	0.4639(2)	0.1588(2)	0.07258(16)	0.020(1)
C(10)	0.5527(2)	0.22136(19)	0.11640(16)	0.019(1)
C(11)	0.5788(2)	0.2925(2)	0.16499(17)	0.022(1)
C(13)	0.6979(2)	0.1574(2)	0.27040(19)	0.029(1)
C(14)	0.8307(2)	0.2733(2)	0.22620(18)	0.028(1)
C(15)	0.7506(2)	0.1144(2)	0.13195(18)	0.027(1)
C(16)	0.5196(2)	0.3732(2)	0.00612(18)	0.027(1)
C(17)	0.6908(3)	0.2604(2)	0.00682(19)	0.031(1)
C(18)	0.7149(2)	0.4181(2)	0.11370(18)	0.027(1)
C(19)	0.0701(2)	0.1522(2)	-0.06129(18)	0.030(1)
C(20)	0.0127(3)	0.2341(2)	0.0590(2)	0.037(1)
C(21)	0.0014(3)	0.3303(2)	-0.0857(2)	0.036(1)
C(22)	0.3309(2)	0.4406(2)	0.10289(18)	0.027(1)
C(23)	0.1359(2)	0.4879(2)	0.00029(18)	0.027(1)
C(24)	0.1406(2)	0.3990(2)	0.14149(19)	0.029(1)
P(1)	0.38612(6)	0.35723(6)	0.34160(4)	0.028(1)
F(1)	0.29302(14)	0.36347(12)	0.38457(10)	0.037(1)
F(2)	0.46178(15)	0.42481(13)	0.40581(10)	0.045(1)
F(3)	0.43749(16)	0.27116(13)	0.39425(11)	0.047(1)
F(4)	0.31041(16)	0.29072(13)	0.27815(10)	0.044(1)

F(5)	0.33575(15)	0.44470(13)	0.28989(10)	0.042(1)
F(6)	0.48016(16)	0.35290(17)	0.29930(12)	0.059(1)
H(1A)	0.3525	0.0107	0.0490	0.025
H(1B)	0.2671	0.0899	0.0104	0.025
H(2A)	0.1779	-0.0283	0.0583	0.032
H(2B)	0.1709	0.0662	0.1021	0.032
H(3A)	0.3209	-0.0808	0.1633	0.038
H(3B)	0.2210	-0.0502	0.1953	0.038
H(4A)	0.3077	0.0889	0.2415	0.034
H(4B)	0.3944	0.0085	0.2744	0.034
H(5A)	0.4755	0.1340	0.2261	0.028
H(5B)	0.4870	0.0398	0.1836	0.028
H(6A)	0.2665	0.1931	0.1585	0.025
H(6B)	0.3668	0.2584	0.1576	0.025
H(8A)	0.268(2)	0.305(2)	-0.0489(17)	0.028
H(9A)	0.4986	0.1024	0.0598	0.024
H(9B)	0.4252	0.1890	0.0231	0.024
H(11A)	0.549(2)	0.3278(19)	0.2003(17)	0.026

Appendix Table 20: Anisotropic displacement parameters $(Å)^2$ for $(Co_2(CO)_6)_2$**4b**. The anisotropicdisplacement factor exponent takes the form: $-2\pi^2[\, h^2 a^{*2} U_{11} + \ldots + 2\, h\, k\, a^*\, b^*\, U_{12}\,]$

	U_{11}	U_{22}	U_{33}	U_{23}	U_{13}	U_{12}
Co(1)	0.0130(2)	0.0259(2)	0.0208(2)	0.0008(2)	-0.0005(2)	0.0002(2)
Co(2)	0.0158(2)	0.0262(2)	0.0211(2)	0.0020(2)	0.0025(2)	0.0004(2)
Co(3)	0.0126(2)	0.0314(3)	0.0272(2)	-0.0043(2)	-0.0028(2)	0.0019(2)
Co(4)	0.0141(2)	0.0275(2)	0.0237(2)	-0.0019(2)	0.0001(2)	0.0026(2)
O(1)	0.0346(13)	0.0526(16)	0.0298(13)	0.0108(12)	0.0006(11)	-0.0088(11)
O(2)	0.0240(12)	0.0448(15)	0.0379(14)	-0.0032(11)	-0.0023(10)	-0.0082(10)
O(3)	0.0349(13)	0.0325(14)	0.0447(14)	-0.0088(12)	0.0127(11)	0.0037(10)
O(4)	0.0461(15)	0.0559(16)	0.0349(14)	-0.0004(13)	0.0195(12)	0.0148(12)
O(5)	0.0319(12)	0.0366(14)	0.0352(13)	-0.0045(11)	0.0070(10)	-0.0091(11)
O(6)	0.0290(12)	0.0292(13)	0.0354(13)	0.0063(11)	-0.0019(11)	0.0018(10)
O(7)	0.0284(13)	0.0374(15)	0.0506(16)	-0.0123(13)	-0.0088(11)	0.0032(11)
O(8)	0.0407(15)	0.075(2)	0.0604(18)	-0.0120(15)	0.0284(14)	-0.0182(14)
O(9)	0.0418(15)	0.0446(16)	0.0469(16)	-0.0014(13)	-0.0215(12)	0.0104(12)
O(10)	0.0208(12)	0.0355(13)	0.0451(14)	-0.0085(11)	0.0009(10)	-0.0014(10)
O(11)	0.0256(12)	0.0395(14)	0.0419(14)	0.0114(12)	0.0085(10)	0.0089(10)
O(12)	0.0346(13)	0.0596(17)	0.0296(13)	-0.0031(12)	0.0102(11)	0.0045(12)
N(1)	0.0120(11)	0.0256(14)	0.0160(12)	0.0009(10)	-0.0004(9)	0.0008(9)
C(1)	0.0135(14)	0.0254(16)	0.0205(15)	-0.0023(13)	-0.0019(12)	-0.0009(12)
C(2)	0.0181(15)	0.0333(18)	0.0255(16)	0.0018(14)	0.0025(13)	-0.0044(13)
C(3)	0.0240(16)	0.038(2)	0.0299(18)	0.0063(15)	0.0027(14)	-0.0057(14)
C(4)	0.0211(16)	0.0384(19)	0.0234(16)	0.0085(15)	0.0024(13)	-0.0009(14)
C(5)	0.0164(14)	0.0332(18)	0.0173(15)	0.0055(13)	-0.0014(12)	0.0030(13)
C(6)	0.0106(13)	0.0285(17)	0.0208(15)	-0.0007(13)	0.0000(12)	0.0014(12)
C(7)	0.0110(14)	0.0277(17)	0.0238(16)	-0.0045(13)	0.0016(12)	-0.0004(12)
C(8)	0.0148(15)	0.0284(18)	0.0253(17)	-0.0044(14)	0.0017(13)	0.0004(12)
C(9)	0.0112(13)	0.0290(17)	0.0181(15)	-0.0005(13)	0.0013(11)	0.0007(12)
C(10)	0.0127(14)	0.0256(16)	0.0176(14)	0.0036(13)	0.0025(11)	0.0034(11)
C(11)	0.0152(14)	0.0265(17)	0.0219(16)	0.0039(13)	0.0026(12)	0.0022(12)
C(13)	0.0123(15)	0.0333(19)	0.035(2)	0.0019(16)	-0.0029(13)	-0.0015(13)

C(14)	0.0214(17)	0.0318(19)	0.0271(17)	0.0031(15)	0.0018(14)	0.0024(14)
C(15)	0.0185(15)	0.0299(18)	0.0285(18)	0.0064(15)	-0.0003(13)	-0.0026(13)
C(16)	0.0246(17)	0.0262(18)	0.0306(18)	-0.0027(15)	0.0085(14)	-0.0062(14)
C(17)	0.0257(17)	0.037(2)	0.0260(18)	0.0099(15)	0.0009(14)	0.0022(14)
C(18)	0.0216(16)	0.0341(19)	0.0266(17)	0.0050(15)	0.0074(14)	0.0016(14)
C(19)	0.0145(15)	0.037(2)	0.0303(18)	0.0008(16)	-0.0049(13)	0.0041(13)
C(20)	0.0194(17)	0.039(2)	0.046(2)	-0.0097(17)	0.0004(16)	-0.0036(14)
C(21)	0.0240(17)	0.036(2)	0.041(2)	-0.0117(17)	-0.0022(15)	0.0012(15)
C(22)	0.0216(17)	0.0268(17)	0.0308(17)	-0.0025(14)	0.0067(14)	0.0051(13)
C(23)	0.0149(15)	0.0345(19)	0.0310(18)	-0.0039(15)	0.0044(13)	-0.0005(13)
C(24)	0.0198(16)	0.0305(18)	0.0315(19)	-0.0018(15)	-0.0008(14)	0.0027(13)
P(1)	0.0279(4)	0.0358(5)	0.0190(4)	-0.0005(4)	0.0046(3)	-0.0034(4)
F(1)	0.0355(11)	0.0459(12)	0.0315(10)	-0.0035(9)	0.0139(8)	-0.0038(9)
F(2)	0.0448(12)	0.0566(13)	0.0250(10)	-0.0008(9)	-0.0015(9)	-0.0265(10)
F(3)	0.0547(13)	0.0454(12)	0.0344(11)	0.0086(9)	0.0053(10)	0.0153(10)
F(4)	0.0572(13)	0.0438(12)	0.0243(10)	-0.0120(9)	0.0013(9)	-0.0089(10)
F(5)	0.0468(12)	0.0418(12)	0.0322(11)	0.0104(9)	0.0014(9)	-0.0044(9)
F(6)	0.0451(13)	0.1006(18)	0.0408(12)	0.0042(12)	0.0257(10)	0.0110(12)

Appendix Table 21: Bond lengths [Å] for $(Co_2(CO)_6)_2$ **4b**.

Atom-atom	Distance	Atom-atom	distance
Co(1)-C(13)	1.785(3)	Co(1)-C(14)	1.818(3)
Co(1)-C(15)	1.838(3)	Co(1)-C(11)	1.965(3)
Co(1)-C(10)	1.970(3)	Co(1)-Co(2)	2.4560(5)
Co(2)-C(16)	1.799(3)	Co(2)-C(17)	1.820(4)
Co(2)-C(18)	1.826(3)	Co(2)-C(11)	1.957(3)
Co(2)-C(10)	1.984(3)	Co(3)-C(19)	1.814(4)
Co(3)-C(20)	1.820(4)	Co(3)-C(21)	1.825(4)
Co(3)-C(8)	1.958(3)	Co(3)-C(7)	1.975(3
Co(3)-Co(4)	2.4626(6)	Co(4)-C(22)	1.790(3)
Co(4)-C(23)	1.812(3)	Co(4)-C(24)	1.843(3)
Co(4)-C(8)	1.960(3)	Co(4)-C(7)	1.967(3)
O(1)-C(13)	1.144(4)	O(2)-C(14)	1.135(3)
O(3)-C(15)	1.130(4)	O(4)-C(17)	1.137(4)
O(5)-C(18)	1.136(3)	O(6)-C(16)	1.141(3)
O(7)-C(19)	1.128(4)	O(8)-C(20)	1.132(4)
O(9)-C(21)	1.136(4)	O(10)-C(22)	1.137(3)
O(11)-C(23)	1.143(3)	O(12)-C(24)	1.137(4)
N(1)-C(1)	1.511(3)	N(1)-C(5)	1.521(3)
N(1)-C(9)	1.524(3)	N(1)-C(6)	1.526(3)
C(1)-C(2)	1.516(4)	C(2)-C(3)	1.519(4)
C(3)-C(4)	1.535(4)	C(4)-C(5)	1.521(4)
C(6)-C(7)	1.480(4)	C(7)-C(8)	1.328(4)
C(9)-C(10)	1.489(4)	C(10)-C(11)	1.336(4)
P(1)-F(4)	1.5937(19)	P(1)-F(1)	1.5945(18)
P(1)-F(3)	1.595(2)	P(1)-F(6)	1.595(2)
P(1)-F(5)	1.600(2)	P(1)-F(2)	1.6105(19)
C(1)-H(1A)	0.99	C(1)-H(1B)	0.99
C(2)-H(2A)	0.99	C(2)-H(2B)	0.99
C(3)-H(3A)	0.99	C(3)-H(3B)	0.99
C(4)-H(4A)	0.99	C(4)-H(4B)	0.99

C(5)-H(5A)	0.99	C(5)-H(5B)	0.99
C(6)-H(6A)	0.99	C(6)-H(6B)	0.99
C(8)-H(8A)	0.91(3)	C(9)-H(9A)	0.99
C(9)-H(9B)	0.99	C(11)-H(11A)	0.98(3)

Appendix Table 22: Bond angles [°] for $(Co_2(CO)_6)_2$ **4b**.

Atom-atom-atom	Angle	Atom-atom-atom	Angle
C(13)-Co(1)-C(14)	95.52(13)	C(13)-Co(1)-C(15)	103.11(14)
C(14)-Co(1)-C(15)	103.87(13)	C(13)-Co(1)-C(11)	98.81(13)
C(14)-Co(1)-C(11)	109.18(13)	C(15)-Co(1)-C(11)	138.00(13)
C(13)-Co(1)-C(10)	106.28(12)	C(14)-Co(1)-C(10)	143.52(13)
C(15)-Co(1)-C(10)	99.28(12)	C(11)-Co(1)-C(10)	39.68(11)
C(13)-Co(1)-Co(2)	149.90(10)	C(14)-Co(1)-Co(2)	95.76(10)
C(15)-Co(1)-Co(2)	101.11(9)	C(11)-Co(1)-Co(2)	51.09(9)
C(10)-Co(1)-Co(2)	51.87(8)	C(16)-Co(2)-C(17)	97.69(14)
C(16)-Co(2)-C(18)	98.83(13)	C(17)-Co(2)-C(18)	108.45(14)
C(16)-Co(2)-C(11)	105.29(12)	C(17)-Co(2)-C(11)	141.85(13)
C(18)-Co(2)-C(11)	97.74(13)	C(16)-Co(2)-C(10)	101.08(12)
C(17)-Co(2)-C(10)	106.69(13)	C(18)-Co(2)-C(10)	136.48(13)
C(11)-Co(2)-C(10)	39.61(12)	C(16)-Co(2)-Co(1)	151.90(9)
C(17)-Co(2)-Co(1)	96.14(10)	C(18)-Co(2)-Co(1)	99.79(9)
C(11)-Co(2)-Co(1)	51.36(8)	C(10)-Co(2)-Co(1)	51.35(8)
C(19)-Co(3)-C(20)	98.55(15)	C(19)-Co(3)-C(21)	97.30(14)
C(20)-Co(3)-C(21)	107.07(15)	C(19)-Co(3)-C(8)	104.39(13)
C(20)-Co(3)-C(8)	140.19(14)	C(21)-Co(3)-C(8)	101.81(14)
C(19)-Co(3)-C(7)	106.96(12)	C(20)-Co(3)-C(7)	102.77(13)
C(21)-Co(3)-C(7)	137.90(13)	C(8)-Co(3)-C(7)	39.45(12)
C(19)-Co(3)-Co(4)	154.65(9)	C(20)-Co(3)-Co(4)	99.12(10)
C(21)-Co(3)-Co(4)	94.73(10)	C(8)-Co(3)-Co(4)	51.09(9)
C(7)-Co(3)-Co(4)	51.18(8)	C(22)-Co(4)-C(23)	98.05(13)
C(22)-Co(4)-C(24)	99.45(13)	C(23)-Co(4)-C(24)	102.14(13)
C(22)-Co(4)-C(8)	100.36(12)	C(23)-Co(4)-C(8)	107.12(13)
C(24)-Co(4)-C(8)	141.68(14)	C(22)-Co(4)-C(7)	99.00(12)
C(23)-Co(4)-C(7)	144.94(13)	C(24)-Co(4)-C(7)	104.95(13)
C(8)-Co(4)-C(7)	39.53(12)	C(22)-Co(4)-Co(3)	148.59(9)
C(23)-Co(4)-Co(3)	102.69(9)	C(24)-Co(4)-Co(3)	98.93(10)
C(8)-Co(4)-Co(3)	51.03(8)	C(7)-Co(4)-Co(3)	51.49(8)
C(1)-N(1)-C(5)	109.3(2)	C(1)-N(1)-C(9)	106.2(2)
C(5)-N(1)-C(9)	110.36(19)	C(1)-N(1)-C(6)	112.3(2)
C(5)-N(1)-C(6)	107.9(2)	C(9)-N(1)-C(6)	110.8(2)
N(1)-C(1)-C(2)	113.3(2)	C(1)-C(2)-C(3)	110.8(2)
C(2)-C(3)-C(4)	110.4(2)	C(5)-C(4)-C(3)	112.3(2)
N(1)-C(5)-C(4)	113.0(2)	C(7)-C(6)-N(1)	117.4(2)
C(8)-C(7)-C(6)	147.0(3)	C(8)-C(7)-Co(4)	69.97(18)
C(6)-C(7)-Co(4)	123.3(2)	C(8)-C(7)-Co(3)	69.59(17)
C(6)-C(7)-Co(3)	139.3(2)	Co(4)-C(7)-Co(3)	77.33(10)
C(7)-C(8)-Co(3)	70.96(18)	C(7)-C(8)-Co(4)	70.50(18)
Co(3)-C(8)-Co(4)	77.87(11)	C(10)-C(9)-N(1)	116.8(2)
C(11)-C(10)-C(9)	146.1(3)	C(11)-C(10)-Co(1)	69.93(17)
C(9)-C(10)-Co(1)	136.9(2)	C(11)-C(10)-Co(2)	69.09(17)
C(9)-C(10)-Co(2)	128.39(19)	Co(1)-C(10)-Co(2)	76.78(10)

C(10)-C(11)-Co(2)	71.30(18)	C(10)-C(11)-Co(1)	70.38(17)
Co(2)-C(11)-Co(1)	77.55(11)	O(1)-C(13)-Co(1)	176.7(3)
O(2)-C(14)-Co(1)	179.5(3)	O(3)-C(15)-Co(1)	176.4(3)
O(6)-C(16)-Co(2)	178.8(3)	O(4)-C(17)-Co(2)	178.3(3)
(5)-C(18)-Co(2)	175.5(3)	O(7)-C(19)-Co(3)	177.1(3)
O(8)-C(20)-Co(3)	177.7(3)	O(9)-C(21)-Co(3)	177.2(3)
O(10)-C(22)-Co(4)	177.4(3)	O(11)-C(23)-Co(4)	177.8(3)
O(12)-C(24)-Co(4)	177.7(3)	F(4)-P(1)-F(1)	90.27(10)
F(4)-P(1)-F(3)	90.50(11)	F(1)-P(1)-F(3)	89.36(10)
F(4)-P(1)-F(6)	90.74(11)	F(1)-P(1)-F(6)	178.88(13)
F(3)-P(1)-F(6)	91.11(11)	F(4)-P(1)-F(5)	90.46(10)
F(1)-P(1)-F(5)	90.57(10)	F(3)-P(1)-F(5)	179.04(12)
F(6)-P(1)-F(5)	88.94(11)	F(4)-P(1)-F(2)	179.55(12)
F(1)-P(1)-F(2)	89.34(10)	F(3)-P(1)-F(2)	89.71(11)
F(6)-P(1)-F(2)	89.65(11)	F(5)-P(1)-F(2)	89.33(11)
N(1)-C(1)-H(1A)	108.9	C(2)-C(1)-H(1A)	108.9
N(1)-C(1)-H(1B)	108.9	C(2)-C(1)-H(1B)	108.9
H(1A)-C(1)-H(1B)	107.7	C(1)-C(2)-H(2A)	109.5
C(3)-C(2)-H(2A)	109.5	C(1)-C(2)-H(2B)	109.5
C(3)-C(2)-H(2B)	109.5	H(2A)-C(2)-H(2B)	108.1
C(2)-C(3)-H(3A)	109.6	C(4)-C(3)-H(3A)	109.6
C(2)-C(3)-H(3B)	109.6	C(4)-C(3)-H(3B)	109.6
H(3A)-C(3)-H(3B)	108.1	C(5)-C(4)-H(4A)	109.2
C(3)-C(4)-H(4A)	109.2	C(5)-C(4)-H(4B)	109.2
C(3)-C(4)-H(4B)	109.2	H(4A)-C(4)-H(4B)	107.9
N(1)-C(5)-H(5A)	109	C(4)-C(5)-H(5A)	109
N(1)-C(5)-H(5B)	109	C(4)-C(5)-H(5B)	109
H(5A)-C(5)-H(5B)	107.8	C(7)-C(6)-H(6A)	107.9
N(1)-C(6)-H(6A)	107.9	C(7)-C(6)-H(6B)	107.9
N(1)-C(6)-H(6B)	107.9	H(6A)-C(6)-H(6B)	107.2
C(7)-C(8)-H(8A)	144.8(19)	Co(3)-C(8)-H(8A)	131.2(19)
Co(4)-C(8)-H(8A)	133.8(19)	C(10)-C(9)-H(9A)	108.1
N(1)-C(9)-H(9A)	108.1	C(10)-C(9)-H(9B)	108.1
N(1)-C(9)-H(9B)	108.1	H(9A)-C(9)-H(9B)	107.3
C(10)-C(11)-H(11A)	140.0(17)	Co(2)-C(11)-H(11A)	137.3(17)
Co(1)-C(11)-H(11A)	132.4(17)		

Appendix Table 23: Torsion angles [°] for $(Co_2(CO)_6)_2$ **4b**.

Atom-atom-atom-atom	Angle	Atom-atom-atom-atom	Angle
C(13)-Co(1)-Co(2)-C(16)	-37.3(3)	C(14)-Co(1)-Co(2)-C(16)	-148.8(2)
C(15)-Co(1)-Co(2)-C(16)	105.8(2)	C(11)-Co(1)-Co(2)-C(16)	-38.7(2)
C(10)-Co(1)-Co(2)-C(16)	12.7(2)	C(13)-Co(1)-Co(2)-C(17)	-156.4(2)
C(14)-Co(1)-Co(2)-C(17)	92.04(14)	C(15)-Co(1)-Co(2)-C(17)	-13.35(14)
C(11)-Co(1)-Co(2)-C(17)	-157.91(15)	C(10)-Co(1)-Co(2)-C(17)	-106.49(14)
C(13)-Co(1)-Co(2)-C(18)	93.6(2)	C(14)-Co(1)-Co(2)-C(18)	-17.94(13)
C(15)-Co(1)-Co(2)-C(18)	-123.32(13)	C(11)-Co(1)-Co(2)-C(18)	92.12(14)
C(10)-Co(1)-Co(2)-C(18)	143.53(14)	C(13)-Co(1)-Co(2)-C(11)	1.5(2)
C(14)-Co(1)-Co(2)-C(11)	-110.06(15)	C(15)-Co(1)-Co(2)-C(11)	144.56(14)
C(10)-Co(1)-Co(2)-C(11)	51.41(15)	C(13)-Co(1)-Co(2)-C(10)	-50.0(2)
C(14)-Co(1)-Co(2)-C(10)	-161.47(14)	C(15)-Co(1)-Co(2)-C(10)	93.14(14)
C(11)-Co(1)-Co(2)-C(10)	-51.41(14)	C(19)-Co(3)-Co(4)-C(22)	-11.4(3)

C(20)-Co(3)-Co(4)-C(22)	122.2(2)	C(21)-Co(3)-Co(4)-C(22)	-129.6(2)
C(8)-Co(3)-Co(4)-C(22)	-28.2(2)	C(7)-Co(3)-Co(4)-C(22)	23.1(2)
C(19)-Co(3)-Co(4)-C(23)	118.7(3)	C(20)-Co(3)-Co(4)-C(23)	-107.63(14)
C(21)-Co(3)-Co(4)-C(23)	0.53(14)	C(8)-Co(3)-Co(4)-C(23)	101.89(15)
C(7)-Co(3)-Co(4)-C(23)	153.26(14)	C(19)-Co(3)-Co(4)-C(24)	-136.6(3)
C(20)-Co(3)-Co(4)-C(24)	-2.95(14)	C(21)-Co(3)-Co(4)-C(24)	105.21(14)
C(8)-Co(3)-Co(4)-C(24)	-153.42(15)	C(7)-Co(3)-Co(4)-C(24)	-102.05(14)
C(19)-Co(3)-Co(4)-C(8)	16.8(3)	C(20)-Co(3)-Co(4)-C(8)	150.48(16)
C(21)-Co(3)-Co(4)-C(8)	-101.36(16)	C(7)-Co(3)-Co(4)-C(8)	51.38(15)
C(19)-Co(3)-Co(4)-C(7)	-34.6(3)	C(20)-Co(3)-Co(4)-C(7)	99.10(15)
C(21)-Co(3)-Co(4)-C(7)	-152.74(15)	C(8)-Co(3)-Co(4)-C(7)	-51.38(15)
C(5)-N(1)-C(1)-C(2)	55.8(3)	C(9)-N(1)-C(1)-C(2)	174.9(2)
C(6)-N(1)-C(1)-C(2)	-63.8(3)	N(1)-C(1)-C(2)-C(3)	-57.8(3)
C(1)-C(2)-C(3)-C(4)	54.6(3)	C(2)-C(3)-C(4)-C(5)	-53.0(3)
C(1)-N(1)-C(5)-C(4)	-53.2(3)	C(9)-N(1)-C(5)-C(4)	-169.6(2)
C(6)-N(1)-C(5)-C(4)	69.2(3)	C(3)-C(4)-C(5)-N(1)	53.2(3)
C(1)-N(1)-C(6)-C(7)	-53.4(3)	C(5)-N(1)-C(6)-C(7)	-173.9(2)
C(9)-N(1)-C(6)-C(7)	65.2(3)	N(1)-C(6)-C(7)-C(8)	-51.3(6)
N(1)-C(6)-C(7)-Co(4)	-156.33(19)	N(1)-C(6)-C(7)-Co(3)	92.5(3)
C(22)-Co(4)-C(7)-C(8)	-95.40(19)	C(23)-Co(4)-C(7)-C(8)	22.8(3)
C(24)-Co(4)-C(7)-C(8)	162.22(18)	Co(3)-Co(4)-C(7)-C(8)	72.63(16)
C(22)-Co(4)-C(7)-C(6)	50.6(2)	C(23)-Co(4)-C(7)-C(6)	168.8(2)
C(24)-Co(4)-C(7)-C(6)	-51.8(2)	C(8)-Co(4)-C(7)-C(6)	145.9(3)
Co(3)-Co(4)-C(7)-C(6)	-141.4(3)	C(22)-Co(4)-C(7)-Co(3)	-168.03(11)
C(23)-Co(4)-C(7)-Co(3)	-49.8(2)	C(24)-Co(4)-C(7)-Co(3)	89.59(12)
C(8)-Co(4)-C(7)-Co(3)	-72.63(16)	C(19)-Co(3)-C(7)-C(8)	92.2(2)
C(20)-Co(3)-C(7)-C(8)	-164.59(19)	C(21)-Co(3)-C(7)-C(8)	-30.2(3)
Co(4)-Co(3)-C(7)-C(8)	-73.09(17)	C(19)-Co(3)-C(7)-C(6)	-67.7(3)
C(20)-Co(3)-C(7)-C(6)	35.5(3)	C(21)-Co(3)-C(7)-C(6)	169.9(3)
C(8)-Co(3)-C(7)-C(6)	-159.9(4)	Co(4)-Co(3)-C(7)-C(6)	127.0(3)
C(19)-Co(3)-C(7)-Co(4)	165.29(12)	C(20)-Co(3)-C(7)-Co(4)	-91.50(13)
C(21)-Co(3)-C(7)-Co(4)	42.9(2)	C(8)-Co(3)-C(7)-Co(4)	73.09(17)
C(6)-C(7)-C(8)-Co(3)	155.7(5)	Co(4)-C(7)-C(8)-Co(3)	-83.48(8)
C(6)-C(7)-C(8)-Co(4)	-120.8(5)	Co(3)-C(7)-C(8)-Co(4)	83.48(8)
C(19)-Co(3)-C(8)-C(7)	-99.33(19)	C(20)-Co(3)-C(8)-C(7)	23.9(3)
C(21)-Co(3)-C(8)-C(7)	159.86(19)	Co(4)-Co(3)-C(8)-C(7)	73.32(17)
C(19)-Co(3)-C(8)-Co(4)	-172.65(11)	C(20)-Co(3)-C(8)-Co(4)	-49.5(2)
C(21)-Co(3)-C(8)-Co(4)	86.54(13)	C(7)-Co(3)-C(8)-Co(4)	-73.32(17)
C(22)-Co(4)-C(8)-C(7)	91.63(19)	C(23)-Co(4)-C(8)-C(7)	-166.53(17)
C(24)-Co(4)-C(8)-C(7)	-28.4(3)	Co(3)-Co(4)-C(8)-C(7)	-73.86(16)
C(22)-Co(4)-C(8)-Co(3)	165.49(12)	C(23)-Co(4)-C(8)-Co(3)	-92.66(12)
C(24)-Co(4)-C(8)-Co(3)	45.5(2)	C(7)-Co(4)-C(8)-Co(3)	73.86(16)
C(1)-N(1)-C(9)-C(10)	-174.3(2)	C(5)-N(1)-C(9)-C(10)	-55.9(3)
C(6)-N(1)-C(9)-C(10)	63.5(3)	N(1)-C(9)-C(10)-C(11)	-37.0(6)
N(1)-C(9)-C(10)-Co(1)	96.8(3)	N(1)-C(9)-C(10)-Co(2)	-148.3(2)
C(13)-Co(1)-C(10)-C(11)	84.15(19)	C(14)-Co(1)-C(10)-C(11)	-40.2(3)
C(15)-Co(1)-C(10)-C(11)	-169.17(18)	Co(2)-Co(1)-C(10)-C(11)	-72.28(17)
C(13)-Co(1)-C(10)-C(9)	-70.5(3)	C(14)-Co(1)-C(10)-C(9)	165.2(3)
C(15)-Co(1)-C(10)-C(9)	36.2(3)	C(11)-Co(1)-C(10)-C(9)	-154.6(4)
Co(2)-Co(1)-C(10)-C(9)	133.1(3)	C(13)-Co(1)-C(10)-Co(2)	156.42(12)
C(14)-Co(1)-C(10)-Co(2)	32.1(2)	C(15)-Co(1)-C(10)-Co(2)	-96.89(11)
C(11)-Co(1)-C(10)-Co(2)	72.28(17)	C(16)-Co(2)-C(10)-C(11)	-100.66(18)
C(17)-Co(2)-C(10)-C(11)	157.73(17)	C(18)-Co(2)-C(10)-C(11)	15.0(2)

Co(1)-Co(2)-C(10)-C(11)	73.29(16)	C(16)-Co(2)-C(10)-C(9)	45.6(3)
C(17)-Co(2)-C(10)-C(9)	-56.0(3)	C(18)-Co(2)-C(10)-C(9)	161.2(2)
C(11)-Co(2)-C(10)-C(9)	146.2(3)	Co(1)-Co(2)-C(10)-C(9)	-140.5(3)
C(16)-Co(2)-C(10)-Co(1)	-173.95(11)	C(17)-Co(2)-C(10)-Co(1)	84.45(12)
C(18)-Co(2)-C(10)-Co(1)	-58.27(18)	C(11)-Co(2)-C(10)-Co(1)	-73.29(16)
C(9)-C(10)-C(11)-Co(2)	-128.6(5)	Co(1)-C(10)-C(11)-Co(2)	83.05(8)
C(9)-C(10)-C(11)-Co(1)	148.4(5)	Co(2)-C(10)-C(11)-Co(1)	-83.05(8)
C(16)-Co(2)-C(11)-C(10)	88.96(18)	C(17)-Co(2)-C(11)-C(10)	-36.0(3)
C(18)-Co(2)-C(11)-C(10)	-169.63(17)	Co(1)-Co(2)-C(11)-C(10)	-73.25(16)
C(16)-Co(2)-C(11)-Co(1)	162.21(11)	C(17)-Co(2)-C(11)-Co(1)	37.3(2)
C(18)-Co(2)-C(11)-Co(1)	-96.38(12)	C(10)-Co(2)-C(11)-Co(1)	73.25(16)
C(13)-Co(1)-C(11)-C(10)	-104.92(18)	C(14)-Co(1)-C(11)-C(10)	156.05(18)
C(15)-Co(1)-C(11)-C(10)	16.1(3)	Co(2)-Co(1)-C(11)-C(10)	74.34(16)
C(13)-Co(1)-C(11)-Co(2)	-179.26(11)	C(14)-Co(1)-C(11)-Co(2)	81.71(13)
C(15)-Co(1)-C(11)-Co(2)	-58.2(2)	C(10)-Co(1)-C(11)-Co(2)	-74.34(16)
C(14)-Co(1)-C(13)-O(1)	51(5)	C(15)-Co(1)-C(13)-O(1)	157(4)
C(11)-Co(1)-C(13)-O(1)	-60(5)	C(10)-Co(1)-C(13)-O(1)	-100(5)
Co(2)-Co(1)-C(13)-O(1)	-61(5)	C(13)-Co(1)-C(14)-O(2)	-130(41)
C(15)-Co(1)-C(14)-O(2)	125(41)	C(11)-Co(1)-C(14)-O(2)	-28(41)
C(10)-Co(1)-C(14)-O(2)	-2(42)	Co(2)-Co(1)-C(14)-O(2)	22(41)
C(13)-Co(1)-C(15)-O(3)	153(4)	C(14)-Co(1)-C(15)-O(3)	-108(4)
C(11)-Co(1)-C(15)-O(3)	33(4)	C(10)-Co(1)-C(15)-O(3)	43(4)
Co(2)-Co(1)-C(15)-O(3)	-9(4)	C(17)-Co(2)-C(16)-O(6)	-73(15)
C(18)-Co(2)-C(16)-O(6)	37(15)	C(11)-Co(2)-C(16)-O(6)	138(15)
C(10)-Co(2)-C(16)-O(6)	179(100)	Co(1)-Co(2)-C(16)-O(6)	168(14)
C(16)-Co(2)-C(17)-O(4)	-132(10)	C(18)-Co(2)-C(17)-O(4)	126(10)
C(11)-Co(2)-C(17)-O(4)	-5(10)	C(10)-Co(2)-C(17)-O(4)	-28(10)
Co(1)-Co(2)-C(17)-O(4)	24(10)	C(16)-Co(2)-C(18)-O(5)	85(4)
C(17)-Co(2)-C(18)-O(5)	-173(4)	C(11)-Co(2)-C(18)-O(5)	-22(4)
C(10)-Co(2)-C(18)-O(5)	-31(4)	Co(1)-Co(2)-C(18)-O(5)	-74(4)
C(20)-Co(3)-C(19)-O(7)	35(6)	C(21)-Co(3)-C(19)-O(7)	-73(6)
C(8)-Co(3)-C(19)-O(7)	-178(100)	C(7)-Co(3)-C(19)-O(7)	141(6)
Co(4)-Co(3)-C(19)-O(7)	169(6)	C(19)-Co(3)-C(20)-O(8)	100(8)
C(21)-Co(3)-C(20)-O(8)	-160(8)	C(8)-Co(3)-C(20)-O(8)	-25(8)
C(7)-Co(3)-C(20)-O(8)	-10(8)	Co(4)-Co(3)-C(20)-O(8)	-62(8)
C(19)-Co(3)-C(21)-O(9)	-118(6)	C(20)-Co(3)-C(21)-O(9)	141(6)
C(8)-Co(3)-C(21)-O(9)	-12(6)	C(7)-Co(3)-C(21)-O(9)	7(6)
Co(4)-Co(3)-C(21)-O(9)	40(6)	C(23)-Co(4)-C(22)-O(10)	-102(7)
C(24)-Co(4)-C(22)-O(10)	154(7)	C(8)-Co(4)-C(22)-O(10)	7(7)
C(7)-Co(4)-C(22)-O(10)	47(7)	Co(3)-Co(4)-C(22)-O(10)	29(7)
C(22)-Co(4)-C(23)-O(11)	-28(7)	C(24)-Co(4)-C(23)-O(11)	73(7)
C(8)-Co(4)-C(23)-O(11)	-132(7)	C(7)-Co(4)-C(23)-O(11)	-147(7)
Co(3)-Co(4)-C(23)-O(11)	175(100)	C(22)-Co(4)-C(24)-O(12)	157(7)
C(23)-Co(4)-C(24)-O(12)	57(7)	C(8)-Co(4)-C(24)-O(12)	-83(7)
C(7)-Co(4)-C(24)-O(12)	-101(7)	Co(3)-Co(4)-C(24)-O(12)	-49(7)

Appendix 4: Spectra for ESI-MS from non-polar solvents

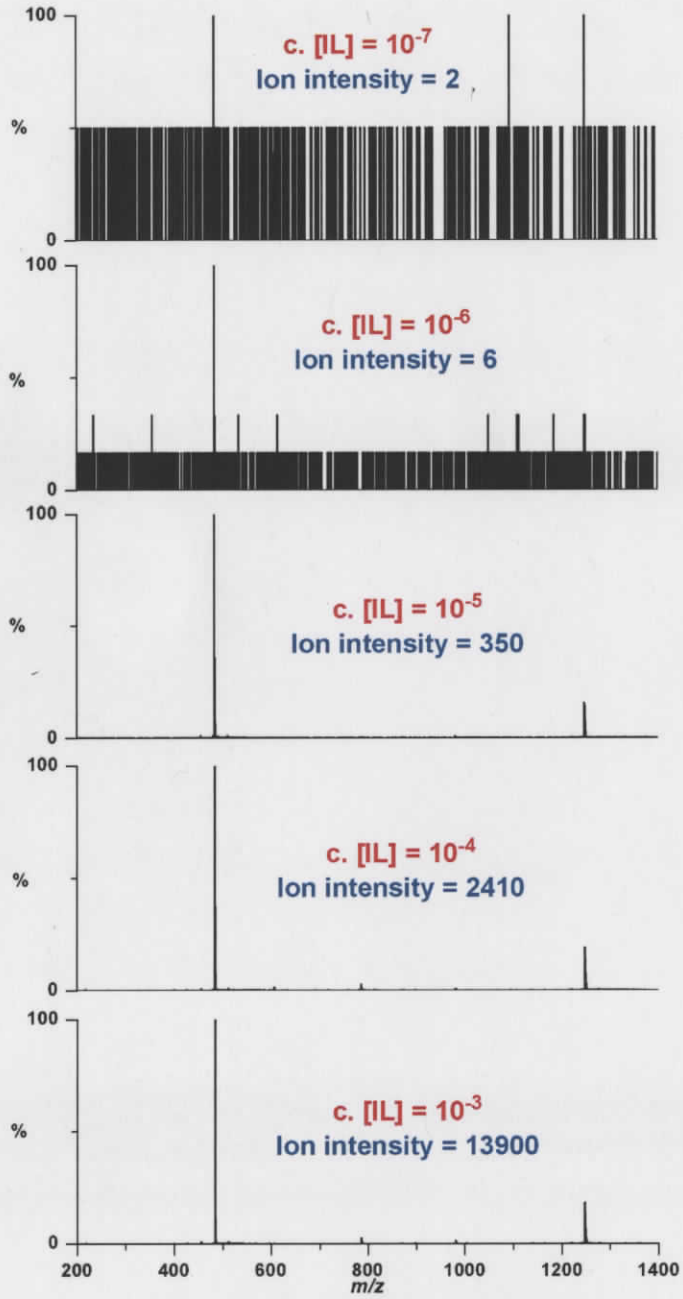

Appendix fig. 21: IL-**1** in pentane

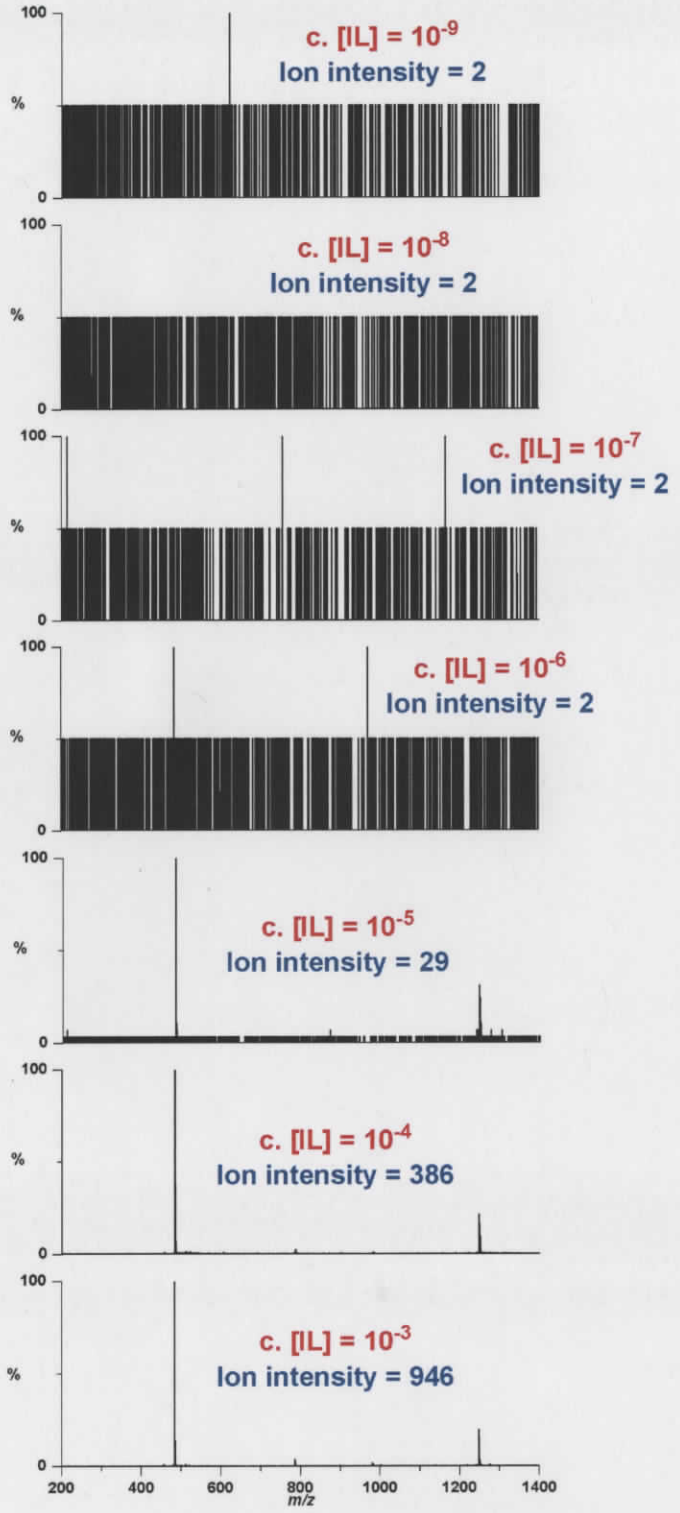

Appendix fig. 22: IL-**1** in cyclohexane.

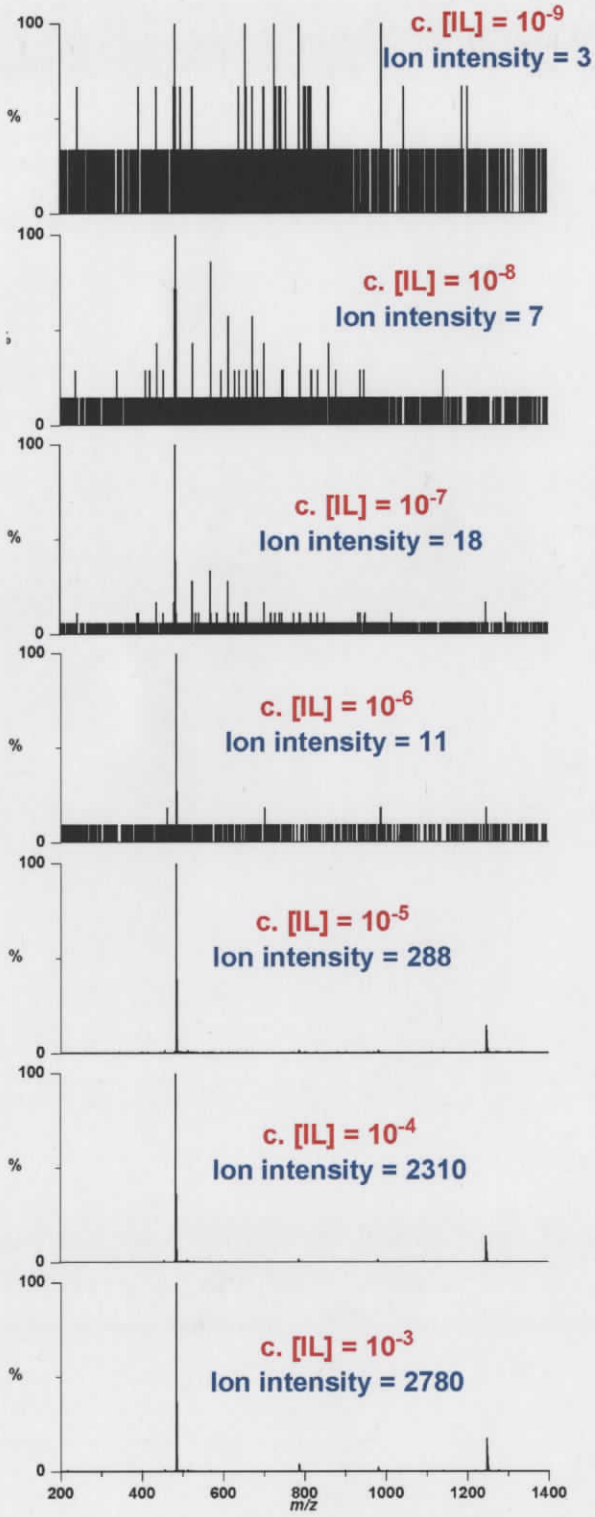

Appendix fig. 23: IL-**1** in benzene

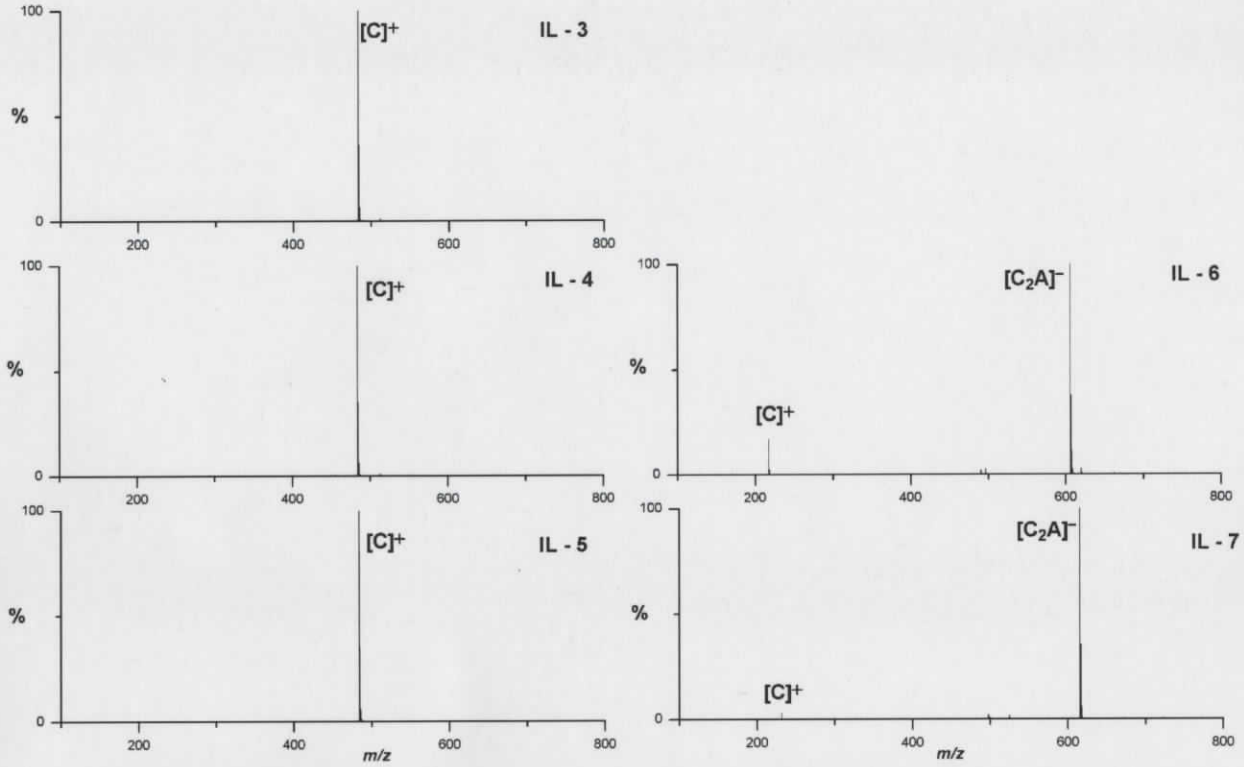

Appendix fig. 24: ESI-MS of IL's **3-7** dissolved in toluene at a concentration of 10^{-6} M.

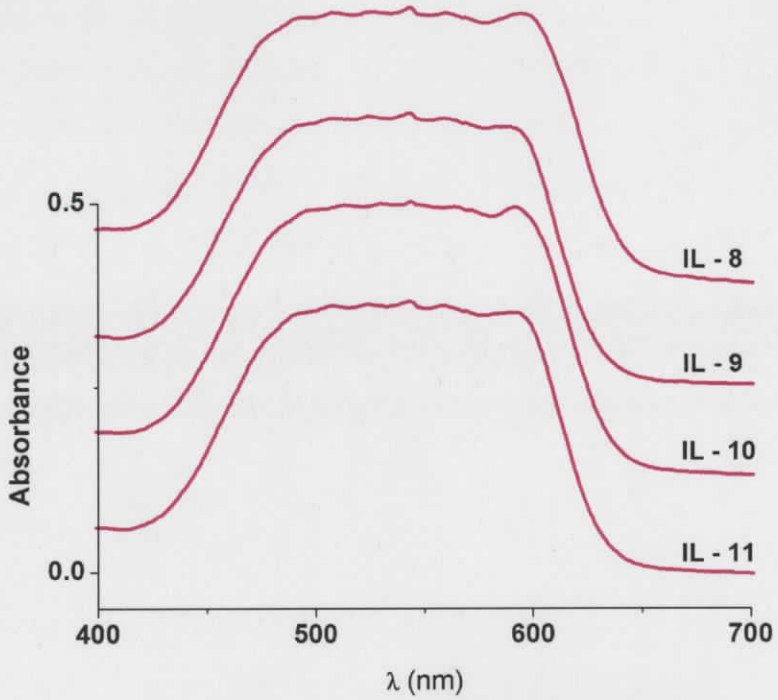

Appendix fig. 25: Solvatochromic shifts of NR in ILs **8-11**.

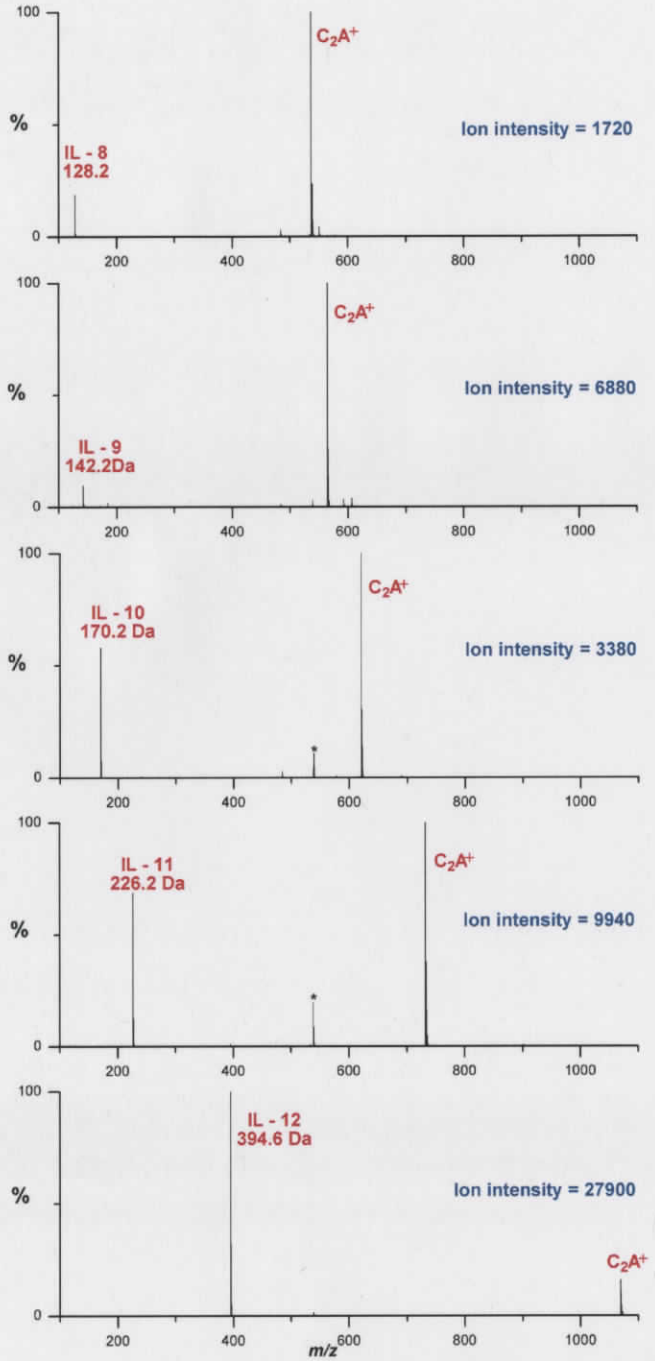

Appendix fig. 26: Spectra of ILs **8-12** at concentrations of 10^{-5} mol L^{-1} in toluene (* = $[PPh_3NPPh_3]^+$ contaminant).

Appendix 5: MS/MS spectra of MAO species and Python programming

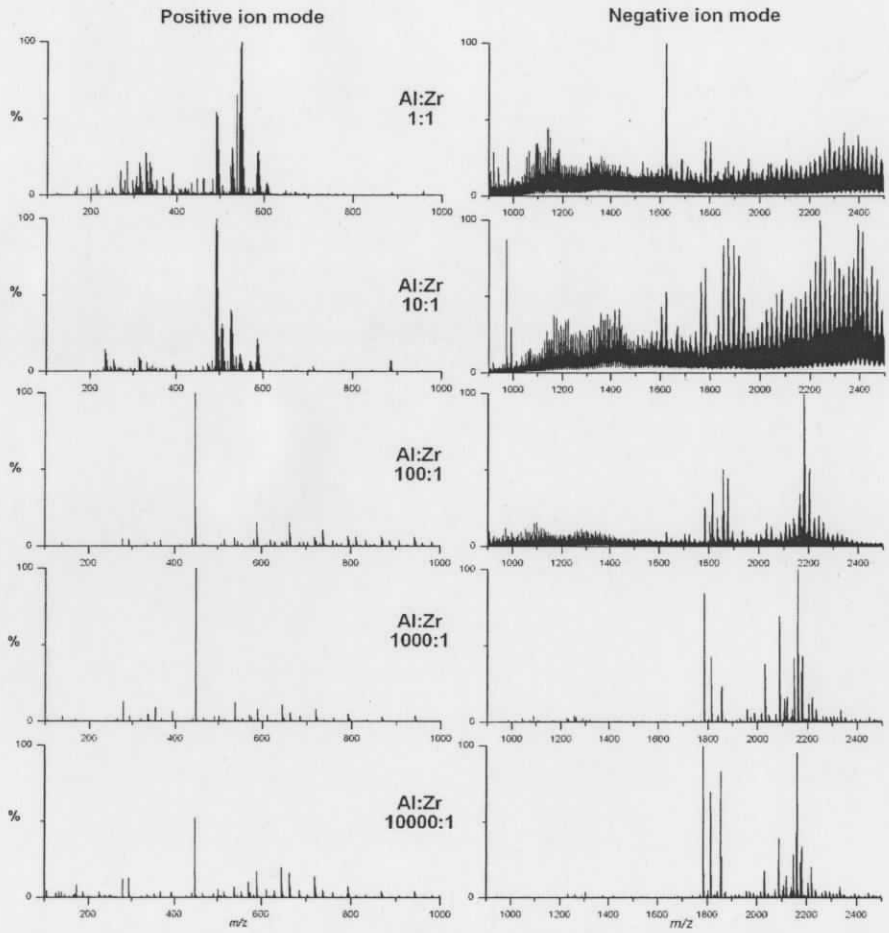

Appendix fig. 27: Positive ion and negative ion spectra of the mixture of Cp_2ZrCl_2 with increasing concentration of MAO.

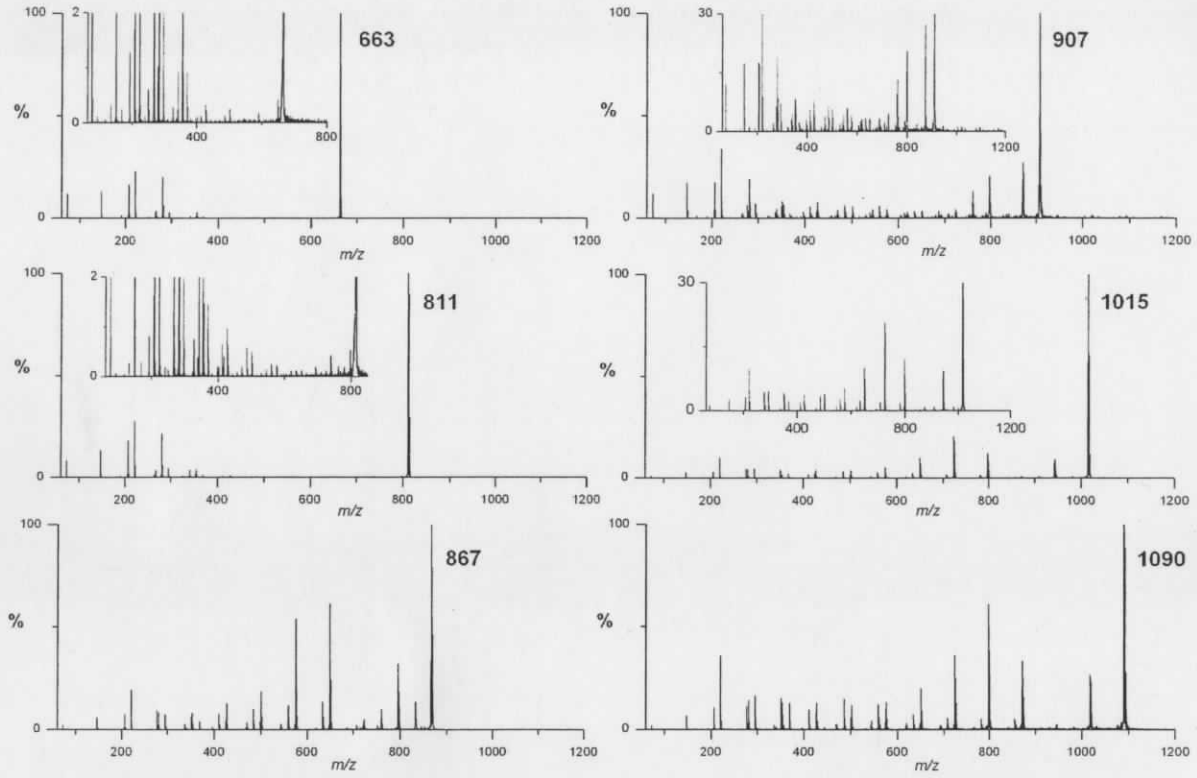

Appendix fig. 28: MS/MS of several peaks in the positive ion spectrum of pure MAO.

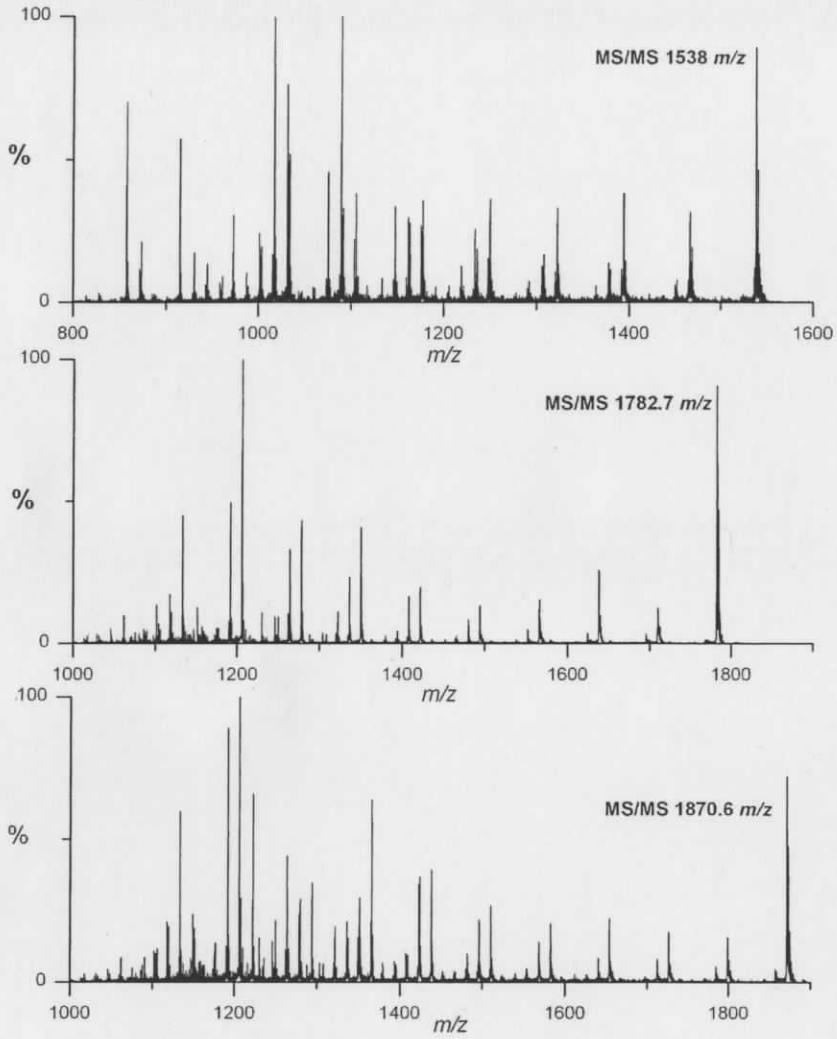

Appendix fig. 29: MS/MS spectra of three peaks from Figure 5-8.

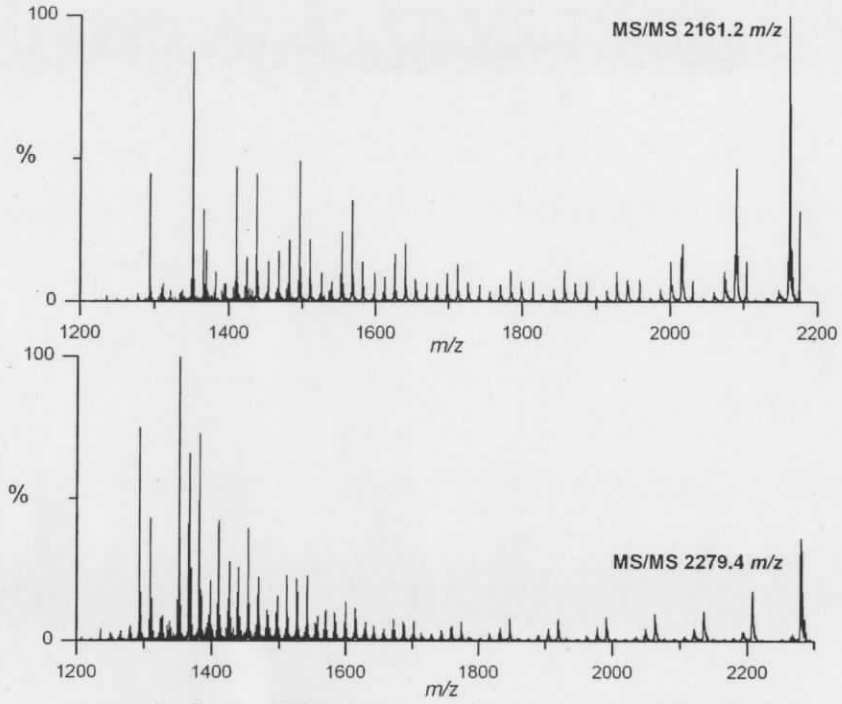

Appendix fig. 30: MS/MS spectra of two peaks from Figure 5-8.

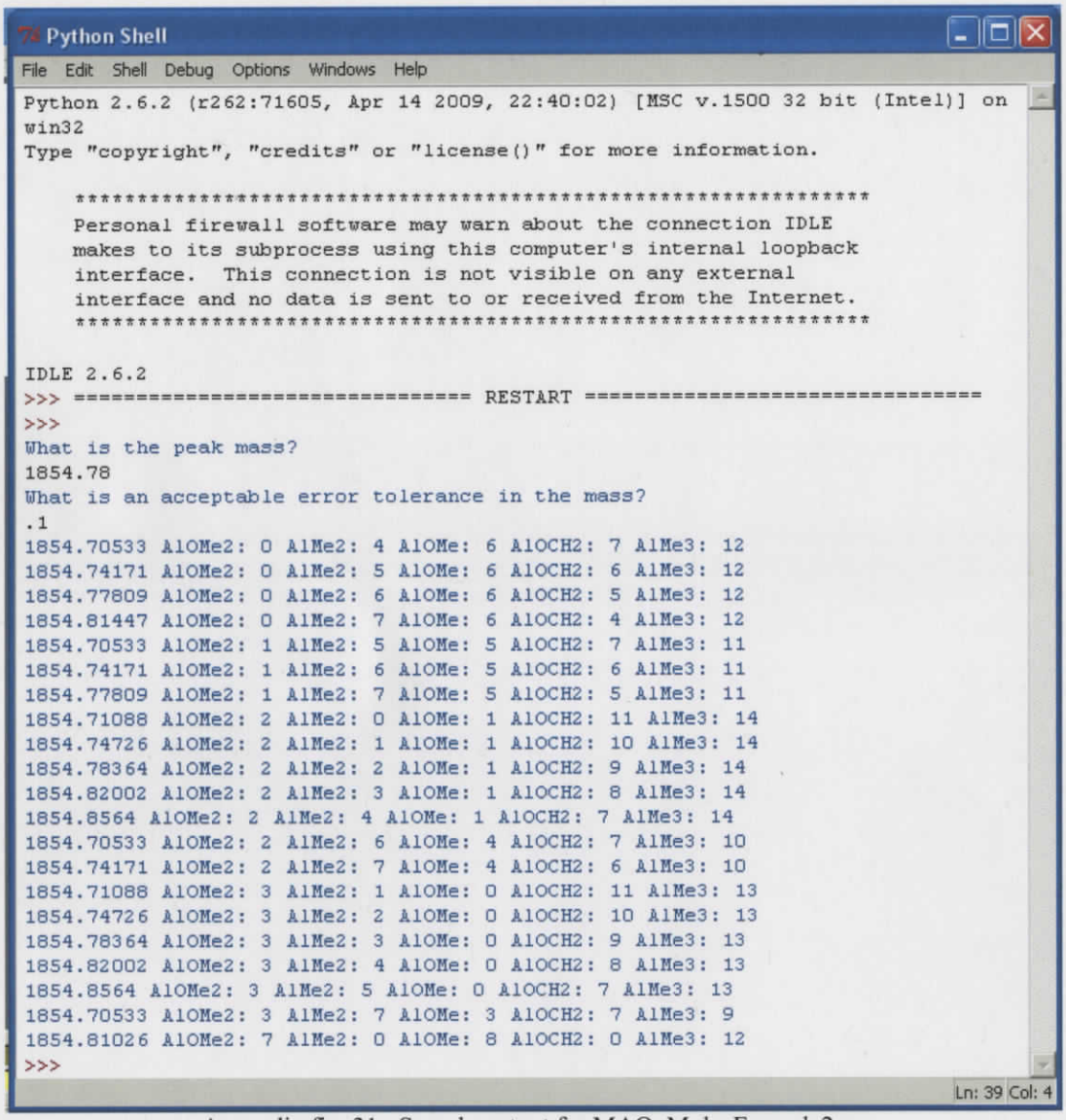

Appendix fig. 31: Sample output for MAO_MolecFormula2.py

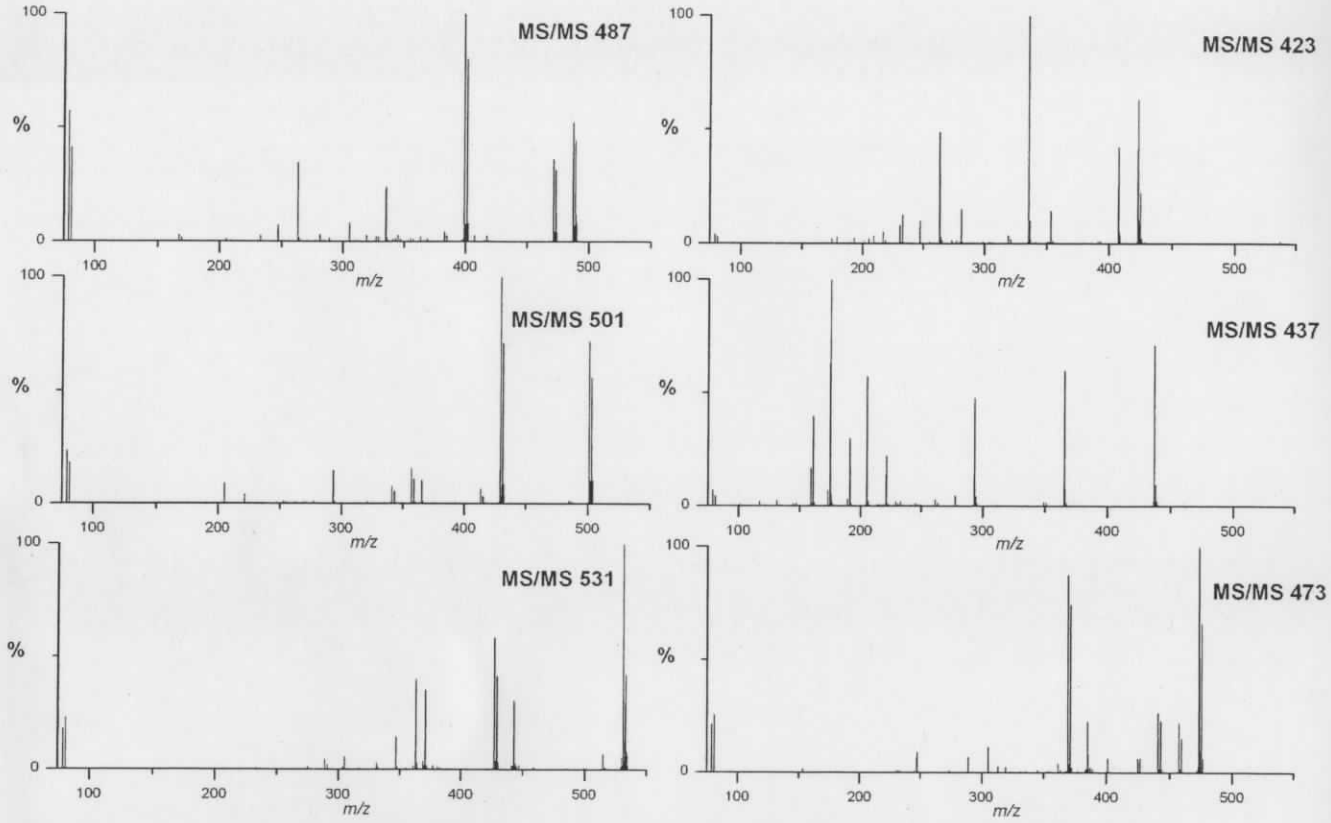

Appendix fig. 32: MS/MS of several peaks in the mixture of MAO + 1/100th Br^-.

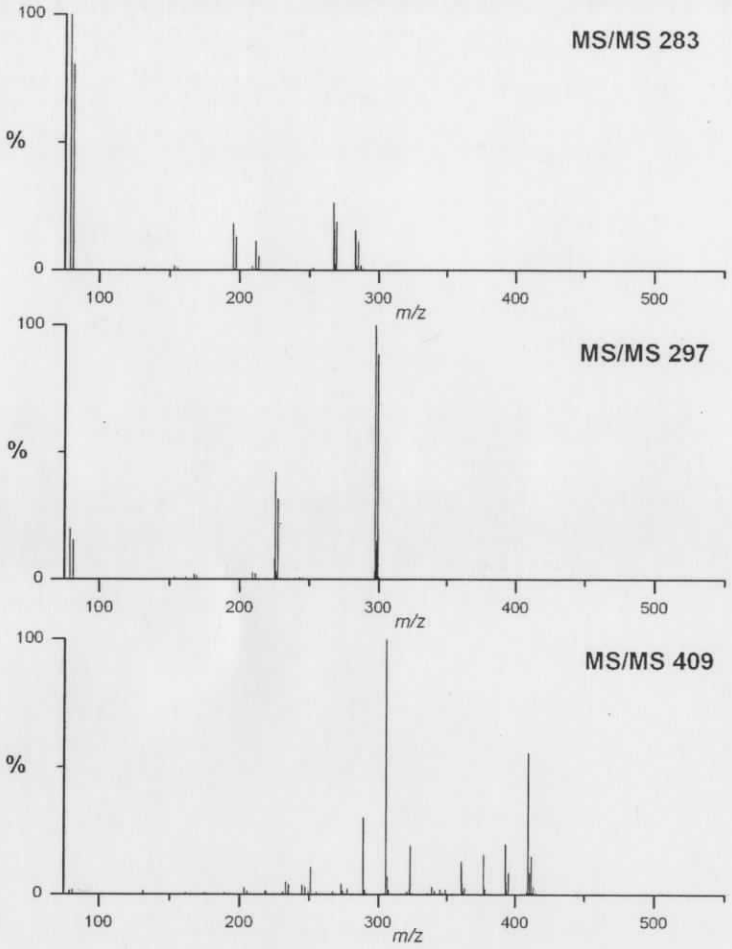

Appendix fig. 33: MS/MS of several peaks in the mixture of MAO + 1/100th Br^-.

5.10.1 Python Programming

These programs were written using the Python programming language (version 2.6.2). This is a freely downloadable programming language available from: http://www.python.org/ . To use these programs, follow these steps:

1. Go to the above website and download Python 2.6.2. Make sure that the version corresponding to the proper operating system is chosen.

2. Once downloaded, open "IDLE (Python GUI)." This will open the interactive development environment (IDLE).

3. Open a blank text window by clicking on "File", then selecting "New Window."

4. Copy the programs below into the text window exactly as they appear below. Any incorrect indents, forgotten commas, different spaces, etc. will make the program freeze and require debugging.

5. Save the program as a .py file. The location of the file does not matter, although if a more complicated program is used it may require being saved in the same folder as the python program.

6. Run the program. The user will be prompted in the IDLE environment, and if successive runs are desired, the user will have to switch back and forth between the text file and the IDLE window. To halt the program in the middle press "CRTL + F6."

MAO_MolecularFormula1.py

```
Al = 26.9815
O = 15.9994
Me = 15.0235

mass = float(raw_input("What is the peak mass?\n"))
tolerance = float(raw_input("What is an acceptable error tolerance in the mass?\n"))

for x in range(100):
    trial1 = x * Al
    for y in range(100):
        trial2 = y * O
        for z in range (200):
            trial3 = z *  Me
            totalmass = trial1 + trial2 + trial3
            if (abs(totalmass - mass) <= tolerance):
                print totalmass, "Al", x, "O", y, "Me", z
```

MAO_MolecularFormula2.py

```
Al = 26.9815
O = 15.9994
Me = 15.0235
OMe = 31.0229
AlMe3 = 72.05196

mass = float(raw_input("What is the peak mass?\n"))
tolerance = float(raw_input("What is an acceptable error tolerance in the mass?\n"))
```

```
# Aluminums only, starts at 10 and goes up to 40
# charge is +3
for x in range(40):
   m = x + 10
   trial1 = m * Al
   charge1 = m * 3

   # Oxygens only, starts at 10 and goes up to 40
   # Charge is -2
   for y in range(30):
      n = y + 10
      trial2 = n * O
      charge2 = n * -2

   # OMe; methoxides, not oxygen and methyls
   # Charge is -1 for a methoxide ligand
      for a in range (20):
         trial3 = a * OMe
         charge3 = a * -1
         totalcharge = charge1 + charge2 + charge3
         totalmass = trial1 + trial2 + trial3
         if (abs(totalmass - mass) <= tolerance):
            if (totalcharge == -1):
               print totalmass, "Al", m, "O", n, "Me", z, "OMe", a

   # TMA
   # No charge
         for c in range (20):
            trial4 = c * AlMe3
            totalmass = trial1 + trial2 + trial3 + trial4
            if (abs(totalmass - mass) <= tolerance):
               if (totalcharge == -1):
                  print totalmass, "Al", m, "O", n, "Me", z, "OMe", a, "TMA", c

   # Methyl ligands bound to Al center
   # Charge is -1
            for z in range (70):
               trial5 = z *  Me
               charge4 = z * -1
               totalcharge = charge1 + charge2 + charge3 + charge4
               totalmass = trial1 + trial2 + trial3 + trial4 + trial5
               if (abs(totalmass - mass) <= tolerance):
                  if (totalcharge == -1):
                     print totalmass, "Al", m, "O", n, "Me", z, "OMe", a, "TMA", c
```

TIBA_MolecFormula.py

```
### Define potential components of the molecule
Al = 26.9815
O = 15.9994
Bu = 57.07042
OBu = 73.06982
OC4 = 72.06192
```

```
### Define the peak mass and an acceptable error in the spectral mass

mass = float(raw_input("What is the peak mass?\n"))
tolerance = float(raw_input("What is an acceptable error tolerance in the mass?\n"))

###Begin searching for potential formulae that fit the spectral mass
for x in range(20):
    trial1 = x * Al
    charge1 = x * 3

    for y in range(20):
      trial2 = y * O
      charge2 = y * -2

      for z in range (20):
        trial3 = z *  Bu
        charge3 = z * -1

        for a in range (20):
          trial4 = a * OBu
          charge4 = a * -1
          totalmass = trial1 + trial2 + trial3 + trial4
          totalcharge = charge1 + charge2 + charge3 + charge4

          if (abs(totalmass - mass) <= tolerance):
            if (totalcharge == -1):
              print totalmass, "Al", x, "O", y, "Bu", z, "OBu", a, "charge", totalcharge

          for b in range (20):
            trial5 = b * OC4
            charge5 = b * -2
            totalmass = trial1 + trial2 + trial3 + trial4 + trial5
            totalcharge = charge1 + charge2 + charge3 + charge4 + charge5

            if (abs(totalmass - mass) <= tolerance):
              if (totalcharge == -1):
                print totalmass, "Al", x, "O", y, "Bu", z, "OBu", a, "OC4H8", b, "charge", totalcharge
```